LINEAR POLYSULFIDES:

THEIR CHARACTERISATION AND

DEGRADATION PATHWAYS

Andrea Mahon

Submitted for the degree of Doctor of Philosophy

University of Warwick
Department of Chemistry

Submitted October 1996

TABLE OF CONTENTS

Title Page		i
Table of Contents		ii
List of Figures		xi
List of Tables		xxi
Acknowledgements		xxiii
Declaration		xxiv
List of Abbreviations		xxv
Abstract		xxvii
Main Text		1

CHAPTER 1: INTRODUCTION

1.1	**Polysulfides**	
1.1.1	History and Development	1
1.1.2	The Materials and their Applications	3
1.1.3	Degradation of Linear Polysulfides	5
1.1.4	Characterisation of LPs	9
1.2	**Polymer Degradation**	
1.2.1	General	10
1.2.2	General Mechanisms of Oxidative Degradation in Linear Polymers	12
1.2.3	Stabilisation and Protection of Polymers	21
1.2.4	Techniques for Monitoring Polymer Degradation	23

1.3 Mass Spectrometry of Polymers

1.3.1 General 24

1.3.2 Electrospray Ionisation 25

1.3.3 Matrix Assisted Laser Desorption Ionisation 31

1.3.4 Field Desorption 34

1.3.5 Mass Spectrometry of Polysulfides 35

1.4 Object of this Work 36

CHAPTER 2: EXPERIMENTAL

2.1 Instrumental

2.1.1 Infrared (IR) Spectroscopy 47

2.1.1.1 Infrared Spectra of Pre-Polymer Films 47

2.1.1.2 Infrared Spectra of Cured Polymer Films 47

2.1.1.3 Solution Infrared Spectra of Leached Polymer Samples 47

2.1.1.4 Infrared Spectra of Polymer Surfaces using Attenuated Total Reflectance (ATR) Infrared Spectroscopy 50

2.1.2 Nuclear Magnetic Resonance (NMR) Spectroscopy 50

2.1.3 Solid State ^{1}H NMR Experiment 54

2.1.4 Gel Permeation Chromatography (GPC) 54

2.1.5 Electrospray Mass Spectrometry 54

2.1.6 Matrix Assisted Laser Desorption Ionisation (MALDI) 56

2.1.7 Field Desorption (FD) 56

2.1.8	Fast Atom Bombardment (FAB)	56
2.1.9	Gas Chromatography (GC) Mass Spectrometry	57
2.1.10	X-Ray Photoelectron Spectrometer (XPS)	57
2.1.11	Static Secondary Ion Mass Spectrometry	57
2.1.12	Raman Spectroscopy	57
2.1.13	Energy Dispersive X-Ray Analysis (EDAX)	57
2.1.14	CHN Analysis	58
2.1.15	Tensile Testing	58
2.1.16	Optical Microscope	58
2.1.17	Pyrolysis of Samples in the Oven	58
2.1.18	Photolysis of Samples	59
2.1.18.1	350 W Xenon Lamp	59
2.1.18.2	UV_B Weatherometer	59
2.1.18.3	Sol-2 Light Box	60
2.2	**Chemicals**	
2.2.1	Polymers	61
2.2.2	Solvents	62
2.2.3	Salts and Matrices for Mass Spectrometric Analysis	62
2.2.4	Curative Agents	63
2.2.5	Potential Stabilising Systems	63
2.2.6	Other Chemicals Used in LP-Cured Formulations	63
2.2.7	Other Chemicals Used in Construction Sealants for XPS Surface Studies	64

2.2.8	Chemicals Used in the Determination of SH	64
2.2.9	Column Chromatography	64
2.3	**Experimental Procedures**	
2.3.1	Titrimetric Estimation of Thiol	65
2.3.2	Preparation of Cured Thin Films of LP	65
2.3.3	Preparation of Cured Cast Blocks of LP	66
2.3.4	Preparation of 'H' Block Samples	66
2.3.5	Formulation of Construction Sealant	68
2.3.6	Actinometry	69

CHAPTER 3: RESULTS AND DISCUSSION CHARACTERISATION OF LINEAR POLYSULFIDES BY ELECTROSPRAY IONISATION MASS SPECTROMETRY

3.1	General Features	71
3.2	Effect of End Group	81
3.3	Effect of Mer Unit	81
3.4	Variation of the Composition of the Mobile Phase	85
3.5	Effect of RMM of LP	85
3.6	Variation in the Cone Voltage	87
3.7	CID and Precursor-Ion Experiments	89
3.8	ESI Spectra of Reaction Systems	101
3.9	Fast Atom Bombardment Experiments	101
3.10	Discussion and Conclusions	101

CHAPTER 4: RESULTS AND DISCUSSION IONS DERIVED FROM LINEAR POLYSULFIDE OLIGOMERS USING MALDI AND FIELD DESORPTION IONISATION MASS SPECTROMETRY

4.1	Introduction	106
4.2	MALDI Studies of LPs	106
4.3	The Appearance of Silver Sulfide Clusters in MALDI Experiments on Linear Polysulfides	113
4.4	Field Desorption Experiments with Linear Polysulfide Oligomers	116
4.5	Discussion and Conclusions	116

CHAPTER 5: RESULTS AND DISCUSSION PHOTO- AND THERMAL DEGRADATION OF LP PRE-POLYMERS

5.1	Preliminary Photodegradation Studies of LP Pre-Polymers by IR Spectroscopy	121
5.2	Degradation Studies of LP Pre-Polymers by GPC	127
5.3	Photodegradation Studies of Bulk Samples of LP Pre-Polymers under UV_B Irradiation by IR Spectroscopy	128
5.4	Chromatography Experiments Carried out on Heavily Irradiated LP-1400C Pre-Polymer to Help Identify New NMR Peaks	134
5.5	Bulk Thermal Degradation Studies of LP Pre-Polymers by IR Spectroscopy	135

5.6 2-D NMR Experiment on Heavily UV-Exposed Pre-Polymer Sample 137

5.7 Experiment to Analyse Volatiles Produced when a Pre-Polymer Sample Undergoes UV Irradiation 137

5.8 Electrospray Mass Spectrometry Studies of Thermally- and Photo-Degraded Pre-Polymers 140

5.9 Discussion and Conclusions 151

CHAPTER 6: RESULTS AND DISCUSSION STUDY OF PHOTODEGRADATION OF CURED-LP FILMS USING INFRA-RED SPECTROSCOPY

6.1 Preliminary Experiments using 350 W Xenon Lamp 157

6.2 Experiment to Ascertain Whether Film Thickness Affects the Rate of Photodegradation 158

6.3 Experiments to Control Film Thickness 161

6.4 Experiment to Ascertain Whether MnO_2 Loading Affects the Rate of Photodegradation 161

6.5 Experiment to Ascertain Whether an Increase in Temperature Affects the Rate of Carbonyl Group Development in Films 165

6.6 To Ascertain the Effects of Photodegrading a Cured LP on a Silica Surface 165

6.7	Experiment to Assess the Effect of the Presence of Tertiary Carbon Atoms in the LP on the Rate of Degradation	169
6.8	The Relative Effects of UV_A and UV_B Radiation in Photodegradation	171
6.9	Experiment to Assess Effect of Carbon Black (ELFLEX 415) on the Rate of Photodegradation	172
6.10	Experiments to Assess Effect of Adhesion Promoter (A187) on Rate of Degradation	172
6.11	Experiment to Assess Effect of the Accelerator Tetramethylthiuram Disulfide (TMTD) on Rate of Degradation	175
6.12	Photodegradation of LPs Cured Using Alternative Curatives	177
6.13	Photographs of UV-Exposed and Non-Exposed Films	183
6.14	Optical Microscopic Examination of LP Films Before and After Photodegradation	190
6.15	Effect of Adding Carbon Black to LP Films Cured with Various Agents	190
6.16	Effect of Varying TBHP Level in LP-977C Cured Films	195
6.17	Effect of Using $CuCl_2$ / KI as a Potential Inhibitor System for LP Photodegradation	197
6.18	Effects of using Tinuvins 1130 and 292 as Potential Inhibitors for LP Photodegradation	199

6.19 Experiments to Assess the Level of Tinuvin 292 Required to Reduce LP Photodegradation 199

6.20 Experiments to Assess Whether Cured Films of LP ZL-2264 Produce Carbonyl Bands When Exposed to UV Irradiation 201

6.21 Solid State ^{1}H NMR Experiment 202

6.22 Discussion and Conclusions 202

CHAPTER 7: RESULTS AND DISCUSSION PHOTO- AND THERMAL DEGRADATION OF CURED LP BLOCKS

7.1 Thermal Degradation at 140°C of TBHP-Cured LP Blocks 209

7.2 Thermal Degradation at 80°C of TBHP-Cured LP Blocks 219

7.3 Photodegradation of TBHP-Cured LP Blocks 221

7.4 Degradation of TBHP-Cured LP 'H' Blocks 223

7.5 Degradation of MnO_2- and $NaBO_3$- Cured LP Samples 225

7.6 Degradation of HDDA-Cured Samples 226

7.7 Discussion and Conclusions 228

CHAPTER 8: RESULTS AND DISCUSSION PHOTODEGRADATION OF POLYSULFIDE POLYMERS AT THEIR INTERFACE WITH GLASS

8.1 X-Ray Photoelectron Spectroscopy (XPS) of the Surfaces of a Ruptured LP-Glass Seal 232

8.2	FTIR-ATR Study of the Polymer Surface of Ruptured MnO_2-Cured Polysulfide Glass Bonds	240
8.3	Static Secondary Ion Mass Spectrometry Studies of LP Polymer Surfaces	244
8.4	Raman Studies of LP Pre-Polymers and Cured LP Surfaces	244
8.5	EDAX Studies of Cured LP Surfaces	246
8.6	Elemental Analysis by C H N Analysis	247
8.7	Attempted Leaching of MnO_2-Cured LP Surfaces	248
8.8	Study of Yellow Discolouration at Exposed Polymer/ Glass Interface by FTIR	249
8.9	Tensile Testing of MnO_2-Cured LP-32C Samples Exposed to UV Radiation with Various Levels of Adhesion Promoter	249
8.10	Discussion and Conclusions	254

CHAPTER 9: CONCLUSIONS AND FUTURE WORK

9.1	Mass Spectrometric Characterisation	257
9.2	Degradation Studies of Linear Polysulfides	260
9.3	Photodegradation of MnO_2-Cured Linear Polysulfides at their Interface with Glass	263
9.4	Future Work	265

LIST OF FIGURES

Figure	Title	Page No.
Fig. 1.1	A schematic diagram of the interface of an electrospray source to a triple quadrupole mass spectrometer	28
Fig. 2.1	IR spectrum of a commercial LP	48
Fig. 2.2	^{1}H NMR spectrum of a commercial LP	51
Fig. 2.3	^{13}C NMR spectrum of a commercial LP	53
Fig. 2.4	'H' block assembly used	67
Fig. 3.1	ESI spectrum of LP-1400C, mobile phase THF/MeOH containing 0.5% aqueous NH_4Cl	75
Fig. 3.2	ESI spectrum of LP-980C, mobile phase THF/MeOH containing 0.5% aqueous NH_4Cl	76
Fig. 3.3	ESI spectrum of LP-12C, mobile phase THF/MeOH containing 0.5% aqueous NH_4Cl	77
Fig. 3.4	ESI spectrum of Model Compound A, mobile phase THF/MeOH containing 0.5% aqueous NH_4Cl	80
Fig. 3.5	ESI spectrum of ELP-3, mobile phase THF/MeOH containing 0.5% aqueous NH_4Cl	82
Fig. 3.6	ESI spectra of ZL-2264, to compare effect of mobile phase on spectral quality: A) THF/MeOH Containing 0.5% aqueous NH_4Cl B) Acetone containing KI	83

Fig. 3.7 ESI-MS spectra of LP pre-polymers of varying molecular weights a) RMM ≈ 1000 b) RMM ≈ 2600 and c) RMM ≈ 4000. Mobile phase THF/MeOH containing 0.5% aqueous NH_4Cl 86

Fig. 3.8 Effect of varying cone voltage on ESI mass spectrum of LP-1400C in a mobile phase of THF/MeOH containing 0.5% aqueous NH_4Cl. (mass range 100-1600 Da). 88

Fig. 3.9 CID spectra of ions selected from the spectrum of LP-1400C 91

Fig. 3.10 Precursor ion spectrum of ion with *m/z* 137.2 derived from the CID of LP-1400C 98

Fig. 3.11 CID spectrum of *m/z* 764.4 ion from ELP-3 100

Fig. 3.12 ESI spectrum of a reaction mixture of Model Compound A with hexane-1,6-diol diacrylate. 102

Fig. 3.13 Positive ion FAB spectrum of LP-1400C in 3-nitrobenzyl alcohol matrix 103

Fig 4.1 MALDI spectrum of LP-2C with 10 μl of silver salt 108

Fig. 4.2 MALDI spectrum of Model A with 10 μl of silver salt 110

Fig. 4.3 MALDI spectrum of ZL-2264 with 10 μl of silver salt 112

Fig. 4.4	MALDI spectrum of ZL-2264 with 200 μl of silver salt	114
Fig. 4.5	Field desorption (FD) spectrum of LP-1400C	117
Fig. 5.1	Layout of apparatus	121
Fig. 5.2	Spectrum showing the development of C=O and O-H frequencies in LP-980C following 20 h UV irradiation with a xenon lamp	122
Fig. 5.3	Profile showing the growth of carbonyl peaks during UV irradiation of LP-1400C	124
Fig. 5.4	Profile showing the growth of carbonyl peaks during UV irradiation of LP-980C	124
Fig. 5.5	Graph showing the effect of oxygen supply on the time dependence of the development of peak at 1726 cm^{-1}	126
Fig. 5.6	Plot to show UV induced changes observed in RMMD for LP-32C	127
Fig. 5.7	Spectrum showing the development of O-H and C=O frequencies in LP-2C after 4820.5 hours UV irradiation in a plentiful supply of oxygen	129
Fig. 5.8	Spectrum of LP-2C after 5205.5 hours UV irradiation in a limited supply of oxygen	130
Fig. 5.9	^1H NMR spectrum of LP-977C after 4820 hours UV_B exposure in 'Weatherometer'	131

Fig. 5.10	^{13}C NMR spectrum of LP-977C after 4820 hours UV_B exposure in 'Weatherometer'	132
Fig. 5.11	Overview of column	135
Fig. 5.12	IR spectrum showing O-H and C=O frequencies in LP-980C after 200 hours at 100°C	136
Fig. 5.13	2-D NMR spectrum of LP-977C after 4820 hours UV_B exposure in 'Weatherometer'	138
Fig. 5.14	Overview of sample tube containing pre-polymer	139
Fig. 5.15	ESI-MS spectrum of LP-977C after 2500 hours UV_B exposure in 'Weatherometer'	141
Fig. 5.16	ESI-MS spectrum of Model A after 5150 hours UV_B exposure in 'Weatherometer'	142
Fig. 5.17	^{13}C NMR spectrum of Model A after 5150 hours UV_B exposure in 'Weatherometer'	144
Fig. 5.18	Overall scheme of hydrolysis for LP pre-polymers	148
Fig. 5.9	Overall scheme of degradation of thermally or UV-irradiated LP featuring duality of mechanism	152
Fig. 6.1	Spectrum showing the development of C=O frequencies in LP-980C with MnO_2 loading of 10% after 20 h UV irradiation using xenon lamp	157
Fig. 6.2	Overview of mounted cured polymer film	158
Fig. 6.3	Profile of growth of 1726 cm^{-1} peak for LP-980C and LP-977C with and without MnO_2 (10%)	159

Fig. 6.4 Profile of growth of carbonyl peaks in cured LP-977C films of varying thickness (with a constant *ca.* 2% of MnO_2), following UV irradiation in 'Weatherometer' 160

Fig. 6.5 Spectrum showing the development of C=O and O-H frequencies in LP-980C with MnO_2 loading of 2% after 1890 h UV irradiation using 'Weatherometer' 162

Fig. 6.6 Profile of growth of carbonyl peaks in cured LP-980C films with varying quantities of MnO_2 following UV irradiation in 'Weatherometer' 164

Fig. 6.7 Overview of mounted film on microscope slide 166

Fig. 6.8 Spectrum showing development of C=O frequencies in LP-977C with a MnO_2 loading of 10% after 155 h UV irradiation through silica using xenon lamp 167

Fig. 6.9 Profile of the development of C=O frequencies in LP-977C with a MnO_2 loading of 10%, coated on a silica disc, after 155 h UV irradiation using xenon lamp 168

Fig. 6.10 Profile of growth of carbonyl peaks in MnO_2 cured LP-12C and LP-2C following UV irradiation in 'Weatherometer' 170

Fig. 6.11 Profile of growth of 1726 cm^{-1} peak for MnO_2 cured LP films using i) UV_A ii) UV_B irradiation 171

Fig. 6.12 Profile of growth of carbonyl peaks in MnO_2 cured LP-977C films with varying levels of carbon black following UV irradiation in UV_B 'Weatherometer' 173

Fig. 6.13 Profile of growth of carbonyl peaks in MnO_2 cured LP-977C films with varying levels of A187 following UV irradiation in UV_B 'Weatherometer' 174

Fig. 6.14 Profile of growth of carbonyl peaks in MnO_2 cured LP-977C films with varying levels of TMTD, following UV irradiation in UV_B 'Weatherometer' 176

Fig. 6.15 Spectrum shows the development of O-H and C=O frequencies in LP-980C with $NaBO_3$ as curative after 2793.4 hours UV_B irradiation using the 'Weatherometer' 178

Fig. 6.16 Spectra showing the development of O-H and C=O frequencies in LP-977C with TBHP as curative after a) 484.3 hours and b) 2468.9 hours UV_B irradiation using 'Weatherometer' 179

Fig. 6.17 Profile of growth of carbonyl peaks in $NaBO_3$-cured LP films following UV_B irradiation in 'Weatherometer' 181

Fig. 6.18	Profile of growth of carbonyl peaks in TBHP-cured LP films following UV_B irradiation in 'Weatherometer'	182
Fig. 6.19a	Photographs of MnO_2-cured LP films before exposure	184
Fig. 6.19b	Photographs of MnO_2-cured LP films after UV exposure	185
Fig. 6.20a	Photographs of $NaBO_3$-cured LP films before exposure	186
Fig. 6.20b	Photographs of $NaBO_3$-cured LP films after UV exposure	187
Fig. 6.21a	Photographs of TBHP-cured LP films before exposure	188
Fig. 6.21b	Photographs of TBHP-cured LP films after UV exposure	189
Fig. 6.22a	Surface morphology photograph of TBHP-cured film before UV exposure	191
Fig. 6.22b	Surface morphology photograph of TBHP-cured film after UV exposure	191
Fig. 6.22c	Surface morphology photograph of $NaBO_3$-cured film before UV exposure	192
Fig. 6.22d	Surface morphology photograph of $NaBO_3$-cured film after UV exposure	192

Fig. 6.22e	Surface morphology photograph of MnO_2-cured film before UV exposure	193
Fig. 6.22f	Surface morphology photograph of MnO_2-cured film after UV exposure	193
Fig. 6.23	Profile of growth of carbonyl peaks with various cured LP-977C films with constant carbon black content, but cured with different curatives, following UV_B irradiation in 'Weatherometer'	194
Fig. 6.24	Profile of growth of carbonyl peaks in LP-977C films cured with varying levels of TBHP following UV_B irradiation in 'Weatherometer'	196
Fig. 6.25	Profile of growth of carbonyl peaks in MnO_2 cured LP-977C films using $Cu(II)Cl_2$ and KI as an inhibitor following UV_B irradiation in 'Weatherometer'	198
Fig. 6.26	Profile of growth of carbonyl peaks in MnO_2 cured LP-977C films containing Tinuvins 292 and 1130 as inhibitors, following UV irradiation in 'Weatherometer'	200
Fig. 6.27	Profile of growth of carbonyl peaks in MnO_2 cured LP-977C films experiment to assess the optimum level of Tinuvin 292 to inhibit degradation following UV_B irradiation in 'Weatherometer'	201

Fig. 7.1	ESI-MS spectrum of TBHP-cured LP exudate exposed to 140°C for 120 hours	211
Fig. 7.2	IR spectrum of TBHP-cured LP exudate exposed to 140°C for 120 hours	212
Fig. 7.3	^{1}H NMR spectrum of TBHP-cured LP exudate exposed to 140°C for 120 hours	213
Fig 7.4	^{13}C NMR spectrum of TBHP-cured LP exudate exposed to 140°C for 120 hours	214
Fig. 7.5	ESI-MS spectrum of TBHP-cured LP exudate exposed to 140°C for 310 hours	218
Fig. 8.1	XPS spectrum of a virgin glass surface	234
Fig. 8.2	XPS spectrum of a virgin glass surface after bombardment with low energy electrons	235
Fig. 8.3	XPS spectrum of a glass surface ruptured from exposed polymer	235
Fig. 8.4	XPS spectrum of an unexposed polymer surface ruptured from glass	236
Fig. 8.5	XPS spectrum of the C(1s) peak of an unexposed polymer surface ruptured from glass	238
Fig. 8.6	XPS spectrum of an unexposed polymer surface taken from centre of bond	238
Fig. 8.7	FTIR-ATR spectra of MnO_2-cured LP-977C surface after a) 286 hours b) 929 hours in dark	241

Fig. 8.8 FTIR-ATR spectra of MnO_2-cured LP-977C 'near' polymer surface after a) 286 hours and b) 929 hours exposed to UV irradiation 242

Fig. 8.9 FTIR-ATR spectra of MnO_2-cured LP-977C 'remote' polymer surface after a) 286 hours and b) 929 hours exposed to UV irradiation 243

Fig. 8.10 Raman spectrum of LP-32C 245

Fig. 8.11 IR spectrum of yellow/brown discolouration 250

Fig. 8.12 Graph to show load in Newtons against UV exposure time in hours with no adhesion promoter present 252

Fig. 8.13 Graph to show load in Newtons against UV exposure time in hours with 1phr adhesion promoter present 252

Fig. 8.14 Graph to show load in Newtons against UV exposure time in hours with 3 phr adhesion promoter present 253

LIST OF TABLES

Table	Title	Page No.
TABLE 2.1	Assignments of the principal peaks in the IR spectrum of an LP	49
TABLE 2.2	General properties of LPs	61
TABLE 2.3	Actinometry results for 350 W xenon lamp	69
TABLE 2.4	Actinometry results for UV_B 'Weatherometer'	69
TABLE 3.1	Assignments of principal peaks in the ESI spectrum of LP-1400C	71
TABLE 3.2	Level of appearance of series A to K in individual LPs	78
TABLE 3.3	ESI spectral peaks and associated assignments in the spectrum of Model Compound A	79
TABLE 3.4	Assignments of principal peaks in series A of the ESI spectrum of ELP-3	81
TABLE 3.5	ESI spectral peaks and associated assignments in the spectrum of ZL-2264	84
TABLE 3.6	Summary chart of ion fragmentation observed in CID of selected ions from LP-1400C	93
TABLE 3.7	Scheme for the fragmentation of ELP-3 on CID	99
TABLE 5.2	Comparison of initial slopes obtained for the development of carbonyl frequencies	125
TABLE 5.3	Carbonyl frequencies in heavily degraded pre-polymer samples	133

TABLE 6.1	Comparison of ν(C=O) frequencies for MnO_2-cured LP films	163
TABLE 6.2	Table to compare position of ν(C=O) in $NaBO_3$-cured LP films	180
TABLE 8.1	Origins of elements identified in XPS spectra of cured LP-glass interfaces following rupture	239
TABLE 8.2	Assignments of peaks in Raman spectrum of LP-32C	246
TABLE 8.3	Elemental analysis of LP samples	247

ACKNOWLEDGEMENTS

I wish to thank my academic supervisor Professor Terry Kemp, for his guidance, advice, encouragement and patience over the last three years. I would like to thank the University of Warwick for a "fees only" graduate award and Morton International Ltd., Coventry for a research studentship.

Staff at Morton International Ltd., Coventry, are thanked for their help and advice, especially my industrial supervisor Dr. Tim Lee, and also Mr. Tom Rees and Mr. Robert Coates. I would also like to thank Dr. Steve Hobbs of Morton International, Woodstock, U.S.A. for synthesising the relatively simple LP known as 'Model A'.

Dr. Armelle Buzy and Professor Keith Jennings are thanked for discussion and use of the ESI-MS which proved extremely useful to my research. I would also like to thank Miss Julie Varney for her help and advice on MALDI-MS and Dr. Tony Jackson of ICI, Wilton is thanked for running the FD-MS spectrum.

Neil Jepson is thanked for his constant help and support throughout my studies.

Finally, I would like to express my dearest thanks to my family, particularly my parents, for their constant support and encouragement. Thank you for believing.

DECLARATION

The work described in this thesis is entirely original and my own, except where otherwise indicated.

Parts of this work were presented at conferences, namely:

20th Annual Meeting of the Polymer Degradation Discussion Group,

at Glasgow University, 13th to 15th September 1995.

21st Annual Meeting of the Polymer Degradation Discussion Group,

at the University of Warwick, 11th to 13th September 1996

and selected for oral and poster presentations for the Spring National ACS meeting,

New Orleans, March 24th to 29th.

Parts of the work contained in this thesis have been published or have been accepted for publication in the scientific literature:

Mahon, A., Kemp, T.J., Buzy, A., Jennings, K.R., *Polymer* **27,** (1996) 531.

(a short communication on the characterisation of polysulfides by electrospray ionisation mass spectrometry combined with collision induced decomposition).

Mahon, A., Kemp, T.J., Buzy, A., Jennings, K.R., *Polymer.* In the press.

(a full paper on the continued work of the characterisation of polysulfide-based polymers by electrospray ionisation mass spectrometry combined with collision induced decomposition).

LIST OF ABBREVIATIONS

amu	atomic mass unit
ATR	attenuated total reflectance
CID	collision-induced dissociation
CRM	charge residue model
cv	cone voltage
Da	Daltons
DMF	dimethyl formamide
DMSO	dimethyl sulphoxide
ESI	electrospray ionisation
EDAX	energy dispersive X-ray analysis
FAB	fast atom bombardment
FD	field desorption
FT	fourier transform
FTIR	fourier transform infrared
GC	gas chromatography
GPC	gel permeation chromatography
HALS	hindered amine light stabiliser
HDDA	hexane-1,6-diol diacrylate
HV	high voltage
IEM	ion evaporation model
IR	infrared
LP	linear polysulfide
MALDI	matrix assisted laser desorption ionisation

MS	mass spectrometry
NMR	nuclear magnetic resonance
PEO	poly(ethylene oxide)
phr	parts per hundred rubber
PPO	poly(propylene oxide)
QhQ	quadrupole-hexapole-quadrupole
RMM	relative molecular mass
RMMD	relative molecular mass distribution
SIDT	single ion droplet theory
SIMS	secondary ion mass spectrometry
TBHP	tertiary butyl hydroperoxide
THF	tetrahydrofuran
TLC	thin layer chromatography
TMTD	tetra-methylthiuram disulfide
TOF	time of flight
UV	ultra violet
XPS	X-ray photoelectron spectrometry

ABSTRACT

Linear polysulfides (LPs) are widely used in high performance sealants. The typical structure of the polymer is:

$$H(SC_2H_4OCH_2OC_2H_4S)_nH.$$

We have completely characterised the complex components that make up commercially used LPs, by means of electrospray ionisation mass spectrometry (ESI-MS), combined with collision induced dissociation (CID). ESI has proved to be an invaluable mass spectroscopic technique in the characterisation of linear polysulfides. The individual spectra are well–resolved, enabling conclusions to be reached about the presence of variant mers (usually associated with additional oxymethylene or oxyethylene units or a monosulfide linkage, or some combination of these), and about the identity of end–groups and nature of the repeat unit. We have also been able to use ESI-MS to study the degradation reactions of LP pre-polymers.

We have obtained spectra of LPs using matrix assisted laser desorption ionisation time-of-flight mass spectrometry, (MALDI-TOF-MS), but these are not as informative as spectra obtained by ESI-MS. Field desorption mass spectrometry (FD-MS) has also been successful in characterising LP samples, but this technique is less generally accessible and much more time-consuming than either ESI-MS or MALDI-TOF-MS.

LPs degrade thermally and photochemically by two competing degradation pathways:

i) a free radical autoxidation mechanism, and
ii) a hydrolysis mechanism.

UV photolysis or pyrolysis of LP pre-polymers in the presence of air or oxygen resulted in the development of carbonyl groups detectable by IR and ^{13}C NMR spectroscopy, while 2-D NMR studies and the highly characteristic field positions of the NMR resonances show the carbonyl group to be due to a formate ester. All thin film samples of cured LP, irrespective of the LP structure and curing agent, including ZL-2264 (with an extra CH_2 linkage in the repeat unit), also produce this carbonyl absorption at 1725 cm^{-1} when exposed to UV irradiation. The formate ester arises as a result of a conventional free radical mechanism of autoxidation; attack at the C-H bond adjacent to the ether oxygen atom leads to a hydroperoxide and hence an alkoxyl radical, followed by scission to give the formate ester. The study of liquid exudates formed when TBHP- and HDDA- cured LP cast blocks are exposed to prolonged periods of heat or UV irradiation also show the development of carbonyl bands at 1724 cm^{-1} in their IR spectra, again indicating that degradation is occurring at least in part via a free radical mechanism.

ESI-MS studies of degraded pre-polymer samples and liquid exudates show that, in parallel with the degradation route involving oxygenation of a methylene group, there is a hydrolysis mechanism involving initial cleavage of the formal group to release formaldehyde, followed by secondary reactions to give other products detected in the ESI-MS spectrum of the photolysate/pyrolysate. This mechanism is supported by the extremely slow degradation of ZL-2264, which has no formal group. The hydrolysis mechanism is the principal route for the degradation of LP pre-polymers and TBHP- and HDDA- cured LP block samples, while LPs cured using MnO_2 and $NaBO_3$ degrade almost exclusively via the free radical autoxidation pathway.

CHAPTER 1

INTRODUCTION

1.1 POLYSULFIDES

1.1.1 HISTORY AND DEVELOPMENT

The history of aliphatic polysulfides began in 1839 when Lowig and Weidmann reacted an aliphatic-alkylene derivative and an inorganic polysulfide[1]. Subsequently, they reacted 1,2-dichloroethane (chloratherin) with potassium trisulfide (K_2S_3) and produced a rubber-elastic substance[2]. At the time, the actual importance of their discovery was not recognised: by synthesising this aliphatic polysulfide they had actually produced the world's first synthetic rubber.

The next significant development came 85 years later in 1924 when C.J. Patrick attempted to develop an inexpensive anti-freeze compound. He attempted to convert 1,2-dichloroethane into ethylene diglycol using substances which reacted hydrolytically; e.g. sodium tetrasulfide (Na_2S_4)[3]. However, instead of the desired product he always finished up with a synthetic rubbery material. Patrick realised the commercial potential of this polysulfide latex because of its exceptional resistance to solvents such as benzene, gasoline and mineral oil. It also possessed excellent characteristics. An extensive research programme followed and in 1927 a patent on the manufacture of polysulfide elastomers was issued[4], the first of many.

Polysulfide production is based on the mechanistically simple procedure of nucleophilic displacement of the chlorine substituent by the polysulfide anion[5]. The equation below for the manufacture of "Thiokol Type A" is typical:

$$Cl\text{-}CH_2\text{-}CH_2\text{-}Cl + nNa_2S_4 \longrightarrow (CH_2\text{-}CH_2\text{-}S\text{-}S\text{-}S\text{-}S)_n + 2nNaCl$$

1,2-dichloroethane + sodium tetrasulfide ⟶ polyethylene tetrasulfide + sodium chloride

Global interest soon increased owing to the inexpensive and readily accessible raw materials such as sulfur, caustic soda, ethylene and chlorine used in the manufacturing process of polysulfide rubbers. However, these early polysulfide rubbers were far from ideal: they were difficult to process, had poor physical properties, possessed foul odours even after curing and gave off irritating fumes during manufacture[6]. To alleviate these problems, from around 1940 onwards the monomer bis(2-chloroethyl)formal ($Cl\text{-}CH_2CH_2OCH_2OCH_2CH_2\text{-}Cl$) was used instead of 1,2-dichloroethane[7].

A few years later, Patrick and Ferguson invented a process whereby the polymeric polysulfide chains were cleaved to a predetermined stage producing curable thiol (-SH) chain termination[8]. Curing of these polymeric liquid materials by a simple oxidation process, i.e oxidation of the thiol end groups to form disulfide linkages, resulted in the formation of a fully-chain extended, high molecular weight, crosslinked polymer. This resulted in an entirely new manufacturing concept; no longer was troublesome mixing equipment required and these liquid polymers could be moulded, absorbed in materials and cast as thin films[6], all because of the chemical reactivity of the thiol end groups.

Today, the thiol-terminated linear polysulfide (LP), represents the major proportion of all polysulfides produced. The modern manufacturing process[3,6] involves mixing bis(2-chloroethyl)formal and sodium polysulfide (doped with sodium sulfonate and magnesium hydroxide), with 1,2,3-trichloropropane being added as a crosslinking agent. This mixture is reacted for three hours at 100°C. The depleted polysulfide is then removed with warm water after which Patrick and Ferguson's

splitting process is performed. Addition of Na_2SO_3 chemically reduces the polysulfide linkages to disulfide groups and the addition of NaSH splits the disulfide linkages forming -SH and -SSH end groups. This cleavage occurs at both the internal and terminal groups. The final molecular weight is determined by the amount of sodium hydrosulfide and sodium sulfite added and normally ranges from 500 to 8000. The sulfite is understood to remove the labile sulfur in any thiomercaptide (RSSH) terminal groups formed on reduction by sodium hydrosulfide and remove any sulfur linkages of ranks higher than two.

$$\sim RSSSR\sim + Na_2SO_3 \longrightarrow \sim RSSR\sim + Na_2S_2O_3$$

$$\sim RSSR\sim + NaSH \longrightarrow \sim RSH + NaSSR$$

$$\sim RSSNa + Na_2SO_3 \longrightarrow \sim RSNa + Na_2S_2O_3$$

Any small impurities formed during this manufacturing process could effect the degradation of these compounds. Clarified polysulfides, e.g. LP-32C, LP-2C etc., have recently become available: filtration leads to a lightened polymer with reduced alkalinity and this results in a more uniform, higher quality product.

The general LP structure is as follows:

$$H(SC_2H_4OCH_2OC_2H_4S)_nH \qquad (n = 7 \text{ to } 42)$$

1.1.2. THE MATERIALS AND THEIR APPLICATIONS

Curing LPs to high molecular weight elastomers is normally accomplished by oxidising the thiol end groups to disulfide bonds[3,6].

$$2\text{-}RSH + O \longrightarrow R\text{-}S\text{-}S\text{-}R + H_2O$$

The curing agents most commonly used are oxygen donating materials[3,6] such as manganese dioxide, lead dioxide, calcium dioxide and sodium perborate, with lead

dioxide and manganese dioxide being the most efficient inorganic curatives for LP polymerisation. There have been few mechanistic studies applied to the curing of polysulfides, however, there is strong experimental evidence from spin trapping experiments[9] to suggest that the curing reaction occurs via the thiyl radical, its subsequent dimerisation leading to the disulfide.

$$RSH \xrightarrow{MnO_2} RS\bullet$$

$$RS\bullet \longrightarrow RSSR$$

There are frequent references in the literature that temperature and humidity affect the rate of cure. It has been shown that increasing the trace levels of water in LPs leads to an acceleration in cure using a lead dioxide curing system[10]. The cure rate of a formulation involving an LP and lead dioxide increased significantly at higher temperatures[11].

Organic oxidants such as benzoyl peroxide and tertiary-butyl hydroperoxide can also be used to polymerise LPs but are a less popular choice because they are more expensive and, unless reactions are carefully controlled, can result in unwanted side reactions.

Cured polysulfides are now used in applications far beyond those based on solvent and fuel resistance[6], for instance they have been employed as binders in solid fuel rockets. LPs are utilised as sealants in various industries[3,6,12-14] such as construction, automotive, marine, aircraft and insulating glass. Since their development in the 1940's they have had a long history of commercial use because they show good ageing properties and excellent weatherability. Typically the LPs are cured and compounded with fillers, plasticisers, dilutents, adhesion promoters,

pigments and thixotropic agents. The actual formulation of the sealant depends on its final application.

Many LP-based sealants are involved in outdoor applications and consequently the durability and service lifetime of these materials are important. Sunlight, temperature, humidity and ozone are all constituents of the environment which are known to influence polymer degradation. Degradation mechanisms for LP polymers therefore need to be identified in order to understand and improve their service lifetime.

1.1.3 DEGRADATION OF LINEAR POLYSULFIDES

The first extensive investigation into the degradation of LPs was due to Rosenthal and Berenbaum of the Thiokol Chemical Corporation, New Jersey. Their in-house report[15] emphasises the hydrolysis of the formal link as the initiating step in the thermal degradation, with the secondary reduction of disulfide links in the polymer backbone by the formaldehyde liberated in the first step. They also refer to an oxidation step, of the formal bond, to produce formic acid which then catalyses the hydrolysis step. In support of this conjecture, CaO acts as a stabilising agent against degradation. Another key feature of the overall degradation process is the conversion of the SH bands (2560 cm^{-1}) into OH (3500 cm^{-1}) as degradation proceeds. Heating an LP in a sealed tube for a week led to a gas (mostly CO and CO_2), a liquid (H_2O + HCO_2H) and a solid consisting of dithiane, poly(ethylene monosulfide) and another polymeric substance with elemental analysis indicating a structure containing a formate ester group:

$$HOCH_2CH_2(SCH_2CH_2)_nSCH_2CH_2OCOH$$

This had IR frequencies of 1725 cm^{-1} and 3500 cm^{-1}. It underwent pyrolysis to form dithiane. The latter observation, together with experiments using model compounds, pointed to a marked tendency for disulfide links to be converted, under these high temperature conditions, to monosulfide, the reductants being formaldehyde and formic acid. Hydroxylated thiols are known to undergo polymerisation reactions of the type:

$$HOCH_2CH_2SH \xrightarrow{H+} HOCH_2CH_2(SCH_2CH_2)_xOH \xrightarrow{\Delta} (CH_2CH_2S)_2$$

The role of oxygen is important in the degradation of cured LP polymers: degradation occurs initially at the exposed surface of the bulk polymer and then proceeds inwards. Both blanketing the polymer with N_2 and incorporating antioxidants exercise a stabilising influence. The existence of an induction period before the onset of serious hydrolytic degradation was attributed by these authors to the clear build up of formic acid via an autoxidation route; a scheme is illustrated overleaf.

More recent studies[16-22] involving the effects of heat, water and the environment on the curing, storage and service lifetime of polysulfide-based aircraft sealants, have been extensively researched by a group in Australia led by Brenton Paul working for DSTO Materials Research Laboratory. This work summarises mainly means to improve the service lifetime and performance properties of these sealants, such as storage at sub-zero temperatures, rather than mechanistic details of how these sealants actually degrade.

Scheme for LP autoxidation

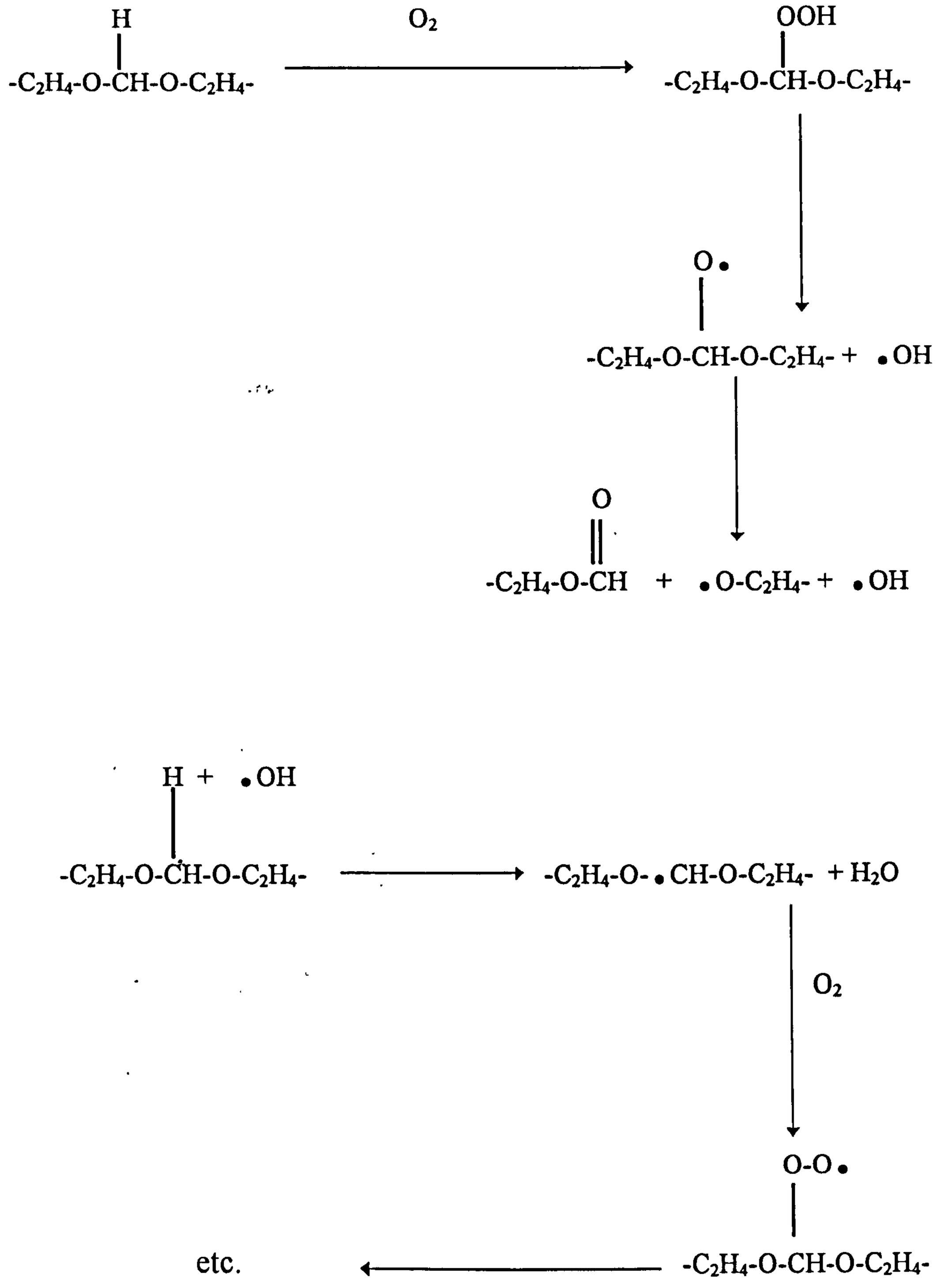

Brenton Paul, Hanhela and Huang accept the importance of the hydrolysis mechanism in the degradation of LPs but draw attention to a parallel radical pathway for pyrolysis and the existence of backbiting mechanisms[16].

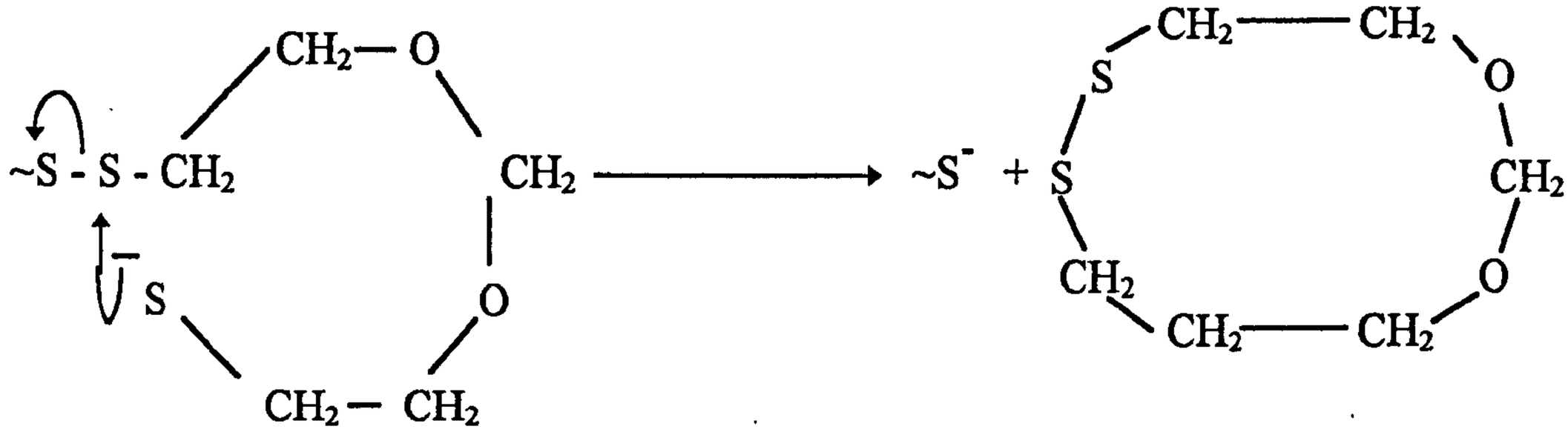

These authors noted the important role of the curative itself on the rate of thermal degradation. MnO_2 for example, is basic in character, which tends to suppress the acidolysis of the formal group but does not inhibit autoxidation. One of the findings of this thesis is that MnO_2-cured LP pre-polymers degrade solely by autoxidation and there is no trace of a hydrolysis mechanism, whereas t-butyl hydroperoxide-cured LPs are extremely vulnerable to thermally induced and photo-induced hydrolysis.

In their 1995 review, Kishore and Ganesh[23] concentrate largely on the hydrolysis mechanism and subsequent steps, e.g.

$$-CH_2CH_2SSCH_2CH_2- + CH_2O \longrightarrow 2\ -CH_2CH_2SH + HCO_2H$$

$$-CH_2CH_2SH + HOCH_2CH_2S- \longrightarrow -CH_2CH_2SCH_2CH_2S- + H_2O$$

1.1.4 CHARACTERISATION OF LPs

Again there are surprisingly few documented accounts of the characterisation of LP polymers. Despite being developed in the 1940's and having a long commercial history, the detailed composition of these polymers was not established until 1991, when Mazurek and Moritz published their ^{13}C NMR assignments of LP pre-polymers[24]. Their analysis revealed the presence of a number of minor components incorporated in the polymers, the most important being the monosulfide and diformal ether analogues of the expected monomer unit. An earlier publication[25] in 1985 did report a preliminary ^{13}C NMR analysis of LPs but contains a number of incorrect assignments.

Other documented analysis of polysulfides includes the determination of the thiol end groups by titration[26] and the monitoring of the SH band at 2560 cm^{-1} in the IR spectrum[27]. This allows molecular weights to be calculated for the polymers and allows chemical cure levels to be estimated. It can also be used as a means of monitoring ageing because polysulfides can undergo a self-curing reaction with time leading to a reduction of the thiol groups. Other attempts to determine the molecular weight distribution, weight average and number average molecular weight have been carried out by Morton Thiokol using gel permeation chromatography[28].

A recent publication by R.J. Coates et al [9] included the assignment of a ^{1}H NMR spectrum for an LP.

At the time the research on which this thesis is based was begun, the results detailed by Mazurek and Moritz[24] offered the most comprehensive and accurate analysis available. Therefore a fully detailed characterisation of LP pre-polymers seemed crucial, bearing in mind that any impurities found within the polymer may

influence its degradation and result in a shorter service lifetime. This thesis includes development of a method of completely characterising the complex components that make up commercially used LPs, by means of electrospray ionisation mass spectrometry (ESI-MS), combined with collision induced dissociation (CID) to confirm the assignments made[29,30]. This is quite possibly the most detailed and comprehensive study of LP characterisation, offering a greater level of detail than the analytical methods associated with previous studies summarised in this section.

1.2 POLYMER DEGRADATION

1.2.1 GENERAL

Most organic polymers undergo degradation or oxidation reactions when exposed to outdoor environments[31-38]; this results in the deterioration of the mechanical properties of the bulk polymer and hence reduces the service lifetime of the material.

When undergoing degradative and oxidative reactions, polymers undergo both chemical and physical changes. The usual physical changes are discolouration, crazing, cracking and loss of tensile strength, all of which are normally associated with chain scission reactions, i.e. cleavage of the polymer backbone, although sometimes crosslinking reactions may occur[37]. Chemical changes normally involve the formation of new functional groups, for example most polymers form a variety of hydroxyl/peroxide and carbonylic products when undergoing oxidative degradation reactions[32,36,37]. When oxygen is readily available, free radicals, formed during cleavage of chemical bonds by exposure to UV or heat, react to form peroxyl radicals, which initiate a series of radical chain reactions[31-36].

initiation	initiator $\rightarrow X\bullet$
	$X\bullet + RH \rightarrow R\bullet + HX$
propagation	$R\bullet + O_2 \rightarrow ROO\bullet$
	$ROO\bullet + RH \rightarrow ROOH + R\bullet$
termination	$ROO\bullet + ROO\bullet \rightarrow$ non-radical products
	$ROO\bullet + R\bullet \rightarrow$ non-radical products
	$R\bullet + R\bullet \rightarrow$ non radical products

Autoxidation accounts for most failures of polymers exposed to outdoor environments by converting small amounts of hydrocarbon groups (RH) into hydroperoxide (ROOH)[32]. The exact nature of the initiation step remains unresolved but possible candidates are:

i) residual impurities from the polymerisation process[32],

ii) C-C cleavage processes occurring under mechanical strain or at defect centres[39], and

iii) attack by singlet oxygen produced by some photochemical process[32].

Once hydroperoxides are present, they can be photolysed to RO• and •OH radicals[31,32] while carbonyl compounds can act as photogenerators of radicals via abstraction processes[32].

$$\text{i.e.} \quad R_1R_2C{=}O \xrightarrow{h\nu} {}^1(R_1R_2C{=}O)^* \longrightarrow {}^3(R_1R_2C{=}O)^*$$

$${}^3(R_1R_2C{=}O) + R_3H \longrightarrow R_1R_2C\bullet\text{-}OH + R_3\bullet$$

With an ever-increasing demand for polymer usage in outdoor applications, research on polymer degradation and stabilisation has become increasingly important in recent years.

1.2.2 GENERAL MECHANISMS OF OXIDATIVE DEGRADATION IN LINEAR POLYMERS.

Hydroperoxides are widely accepted as the vital intermediate stage in the oxidative mechanism for the thermal and photochemical degradation of polyolefins. Over the past thirty years, extensive research has been carried out by various groups[40-55] to investigate the nature and role of these hydroperoxides in order to propose degradative mechanisms, particularly for polyethylene and polypropylene.

Mechanisms for the oxidative degradation of polyolefins have been widely researched, and many general reviews are avaliable[31-35]. Although, schemes 1 and 2 are widely accepted for the oxidation of polyethylene initiated thermally or photochemically, there is still some dispute over the exact initiation mechanisms[56]. Scheme 1 illustrates a mechanism for oxidative chain scission in polyethylene while scheme 2 outlines a decomposition route which may occur in polyethylene if residual double bonds are present as an impurity in the polymer backbone. A mechanism for the autoxidation of polypropylene is illustrated in scheme 3.

Scheme 1:

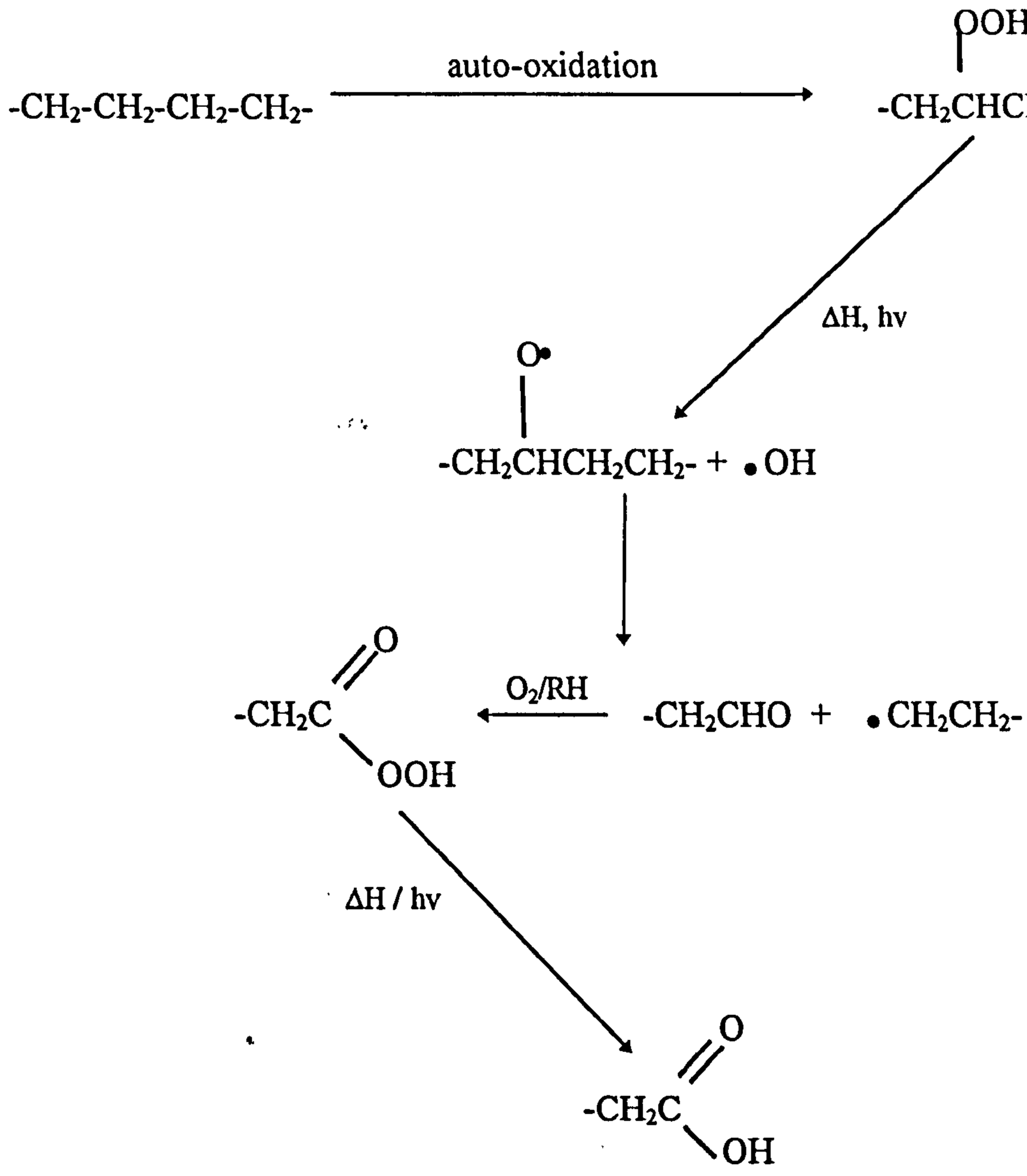
auto-oxidation
-CH2-CH2-CH2-CH2-
OOH
-CH2CHCH2CH2-
ΔH, hv
O•
-CH2CHCH2CH2- + •OH
O
-CH2C
OOH
O2/RH
-CH2CHO + •CH2CH2-
ΔH / hv
O
-CH2C
OH

Scheme 2:

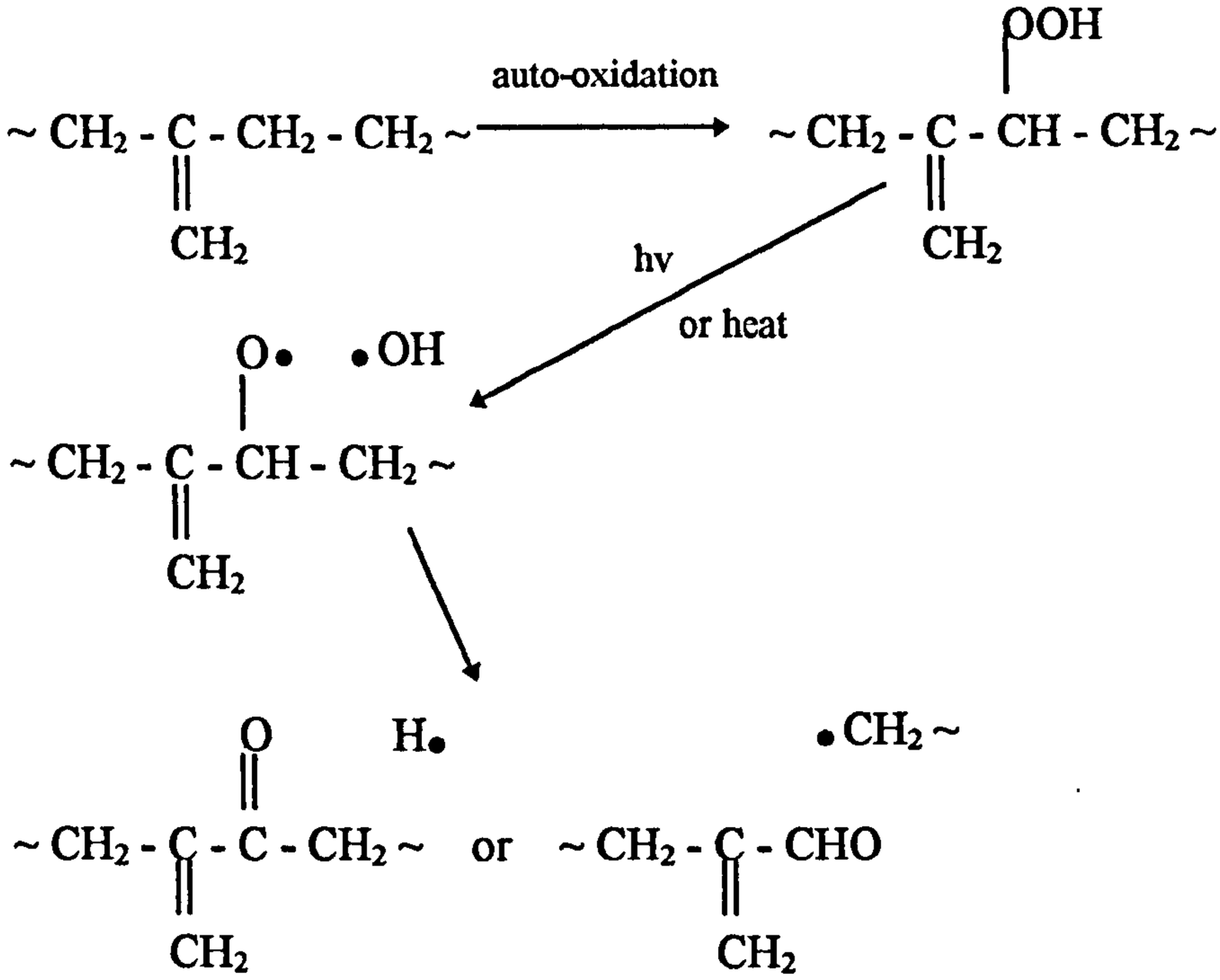

Scheme 3

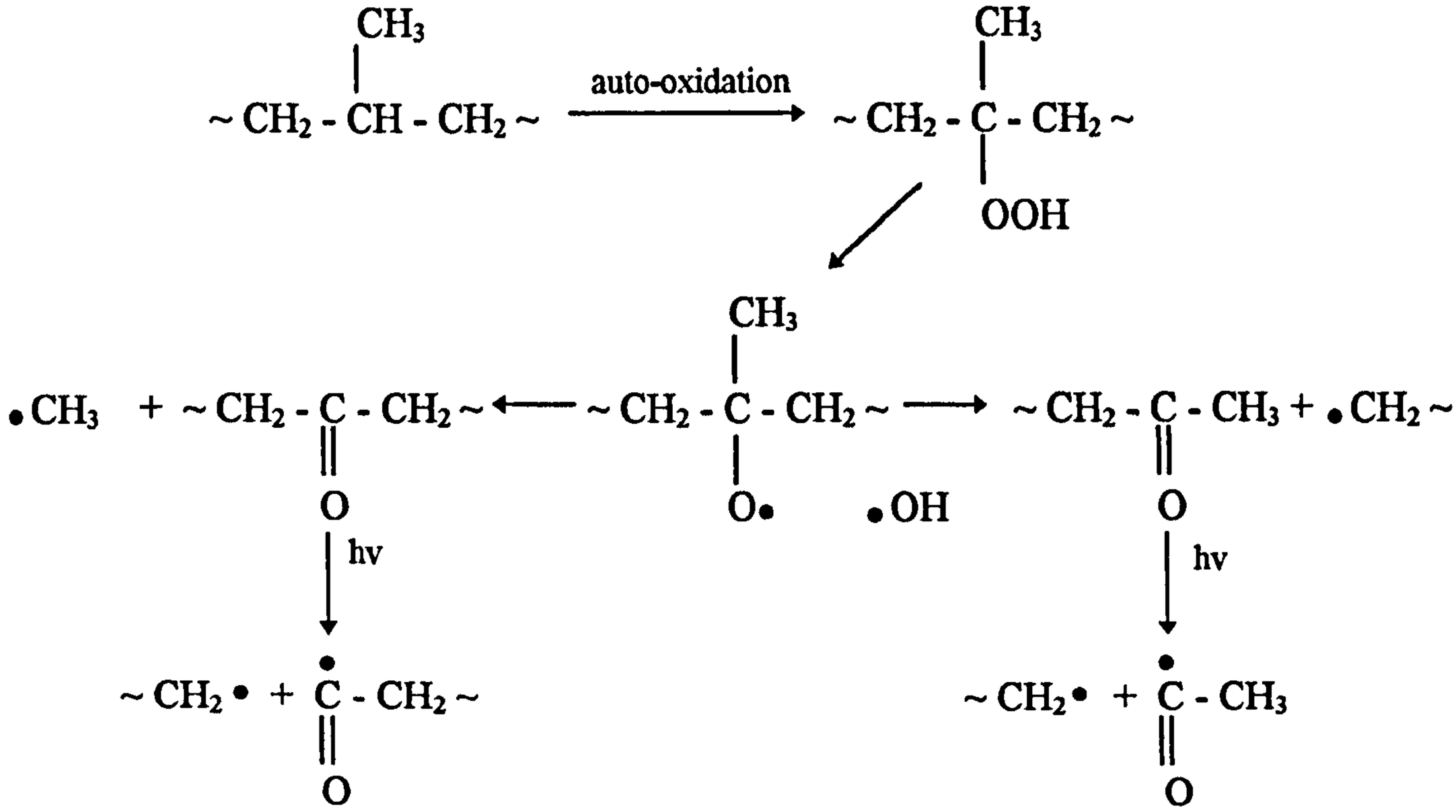

The most important reactions which occur within the degradative oxidation of polyethylene are as follows[56].

i) α-hydroperoxide formation from the vinylidene groups, present in the polymer backbone as impurities.

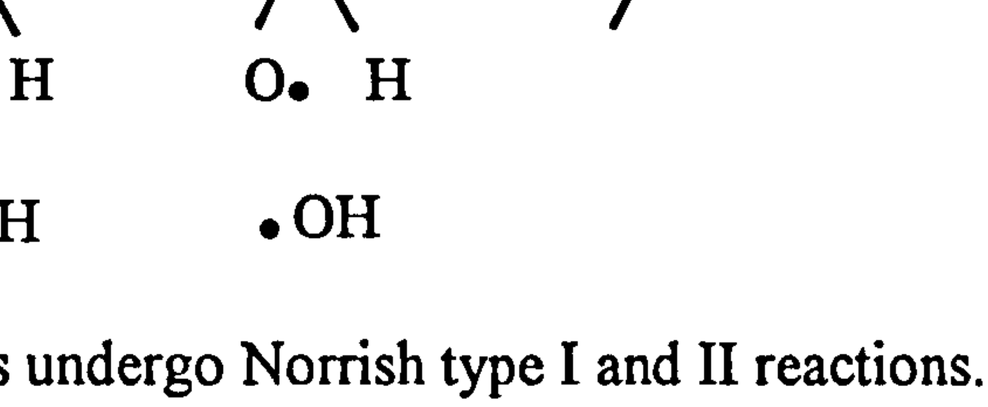

ii) Reactions induced by UV, heat and free radicals produce carbonyl groups and water, by the destabilisation and direct decomposition of these α-hydroperoxides.

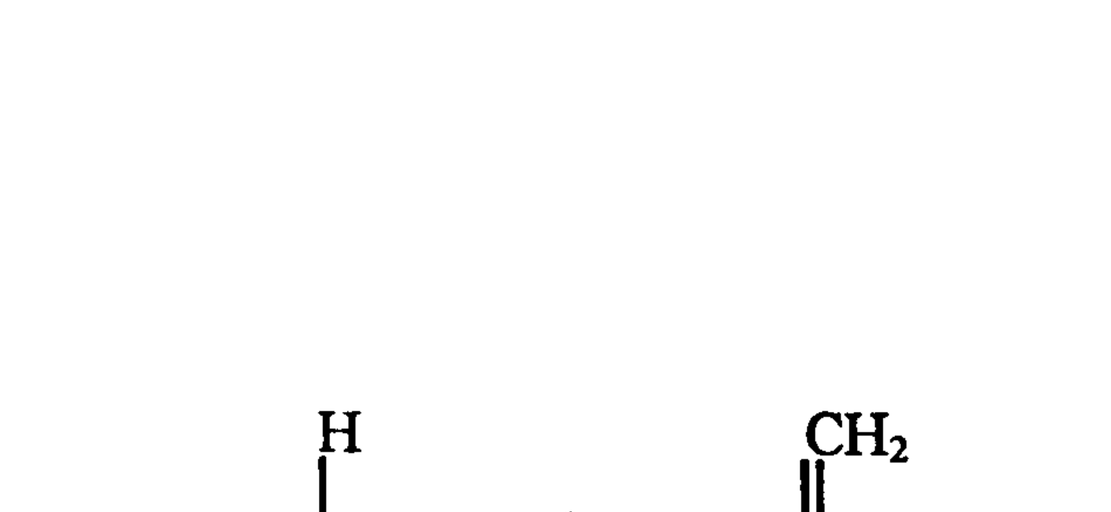

iii) The carbonyl groups undergo Norrish type I and II reactions.

and

iv) The formation of charge transfer complexes results in the generation of free radicals.

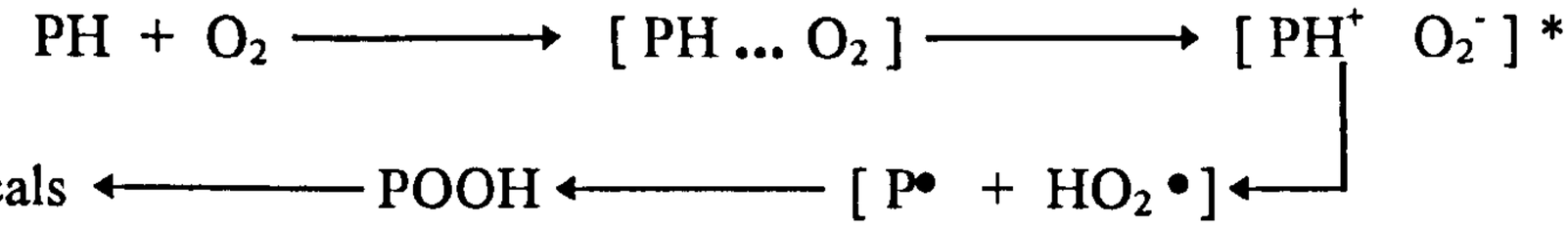

v) Hydroperoxide decomposition and photo-initiation by trace metal ions, usually found in the polymer as an impurity during the manufacturing process, to yield free radicals.

vi) Alkoxyl radical recombinations.

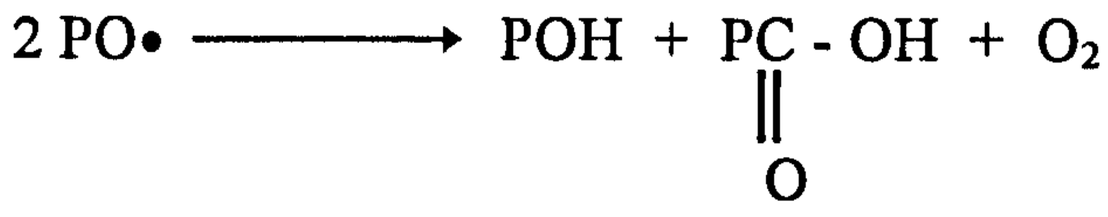

As one would expect, polypropylene undergoes a similar oxidation route to polyethylene (see scheme 3). Most degradation mechanisms for polypropylene are based on the mechanism first published by Bolland and Gee[57,58] in 1946, whereby peroxide formation is vital to the formation of free radicals. In recent years, the photo- and thermal initiated oxidation of polypropylene has been extensively researched by Lacoste et al.[59-61] and Yang et al.[62]; their work has shown the predominant formation of the tertiary hydroperoxide during oxidative degradation.

A surface analysis study involving the photo-oxidation of polypropylene blocks[63, 64] showed high levels of chromophores at the exposed polymer surface; these decrease in quantity with depth and are associated with restriction on oxygen diffusion and the usual competition with alkyl radicals in the inner layers of the polymer. Chromophore formation in the bulk polymer layers progressively increases with longer exposure times due to the development of cracks, which accelerates the

diffusion of oxygen to deeper layers. A relationship between carbonyl group development and loss of tensile properties was discovered.

Publications concerning the degradation pathways of poly(ethylene oxide) (PEO) and poly(propylene oxide) (PPO) have become available in the last decade; although the major degradation products have been completely defined, there still appears to be some dispute about the exact degradation mechanism. Griffiths et al.[65] have studied the thermal degradation of PPO by ^{1}H NMR and gas phase infra-red spectroscopy, and have proposed two mechanisms operating simultaneously based on hydroperoxide formation; they propose that oxidation occurs predominantly at the tertiary carbon atom as follows:

$$HO\text{-}[CH_2\text{-}CH(CH_3)\text{-}O]_x\text{-}CH_2\text{-}C(CH_3)(\mathbf{OOH})\text{-}O\text{-}[CH_2\text{-}CH(CH_3)\text{-}O]_yH$$

$$\downarrow$$

$$HO\text{-}[CH_2\text{-}CH(CH_3)\text{-}O]_x\text{-}CH_2\text{-}C(CH_3)(\mathbf{O}\bullet)\text{-}O\text{-}[CH_2\text{-}CH(CH_3)\text{-}O]_yH$$

$$\mathbf{HO}\bullet + RH \longrightarrow H_2O + \mathbf{R}\bullet$$

where the RH is the polymer molecule and the $\mathbf{R}\bullet$ radical generates further hydroperoxide.

Mechanism 1: C-C bond cleavage adjacent to the alkoxyl radical centre takes place to generate the following products, followed by further peroxidation.

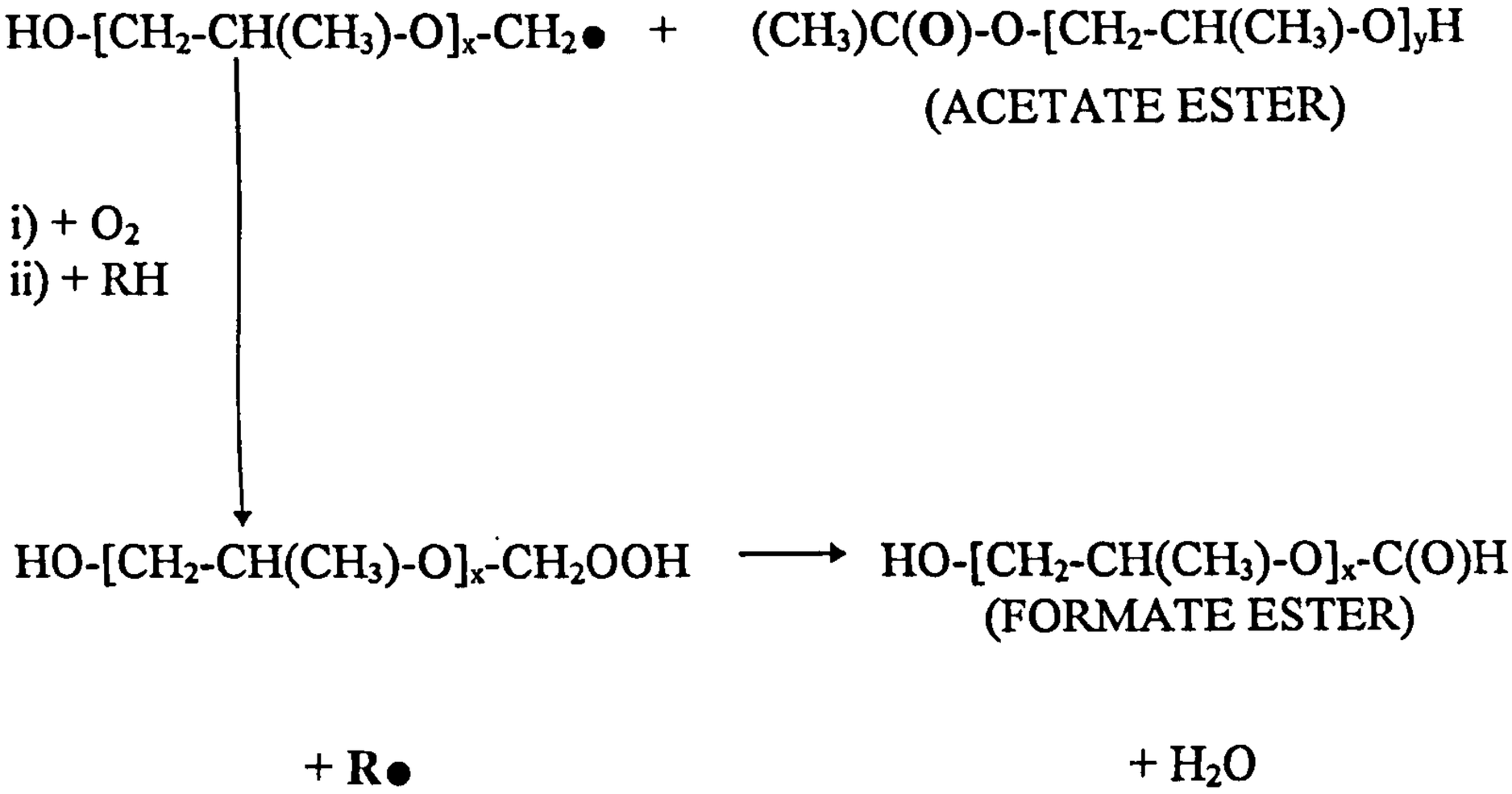

Mechanism 2: C-O bond cleavage adjacent to the alkoxyl radical group occurs to generate the following

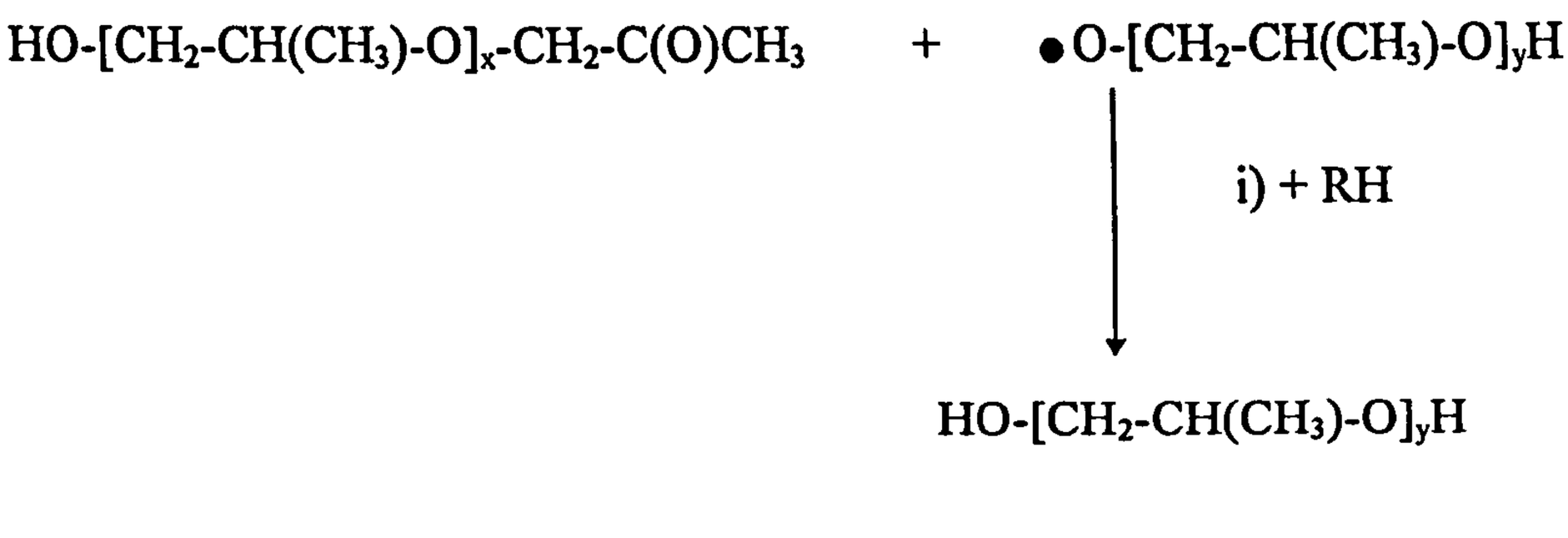

Both of these pathways involve reaction with an oxygen molecule to form a tertiary hydroperoxide followed by decomposition to an alkoxyl radical and an OH

radical, hence resulting in H_2O. These processes when occurring in parallel produce the acetate, formate and ketone end groups, but the acetate and formate are predicted to be present in equal amounts instead of the 2:3 ratio found by NMR analysis. The authors suggest that more formate may be produced from the breakdown of the less probable secondary hydroperoxide.

Lemaire et al.[66] have studied the photodegradation of PPO using solution infra-red spectroscopy, and have proposed a scheme whereby oxidation predominates via the secondary carbon atom; oxidative degradation is proposed to occur by two pathways operating simultaneously. A cage recombination mechanism is also invoked. Although they suggest that the secondary hydroperoxide mechanism is preferred to the tertiary hydroperoxide mechanism (proposed by Griffiths et al.[65]), they offer no detailed mechanism for this oxidation process. Schemes of these pathways are clearly explained in a publication by Barton et al.[67] whereby the thermal degradation of PPO was studied by ESI and MALDI; their results support the role of the secondary alkoxyl radical. Their schemes of oxidation are illustrated as follows:

$$HO\text{-}[CH_2\text{-}CH(CH_3)\text{-}O]_x\text{-}CH(\mathbf{OOH})\text{-}CH(CH_3)\text{-}O\text{-}[CH_2\text{-}CH(CH_3)\text{-}O]_yH$$

$$\downarrow$$

$$HO\text{-}[CH_2\text{-}CH(CH_3)\text{-}O]_x\text{-}CH(\mathbf{O}\bullet)\text{-}CH(CH_3)\text{-}O\text{-}[CH_2\text{-}CH(CH_3)\text{-}O]_yH$$

$$\downarrow \quad \text{CAGE REACTION WITH HO}\bullet$$

$$HO\text{-}[CH_2\text{-}CH(CH_3)\text{-}O]_x\text{-}C(O)\text{-}CH(CH_3)\text{-}O\text{-}[CH_2\text{-}CH(CH_3)\text{-}O]_yH + H_2O$$

The alkoxyl radical either undergoes a cage reaction as illustrated above or undergoes scission reactions as follows:

Mechanism 1: C-C bond cleavage adjacent to the alkoxyl radical centre takes place to generate the following products.

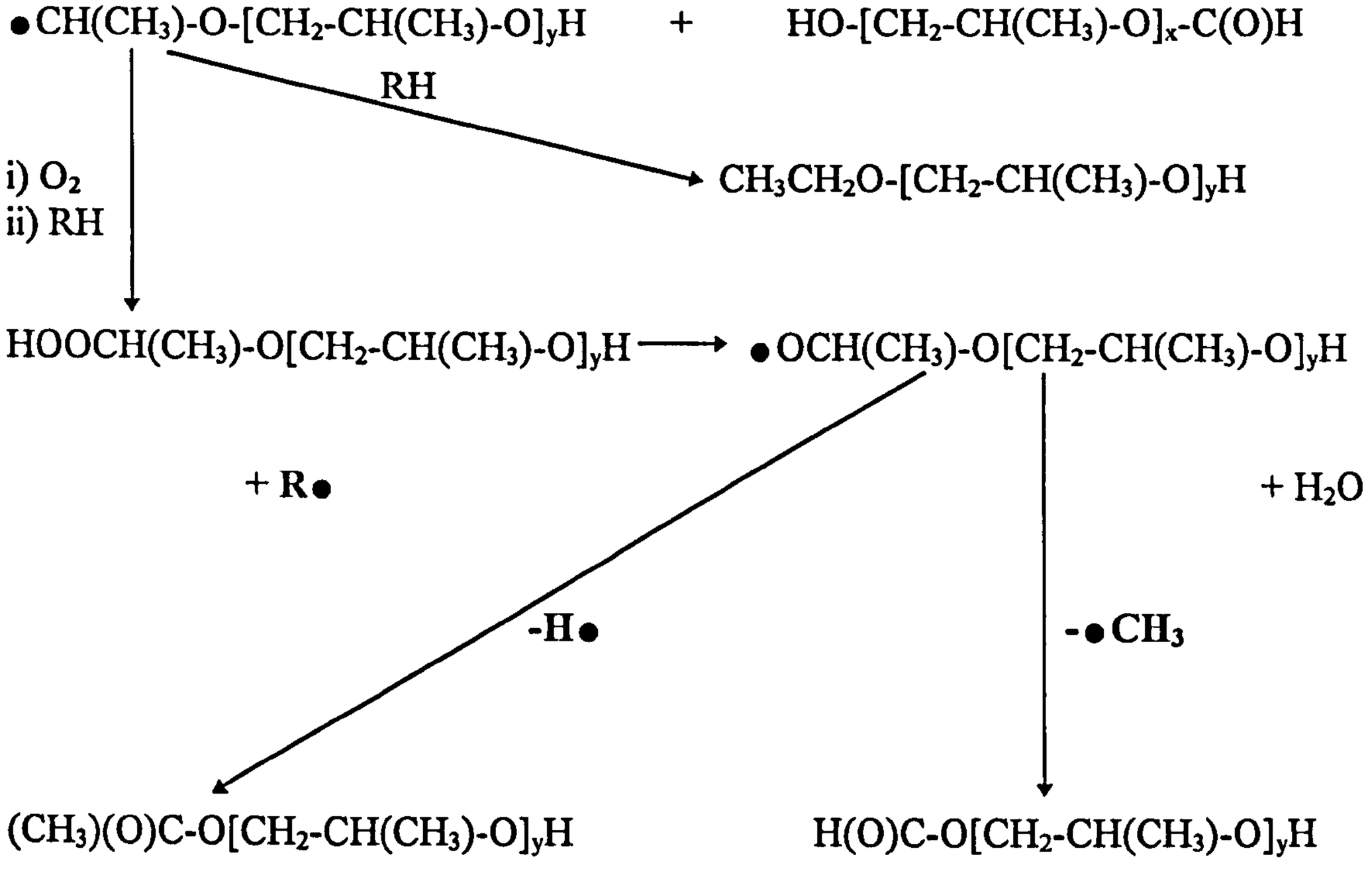

Mechanism 2: C-O bond cleavage adjacent to the alkoxyl group takes place to generate the following products:

H(O)C-CH(CH3)-O-[CH2-CH(CH3)-O]yH

+

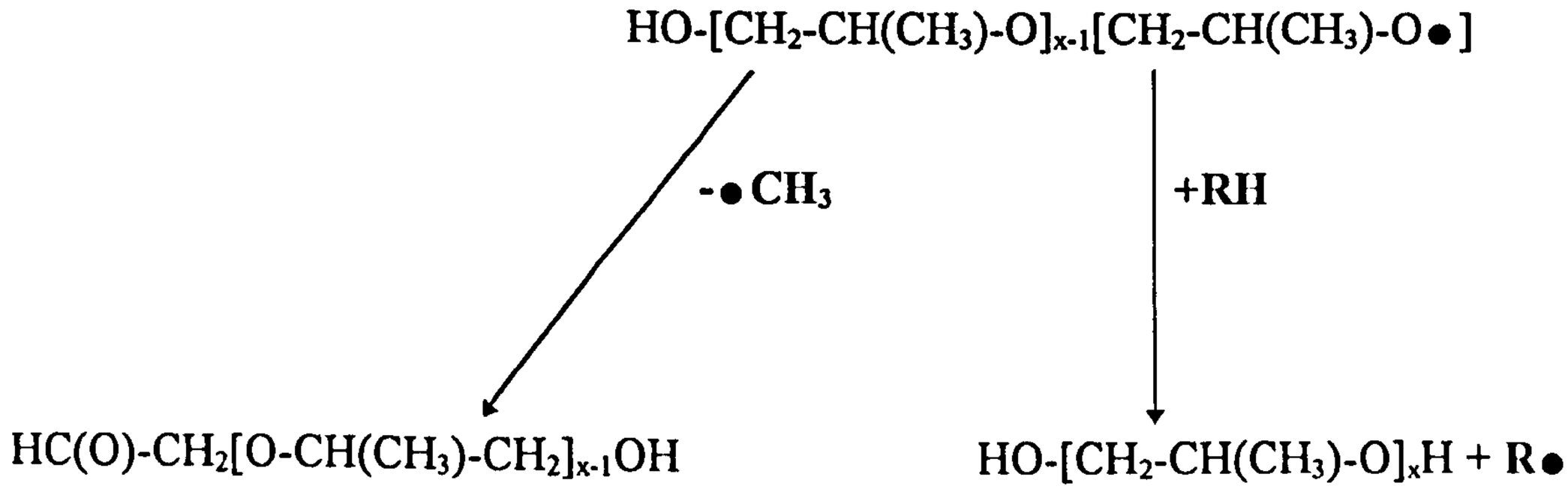

Although there may be dispute over the exact mechanism for the oxidative degradation of PPO, all publications outlined[65-67] agree that a formate ester is formed during pyrolysis[65,67] and photolysis[66].

PEO also undergoes a similar degradation mechanism to poly(propylene)[59-62] and PPO[65-67]; whereby the hydroperoxyl radical formed as a result of UV or heat exposure decomposes by the loss of a hydroxyl radical to produce an alkoxyl radical, which undergoes further reactions like those illustrated previously for PPO. Cameron et al[68,69] have studied the thermal degradation of PEO and its complex with metal salts; they found that the IR spectrum of the degraded material suggested a high concentration of formate was produced, with a lower concentration of ester and no aldehyde. This suggests that beta-2 scission of the alkoxyl radical is preferred to beta-1 scission. They also attempted to characterise the secondary thermal decomposition products of PEO[68]. The degradation products of PEO have also been characterised using pyrolysis mass spectrometry by Fares et al[70], who conclude that thermal degradation occurs via C-O and C-C scission reactions, with products formed as a result of C-O scission being the most abundant.

The photodegradation of PEO has been researched by Rabek et al.[71] and Lemaire et al.[66]; who propose that degradation occurs via the secondary hydroperoxide; the resulting alkoxyl and hydroxyl radicals then react as illustrated for PPO.

1.2.3 STABILISATION AND PROTECTION OF POLYMERS.

As discussed in section 1.2.2, polymers when exposed to heat or UV light are susceptible to the free radical process of autoxidation. In order to prevent the

degradation of polymers and so increase their service lifetimes, many types of stabilisers have been developed in recent years.

The use of carbon black as a stabiliser is widespread[72,73]; the black powder absorbs incident light leading to the protection of the polymer against UV. Carbon black is also believed to act effectively as an antioxidant in polymer systems due to the presence of phenolic and quinonoid groups in its structure acting as radical scavengers[73]. Although the use of carbon black is efficient and economical, its use is limited by its colour.

Gijsman et al.[74] have found that the most effective stabilisers for aliphatic polyamides against thermoxidative degradation is a combination of metal (mainly Cu and Mn) and halogen (mainly Br and I) salts. The stabilisation mechanism is most probably based on the metal ion catalysed decomposition of hydroperoxides by the halogen salt.

Antioxidants are widely used in polymer systems to prevent/reduce the autoxidation process. Hindered phenols and aromatic amines are common chain-breaking donor antioxidants, and their mechanism of stabilisation, which has been documented by Pospisil[75-77], involves the reduction of the alkoxyl and peroxyl radicals. Their reaction with ROO radical leads to the formation of a hydroperoxide molecule and the (relatively stable) antioxidant free radical[78]. Alternatively, chain-breaking acceptor antioxidants oxidise alkyl radicals; hindered amine light stabilisers (HALS) are a common example of this type of UV stabiliser. Extensive studies to establish the efficiency and mechanism of operation of HALS have been carried out in recent years[76-81]. Preventative antioxidants may also be used to stabilise polymers, the

most important of these being destroyers of peroxides such as phosphite esters, which act by removing hydroperoxides in a non-radical process[78].

1.2.4 TECHNIQUES FOR MONITORING POLYMER DEGRADATION.

Classical analytical techniques such as infrared (IR) spectroscopy, nuclear magnetic resonance (NMR) spectroscopy and gel permeation chromatography (GPC) have been applied to study the degradation of polysulfides. These techniques are well documented[82-84] and heavily utilised in polymer analysis.

Chemical changes resulting from polymer degradation have been successfully monitored using IR spectroscopy, especially for polyolefin type polymers[32,33,37], whereby the principal discernible changes are the development of hydroxyl bands in the region of 3000-4000 cm^{-1}, and carbonyl bands in the region of 1500-2000 cm^{-1}. This technique has been applied in this thesis to study polysulfide degradation, especially in cured-LP films (chapter 6).

Degradation products have been identified successfully in polymers such as poly(ethylene oxide)[85], poly(propylene oxide)[65] and polypropylene[61] using NMR spectroscopy. We have been able to use this technique as an aid in establishing the degradation products formed in LP pre-polymers and to analyse the liquid exudate which forms in heavily degraded TBHP-cured polysulfide. GPC has also been successful in monitoring molecular weight changes occurring in polystyrene and polypropylene as a result of photo-oxidation[86]. We have used this technique to study molecular weight changes in degraded pre-polymer samples.

We have also applied certain of the relatively new soft ionisation mass spectrometry techniques, such as electrospray ionisation (ESI), matrix assisted laser desorption ionisation (MALDI) and field desorption (FD) to characterise fully polysulfides and to study their degradation pathways. These ionisation techniques are able to offer analysis of polymer samples without causing significant *in situ* degradation. MALDI and ESI have been used recently to characterise the thermal degradation pathways of PPO[67]. We have successfully applied ESI combined with collision induced decomposition (CID) to characterise undegraded and degraded polysulfides.

We have also made an attempt to characterise UV-induced changes at the polymer surface by using techniques such as X-ray photoelectron spectroscopy (XPS), static secondary ion mass spectrometry (SIMS), attenuated total reflectance infrared spectroscopy (FTIR-ATR) and surface Raman spectroscopy but with only very limited success.

1.3 MASS SPECTROMETRY OF POLYMERS

1.3.1 GENERAL

Mass spectrometry is the commonest technique used to determine the relative molecular masses (RMM) of large organic molecules. Although commercial mass spectrometers have been available for more than 50 years, their real potential has been fully realised only in the last twenty years, when research groups in biosciences were able to obtain molecular weight and structural information of proteins, peptides and other biological polymers by means of using mass spectrometry[87].

In recent years, the analysis of synthetic polymers by mass spectrometry has been carried out with the use of soft ionisation techniques such as FD, MALDI and ESI. Mass spectrometry is a powerful analytical tool for polymer analysis, and modern instruments can directly measure the molecular masses of oligomers and give detailed structural information[87]. The development of tandem mass spectrometers has permitted the application of CID experiments, which may be used to obtain structural information to confirm the assignments of individual oligomers.

1.3.2 ELECTROSPRAY IONISATION

Electrospray ionisation (ESI) is a method whereby ions present in solution are converted into characteristic gas phase ions which the mass spectrometer can analyse. A solution is nebulised under the influence of a high electric field; desolvation of the resultant aerosol is then achieved using a combination of heat, gas flow and vacuum. Employing supersonic beam methods, characteristic gas phase ions are efficiently formed for mass spectrometric analysis[87]. Ions formed by means of using this ionisation method are typically multiply-charged species, i.e. macromolecules with a number of protons/cations attached.

Electrospray ionisation was first applied to macromolecules in 1968 by Dole et al.[88]; in a later study using lysozyme they demonstrated the phenomenon of multiple charging[89]. Publications about ESI coupled to a mass spectrometer were made by two groups in 1984 namely, Fenn et al.[90] and Aleksandrov et al.[91] Fenn et al. have shown that ESI has the ability to produce multiple charging in poly(ethylene glycols), with samples of 17 500 Da bearing up to 23 charges per ion[92].

Many schemes are available to describe the desolvation of the charged droplets in ESI[88,92-98], but the actual mechanism still remains unresolved. The most widely accepted mechanisms are the charge residue model (CRM) sometimes referred to as the single ion droplet theory (SIDT), and the atmospheric pressure ion evaporation model (IEM).

The CRM theory was initially suggested by Dole et al.[88] and later promoted by Rollgen and co-workers[95]. Rollgen suggested that gas phase ions arise from the desolvation of very small droplets at the Rayleigh limit. Droplets formed contain only one analyte ion, and solvent evaporation from the droplet arising from instabilities at the surface results in the formation of gas phase ions. This generates, according to Dole[88], singly-charged molecular ions.

The IEM theory was originally proposed by Thomson and Iribane[96-98] and further developed by Fenn et al.[92-94] Thomson and Iribane proposed the formation of droplets containing many solute ions; as a consequence of the desolvation process the diameter of these droplets decreases, leading to an increase in surface charge density and coulombic repulsive forces. This continues until the repulsive forces overcome the surface tension, i.e. the Rayleigh stability limit is exceeded, and the droplet ruptures to form smaller fragment droplets, and evaporation then continues for this next generation of smaller droplets.

Research by Fenn et al. has further developed the IEM model and attempts to explain how large molecules such as proteins and poly(ethyl glycol)[92] could carry many positive charges from the attachment of metal cations or protons. Multiple charging is thought to occur by shrinkage of the highly charged droplet; as the solvent evaporates the droplet diameter decreases, while the number of charges remains

constant within the liquid volume. The "decreasing size and rupture" process continues until smaller droplets are produced. Studies suggest that at sufficiently high charge densities, multiply charged ions may desorb under the influence of the external electric field[94,96]. The point of ion desorption depends on the size of the molecule and the number of charges attached[94].

A schematic diagram of the electrospray source of the "Quattro II" (Micromass UK Ltd.) tandem quadrupole mass spectrometer is illustrated in fig.1.1. In ESI experiments the source is approximately at ambient temperature and atmospheric pressure.

The sample is injected into the mobile phase which is pumped (rate ≈ 1-20 μ L min^{-1}) through the capillary. An electric potential of 2-5 kV exists between the fine steel spraying capillary and the counter electrode, otherwise known as the high voltage (HV) lens. As a result, the solution emerging from the capillary forms a fine spray of charged droplets containing both analyte ions and solvent. Desolvation is initiated by the use of a nitrogen bath gas which sweeps away any solvent vapour.

These partially desolvated ions then migrate towards the sample cone through the HV lens, which is heated to aid further desolvation and serves to remove involatile material which may cause blockages to the cone; it also focuses the ions through the cone orifice (0.2 mm i.d.) into the first vacuum stage (≈ 1 x 10^{-1} mbar). The sample cone is held at a voltage of 0-200 V but for most experiments, it is set at 30-60 V. As the voltage is increased, the most probable number of charges on a sample molecule falls[99], presumably due to the stripping of protons or other cations.

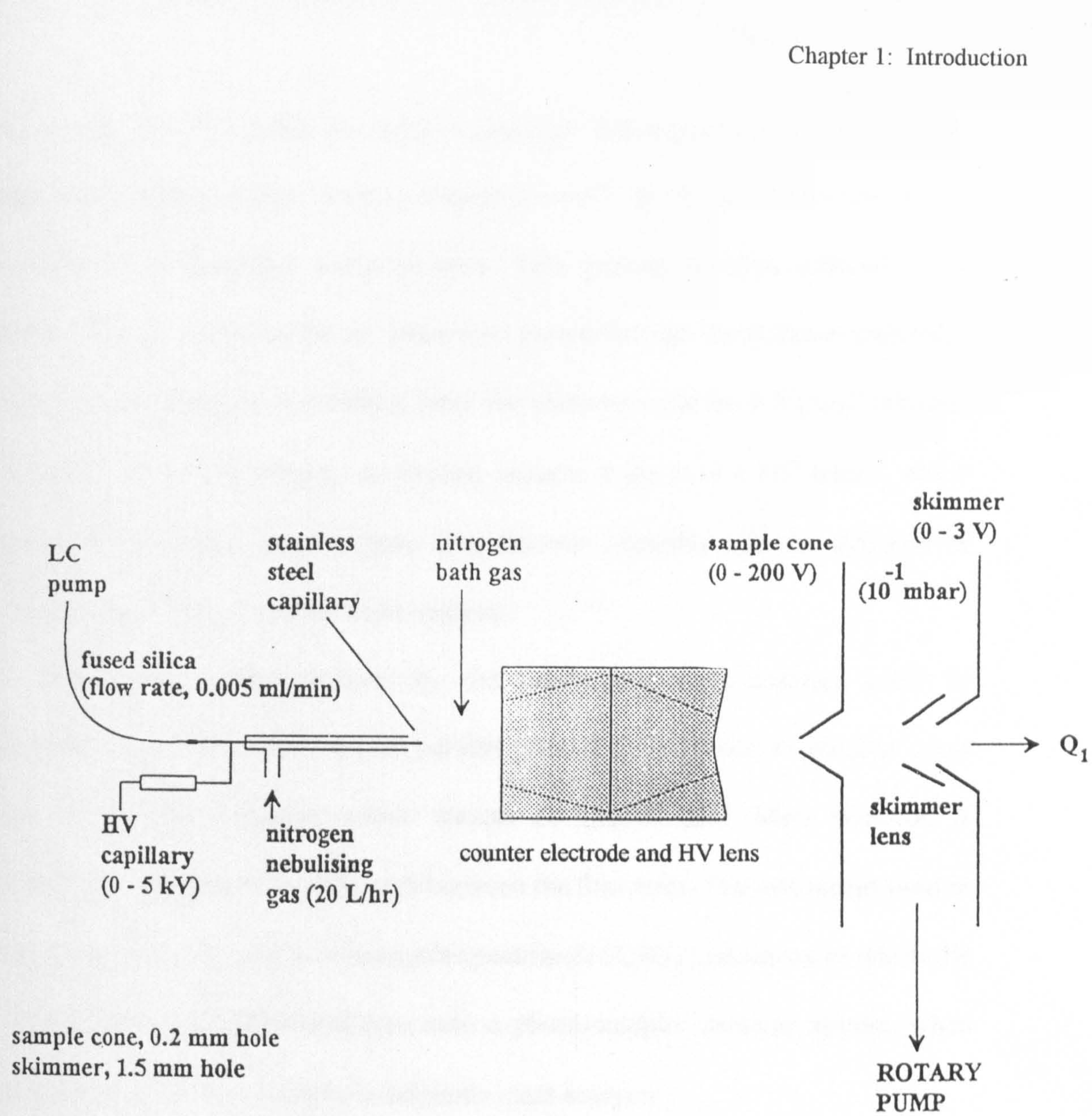

Fig. 1.1: A schematic diagram of the interface of an electrospray source to a triple quadrupole mass spectrometer.

Above about 125 V, significant collision-induced decomposition of the various multiply-charged ions occurs, yielding fragment ions[100] of the type observed in the CID spectra[101] of individual precursor ions. This process is often referred to as 'skimmer CID'. A portion of the ion beam then passes through the skimmer assembly, consisting of the skimmer lens (offset from the skimmer cone by 5 V) and skimmer cone (0-3 V), to be delivered to the second vacuum stage ($\approx 4 \times 10^{-4}$ mbar), which contains the quadrupole mass analyser. The skimmer assembly aids the diffusion of solvent molecules away from the mass analyser.

The ions are then analysed by the quadrupole mass analyser which is constructed from four equally spaced parallel rods of a hyperbolic or circular cross section; a potential is applied which creates an electric field. Mass selection is achieved if the ions follow a stable path between the four rods. The instrument used in our experiments is a quadrupole-hexapole-quadrupole (QhQ) instrument in which the first quadrupole passes deflected ions onto a photomultipler detector system, when the instrument is used as a simple quadrupole mass analyser.

During CID experiments, ions selected by the first quadrupole are deflected into a hexapole collision cell, containing argon as the collision gas, while a second quadrupole is used to select the fragment ions arising during CID. Additional information may be obtained from a precursor ion scan in which all precursors of a chosen product ion are identified by scanning the first quadrupole mass analyser while holding the second quadrupole mass analyser constant to transmit the ion of chosen *m/z*.

The upper mass limit of the quadrupole depends on the length of the rods and rod geometry. Typically, commercial instruments such as the "Quattro II" (used in

our experiments) offer a mass range of 1 to 4000 Daltons for singly-charged ions. Since ions formed by electrospray ionisation are usually multiply-charged species, the *m/z* ratio for macromolecules is a fraction of the actual molecular weight. ESI-MS has successfully analysed poly(ethylene glycol) samples of masses up to 5 000 000[93]. The number of charges formed normally depends on experimental and solution conditions such as pH[87].

Although ESI is an extremely popular technique for analysing biological molecules, its application to polymer characterisation is still in its infancy. This is probably due to the difficulty in finding a suitable solvent system in which the polymer and salt are completely soluble. Corless and co-workers[102] have analysed low molecular weight polystyrene samples by electrospray. They could not however obtain structural information for samples of molecular masses higher than the mass limit of the instrument. This could be due to a lack of multiple-charging of PS oligomers or a problem with higher mass oligomers being less soluble in the solvent system used.

An alternative approach to analysing large synthetic polymers is to couple a GPC column to an electrospray ionisation mass spectrometer. Each oligomeric fraction that elutes from the GPC column is then measured directly by the mass spectrometer without interference from multiply-charged species of adjacent oligomers. This approach has been successfully adopted by Prokai and Simonsick[103,104].

Since ESI is a soft ionisation technique, structural information is usually obtained by collision-induced decomposition (CID)[105]; surprisingly there are few

reported studies using ESI/CID for characterising polymeric materials; however polyglycols[106] have been characterised by this method.

1.3.3 MATRIX ASSISTED LASER DESORPTION IONISATION

Matrix assisted laser desorption ionisation (MALDI) is a recently developed soft-ionisation technique, which has been extremely successful in the analysis of large biological molecules and more recently, in the characterisation of synthetic polymers[107] .

Up until the late 1980's, laser desorption mass spectrometry was a popular technique used to analyse polymers. This ionisation technique involves a pulsed UV laser which is focused on to a solid sample; the energy from the laser is transferred to the analyte molecules, leading to ionisation and vaporisation[107]. The pulsed nature of the laser is an important feature since it allows a simple time-of-flight (TOF) spectrometer to be used, which is able to generate a complete mass spectrum for each ionisation event, with unlimited mass ranges[108]. Generally though, direct UV-laser desorption is only viable for polymer molecules with a mass range below 2 000 Da, owing to the intense laser energy and the fragility of the polymer chains[109].

MALDI as introduced by Karas and Hillenkamp[110,111] is a development of the laser desorption technique, with the major difference being the mode of sample preparation. In MALDI the sample is not irradiated directly but is deposited in a solution containing a large excess of matrix molecules which absorb at the same wavelength as the laser. After solvent evaporation, a residue remains which consists of well-separated analyte molecules homogeneously dispersed in a 'sea' of matrix molecules[107]. The energy of the laser is transferred to the matrix and a small fraction

of the matrix vaporises, carrying with it intact analyte molecules into the gas phase. Although this part of the process is completely understood, the mechanism of transfer of charge to the polymer chains is not resolved. Karas[112] proposes a 'photochemical ionisation' model to explain this phenomenon, whereby protonated matrix molecules generated by the laser irradiation act as proton donors to form analyte ions by gas-phase reactions. While this is conceivable for biological polymers soluble in aqueous media, it is an unlikely explanation for synthetic polymers dissolved in organic solvents.

MALDI analysis of most synthetic polymers has remained problematic even in recent years, which is attributed to the lack of a range of suitable matrices. Most matrices available are used for water soluble biopolymers such as proteins and peptides; evidently more ionic or polar polymers such as polyglycols can be successfully analysed using matrixes such as 2,5-dihydroxybenzoic acid and sinapinic acid, but these matrices are unsuitable for non-polar polymers. The criteria for an appropriate matrix are as follows:[107]

i) absorption in the correct wavelength range (i.e. of the laser frequency)

ii) solubility in a solvent compatible with the analyte,

iii) no interaction with the analyte and

iv) miscibility with the analyte in the condensed phase.

Even if all these criteria are met, the efficiency of the matrix candidate is impossible to predict while the desorption and ionisation processes occurring are not completely understood. The difficulty in finding a suitable matrix is therefore a similar problem to that of finding the correct combination of solvent system and salt in ESI-MS.

Possible matrices suitable for polymer analysis are 2-nitrophenyl octyl ether[110,113], 2-cyano-5-phenyl-2,4-pentadienoic acid[114], quinizarin[115] and indole acrylic acid[116]. For non-polar synthetic polymers, salts such as those of silver, copper and cobalt[115] are often introduced to promote ionisation.

Karas, Hillenkamp and co-workers[113] have used MALDI as a technique to analyse synthetic polymers in the range of 1000 to 70 000 Da. They have obtained positive-ion spectra for poly(ethylene glycol) with masses up to 40 000 using 2,5-dihydroxybenzoic acid as a matrix; they also used this matrix to analyse poly(methyl methacrylate). Analysis of polystyrene samples was unsuccessful using 2,5-dihydroxybenzoic acid as a matrix as the analyte phase separates upon deposition, spectra of these less polar polymers with masses up to 70 000 were obtained using 2-nitrophenyl octyl ether as matrix with added silver trifluoroacetate to promote the production of positive ions. Danis et al.[117] have obtained a negative-ion spectrum for a water-soluble poly(styrene sulfonic acid) sample with a mass of 200 000 Da. Other synthetic polymers analysed recently using MALDI include poly(vinyl acetate)[116] polybutadiene[115] and poly(propylene oxide)[67,113].

Evidently the correct choice of matrix and salt to achieve ionisation of intact polymer chains is necessary to the MALDI process. Another criterion to consider when acquiring MALDI spectra is the ratio of matrix to polymer used to prepare samples prior to analysis.

MALDI is normally only successful in obtaining accurate molecular weight information for polymer samples with narrow molecular weight distributions. Montaudo et al.[118] have been able to obtain accurate molecular weight information for polydisperse samples by fractionating samples using GPC prior to MALDI. Selected

fractions were analysed using MALDI-TOF-MS and the average molecular weights calculated.

No previous studies of LP characterisation by MALDI have been published; therefore a wide variety of matrices, salts and concentration levels were examined before our first MALDI spectrum of an LP was obtained. Since commercial LPs are polydisperse, it seems unlikely that accurate molecular weight information could be obtained unless samples were fractionated using GPC prior to MALDI analysis. The significant advantages of using MALDI for the analysis of LPs are:

i) once a suitable matrix system is found, sample preparation is quick and easy,

ii) MALDI instruments are quicker and significantly easier to operate than many mass spectrometric techniques, including ESI.

It was hoped that MALDI could be utilised as a quick and simple technique to characterise LP samples and study their degradation pathways.

1.3.4 FIELD DESORPTION

Prior to the development of MALDI and ESI, the most utilised ionisation method for obtaining molecular weight measurements of polymers by mass spectrometry was field desorption (FD). FD has been used successfully to analyse a wide variety of synthetic polymers including poly(ethylene glycol)[119] polyethylene[120] and polybutadiene,[121] however, it is most suitable for analysing aromatic polymers such as polystyrene[122-124]. Structural information about synthetic polymers may be confirmed by collision induced decomposition spectra of radical ions[124].

Field desorption was developed by Beckey[125] in 1969; the basic concept of this ionisation technique is that samples are deposited and desorbed from an emitter. The emitter is typically a tungsten wire treated with pyrolysed benzonitrile to create carbonaceous dendrites at the surface. The sample is applied as a solution to the emitter and collects at the dendrite vertices, and a high potential is then applied to the emitter by electrical heating. A very high local field strength is created around the dendrite structures promotes ionisation of the sample into the gas phase.

FD-MS tends to produce ions such as [M+H]+ or [M+Cation]+., where the cation is an alkali metal such as sodium. To obtain good quality spectra by FD-MS an emitter current is established whereby intense molecular ion signals are detected with little fragmentation.

1.3.5 MASS SPECTROMETRY OF POLYSULFIDES

Although there are no previous publications involving the mass spectrometry of LPs, a number of studies involving sulfur-containing polymers have been carried out by Montaudo and co-workers[126-130]. They have utilised direct pyrolysis in the ion source of a mass spectrometer (DPMS) to obtain information on the thermal decomposition processes of the following: poly(phenylene sulfide)[126,127], aliphatic polysufides[128], poly(thiomethylene), poly(thiotrimethylene). poly(thiolethylene), poly(thiohexamethylene) and a variety of aliphatic-aromatic polysulfides[129].

They conclude that the primary thermal degradation products evolving from poly(phenylene sulfide) in the initial stages are cyclic oligomers[126,127]. This behaviour is characteristic of sulfur-containing polymers which have shown a tendency initially to produce cyclic oligomers;[128,129] most likely by a back-biting reaction initiated at the

chain ends. A second thermal degradation stage which often occurs in most sulfur-containing polymers, typically involves a β-CH hydrogen transfer process to produce compounds with thiol and olefin end groups[128,129].

Montaudo et al. have also used fast atom bombardment (FAB) mass spectrometry to identify oligomers formed in the polycondensation reactions leading to aromatic, aliphatic and aliphatic-aromatic polysulfides[130]. Using this technique the formation of complexes was identified between cyclic sulfides and heavy metals such as Ag, Hg and Cu.

1.4 OBJECT OF THIS WORK

Little has been published in the open literature concerning the degradation processes undergone by LPs, despite their wide utilisation, therefore the object of this work was to fully investigate the degradation pathways of linear polysulfides manufactured by Morton Thiokol. In this research, we have utilised a wide range of analytical techniques to characterise this class of polymers and identify their degradation products.

ESI combined with CID made possible a comprehensive study of LP characterisation, followed by an extensive study of the thermal- and photo-degradation products of the pre-polymers and liquid exudates produced on photo- and thermal degradation. ESI-MS spectra of degraded samples, analysed alongside spectra obtained by classical analytical techniques such as IR and NMR, have enabled us to confirm that polysulfides degrade by two competing mechanisms.

We have also attempted to characterise the photochemical processes responsible for the discolouration at the glass-polymer interface by utilising a wide range of surface analysis techniques.

CHAPTER 1

REFERENCES

1. Lowig, K., Weidmann, S., *Poggendorff Annals. Physik,* **46**, (1839) 81.

2. Lowig, K., Weidmann, S., *Poggendorff Annals. Physik,,* **49**, (1840) 123.

3. Lucke, H., Huthig, *Alips - Aliphatic Polysulfides. Monograph of an Elastomer.* Wepf Verlag, Basel, (1994).

4. Patrick, J.C., Mnockin, N.M., *Brit Pat. 302270*, (1927).

5. Patrick, J.C., *Brit Pat 360890*, (1930).

6. Bertozzi, E.R., *Rubber Chemistry and Technology,* **41**, (1968) 114.

7. Schroter, R., Becker, W., *US Pat. 2026875*, (1936).

8. Patrick, J.C., Ferguson, H.R., *U.S. Pat 2466963*, (1949).

9. Coates, R.J., Gilbert, B.C., Lee, T.C.P., *J. Chem.Soc, Perkin Trans 2,* (1992) 1387.

10. Planek, J.R., *Polysulfide Polymers: II Applications in High Polymers, Polyethers, Part III.*, Ed Gaylord, N.G., John Wiley and Sons. New York. **13,** (1962) 115.

11. Berenbaum, M.B., *Polysulfide Polymers* in *Encyclopedia of Polymer Science and Technology*. John Wiley and Sons. New York. **2,** (1969) 425.

12. Ghatage, N.D., Verneker, S.P., Lonikar, S.V., *Rubber Chemistry and Technology.*, **54**, (1981) 197.

13. ASTM Spec Technical Publications, *Building Seals and Sealants.*, Julian Panek edit., **606**, (1976) 40.

14. Panek, J.R., Cook, J.P., *Construction Sealants and Adhesives 3rd edition.*, John Wiley and Sons. New York. (1991) 107.

15. Rosenthal, N.A., Berenbaum M.B., *Thermal Degradation of Ethyl Formal Polysulfide Polymers.* In-house report for Thiokol Chemical Corporation.

16. Brenton Paul, D., Hanhela, P.J., Huans, Robert, H.E., *Adhesives, Sealants and Coatings for Space and Harsh Environments.*, Ed by Lieng-Huang Lee., Plenum Publishing Corporation, New York. (1988) 269.

17. Barber, J.W., Hanhel, P.J.,.Huang, R.H.E., Brenton Paul, D., *Polymer Testing* **9**, (1990) 291.

18. Ennis B.C., Hanhela, P.J., Brenton Paul, D., *Aust. J.Chem* **43**, (1990) 109.

19. Hanhela, P.J., Huang, R.H.E., Brenton Paul, D.,.Symes, T.E.F., *J. Appl. Polym. Sci.*, **32**, (1986) 5415.

20. Barber, J.W., Hanhela, P.J., Huang, R.H.E., Brenton Paul, D., *I and EC Product Research and Development*, **25**, (1986) 328.

21. Hanhela, P.J., Huang, R.H.E., Brenton Paul, D., *I and EC Product Research and Development* **25**, (1986) 321.

22. Huang, R.H.E., Paul, D.B., *Materials Forum*, **17**, (1993) 281.

23. Kishore, K. Ganesh, K. *Adv. Poly. Sci.*, **121**, (1995) 81.

24. Mazurek, W., Moritz, A.G., *Macromolecules*, **24**, (1991) 3261.

25. Averko-Antonovich, M.V.S., Zykova, L.A., Safina,V.V., *NP Kauch Rez* **4**, (1985) 23.

26. Berenbaum, M.B., Marck, H.F., Gaylord, N.G., Birkel, N.M., *Encyclopedia of Polymer Science and Tech*, John Wiley and Sons, New York, **2**, (1969) 445.

27. Davidson, R.G., Mathys, C.I., *Anal. Chim. Acta* **160**, (1984) 197.

28. Morton Thiokol., *Internal Lab Reports.*, 1969, 1970, 1988.

29. Mahon, A., Kemp, T.J., Buzy, A., Jennings, K.R., *Polymer* **27**, (1996) 531.

30. Mahon, A., Kemp, T.J., Buzy, A., Jennings, K.R., *Polymer.* In the press.

31. Davis, A., Sims, D., *Weathering of Polymers,* Applied Science Publishers. Essex. (1983).

32. Ranby, B., Rabek J.F., *Photodegradation, Photo-oxidation and Photostabilization.* Wiley Interscience, London. (1975).

33. Grassie, N., Scott, G., *Polymer Degradation and Stabilisation,* Cambridge University Press, Cambridge. (1985).

34. Ranby, B., Rabek J.F., eds. *Singlet Oxygen; Reactions with Organic Compounds and Polymers.* Wiley Interscience, London. (1978).

35. Allen, N.S. in *Specialist Periodical Reports, " Photochemistry "* **22-26.** Royal Society of Chemistry. London. (1990-94).

36. Allen, N.S. Edge, M. *Fundamentals of Polymer Degradation and Stabilisation.* Elsevier Applied Science, Oxford. (1992).

37. Allen, N.S. *TRIP.* **2,** (1994) 366.

38. Hamid, S.H., Amin, M.B., Maadhah. A.G., *Handbook of Polymer Degradation,* M. Dekker, New York. (1992).

39. Hill, D.J.T., O'Donnell, J.H., Pomery P.J., in *Specialist Periodical Reports, "Electron Spin Resonance"* **9,** Royal Society of Chemistry.London. (1985).

40. Beachell, H.C., Nemphos, S.P., *J.Polym. Sci.,* **21,** (1956) 113.

41. Beachell, H.C., Tarbet, G.W., *J.Polym. Sci.,* **45,** (1960) 451.

42. Luongo, J.P., *J.Polym. Sci.,* **42,** (1960) 139.

43. Adams, J.H., *J.Polym. Sci.,* **8,** (1970) 1077.

44. Adams, J.H., Goodrich, J.E., *J.Polym. Sci.,* **8,** (1970) 1269.

45. Zolotova, N.V., Denisov, E.T., *J.Polym. Sci.,* **9,** (1971) 3311.

46. Denisov, Y.E.T., *J.Polym. Sci.*, **19**, (1978) 2893.

47. Scott, G., in *Ultraviolet Light Induced Reactions in Polymers*, **25**, ed. Labana, S.S., ACS Symposium Series. Washington, D.C. (1976) 340.

48. Chakraborty, K.B., Scott, G., *Eur. Polym. J.*, **13**, (1977) 731.

49. Arnaud, J., Moisan, J.Y., Lemaire, J., *Macromolecules*, **17**, (1984) 332.

50. Fanton, E., Pellereau, B., Arnaud, R., Lemaire, J., *J. Polym. Photochem.* **6**, (1985) 437.

51. Ebner, K., White, J.L., *Intern.Polymer Processing*, **9**, part 3, (1994) 233.

52. Fanton, E., Tidjani. A., Arnaud, R., *Polymer.* **35**, (1994) 433.

53. Vaillant, D., Lacoste, J., Dauphin, G., *Polymer Degradation and Stability*, **45**, (1994) 355.

54. Gugumus, F., *Polymer Degradation and Stability*, **49**, (1995) 29.

55. Gijsman, P., Kroon, M., Van Oorshot, M., *Polymer Degradation and Stability*, **51**, (1996) 3.

56. Cruz-Pinto, J.J.C., Carvalho, M.E.S., Ferreira, J.F.A., *Die Angewandte Makromolekulare Chemie*, **216**, (1994) 113.

57. Bolland, J.L., Gee, G., *Trans.Faraday Soc*, **42**, (1946) 236.

58. Bolland, J.L., *Trans.Faraday Soc*, **44**, (1946) 669.

59. Carlsson, D.J., Chmela, S., Lacoste, J., *Macromolecules*, **23**, (1990) 4934.

60. Lacoste, J., Vaillant, D., Carlsson, D.J., *J. Polym. Sci, Polym. Chem*, **31**, (1993) 715.

61. Vaillant, D., Lacoste, J., Dauphin G., *Polymer Degradation and Stability*, **45**, (1994) 355.

62. Yang, C.Q., Martin, L.K., *J. Appl. Polym. Sci.* **51**, (1994) 389.

63. Schoolenberg, G.E., Vink, P., *Polymer*, **32**, (1991) 432.

64. Schoolenberg, G.E., Vink, P., *Polymer*, **32**, (1991) 438.

65. Griffiths, P.J.F., Hughes, J.H., Park,G.S., *Eur. Polym. J*, **29**, (1993) 437.

66. Lemaire, J., Gauvin, P., Sallet, D., *Makromol. Chem*, **188**, (1987) 1815.

67. Barton, Z., Kemp. T.J., Buzy, A., Jennings, K.R., *Polymer*, **36**, (1995) 4927.

68. Costa, L., Gad, A.M., Camino, G., Cameron, G.G., Qureshi, M.Y., *Macromolecules.* **25**, (1992) 5512.

69. Cameron, G.G., Ingram, M.D., Qureshi, M.Y., Gearing, H.M., *Eur. Polym. J.* **25**, (1989) 779.

70. Fares, M.M., Hacaloglu, J., Suzer, S., *Eur. Polym. J.*, **30**, (1994) 845.

71. Rabek, J.F., *Polymer Photodegradation*, Chapman and Hall. London. (1995).

72. Turley, R.S., Brent Strong, A., *J. Adv. Mater.*, April (1994) 53.

73. Mwila, J., Miraftab, M., Horrocks, A.R., *Polymer Degradation and Stability*, **44**, (1994) 351.

74. Janssen, K., Gijsman, P., Tummers. D., *Polymer Degradation and Stability*, **49**, (1995) 127.

75. Pospisil, J., in *Development in Polymer Stabilisation-7*, Ed. Scott, G., Appl. Sci. Pub. (1984) 1.

76. Pospisil, J., Nespurek, S., *Polymer Degradation and Stability*, **49**, (1995) 99.

77. Pospisil, J., *Die Angewandte Makromolekulare Chemie*, **216**, (1994) 135.

78. Al-Malaika, S., *Intern.J. Polym. Mater*, **24**, (1994) 47.

79. Kikkawa, K., *Polymer Degradation and Stability*, **49**, (1995) 135.

80. Geuskens, G., Kanda, M.N., Nedelkos, G., *Intern.J. Polym. Mater*, **24**, (1994) 19.

81. Step, E.N., Turro, N.J., Gande, M.E., Klemchuk, P.P., *Macromolecules*, **27**, (1994) 2529.

82. Bodor, G., *The Structural Investigation Of Polymers*, Ellis Horwood. London. (1991).

83. Bower, D.I., Maddams, W.F., *The Vibrational Spectroscopy of Polymers*, Cambridge University Press, (1989).

84. Young, R.J., *Introduction to Polymers*, Chapman and Hall. London. (1981).

85. Han, S., Kim, C., Kwon. D., *Polymer Degradation and Stability*, **47**, (1995) 203.

86. O'Donnell, B., White, J.R., Holding, S.R., *J. Appl. Polym. Sci.* **52**, (1994) 1607.

87. Campana, J.E., Sheng, L-S., Shew, S.L., Winger, B.E., *Trends Anal.Chem.* **13**, (1994) 239.

88. Dole, M., Mack, L.L., Hines, R.L., Mobeley, R.C., Ferguson, L.D., Alice, M.B., *J. Chem.Phys.* **49**, (1968) 2240.

89. Gieniec, J., Mack, L.L., Nakamae, K., Gupta, C., Kumar, V., and Dole, M., *Biomed. Mass Spectrom.* **11**, (1984) 259.

90. Yamashita, M., Fenn, J.B., *J. Phys. Chem*, **88**, (1984) 4451.

91. Alexandrov, M.L., Knorre, V.D., Kusner, Y.S., *Bioorg. Kim.* **10**, (1984) 710.

92. Wong, S.F., Meng, C.K., Fenn, J.B., *J. Phys. Chem*, **92**, (1988) 546.

93. Nohmi, T., Fenn, J.B., *J. Am. Chem. Soc.* **114**, (1992) 3241.

94. Fenn, J.B., *J. Am. Chem. Soc. Mass Spectrom.*, **4**, (1993) 524.

95. Rollgen, F.W., Bramer-Weger, E., Buetfering, *J., Phys. Colloq.*, Paris. **48-C6**, (1987) 253.

96. Iribarne, J.V., Thomson, B.A., *J. Chem. Phys.* **64**, (1976) 2287.

97. Thomson, B.A., Iribarne, J.V., *J. Chem. Phys.* **71**, (1979) 4451.

98. Thomson, B.A., Iribarne, J.V., Dziedzic, P.J., *Anal.Chem*, **54**, (1982) 2219.

99. Ashton, D.S., Beddell, C.R., Cooper, D.J., Green B.N., Oliver, W.A., *Org. Mass Spectrom*, **28**, (1993) 721.

100. Smith. R.D., Loo, J.A., Baringa, C.J., Edmonds, C.G., Udseth, H.R., *J. Am. Soc. Mass Spectrom.* **1**, (1990) 53.

101. Smith. R.D., Loo, J.A., Edmonds, C.G., Baringa, C.J., Udseth, H.R., *Anal. Chem*, **62**, (1990) 882.

102. Corless, S., Tetler, L.W., Parr, V., Wood, D., '*Abstracts 42nd ASMS Conference on Mass Spectrometry*' Chicago (1994) 515.

103. Simonsick, W.J., Prokai, L., '*Abstracts 42nd ASMS Conference on Mass Spectrometry*' Chicago (1994) 318.

104. Prokai, L., Simonsick, W.J., *Rapid Commun. Mass Spectrom.*, 7, (1993) 853.

105. Jennings, K.R., *Int. J. Mass Spectrom. Ion Phys.*, **1**, (1968) 227.

106. Sherrand, K.B., Marriott, P.J., McCormick, M.J., Cotton, R., Smith, G., *Anal. Chem.*, **66**, (1994) 3394.

107. Creel, H.S., *TRIP.*, **1**, (1993) 336.

108. Price, D., Milnes, G.J., *Int. J. Mass Spectrom. Ion Proc.*, **99** (1990) 1.

109. Wilkins, C.L., Nuwaysir, L.M., *Anal. Chem.*, **60**, (1988) 279.

110. Karas, M., Bachmann, D., Bahr, U., Hillenkamp, F., *Int. J. Mass Spectrom. Ion Proc.*, **78**, (1987) 53.

111. Karas, M., Hillenkamp, F., *Anal. Chem.*, **60**, (1988) 2299.

112. Karas, M., *Analysis,* **20**, (1992) 31s.

113. Bahr, U., Deppe, A., Karas, M., Hillenkamp, F., Giessmann, U., *J. Anal. Chem.*, **64**, (1992) 2866.

114. Williams, J.B., Gusev, A.I., Hercules, D.M., *Paper presented at 42nd ASMS Conference on Mass Spectrometry*, Chicago (1994).

115. Mowat, I.A., Donovan, R.J., *Rapid Comm. Mass Spectrom.*, **9**, (1995) 82.

116. Danis, P.O., Karr, D.E., Holle, A., Mayer-Posner, F., Watson, C.H., *Paper presented at 41st ASMS Conference on Mass Spectrometry*, (1993).

117. Danis, P.O., Karr, D.E., Mayer-Posner, F., Holle, A., Watson, C.H., *Org. Mass Spectrom.*, **27**, (1992) 843.

118. Montaudo, G., Garozzo, D., Montaudo, M.S., Puglisi, C., Samperi. F., *Macromolecules,* **28**, (1995) 7983.

119. McCrae, C.E., Derrick, P.J., *Org. Mass Spectrom.*, **18**, (1983) 323.

120. Lattimer, R.P., Schulten, H.R., *Int. J. Ion Phys.*, **52**, (1983) 105.

121. Craig, A.C., Cullis, P.G., Derrick, P.J., *Int. J. Mass Spectrom. Ion Phys.*, **38**, (1981) 297.

122. Matsuo, T., Matsuda, H., Katakuse, I., *Anal. Chem.*, **51**, (1979) 1329.

123. Rollins, K., Scrivens, J.H., Taylor, M.J., Major, H., *Rapid Commum. Mass Spectrom.*, **4**, (1990) 355.

124. Craig, A.C., Derrick, P.J., *J. Chem. Soc, Chem. Commun.*, (1985) 891.

125. Beckey, H.D., *Int. J. Mass Spectrom. Ion Phys.*, **2**, (1969) 500.

126. Montaudo, G., Puglisi, C., Scamporrino, E., Vitalini, D., *Macromolecules.* **19**, (1986) 2157.

127. Montaudo, G., Puglisi, C., Samperi, F., *J. Polym. Sci, Polym. Chem.*, **32**, (1994) 1807.

128. Montaudo, G., Scamporrino, E., Puglisi, C., Vitalini, D., *J. Polym. Sci, Polym. Chem.*, **25**, (1987) 475.

129. Montaudo, G., Scamporrino, E., Puglisi, C., Vitalini, D., *Polymer.* **28**, (1987) 477.

130. Montaudo, G., Scamporrino, E., Puglisi, C., Vitalini, D., *Macromolecules.* **21**, (1988) 1594.

CHAPTER 2

EXPERIMENTAL

2.1 INSTRUMENTAL

2.1.1 INFRARED (IR) SPECTROSCOPY

IR spectra were obtained using a Perkin-Elmer 1720X FTIR spectrophotometer (range 5250-400 cm^{-1}). Resolution was predetermined at 4 cm^{-1}.

2.1.1.1 INFRARED SPECTRA OF PRE-POLYMER FILMS

Thin (≈ 0.5 mm) pre-polymer films were mounted onto a sodium chloride plate and the spectra were recorded in the usual way. A library of IR spectra for all LPs listed in table 2.2 was compiled at the beginning of the project, and a typical IR spectrum of a commercial LP is illustrated in fig.2.1. Table 2.1 gives assignments of the major peaks.

2.1.1.2 INFRARED SPECTRA OF CURED POLYMER FILMS

Thin (≈ 1 mm) cured polymer films were mounted onto a cardboard holder (see fig.6.3). Spectra were recorded in the normal manner.

2.1.1.3 SOLUTION INFRARED SPECTRA OF LEACHED POLYMER SAMPLES

Solution IR spectra were recorded using sodium chloride plates and 1 mm spacers. Chloroform was normally used as the leaching solvent.

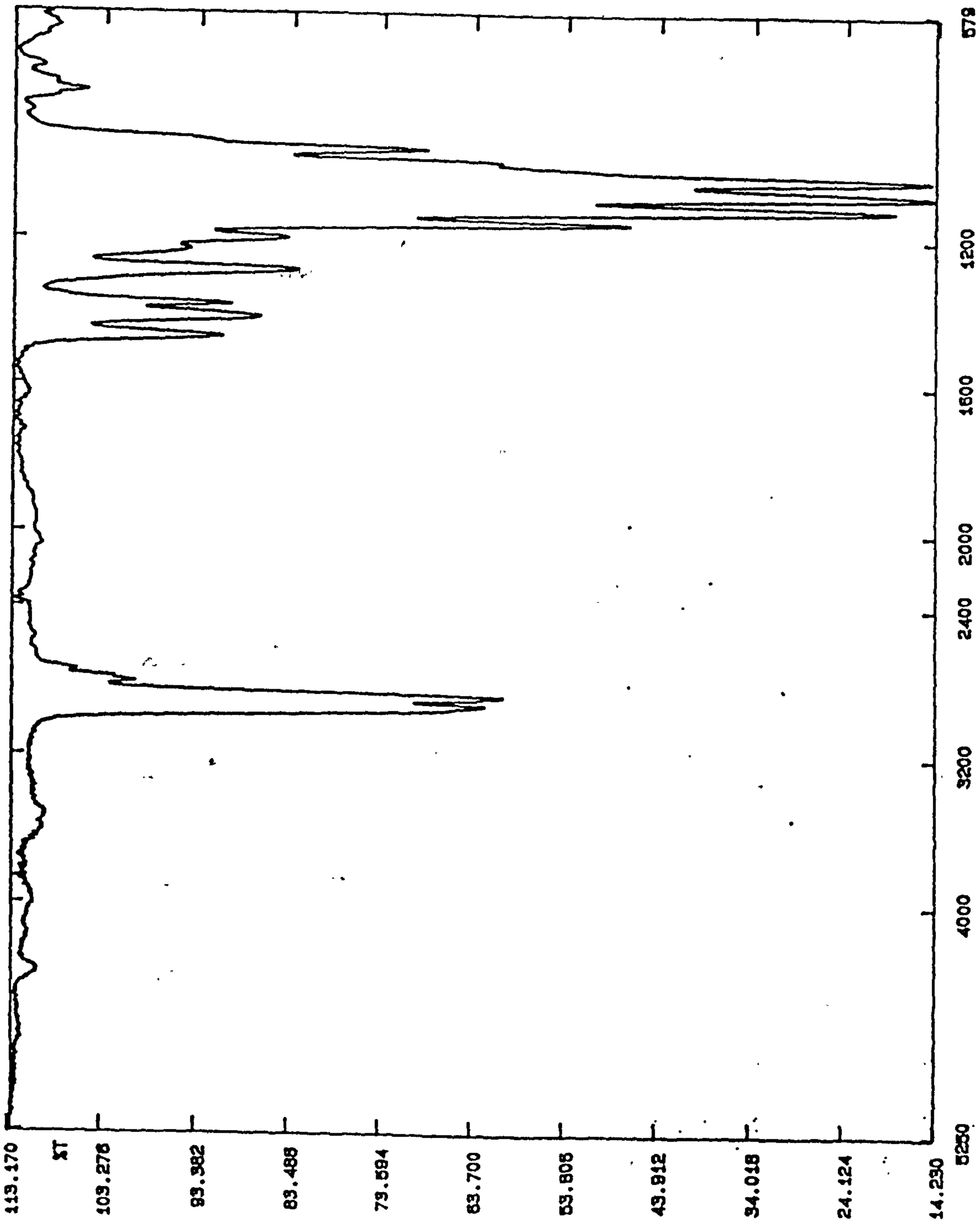

Fig. 2.1: IR spectrum of a commercial LP.

TABLE 2.1 Assignments of the principal peaks in the IR spectrum of an LP.

Frequency / cm^{-1}	Intensity	Assignments and Comments
≈3600	Weak	Free water. Broad
≈3500	Weak	Intramolecular bonded hydroxyl. Broad.
2921 2869	Strong	Asymmetric and symmetric CH_2 stretch. Sharp.
2560	Weak	S-H stretch. Sharp.
2360	Weak	Atmospheric CO_2 in background.
1467	Medium	CH_2-O, CH_2 scissoring deformation. Sharp.
1413	Medium	CH_2-S, CH_2 stretch. Sharp.
1197	Strong	C-C-O stretch. Sharp.
1155	Strong	Symmetric C-O-C stretch (C-O stretching). Sharp.
1114	Strong	Asymmetric C-O-C stretch (C-O stretching). Sharp.

2.1.1.4 INFRARED SPECTRA OF POLYMER SURFACES USING ATTENUATED TOTAL REFLECTANCE (ATR) INFRARED SPECTROSCOPY

Polymer surfaces were examined using a horizontial ATR attachment supplied by Spectra Tech Inc. which was connected to a Unicam Mattson model 1000 FTIR spectrometer. Connection and operation of the ATR attachment was carried out following the manufacturer's instruction manual. Resolution was predetermined at 16 cm^{-1}.

2.1.2 NUCLEAR MAGNETIC RESONANCE (NMR) SPECTROSCOPY

Spectra were obtained using a Bruker ACF 250 spectrometer operating at 250.13 MHz for ^{1}H and 62.86 MHz for ^{13}C NMR; the tubes used were normally 5 mm in diameter, and chloroform-d was the usual solvent. When increased spectral resolution was required, a Bruker ACP 400 spectrometer operating at 400.13 MHz for ^{1}H and 100.62 MHz for ^{13}C NMR was employed.

A library of NMR spectra for all LPs listed in table 2.2 (10% solutions in $CDCl_3$; reference $CDCl_3$) was compiled at the beginning of this project. A typical ^{1}H NMR spectrum of a commercial LP is illustrated in fig.2.2. Assignments are as follows:

<u>Major Peaks</u>

Singlet at 4.71 ppm: CH_2-CH_2-O-C<u>H</u>$_2$-O-CH_2-CH_2,

Triplet at 3.80 ppm (J=6.38 Hz): CH_2-O-C<u>H</u>$_2$-CH_2-SS

Triplet at 2.89 ppm (J=6.38 Hz): CH_2-O-CH_2-C<u>H</u>$_2$-SS

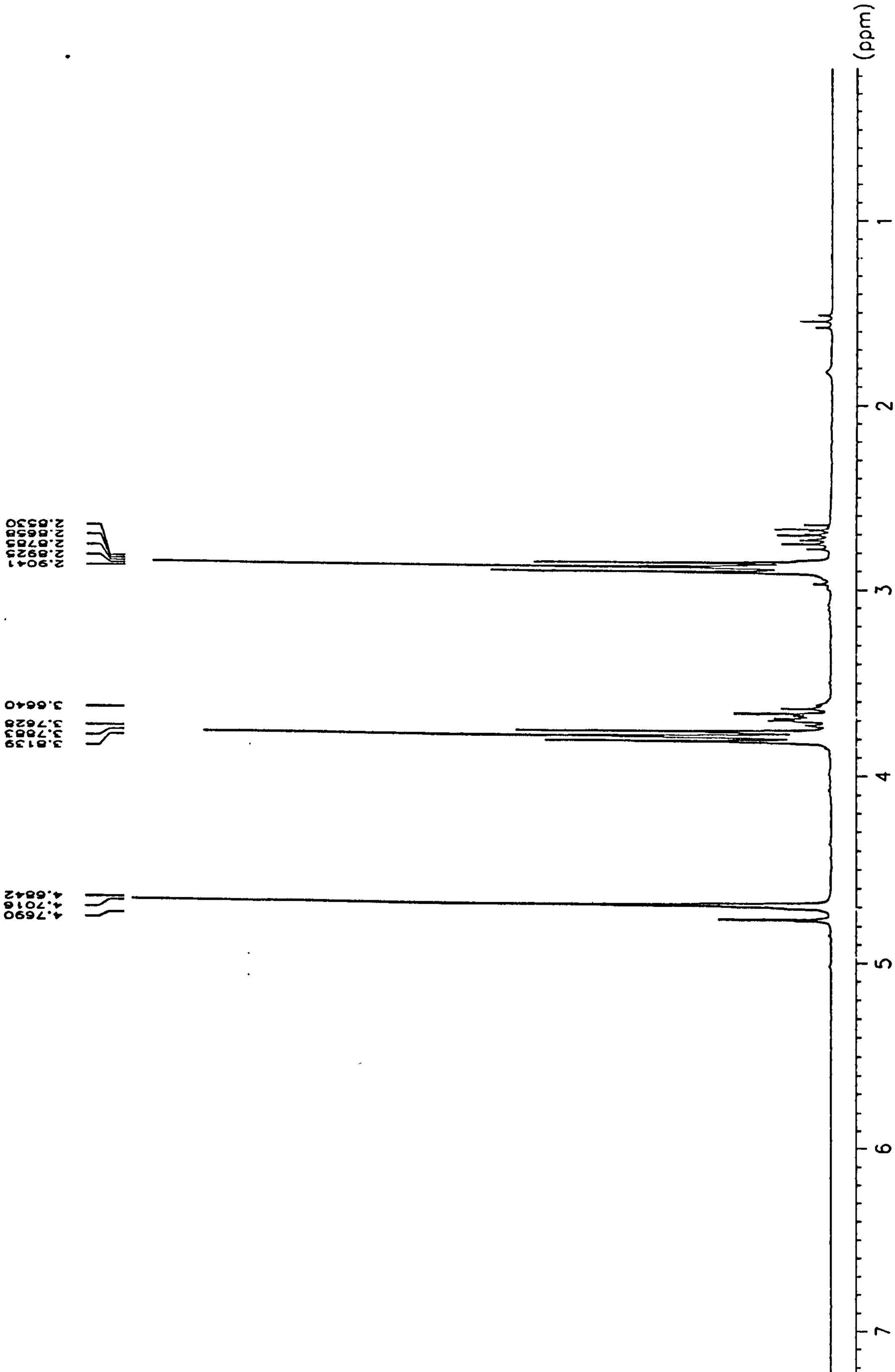

Fig. 2.2: ^{1}H NMR spectrum of a commercial LP.

Minor Peaks

Singlet at 4.79 ppm: CH_2-O-C$\underline{H}_2$-O-C$\underline{H}_2$-O-CH_2

Triplet at 3.68 ppm (J=6.31Hz): O-CH_2-O-C$\underline{H}_2$-CH_2-SH

Multiplet at 3.75-3.63 ppm: Impurities in polymer backbone.

Triplet at 2.76 ppm (J=6.51 Hz): CH_2-S-C$\underline{H}_2$-CH_2-O-CH_2-O-CH_2

Doublet triplet at 2.72 (J=6.32 Hz): HS-C$\underline{H}_2$-CH_2-O

2.68 (J=6.32 Hz):

Triplet at 1.56 ppm (J=8.22 Hz): CH_2-S$\underline{H}$

A typical ^{13}C NMR spectrum of a commercial LP is illustrated in fig.2.3. Assignments are as follows:

Major Peaks

95.30 ppm: CH_2-CH_2-O-$\underline{C}H_2$-O-CH_2-CH_2,

66.00 ppm: O-CH_2-O-$\underline{C}H_2$-CH_2-SS

38.68 ppm: O-CH_2-O-CH_2-$\underline{C}H_2$-SS

Minor Peaks

91.83 ppm: CH_2-O-$\underline{C}H_2$-O-$\underline{C}H_2$-O-CH_2

69.57 ppm: O-CH_2-O-$\underline{C}H_2$-CH_2-SH

32.10 ppm: CH_2-S-$\underline{C}H_2$-CH_2-O-CH_2-O

24.45 ppm: HS-$\underline{C}H_2$-CH_2-O-CH_2-O

Our NMR assignments agree with those made by previous workers[1,2].

DEPT and 2-D $^1J^1H$-^{13}C correlation experiments were carried out using the Bruker ACP 400 spectrometer to identify the photodegradation products in heavily UV exposed pre-polymer samples.

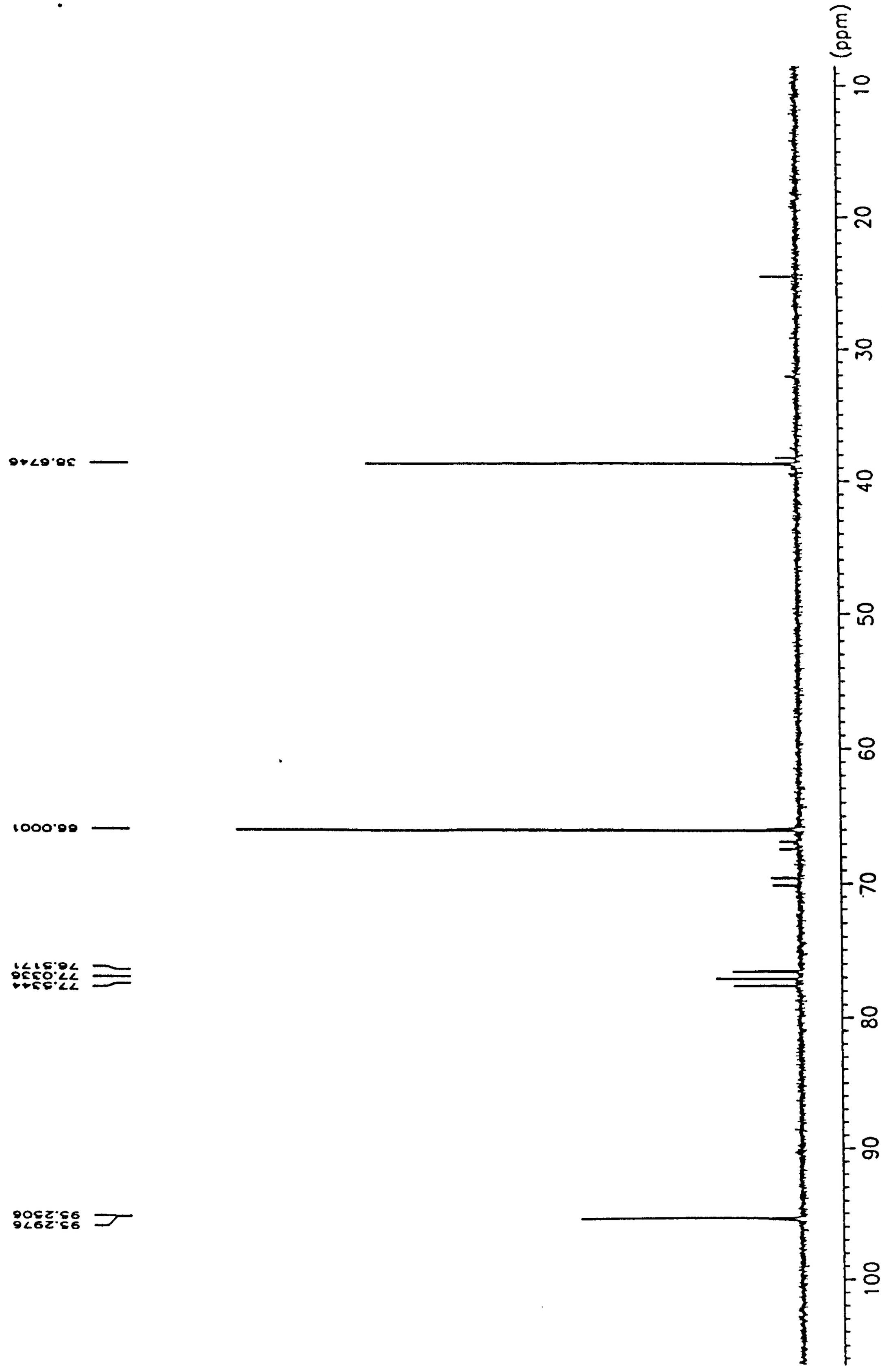

Fig. 2.3: ^{13}C NMR spectrum of a commercial LP.

2.1.3 SOLID STATE ^{1}H NMR EXPERIMENT

A ^{1}H NMR spectrum of a powdered LP film sample was obtained in the Physics Department on a Bruker MSL-360 instrument run at 8.45 T.

2.1.4 GEL PERMEATION CHROMATOGRAPHY (GPC)

The GPC equipment used in these experiments consisted of a dual piston HPLC pump (ICI instruments LC1110), a Rheodyne injection valve with a 20 µl sample loop (Rheodyne 1725), and a differential refractive index detector (ICI instruments LC1240). Data were analysed using Polymer Laboratories Calibre GPC software.

All polymer samples were analysed at a concentration of 50 mg ml^{-1}, with THF as the eluent with a flow rate of 1 ml/min^{-1}; toluene (≈ 0.2 %wt) was used as an internal standard and flow marker for each sample. The columns used were either a Polymer Laboratories (PL) Mixed-D (300 x 7.5 mm) or a Mixed-E depending on the mass range being examined, connected to a Polymer Laboratories 5 µm bead size guard column (50 x 7.5 mm). The PL 3 µm bead size Mixed-E column was calibrated between 200 and 30 000, while the PL 5 µm bead size Mixed-D column was calibrated between 200 and 400 000, using narrow PMMA standards (PL).

2.1.5 ELECTROSPRAY MASS SPECTROMETRY

The ESI/CID experiments were carried out in a Fisons' 'Quattro II' triple quadrupole mass spectrometer (VG Biotech, Altrincham, UK) equipped with an atmospheric pressure ionisation (API) source operated in the nebulizer–assisted

electrospray mode. The potential on the electrospray needle was set at 4 kV and the extraction (cone voltage (cv)) was set at *ca.* 55 V for the THF/MeOH mobile phase and *ca.* 100 V for the acetone/KI phase except during experiments conducted to ascertain the affect of changing the cv on the ESI spectrum. LPs at a concentration of 0.5 μg/μl were dissolved in a solvent compatible with the mobile phase. For most experiments this was a 1:1 (v/v) mixture of tetrahydrofuran (THF) and methanol (MeOH) in the presence of 0.5% aqueous ammonium chloride. A number of experiments were conducted using acetone as the mobile phase containing potassium iodide (0.5 mg/ml) and yet others with a 1:1 THF/MeOH containing 0.5% trifluoracetic acid (TFA), and also THF/DMF with KI and NH_4^+, the latter with little success.

Mass spectra were scanned over the range *m/z* 3500 – *m/z* 350 during a 10 s scan and by operating the data system in the multichannel acquisiton (MCA) mode, several scans were summed to produce the final spectrum. Calibration was carried out using a solution of sodium iodide. In CID experiments, polysulfide ions of selected *m/z* passed at a translational energy of 20 eV from the first quadrupole mass analyser into the r.f. – only hexapole collision cell containing argon at an indicated pressure of 3.8×10^{-3} mbar. Fragment ion spectra were obtained by scanning the final quadrupole mass analyser over the *m/z* range from the mass of the precursor ion down to *m/z* 50 in 10 s using the MCA mode.

2.1.6 MATRIX-ASSISTED LASER DESORPTION IONISATION (MALDI)

All experiments were carried out on a Kratos Kompact III MALDI-TOF mass spectrometer. The instrument is fitted with a nitrogen laser of wavelength 337 nm with a 3 ns pulse duration, and an electron multiplier detector. The spectrometer was operated in the positive ion linear mode with an accelerating potential of 20 kV.

All polymer sample concentrations were approximately 3 mg/ml in THF. Various volumes of silver trifluoroacetate (10-200 μl) was used to dope the analyte solution (0.5 ml). Equal quantities of this solution and the matrix solution (0.1 M 9-nitroanthracene in THF) were mixed and the resulting solution left to stand for up to 4 hours. 1 μl of this mixture was deposited onto the stainless steel sample slide and the solvent was evaporated off.

Every sample was analysed at various laser powers and spectra were averaged over 200 laser shots. Analysis of the data acquired was carried out using software installed on the Kompact III.

2.1.7 FIELD DESORPTION (FD)

All experiments were carried out by Dr. A.T. Jackson of ICI (Wilton) on a ZAB-T four sector mass spectrometer, (Micromass, Manchester UK.).

2.1.8 FAST ATOM BOMBARDMENT (FAB)

All experiments were carried out on a Kratos Analytical MS80 mass spectrometer employing FAB. 3-nitrobenzyl alcohol was used as a matrix.

2.1.9 GAS CHROMATOGRAPHY (GC) MASS SPECTROMETRY

All experiments were carried out on a Kratos Analytical MS80 mass spectrometer, equipped with a OV170 G.C. capillary column using a temperature range of 40-100^0 C.

2.1.10 X-RAY PHOTOELECTRON SPECTROMETER (XPS)

1 cm^3 samples were mounted onto a stand using a carbon adhesive and left in a vacuum for 24 hours. These samples were then examined in the Physics Department by XPS. All experiments were carried out using a VG ESCA LAB 5 instrument.

2.1.11 STATIC SECONDARY ION MASS SPECTROMETRY

All experiments were carried out using a EVA 2000 SIMS quadrupole instrument, built in the Physics Department at the University of Warwick. A beam of oxygen molecules of energy 4 kV was employed.

2.1.12 RAMAN SPECTROSCOPY

All experiments were carried out at the laser facility at Rutherford Appleton Laboratories under the supervision of Dr A.W. Parker. Raman spectra were obtained using the 363 nm line of an argon ion laser as the excitation wavelength.

2.1.13 ENERGY DISPERSIVE X-RAY ANALYSIS (EDAX)

All EDAX experiments were carried out by Ms. J. Buckle using a Princeton Gamma-Tech digital spectrometer equipped with a prism detector, at Shipley Ltd.,

Coventry. All samples were coated with carbon prior to analysis, but the samples still experienced "break-up" under the electron beam.

2.1.14 CHN ANALYSIS

Samples were weighted using a Mettler ultra micro balance (7 decimal places) and sealed in tin capsules. Analysis was performed using a Leeman Laboratories CE440 elemental analyser. Repeat analysis was performed on every sample to ensure reproducibility.

2.1.15 TENSILE TESTING

All samples were tested at Morton International Ltd., Coventry using a Nene M2 tensometer equipped with a 500 N load cell.

2.1.16 OPTICAL MICROSCOPE

Photographs of the surface of cured-LP films were obtained at a magnification of 300 times using an Olympus BH-2 light microscope equipped with Nomarski differential interference contrast objectives. The microscope was fitted with an Olympus PM-10AK microphotographic system.

2.1.17 PYROLYSIS OF SAMPLES IN THE OVEN

Extensive pyrolysis of all polymer samples over long periods of time were carried out in a fan-assisted Gallenkamp Hotbox model oven. The oven temperature

was closely monitored with a Cu/Con thermocouple and a stability of $\pm 0.5^0$ C was attainable.

2.1.18 PHOTOLYSIS OF SAMPLES

Extensive photolysis of polymer samples over long periods of time were carried out using various UV sources as set out below.

2.1.18.1 350 W XENON LAMP

Preliminary studies of LP photodegradation were carried out using a Eurosep Instruments model no. FO160000 350 W air-cooled xenon lamp. No filters were used, see table 2.3 in section 2.3.6 for the light output of the xenon lamp. The pre-polymer films were normally mounted onto a sodium chloride plate and photolysed directly in air at a distance of approximately 10 cm.

2.1.18.2 UV_B WEATHEROMETER

Photodegradation studies of bulk pre-polymer samples and cured LP films were carried out using a QUV accelerated weathering tester at Morton International Ltd., Coventry. UVB-313 fluorescent lamps, purchased from the Q-Panel Company, Bolton, were installed in the "Weatherometer" for all experiments except for the experiment whereby UV_A radiation was monitored and then UVA-340 fluorescent lamps were installed in the instrument. See table 2.4 in section 2.3.6 for the light output of UV_B lamps.

2.1.18.3 SOL-2 LIGHT BOX.

Photodegradation studies of cured-LP cast blocks and 'H' block samples were all carried out using a dr. Honle Sol-2 light box, at Morton International Ltd., Coventry. A sunlight simulation bulb purchased from the manufacturer was installed, and no filters were used.

2.2 CHEMICALS

2.2.1 POLYMERS

Commercially–available LPs, sold under the name Thiokol® LPs, were obtained from Morton International Ltd; their general size characteristics are summarised in Table 2.2. LPs have the general structure:

$$H(-S-C_2H_4-O-CH_2-O-C_2H_4-S-)_nH$$

TABLE 2.2: General properties of LPs.

LP code no	≈ RMM	'n' value	% branching agent/ moles %	Average SH content/ moles kg^{-1}	Average viscosity @ 25^0 C /Pa s
1400C	1000	7	0	2.06	1.15
33	1000	7	0.5	1.75	1.75
3	1000	7	2.0	2.06	1.15
980C	2600	16	0.5	0.91	12.5
977C	2600	16	2.0	0.91	12.5
541C	4000	24	0	0.53	46.5
12C	4000	24	0.2	0.53	46.5
32C	4000	24	0.5	0.53	46.5
2C	4000	24	2.0	0.60	46.5
31	8000	42	0.5	0.38	62.5

Other LPs were also obtained from Morton and are as follows:

(i) Model A. This was considered to be an exceptionally pure LP, *i.e.* free from material with variant mers, with an approximate relative molecular mass of *ca* 2600.

(ii) ZL–2264. This polysulfide has the general formula:

$$H(SC_2H_4OC_2H_4OC_2H_4S)_nH,$$

i.e. the oxymethylene unit in a normal LP is replaced by oxyethylene.

(iii) ELP–3. This polysulfide has the general formula:

$$\overline{OCH_2CHCH_2}(SC_2H_4OCH_2OC_2H_4S)_nCH_2\overline{CHCH_2O}$$

i.e. the terminal thiol groups are replaced by oxirane units, and it has a RMM *ca.* 1000.

2.2.2 SOLVENTS

Chloroform-d_1: 99.8 %, Fluorochem Ltd.

THF, MeOH, DMF, $CHCl_3$, $C_6H_5CH_3$: 99.8 %, HPLC grade, Fisons.

2.2.3 SALTS AND MATRICES FOR MASS SPECTROMETRIC ANALYSIS

NH_4Cl, KI: 99.9 %, Fisons.

NaCl, KCl : 99 %, Aldrich.

Trifluoroacetate acid (ammonium salt): 98%, Aldrich.

Silver trifluoroacetate: 98%, Aldrich.

3-nitrobenzyl alcohol: 99 %, Aldrich.

9-nitroanthracene: 97%, Aldrich.

2,5-Dihydroxybenzoic acid: 99 %, Aldrich.

Dithranol: 98 %, Aldrich.

2.2.4 CURATIVE AGENTS

Activated MnO_2 FA: 74-79 %, Hoechst UK Ltd.

Sodium Perborate Monohydrate: 98 %, Laporte Organics.

TBHP: 70 % aqueous solution, Laporte Organics.

HDDA: 90 %, Aldrich.

2.2.5 POTENTIAL STABILISING SYSTEMS

Carbon Black (Elflex 415): Cabot Leinden Technical Centre.

Tinuvin 1130: Ciba Additives.

Tinuvin 292: Ciba Additives.

$CuCl_2$, KI : 99.9 % Fisons.

2.2.6 OTHER CHEMICALS USED IN LP-CURED FORMULATIONS

Adhesion Promotor, Siquest A187: OSi Ltd.

Tetra-methylthiuram disulfide (TMTD)-Robinson Brothers, UK.

Tributylamine: 99 %, Aldrich.

Sodium hydroxide: 97 %, Aldrich.

2.2.7 OTHER CHEMICALS USED IN CONSTRUCTION SEALANTS FOR XPS SURFACE STUDIES.

Plasticiser, Cereclor 63L: ICI Plc.

Hydrocarbon resin, (used as an adhesion promoter) Necires EPX L5: Neville

Cindu B.V.

Thixatrope, Thixatrol ST: Redland Minerals.

Titanium Dioxide, used as a whitner: Tioxide Ltd.

$CaCO_3$ filler, Winnofil SPT: ICI Plc.

$CaCO_3$ filler, Polcarb S: English China Clay International Ltd.

Sulfur flowers: Fisons

NB: Where possible LPs were cured/formulated using the chemical suppliers that Morton International Ltd., Coventry, recommend to their customers.

2.2.8 CHEMICALS USED IN THE DETERMINATION OF SH

Pyridine: AnalaR grade, 99.5 %, Fisons.

Starch indicator solution: Aldrich

Iodine solution: 0.1 N, see section 2.3.1

Sodium thiosulfate Solution: 0.1 N, AnalaR grade, BDH.

2.2.9 COLUMN CHROMATOGRAPHY

Silica Gel 60: Particle size 0.040-0.063 mm (230-400 mesh ASTM), Merck.

Sand: Low in iron, 40-100 mesh, Fisons.

2.3 EXPERIMENTAL PROCEDURES

2.3.1 TITRIMETRIC ESTIMATION OF THIOL

The primary mercaptan content of each LP used was calculated using a titrimetric method which is a standard testing procedure of Morton Thiokol[3,4].

Between 0.5 to 1.0 grams of LP (weight depending on the approximate RMM of the LP) is weighed accurately into a Erlenmeyer flask and 50 ml of pyridine is added to dissolve the sample. The sample is then titrated against a standardised 0.1 N aqueous iodine solution until the colour changes from clear to pale yellow.

The mercaptan content is calculated as follows:

$$\frac{(\text{ml of } I_2) \times (\text{normality of } I_2) \times 3.307}{\text{weight of LP}}$$

The 0.1 N iodine solution was prepared by dissolving 50 grams of potassium iodide in 100 ml of distilled water; 12.69 grams of iodine crystals were added. This solution was then made up to a litre in a volumetric flask using distilled water. The solution was standardised by titrating against a 0.1 N solution of thiosulfate using starch as indicator until a light blue end-point is reached.

$$\text{Normality of } I_2 = \frac{2.5}{\text{ml } I_2}$$

2.3.2 PREPARATION OF CURED THIN FILMS OF LP

Thin films were cured onto plastic sheets using an appropriate curing agent:

i) MnO_2: addition as stated in experiment.

ii) $NaBO_3$: 1 mole of perborate to every mole of thiol present in the LP, 3 parts per hundred rubber (phr) of 0.5 M NaOH was added to accelerate cure.

iii) TBHP: Unless otherwise stated, 1 mole of TBHP was added for every mole of thiol; 1 phr tributylamine was added to accelerate the rate of cure.

When fully cured, these films were removed from the plastic support and mounted onto cardboard, see fig 6.3. To ensure that films of the same thicknesses were used during experiments, films were selected with comparable IR absorptions at various reference peaks, e.g. 791 cm^{-1} .

2.3.3 PREPARATION OF CURED CAST BLOCKS OF LP

The LP and curative were mixed together and allowed to cure in a plastic dish 50 mm diameter x 18 mm (supplied by Sterilin). The MnO_2-, $NaBO_3$- and TBHP-cured cast blocks were prepared in the same ratios as for the thin films in section 2.3.2.

For HDDA cured cast blocks, 1 mole of acrylate was added for every 2 moles of thiol, while 1 phr of tributylamine was added to accelerate the cure.

2.3.4 PREPARATION OF 'H' BLOCK SAMPLES

'H' block assemblies were constructed, each consisting of a 12 mm x 12 mm x 50 mm bead of cured LP (sealant mixture) held between parallel plates of clear float window glass (50 mm x 50 mm x 6 mm), using spacer bars, see fig.2.4. The assemblies were held together securely using tape to prevent movement during the seven day curing period.

Fig.2.4: 'H' block assembly used.

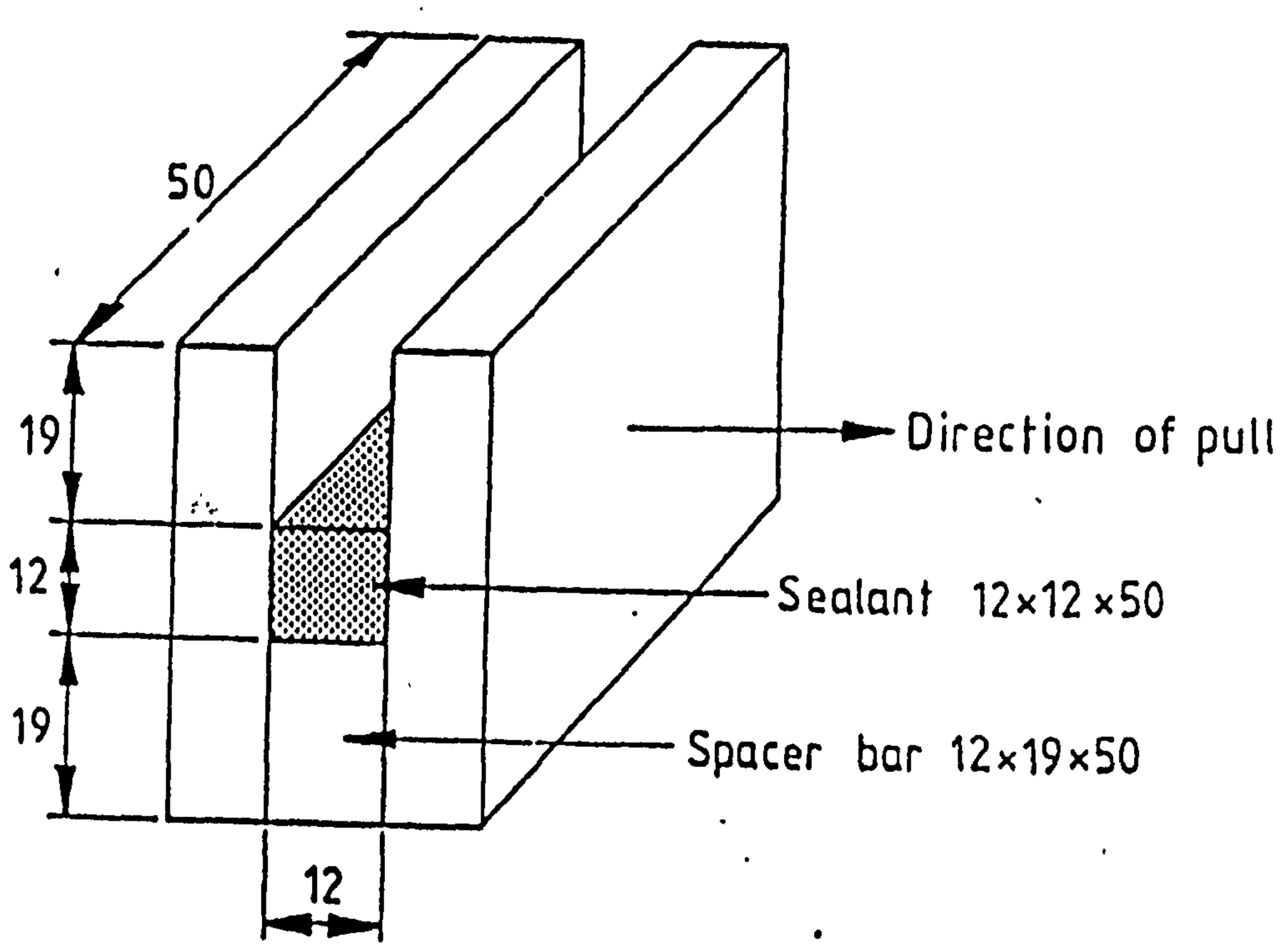

2.3.5 FORMULATION OF CONSTRUCTION SEALANT

The construction sealants examined by XPS, see section 8.1, were prepared to a standard formulation for a two part polysulfide construction sealant. Details were supplied by Morton International[5]:

Ingredient	Parts by Weight
Part A:	
LP-32C	100
Cereclor 63L	60
Necires EPX L5	5
Thrixatrol ST	5
Titanium dioxide RCR2	10
Winnofil SPT	45
Polcarb S	50
Sulfur	0.1
Part B:	
Manganese dioxide FA	10
Cereclor 63L	12
Tetra-methyl thiuram disulfide	0.5

Weight mix ratio: Part A : Part B
275.1 : 22.5

2.3.6 ACTINOMETRY

The light outputs of the xenon lamp and UV_B 'Weatherometer' have been determined using the method of Hatchard and Parker[6], which is based on the photodecomposition of potassium ferrioxalate to yield Fe^{2+} ions which are estimated colorimetrically using 1,10-phenanthroline.

TABLE 2.3 Actinometry results for 350 W xenon lamp.

t /s	Vol / cm^3	Abs	C_{FeII} / 10^{-6}M	C* / 10^{-4}M	n_{FeII} / 10^{-6}M	N/ t / 1.25 /10^{-16}	N /A^2s^{-1}
29.8	2.80	0.2805	12.52	12.4	3.47	5.61	5.61
30.1	2.80	0.2840	12.68	12.56	3.52	5.63	5.63

TABLE 2.4 Actinometry results for UV_B 'Weatherometer'

t /s	Vol / cm^3	Abs	C_{FeII} / 10^{-6}M	C* / 10^{-4}M	n_{FeII} / 10^{-6}M	N/ t / 1.25 /10^{-16}	N /A^2s^{-1}
300	2.80	1.175	5.25	5.20	1.456	2.34	2.34
300	2.80	1.188	5.30	5.25	1.470	2.36	2.36
300	2.80	1.168	5.21	5.16	1.445	2.32	2.32
300	2.80	1.306	5.83	5.78	1.618	2.60	2.60
300	2.80	1.300	5.80	5.75	1.610	2.58	2.58
300	2.80	1.310	5.85	5.80	1.624	2.61	2.61

CHAPTER 2

REFERENCES

1. Mazurek, W., Moritz, A.G., *Macromolecules,* **24**, (1991) 3261.

2. Coates, R.J., Gilbert, B.C., Lee, T.C.P., *J. Chem. Soc., Perkin Trans 2,* (1992) 1387.

3. Berenbaum, M.B., Marck, H.F., Gaylord, N.G., Birkel, N.M., *Encyclopedia of Polymer Science and Tech.*, John Wiley and Sons, New York, **2**, (1969) 445.

4. Morton Thiokol standard testing procedures, *Primary Mercaptan Content,* method number MPQC-37.

5. Morton Thiokol formulation for construction sealant B235M.

6. Hatchard, C.G., Parker, C.A., *Proc. Roy. Soc.*, London. **A235**, (1956) 518.

CHAPTER 3

CHARACTERISATION OF LINEAR POLYSULFIDES BY ELECTROSPRAY IONISATION MASS SPECTROMETRY

3.1 GENERAL FEATURES

All LPs listed in table 2.2 formed singly charged positive ions of the type $[M+NH_4]^+$ when the THF/MeOH/aq.NH_4Cl mobile phase was used. A typical ESI MS spectrum of LP-1400C is shown in fig. 3.1. The complex spectra given by all LPs can be rationalised by postulating the coexistence of several series of oligomers within a single type of LP; each member of each series differs in mass from its neighbours in the same series by 166 Daltons (Da), which corresponds to the most common repeat unit ($SC_2H_4OCH_2OC_2H_4S$). These various different series are labelled by letter (A,B,C...) in Fig. 3.1 and the assignments of individual peaks within each series for LP–1400C are summarised in Table 3.1.

TABLE 3.1 Assignments of principal peaks in the ESI spectrum of LP–1400C ("extra" groups are denoted in bold font)

Series A $H(SC_2H_4OCH_2OC_2H_4S)_nH.NH_4^+$

n	*m/z*
9	1514.6
8	1348.6
7	1182.6
6	1016.5
5	850.5
4	684.4
3	518.4

Series B $H(SC_2H_4OCH_2OC_2H_4S)_n(C_2H_4OCH_2OC_2H_4S)H.NH_4^+$
(*i.e.* one –S–S– link replaced randomly by –S–)

n	*m/z*
8	1482.6
7	1316.6
6	1150.7
5	984.5
4	818.7
3	652.6
2	486.4

Series C $H(SC_2H_4OCH_2OC_2H_4S)_n(SC_2H_4OC_2H_4OCH_2OC_2H_4S)H.NH_4^+$
(*i.e.* one mer unit contains an extra oxyethylene link)

n	*m/z*
7	1392.5
6	1226.6
5	1060.5
4	894.5
3	728.4
2	562.4

Series D $H(SC_2H_4OCH_2OC_2H_4S)_n(SC_2H_4OCH_2OCH_2OC_2H_4S)H.NH_4^+$
(*i.e.* one mer unit contains extra oxymethylene link)

n	*m/z*
6	1212
5	1046
4	880
3	714
2	548

Series E $H(SC_2H_4OCH_2OC_2H_4S)_n(SC_2H_4OC_2H_4OCH_2OC_2H_4S)_2H.NH_4^+$
(*i.e.* two mer units contain an extra oxyethylene unit).

n	*m/z*
6	1436
5	1270
4	1104
3	938.5
2	772.4
1	606.5
0	440.5

Series F

$H(SC_2H_4OCH_2OC_2H_4S)_n(SC_2H_4OC_2\mathbf{H_4O}CH_2OC_2H_4S)(SC_2H_4OCH_2O\mathbf{CH_2O}C_2H_4S)H.NH_4^+$

(*i.e.* one mer unit contains an extra oxyethylene unit and one contains an extra oxymethylene unit.

n	*m/z*
5	1256
4	1090
3	924
2	758
1	592
0	426

Series G $H(SC_2H_4OCH_2OC_2H_4S)_n(SC_2H_4OC_2\mathbf{H_4O}CH_2OC_2H_4S)(C_2H_4OCH_2OC_2H_4S)H.NH_4^+$

(*i.e.* one mer unit contains an extra oxyethylene unit while another has an –S– link replacing –S–S–).

n	*m/z*
5	1194
4	1028
3	862
2	696
1	530

Series H

$H(SC_2H_4OCH_2OC_2H_4S)_n(SC_2H_4OC_2\mathbf{H_4O}CH_2OC_2H_4S)_2(SC_2H_4OCH_2O\mathbf{CH_2O}C_2H_4S)H.NH_4^+$

(*i.e.* two mer units contain an extra oxyethylene unit while one contains an extra oxymethylene unit).

n	*m/z*
5	1467
4	1301
3	1135
2	968.6
1	802.6
0	636.5

Series I

$H(SC_2H_4OCH_2OC_2H_4S)_n(C_2H_4OC_2\mathbf{H_4O}CH_2OC_2H_4S)(SC_2H_4OC_2\mathbf{H_4O}CH_2OC_2H_4S)H.NH_4^+$

i.e one mer unit contains an extra oxyethylene unit while one contains an extra oxyethylene unit and either it or another mer unit has an –S– link instead of an –S–S– link. This series, while clearly apparent, is of only weak intensity..

n	*m/z*
7	1570
6	1405
5	1238
4	1072
3	906
2	740

Series J $H(SC_2H_4OCH_2OC_2H_4S)_n(SC_2H_4OCH_2O\mathbf{CH_2O}C_2H_4S)_2H.NH_4^+$

(*i.e.* Two mer units contain an extra oxymethylene unit. This series, while clearly apparent with some LPs (see Table 3.2), is not apparent in LP–1400C).

Series K

$H(SC_2H_4OCH_2OC_2H_4S)_n(SC_2H_4O\mathbf{C_2H_4O}C_2H_4O\mathbf{C_2H_4O}C_2H_4S)(SC_2H_4O\mathbf{C_2H_4O}CH_2OC_2H_4S)H.NH_4^+$

(*i.e.* Three extra oxyethylene groups are present, possibly in three separate mers or with two extra in a single mer and one in another mer. This series, while clearly apparent with some LPs (see Table 3.2), is not apparent in LP–1400C).

This type of spectrum was obtained with a variety of LPs as indicated by figs. 3.2 and 3.3, from which the situation can be summarised with series having the general formula.

$H(SC_2H_4OCH_2OC_2H_4S)_{n-1}$ (variant mer) $H.NH_4^+$

or $H(SC_2H_4OCH_2OC_2H_4S)_{n-2}$ (variant mer) (variant' mer) $H.NH_4^+$

or $H(S_2H_4OCH_2OC_2H_4S)_{n-3}$ (variant mer)$_2$ (variant' mer) $H.NH_4^+$

Thus it can be seen that all LPs contain series of the following composition, ('extra' groups are denoted in bold font):

Series A: Expected structure of LP and therefore shows no variant mer.

Series B: variant = $(C_2H_4OCH_2OC_2H_4S)$

Series C: variant = $(SC_2H_4O\mathbf{C_2H_4O}CH_2OC_2H_4S)$

Series D: variant = $(SC_2H_4OCH_2\,O\mathbf{CH_2O}C_2H_4S)$

Series E: variant = $(SC_2H_4O\mathbf{C_2H_4O}CH_2OC_2H_4S)$, variant' = $(SC_2H_4O\mathbf{C_2H_4O}\,CH_2OC_2H_4S)$

Series F: variant = $(SC_2H_4O\mathbf{C_2H_4O}CH_2OC_2H_4S)$, variant' = $(SC_2H_4OCH_2O\mathbf{CH_2O}C_2H_4S)$

Series G variant = $(SC_2H_4O\mathbf{C_2H_4O}CH_2OC_2H_4S)$, variant' = $(C_2H_4OCH_2OC_2H_4S)$

Series H: variant = $(SC_2H_4O\mathbf{C_2H_4O}CH_2OC_2H_4S)_2$, variant' = $(SC_2H_4OCH_2O\mathbf{CH_2O}C_2H_4S)$

Series I: variant = $(C_2H_4O\mathbf{C_2H_4O}CH_2OC_2H_4S)(SC_2H_4O\mathbf{C_2H_4O}CH_2OC_2H_4S)$

Series J: variant = $(SC_2H_4OCH_2O\mathbf{CH_2O}C_2H_4S)_2$

Series K: variant =$(SC_2H_4O\mathbf{C_2H_4O}CH_2OC_2H_4S)(SC_2H_4O\mathbf{C_2H_4O}\mathbf{C_2H_4O}CH_2OC_2H_4S)$

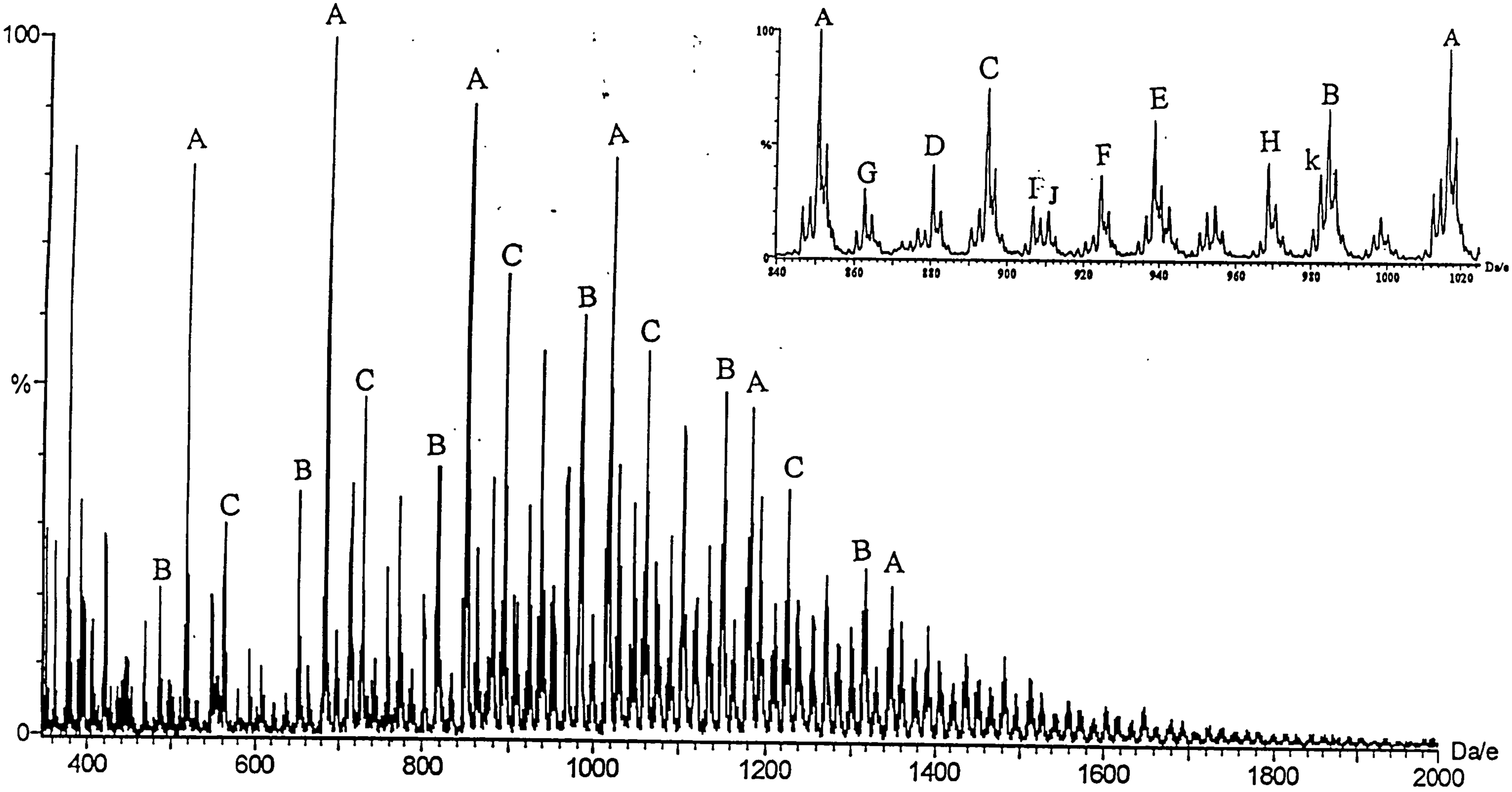

Fig.3.1: ESI spectrum of LP-1400C, mobile phase THF/MeOH containing 0.5% aqueous NH_4Cl. Insert: expansion of spectrum in *m/z* range 840-1020 to reveal greater detail. Assignments of ions are given *in Table 3.1.*

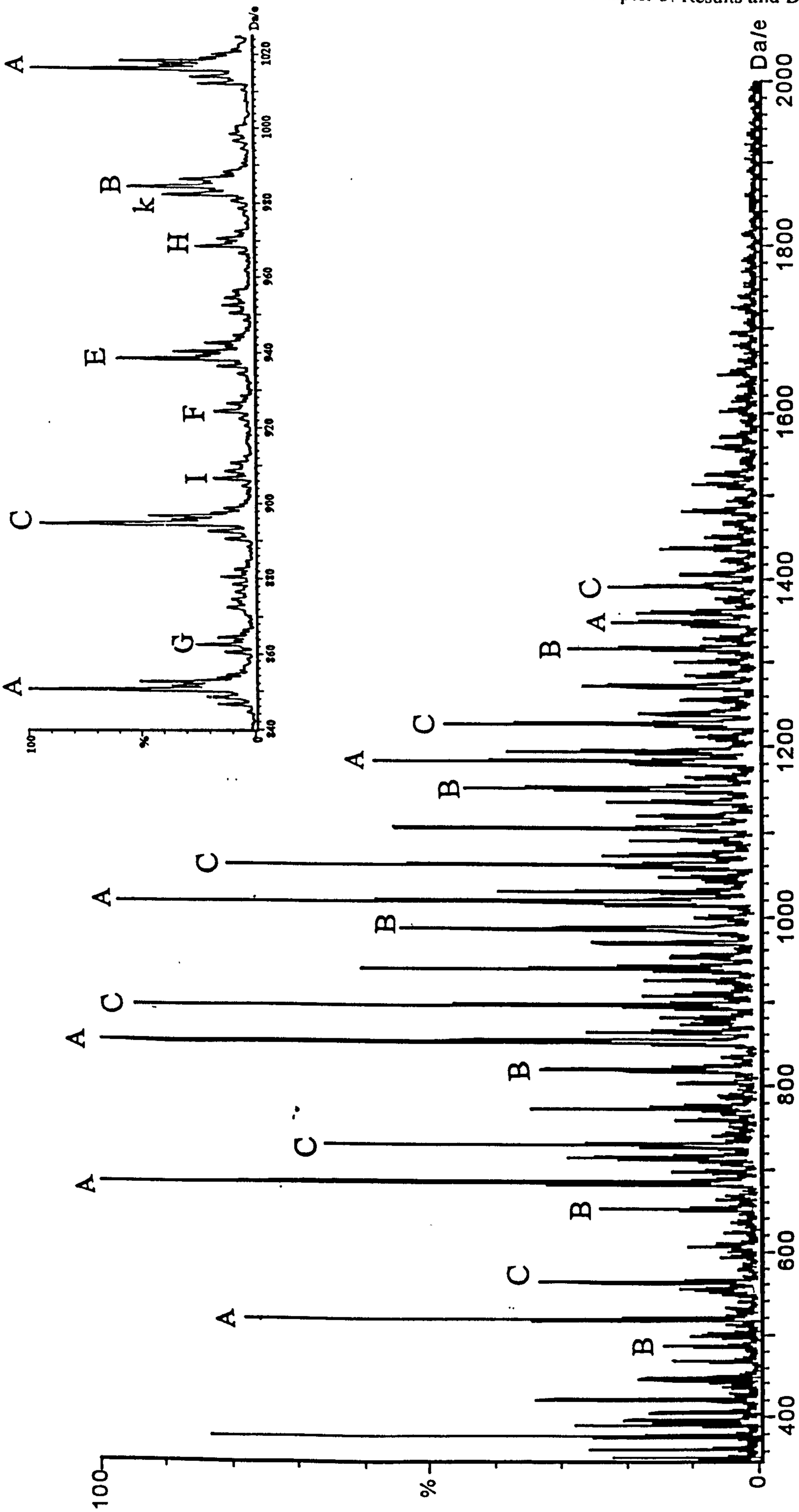

Fig.3.2: ESI spectrum of LP-980C, mobile phase THF/MeOH containing 0.5% aqueous NH_4Cl. Insert: expansion of spectrum in *m/z* range 840-1020 to reveal greater detail.

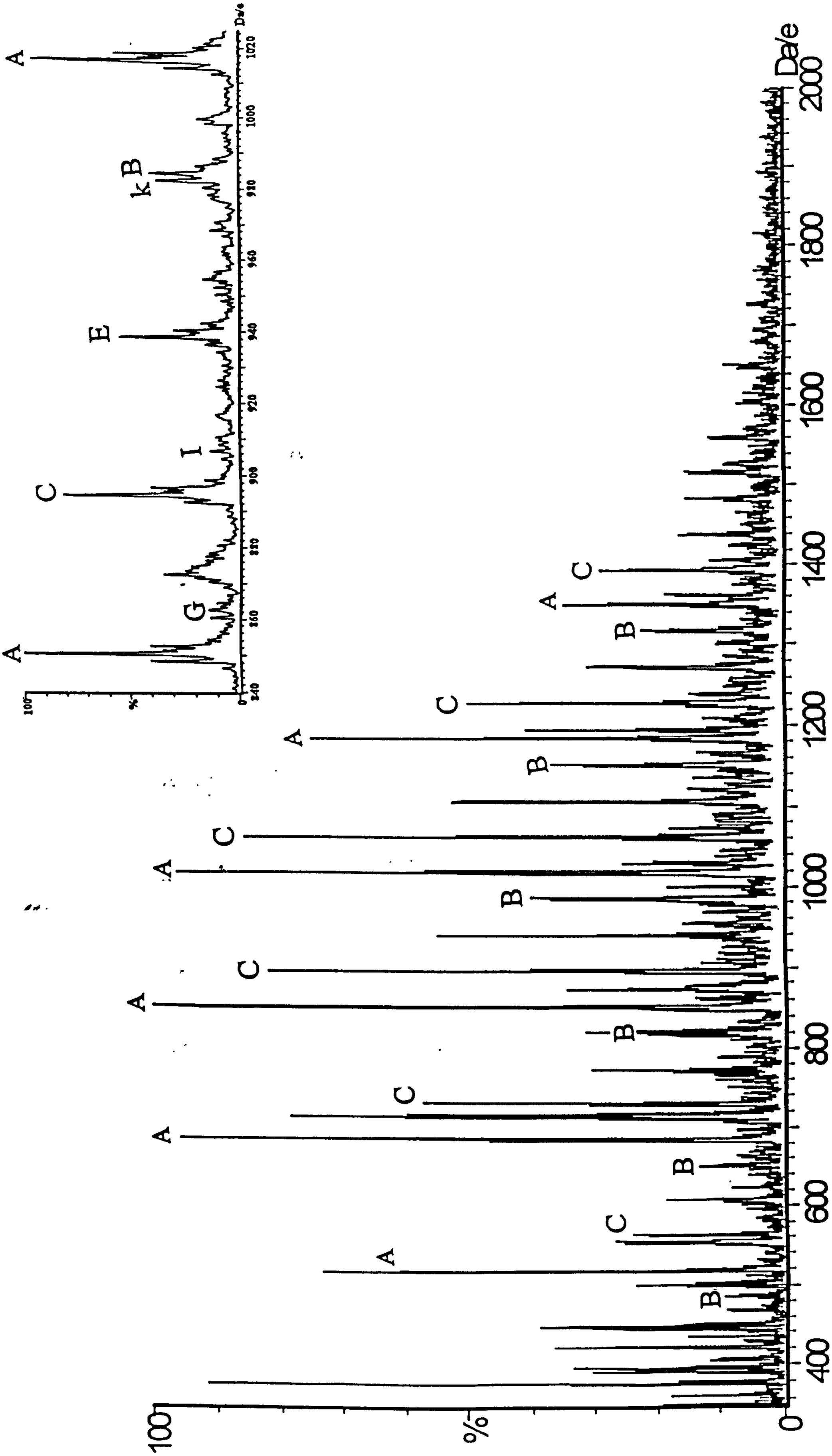

Fig.3.3: ESI spectrum of LP-12C, mobile phase THF/MeOH containing 0.5% aqueous NH_4Cl. Insert: expansion of spectrum in *m/z* range 840-1020 to reveal greater detail.

It should, however, be noted that

(i) the location of the variant mer(s) within the linear sequence is random

(ii) when there are several variants, these may be distributed between several mers or be located (at least partially) within a single mer.

Accordingly the designations given above refer to only one of several possible distributions of variants.

The degrees of prominence of particular series within the various LPs investigated are summarised in table 3.2.

TABLE 3.2 Level of appearance of series A to K in individual LPs.

Series	A	B	C	D	E	F	G	H	I	J	K
LP–1400C	s	s	s	w	m	w	w	w	w	x	x
LP–3	s	s	s	x	s	x	m	w	m	x	s
LP–33	s	s	s	m	s	w	w	m	w	w	w
LP–977C	s	m	s	w	w	w	w	x	w	x	w
LP–980C	s	m	s	x	m	w	w	w	w	x	w
LP–32C	s	m	s	x	m	x	w	x	x	x	m
LP–12C	s	m	s	x	m	x	w	x	w	x	w
LP–541C	s	m	m	w	w	w	x	w	w	x	w
LP–31C	m	w	m	x	w	x	x	x	x	x	w
ELP–3	s	w	s	w	m	w	w	w	w	x	w
Model A	s	m	w	x	x	x	x	x	x	x	x

s = strong, m = moderate, w = weak, x = little sign

The complex distributions observed in the ESI spectra of all ten LPs listed in Table 2.2 results both from the coexistence of polymers having a range of *n* values within a given series and the presence of several series of compounds that are based on 'anomalous' repeat units containing one less sulfur atom or additional oxymethylene and oxyethylene groups. This is not unexpected in view of the method of preparation of LPs[1]. From table 3.2 it can be seen that one series is very prominent in all the LPs, namely Series C with an extra oxyethylene link in one mer unit, while Series B

(lacking a single S atom) and Series E (with an extra oxyethylene link in two mer units) are the only other mers to show any prominence in several LPs. Series featuring three variants in the structure are either absent or barely detectable.

An exceptionally pure LP, model compound A, with an approximate relative molecular mass, (RMM), of *ca.* 2600 was also studied. As expected, this compound shows a simpler ESI spectrum, fig. 3.4, featuring only one significant series in addition to the expected series A, namely series B, i.e. with a single -S- link replacing -S-S-.

A summary of the spectral peaks observed in Model A is given in Table 3.3

TABLE 3.3 ESI spectral peaks and associated assignments in the spectrum of Model Compound A.

Series A $H(SC_2H_4OCH_2OC_2H_4S)_nH.NH_4^+$

n	*m/z*
10	1680.2
9	1514.0
8	1348.0
7	1182.1
6	1016.2
5	850.3
4	684.3
3	518.4
2	352.5

Series B $H(SC_2H_4OCH_2OC_2H_4S)_n(C_2H_4OCH_2OC_2H_4S)H.NH_4^+$
(*i.e.* One –S–S– link replaced randomly by –S–).

n	*m/z*
9	1648.1
8	1482.3
7	1316.3
6	1150.4
5	984.3
4	818.4
3	652.4
2	486.5

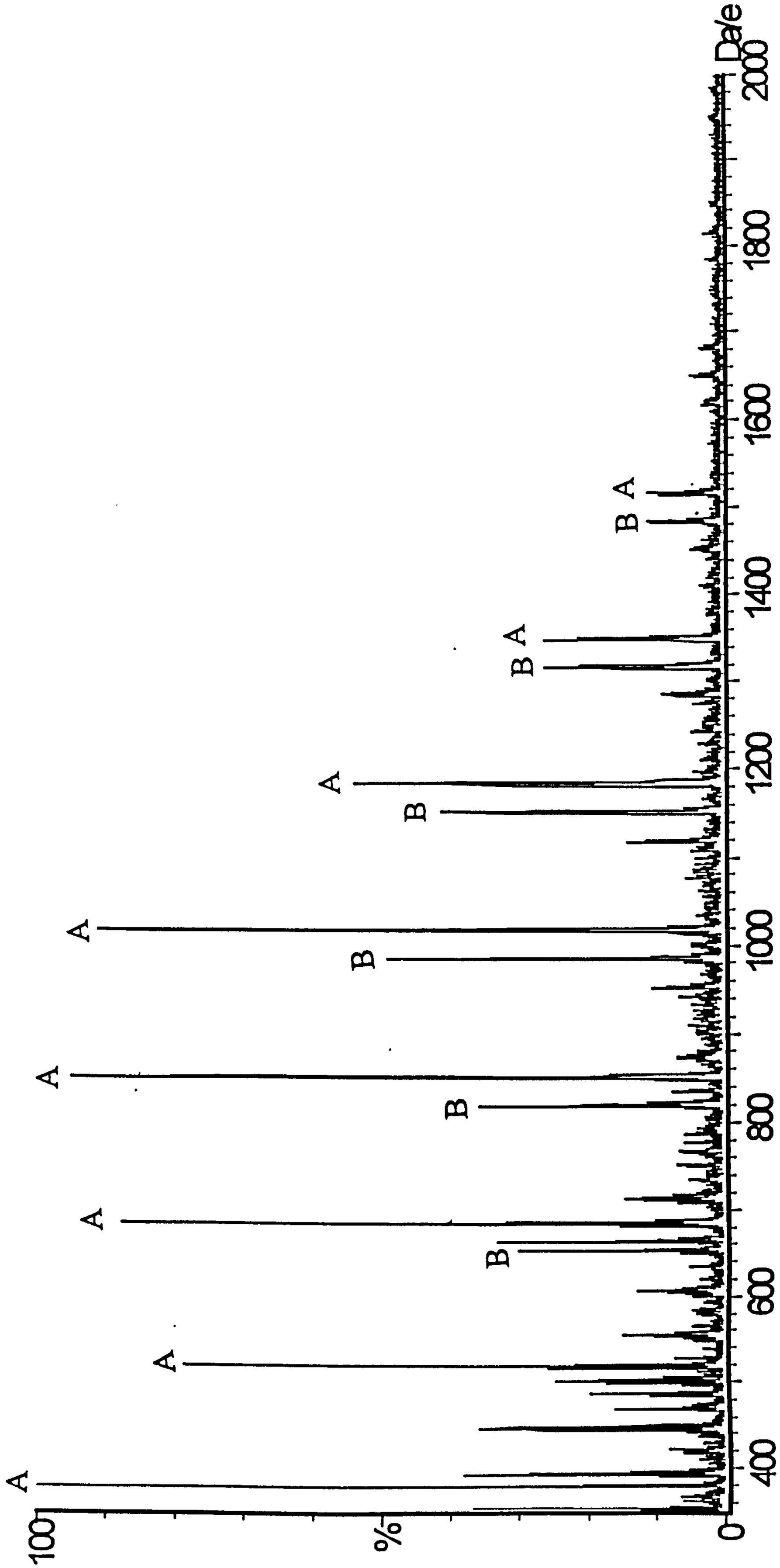

Fig.3.4: ESI spectrum of Model Compound A, mobile phase THF/MeOH containing 0.5% aqueous NH_4Cl.

3.2 EFFECT OF END GROUP

ELP–3 which contains terminal epoxy groups (section 2.2.1), produces an ESI spectrum, Fig. 3.5, displaying the usual series A–K with 166 Da separation but with different masses because of the end groups (the replacement of the thiol hydrogen by epoxy at each end increases the RMM by 112 over the LP analogue). For brevity, only assignments of Series A are given in Table 3.4.

TABLE 3.4 Assignments of principal peaks in Series A of the ESI spectrum of ELP–3

Series A $\overline{OCH_2CH}CH_2(SC_2H_4OCH_2OC_2H_4S)_nCH_2\overline{CHCH_2O}.NH_4^+$

n	*m/z*
9	1626.7
8	1460.7
7	1294.6
6	1128.5
5	962.5
4	796.5
3	630.6
2	464.6

The CID behaviour of ELP 3 is discussed in section 3.7

3.3 EFFECT OF MER UNIT

ZL-2264, an LP whereby the oxymethylene unit within the mer is replaced by oxyethylene was studied; this has the formula $H(SC_2H_4OC_2H_4OC_2H_4S)_nH$. The behaviour of this sample closely resembled that of model compound A, while the RMM of the mer unit ($SC_2H_4OC_2H_4OC_2H_4S$) is 180 Da, giving a larger peak–to–peak separation in each series. Variant mers are once again visualised in the ESI spectrum, Fig. 3.6, although these now refer solely to the presence of one or two

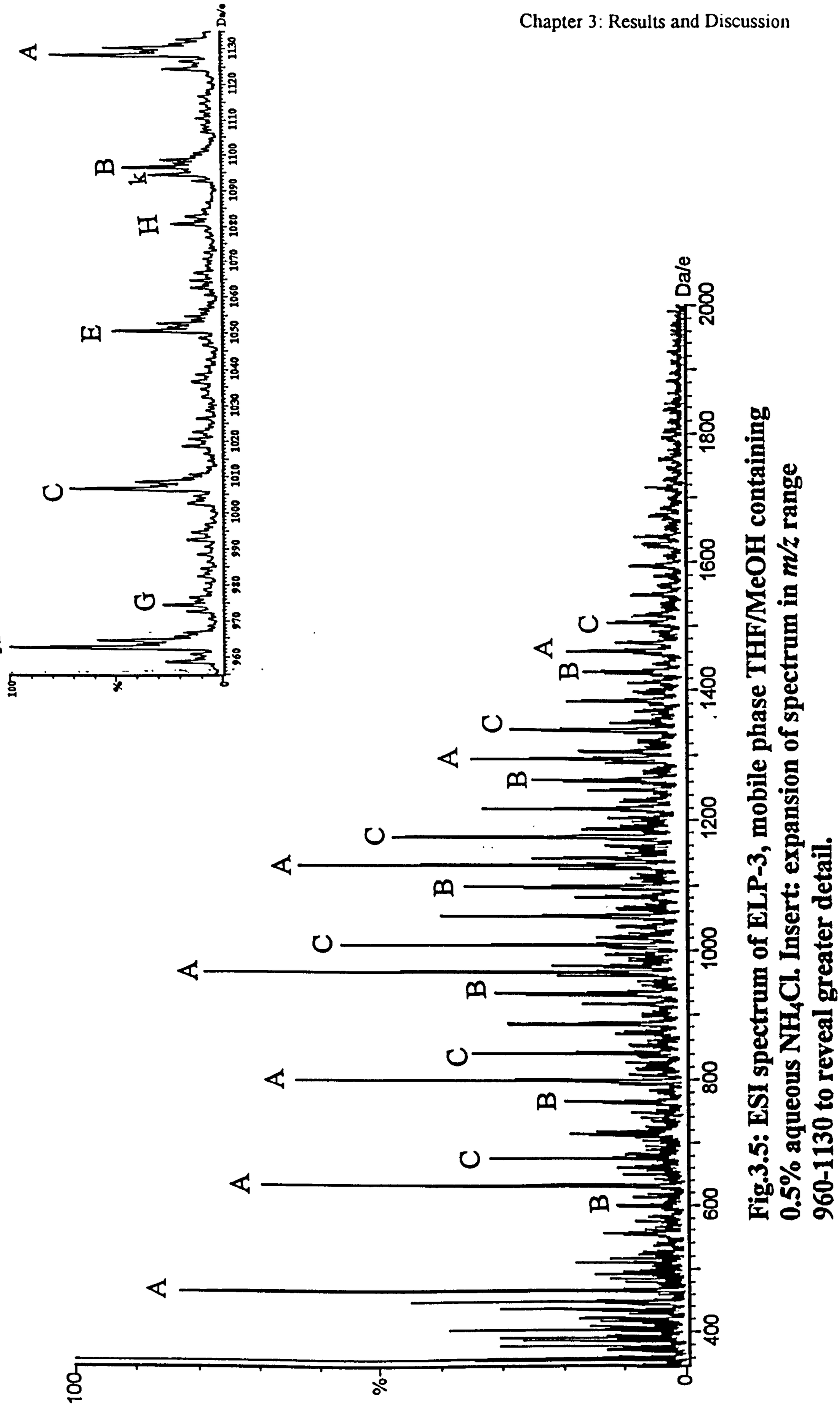

Fig.3.5: ESI spectrum of ELP-3, mobile phase THF/MeOH containing 0.5% aqueous NH_4Cl. Insert: expansion of spectrum in *m/z* range 960-1130 to reveal greater detail.

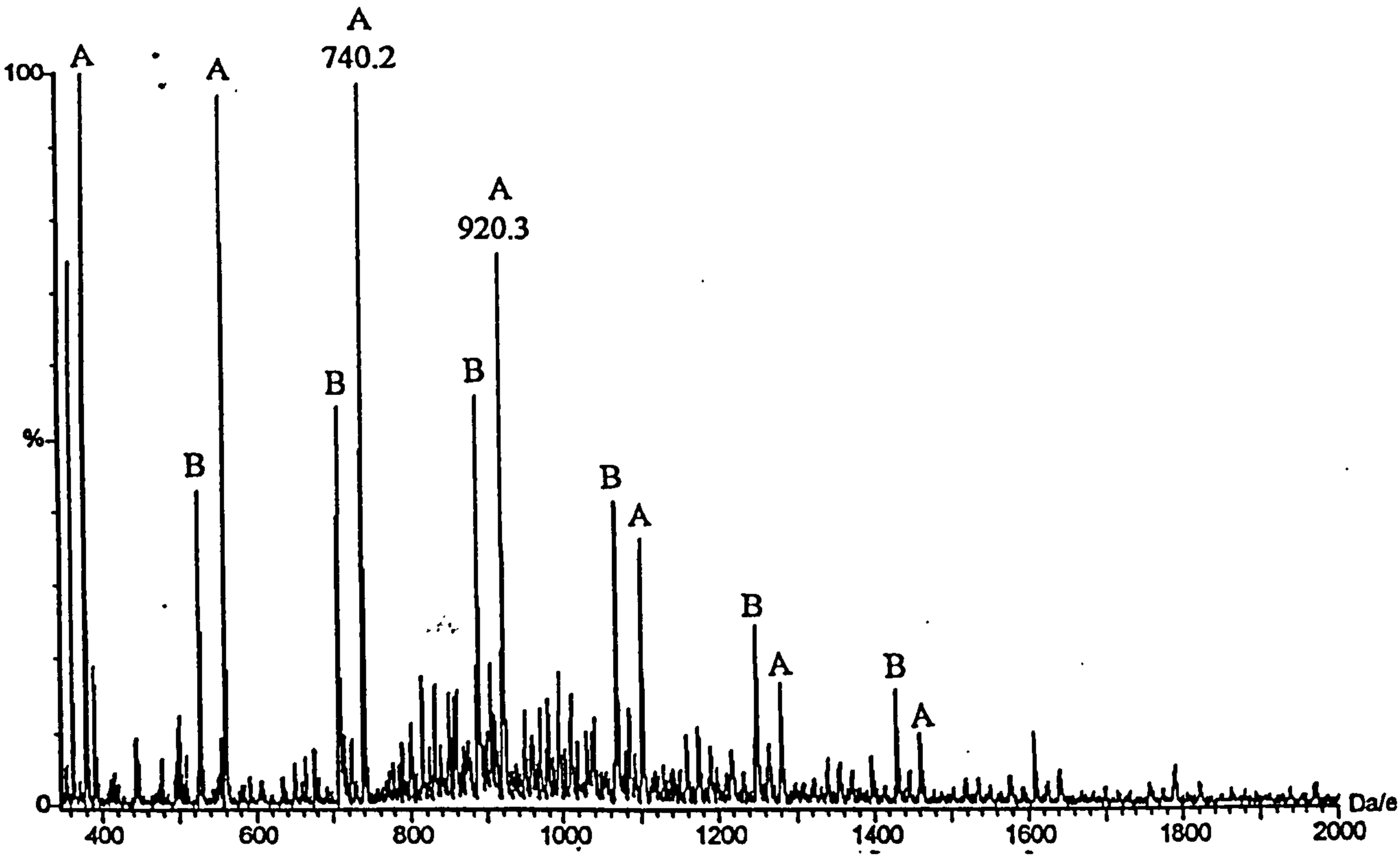

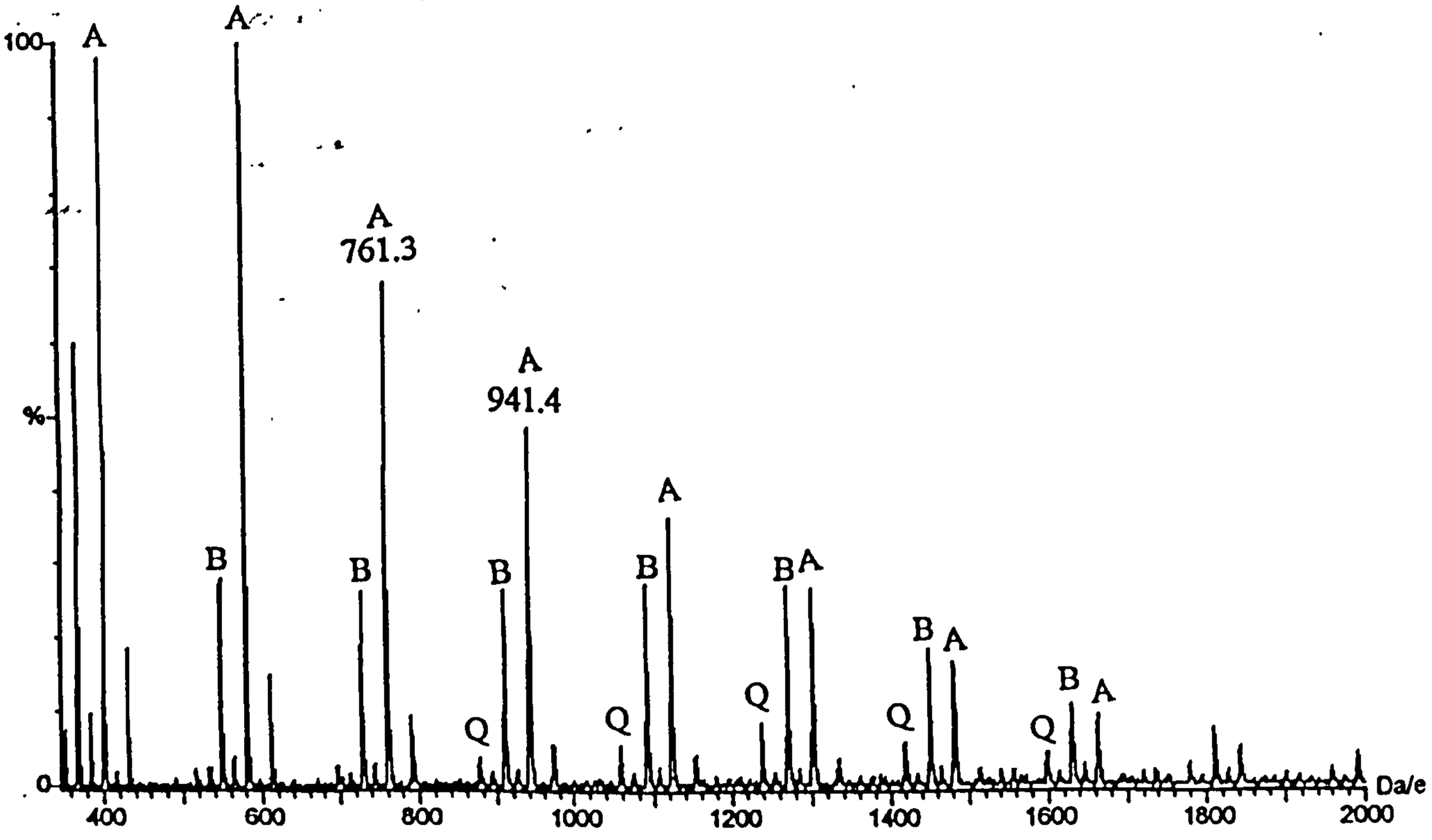

Fig.3.6: ESI spectra of ZL-2264 to compare effect of mobile phase on spectral quality: A) Mobile phase THF/MeOH containing 0.5% aqueous NH_4Cl. B) Acetone containing KI.

monosulfide links at the expense of disulfide links. The assignments of individual peaks are given in Table 3.5.

TABLE 3.5 ESI spectral peaks and associated assignments in the spectrum of ZL–2264.

Series A $H(SC_2H_4OC_2H_4OC_2H_4S)_nH.NH_4^+$

n	*m/z*
10	1820.1
9	1640.2
8	1460.2
7	1280.3
6	1100.2
5	920.3
4	740.2
3	560.5
2	380.4

Series C $H(SC_2H_4OC_2H_4OCH_4S)_n(SC_2H_4OC_2H_4OC_2H_4)H.NH_4^+$
(*i.e.* One –S–S– link replaced randomly by –S–)

n	*m/z*
10	1968.0
9	1788.7
8	1608.4
7	1428.2
6	1248.3
5	1068.3
4	888.3
3	708.4
2	528.4

Series Q $H(SC_2H_4OC_2H_4OC_2H_4S)_n(SC_2H_4OC_2H_4OC_2H_4)_2H.NH_4^+$
(*i.e.* Two –S–S– links have been replaced randomly by –S–).

n	*m/z*
9	1936.1
8	1756.4
7	1576.3
6	1396.5
5	1216.5

3.4 VARIATION OF THE COMPOSITION OF THE MOBILE PHASE.

All previous LP spectra referred to in this chapter were obtained using a mobile phase consisting of a 50/50 THF/MeOH mixture containing 0.5% aqueous NH_4Cl as an electrolyte to charge neutral LP molecules by forming 1:1 ion–molecule adducts, $[M.NH_4]^+$. Changing the mobile phase to an acetone solution of potassium iodide (0.5 mg/ml) resulted in two main effects, *viz.*,

(i) the level of baseline noise in the spectra was considerably reduced . see fig 3.6.

(ii) the K^+ ion adducts of the LP did not undergo dissociation with argon under CID conditions. The ready CID of NH_4^+ ion adducts is associated with initial loss of NH_3 leading to the H^+ ion adducts which then fragment on collision with argon.

3.5 EFFECT OF RMM OF LP.

The relative intensities of peaks in the ESI spectra are not in accord with the expected relative abundances of the various components based on GPC data and titration calculations for these LPs. Even LPs such as LP-2C and LP-12C, with a nominal RMM of approximately 4000, fail to give peaks at *m/z* values above 2000. Fig. 3.7. demonstrates that LPs of nominal RMMs 1000, 2600 and 4000 show very similar spectra with few peaks above *m/z* 1800.

It appears ESI gives a heavy bias towards the detection of low mass oligomers at the expense of those of higher mass. This problem does not seem due to lower solubility of the higher mass oligomers because changing the solvent to THF/DMF offered no advantage. It can therefore be concluded that LP ions of higher mass have

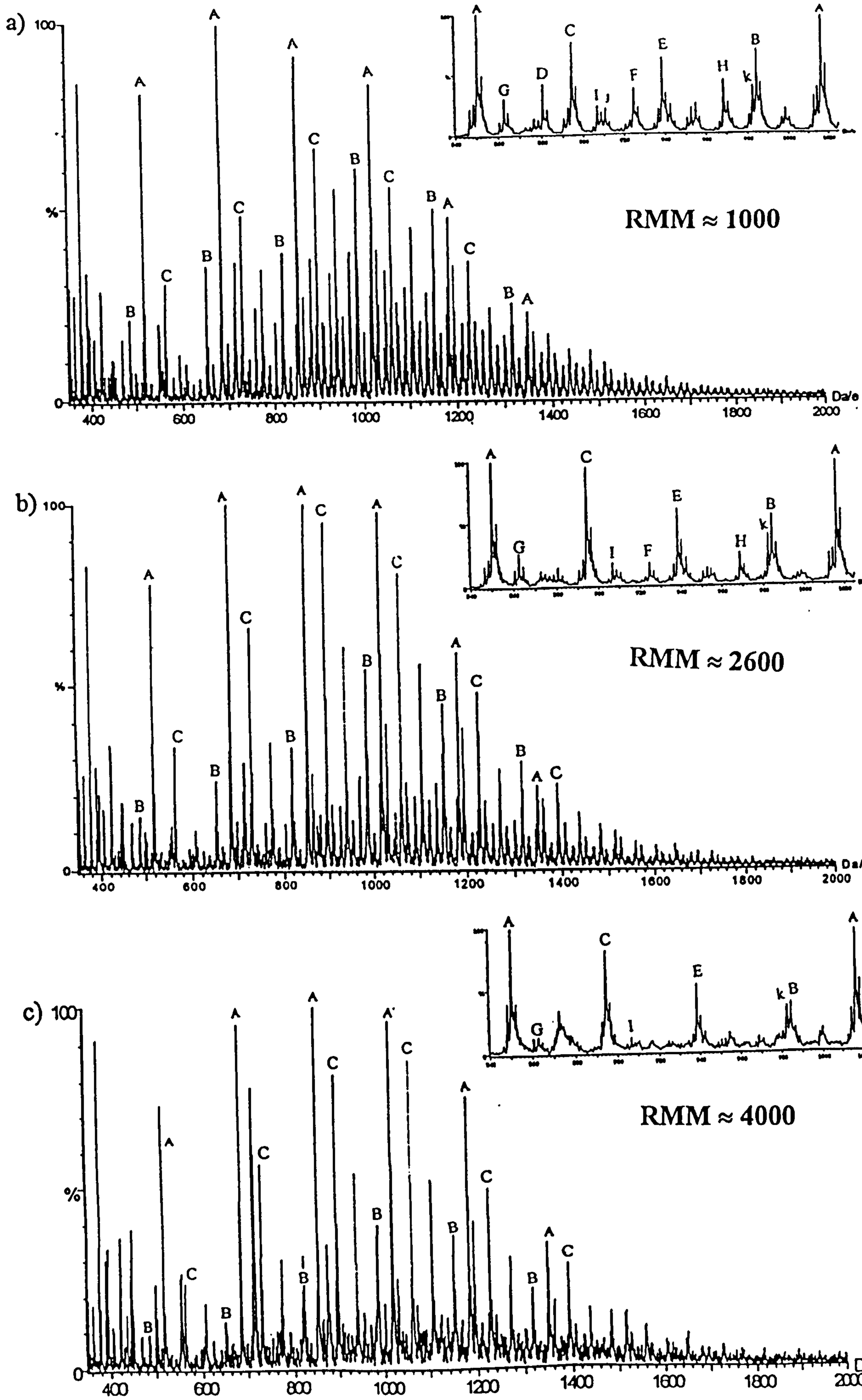

Fig. 3.7: ESI-MS spectra of LP pre-polymers of varying molecular weights: a) RMM ≈ 1000 b) RMM ≈ 2600 and c) RMM ≈ 4000. Mobile phase THF/MeOH containing 0.5 % aqueous NH_4Cl.

(i) a greater tendency to fragment before detection,

(ii) (less probably) transfer their charge to lower mass material, or

(iii) fail to be transmitted or detected.

That higher mass species derived from synthetic polymers **can** be detected by ESI has been demonstrated in the study of polystyrenes[2].

The possibility that the ions carry more than one charge can be ruled out since the separation of *m/z* 166 Da would be reduced to 83 for doubly charged ions or around 55 for triply charged, and ions with these separations are not observed.

3.6 VARIATION IN THE CONE VOLTAGE.

The CID of precursor ions produced in the ESI source was investigated without precursor ion mass analysis by studying the effect of increasing the cone voltage, all other conditions remaining constant. At low cone voltages (*e.g.* 20 V), little CID is expected to occur so that the spectrum shown in Fig. 3.8a is largely of precursor ions formed in the source. As the cone voltage is increased, more CID occurs leading to a reduction in the abundance of higher mass ions and a corresponding increase in the abundance of lower mass fragment ions. This is illustrated in Fig. 3.8b and 3.8c in which the ions of *m/z* 137, 167, 211 and 243 emerge as the dominant ions at high cone voltages. These ions are assigned the structures $(C_2H_4SSC_2H_4O)H^+$, $(SC_2H_4OCH_2OC_2H_4S)H^+$, $(SC_2H_4OCH_2OC_2H_4SC_2H_4O)H^+$ and $(SC_2H_4OCH_2OC_2H_4SSC_2H_4O)H^+$ respectively.

Under the relative mild CID conditions employed, ions of the monomer and terminal species are relatively stable and account for the major species giving rise to the spectra.

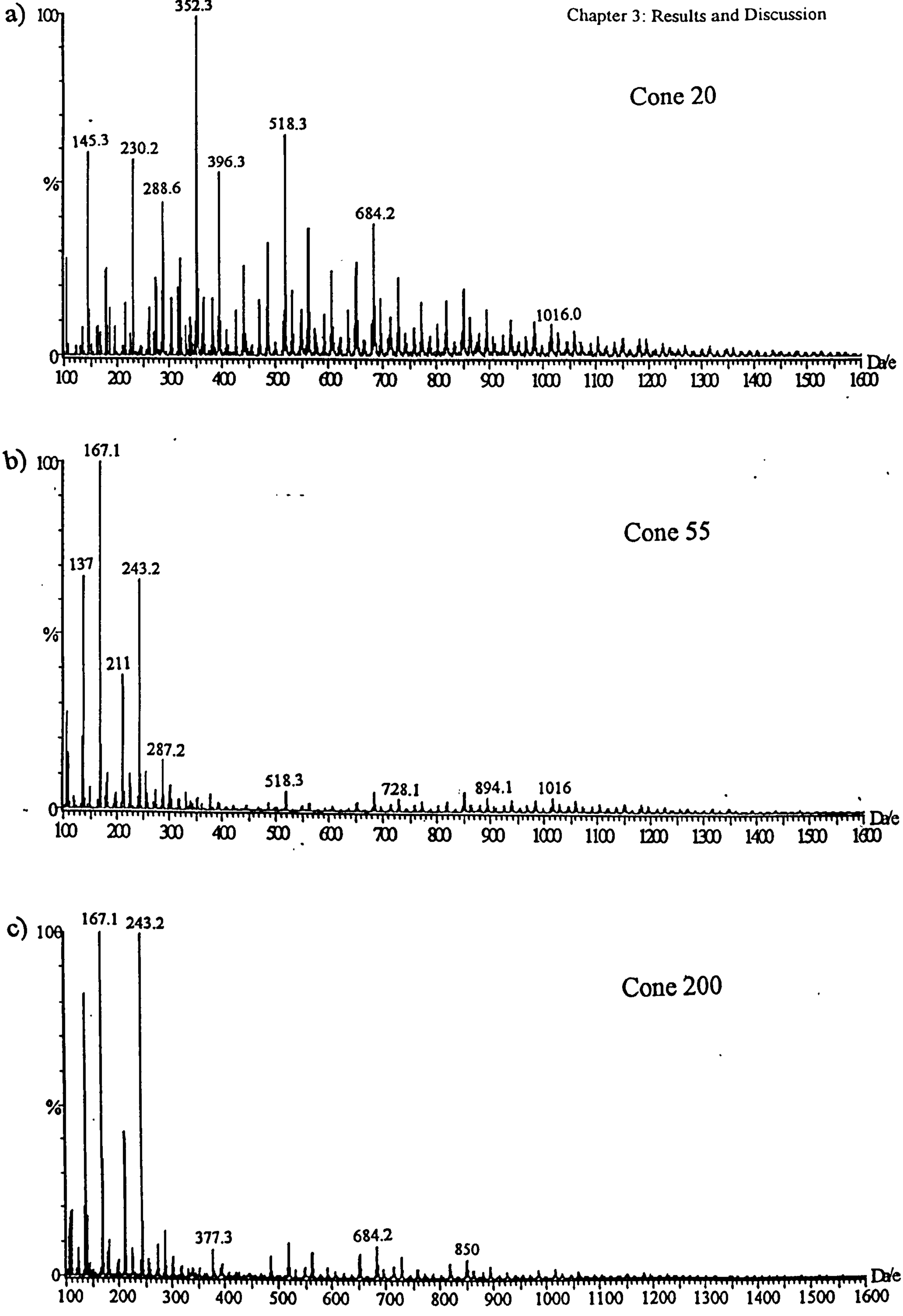

Fig.3.8: Effect of varying cone voltage on ESI mass spectrum of LP-1400C in a mobile phase of THF/MeOH containing 0.5% aqueous NH_4Cl (mass range 100-1600 Da). Each spectrum is normalised to its base peak.

Generally similar behaviour was exhibited when the cv was increased from 20 to 180 with a solution of ELP–3 in THF/MeOH/NH_4Cl: all the high–mass peaks up to 1128.1 disappeared on going from cv 20 to 60, and the intense *m/z* peaks at 281.3 and 298.3 found at cv 20 gave way at cv 60 to new peaks at 149.3, 223.3 and 243.2. At cv 90 the 223.3 peak was about 4 times as abundant as any other ion: this is attributed to the terminal species $\overline{OCH_2CHCH_2}SC_2H_4OCH_2OC_2H_4S^+$. The species with *m/z* 281.3 and 298.3 detected at low cv are assigned to $\overline{OCH_2CHCH_2}SC_2H_4OCH_2OC_2H_4SCH_2\overline{CHCH_2}OH^+$ and $\overline{OCH_2CHCH_2}SC_2H_4OCH_2OC_2H_4SCH_2\overline{CHCH_2}O.NH_4^+$ respectively, while the peak at 149.3 is attributed to $\overline{OCH_2CHCH_2}SC_2H_4OCH_3.H^+$.

3.7 CID AND PRECURSOR-ION EXPERIMENTS

The ESI spectra of LPs give rise to a number of well-defined series differing in *m/z* value within a given series by 166 Da, see figs. 3.1, 3.2 and 3.3. Identification of the origin of each individual series, and the nature of the parallel series, can be partially effected by the inspection of the mass differences between the members of parallel series. To confirm the assignments recorded in Table 3.1, especially where a degree of uncertainty may be attached to series containing "anomalous" repeat units, the CID spectra of selected ions of each series (A-H) for LP-1400C were recorded. These are exemplified in fig. 3.9. All fragment ions are formed with the initial loss of ammonia from the precursor ion; when CID experiments were attempted using the acetone/KI system no fragmentation was observed. The simplicity of the upper spectrum (fig.3.9a) for series A reflects the dominance of a particular mode of fragmentation and the symmetry of the precursor ion. The two major fragment ions

observed (*m/z* 167 and 243) correspond to simple cleavage while the ion at *m/z* 137 was shown by a precursor ion experiment (discussed in detail below) to be generated from the ion at *m/z* 167 via the loss of a CH_2O group.

Considering the ESI spectrum of LP–1400C (mobile phase THF/MeOH/0.5% aqueous NH_4Cl), the fragment ions result from the fragmentations:

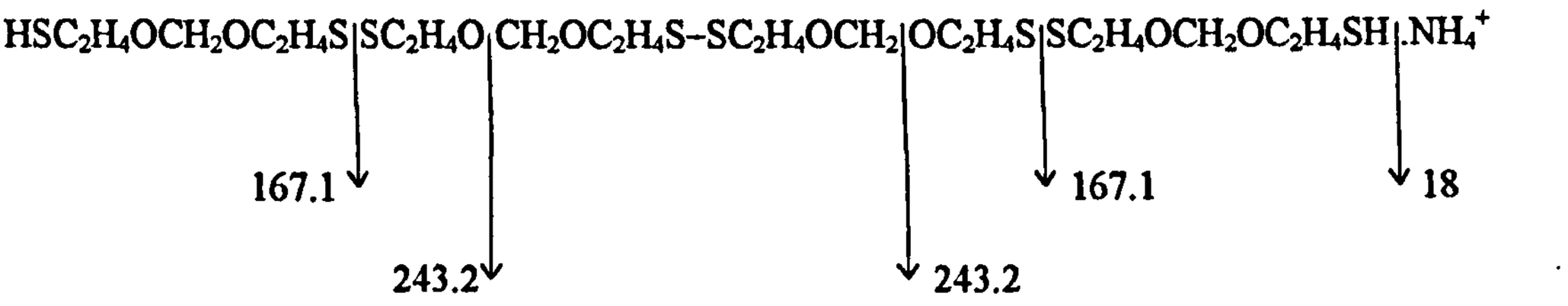

The simplicity of this CID spectrum accords with the high symmetry of the precursor ion. By contrast, the mass 652.4 ion from Series B produces a more complex CID spectrum attributable to the fragmentations:

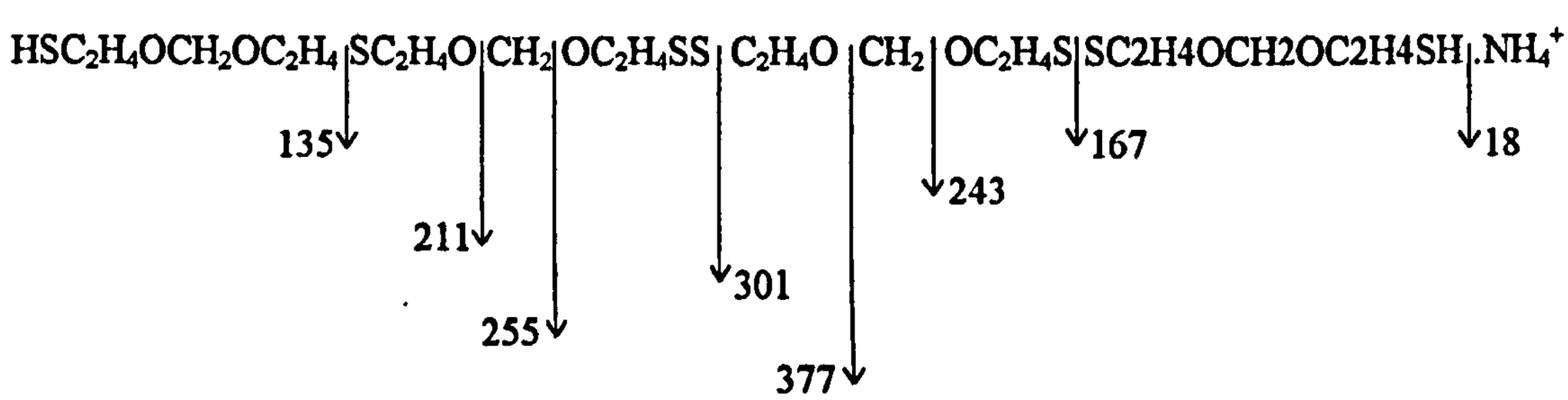

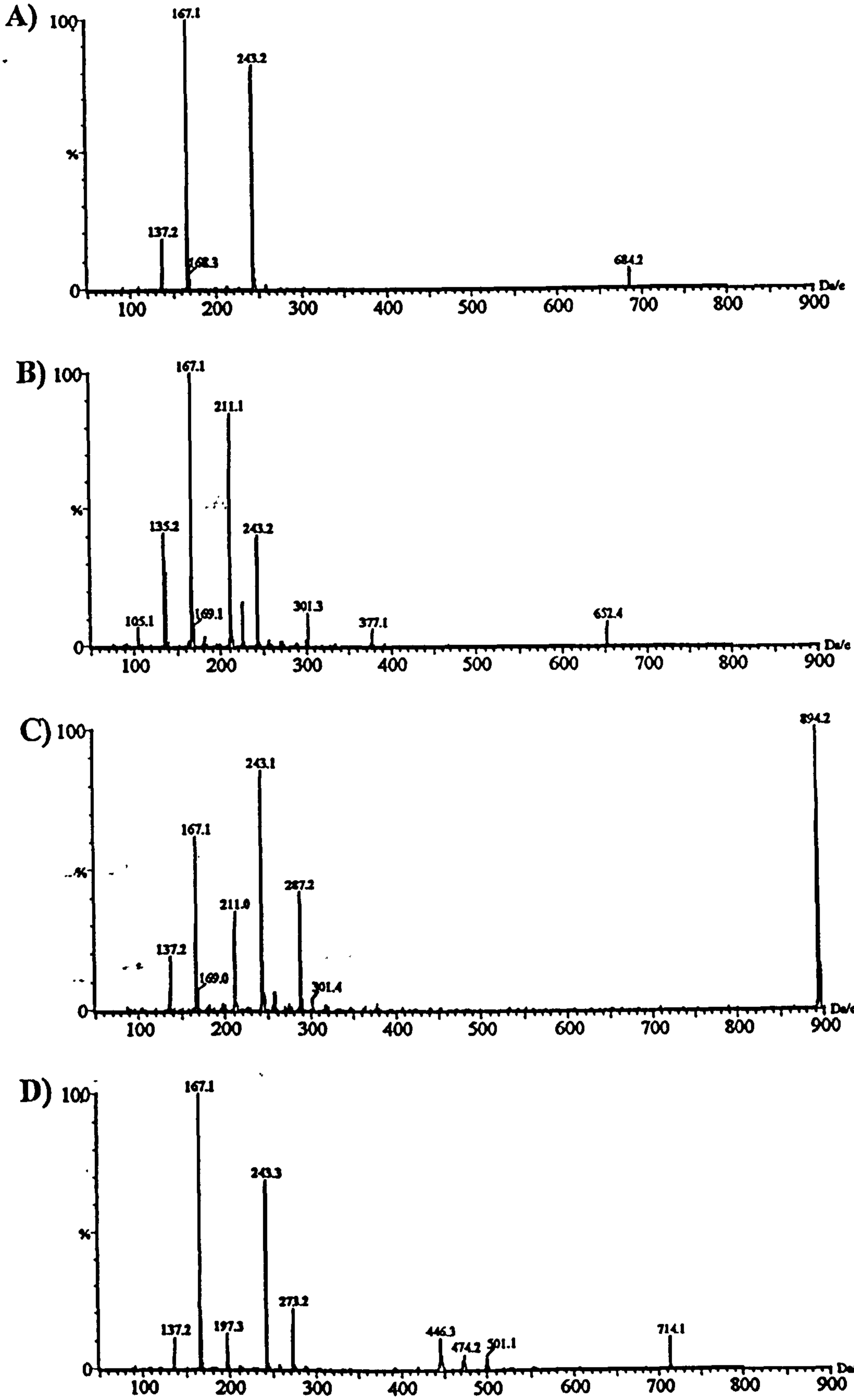

Fig.3.9: CID Spectra of ions selected from the spectrum of LP-1400C (Fig.3.1)

A) ion at *m/z* 684.2 peak in Series A.

B) ion at *m/z* 652.4 peak in Series B.

C) ion at *m/z* 894.2 peak in Series C.

D) ion at *m/z* 714.1 peak in Series D.

CID (20 eV) with argon target gas, 3.8×10^{-3} mbar

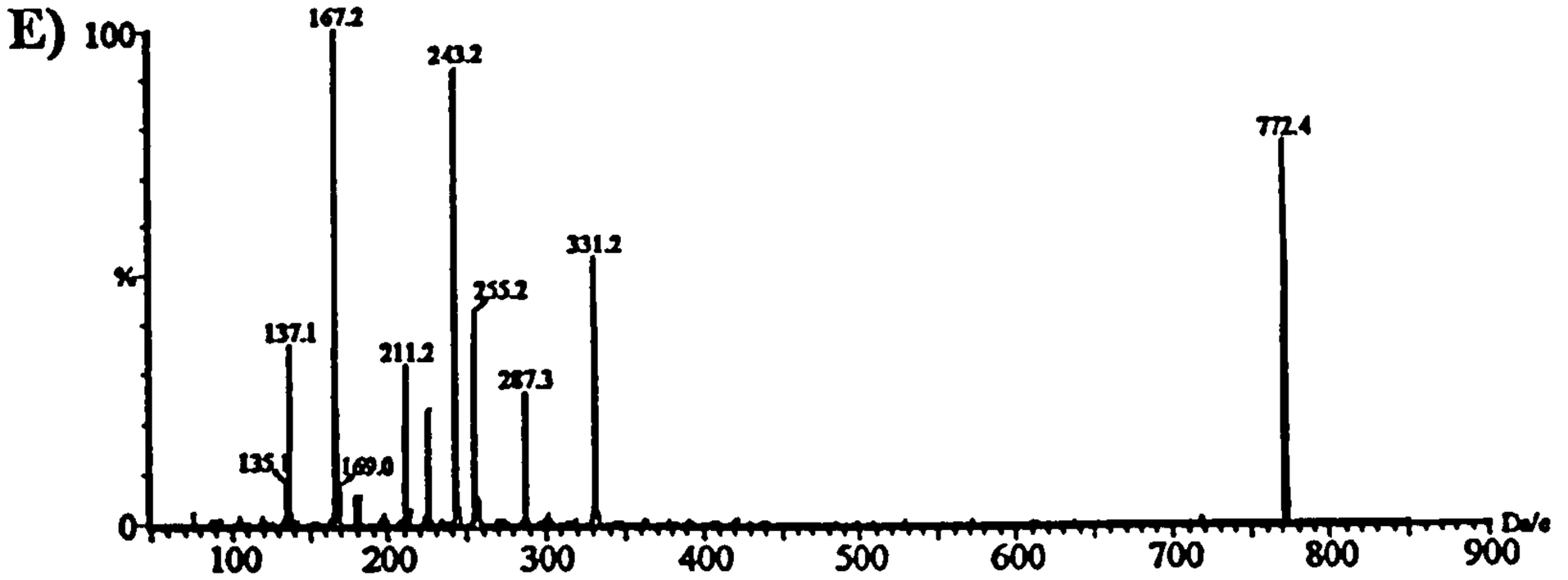

Fig.3.9: CID Spectra of ions selected from the spectrum of LP-1400C (Fig.3.1)

E) ion at *m/z* 772.4 peak in Series E.

F) ion at *m/z* 758.3 peak in Series F.

G) ion at *m/z* 696.5 peak in Series G.

H) ion at *m/z* 802.4 peak in Series H.

CID (20 eV) with argon target gas, 3.8 x 10^{-3} mbar

TABLE 3.6 Summary chart of ion fragmentation observed in CID of selected ions from LP-1400 (all fragments refer to the NH_4^+ - loss species).

Series C - Selected ion 894.2

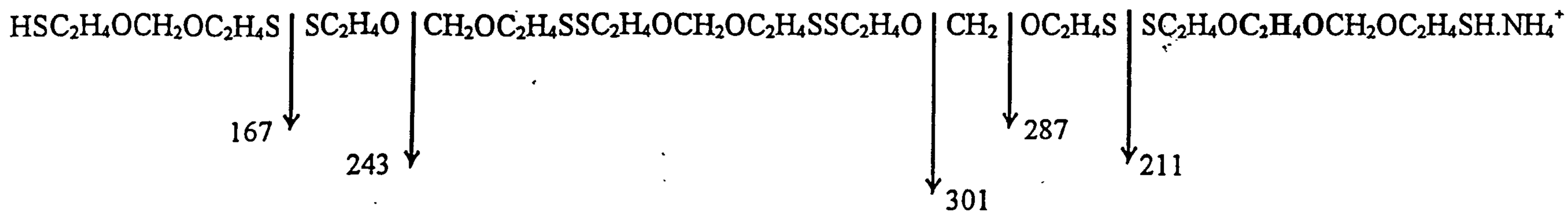

Series D - Selected ion 714.1

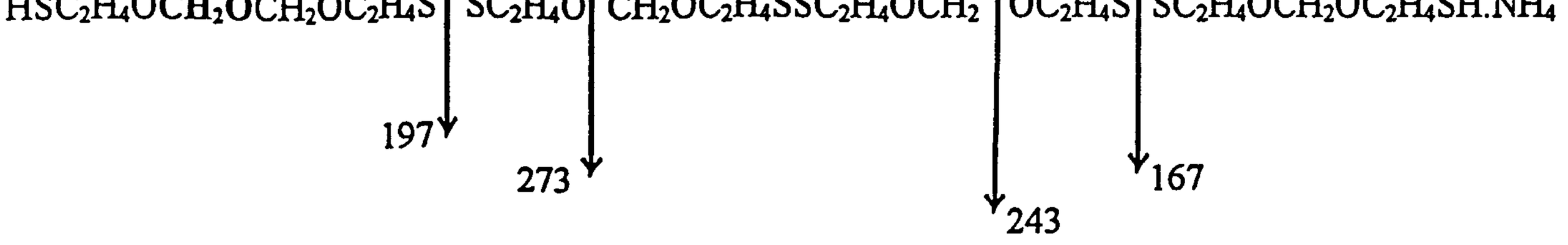

Series E - Selected ion 772.4

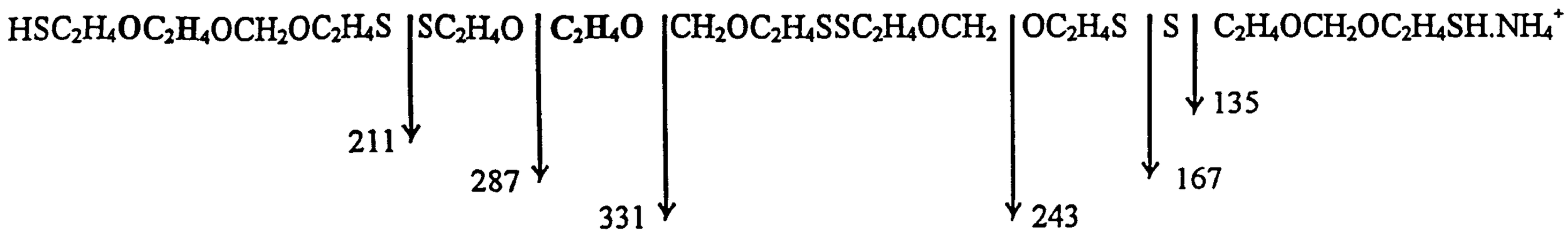

Series F - Selected ion 758.3

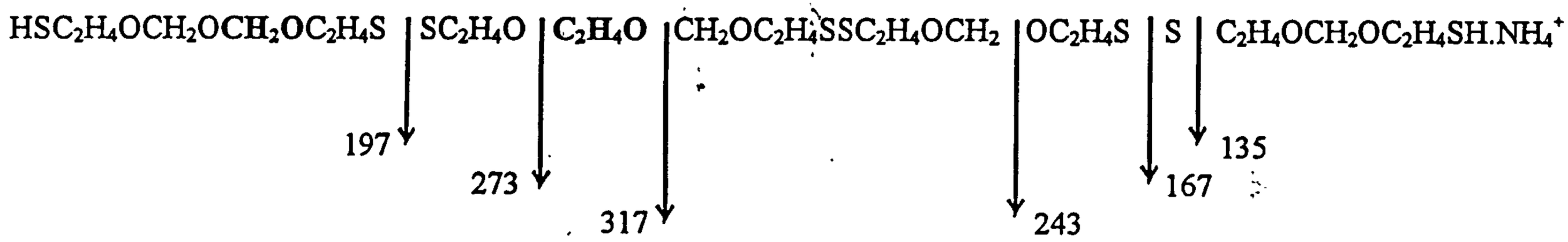

OR

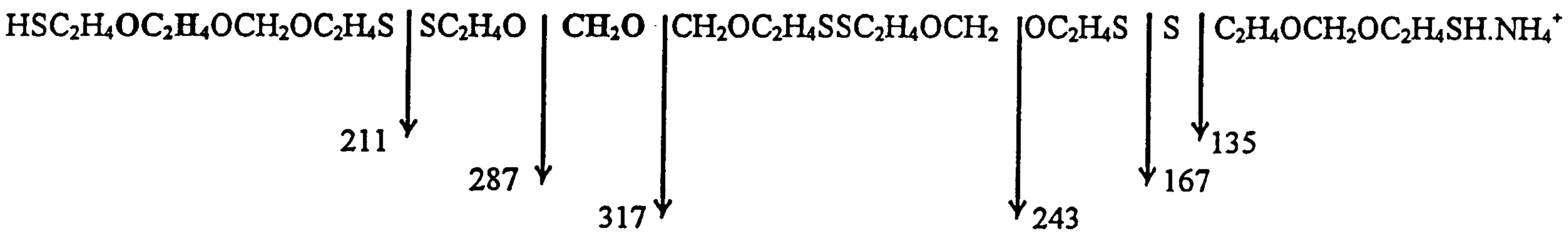

Series G - Selected ion 696.5

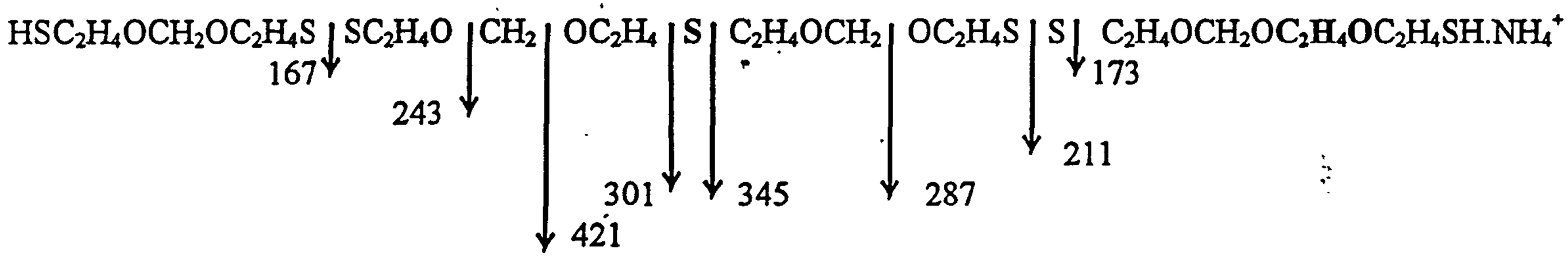

OR

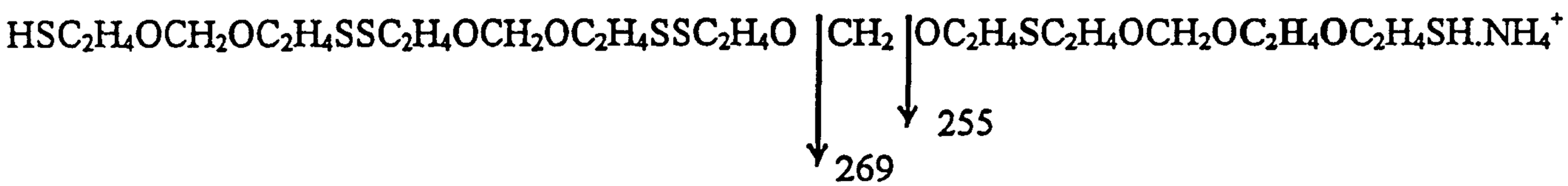

OR

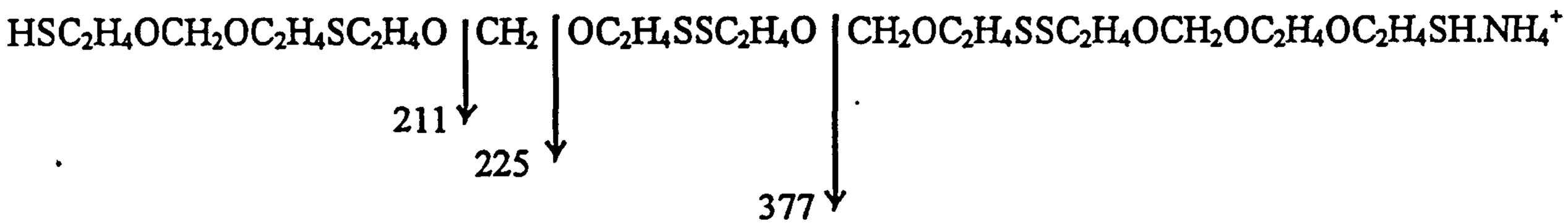

Series H - Selected ion 802.4

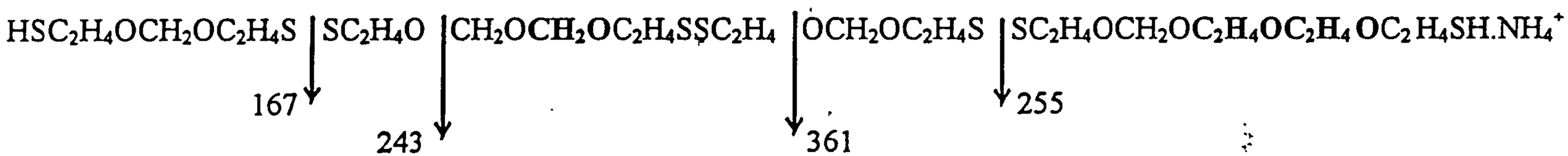

OR

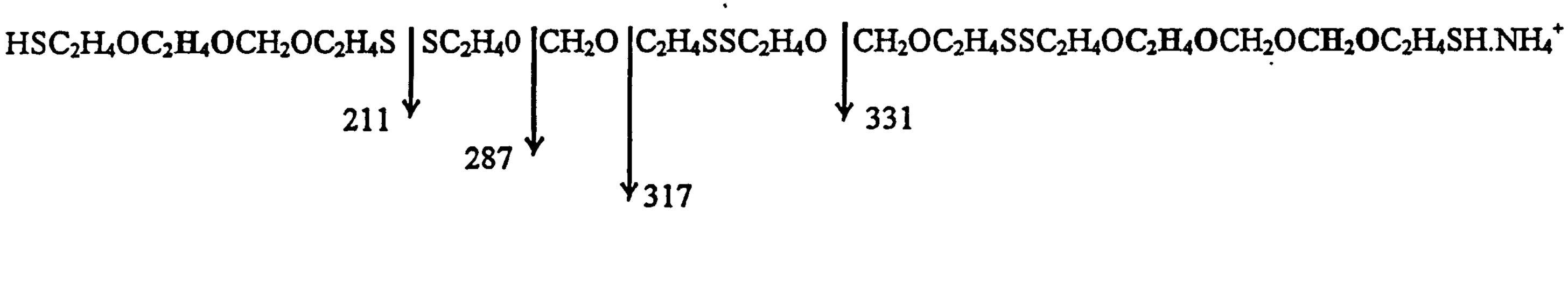

The somewhat more complex spectra obtained for the other series are a consequence of the lower symmetry of the precursor ions. A summary of the ions observed during CID of ions from all the Series C–H is given in Table 3.6. The variation in the parent ion intensity (fig.3.9) is most probably an artefact due to an adventitious fluctuation in pressure. The CID spectra show the following:

(i) the cleavage sites are relatively few and are repeated between different series, with –S–S– and –C–O– fission being particularly prominent, although –C–S– cleavage is also found

(ii) the Series F, G and H, which feature more than one type of structural variant, give rather complex CID spectra indicating the presence of isomers which differ in the location of the variant (one or more CH_2O or C_2H_4O groups, and one fewer S atom) in the polymer chain. While the CID spectral assignments made in Table 3.6 account for virtually all the ions detected, the data cannot allow positional discrimination within a single mer unit, *e.g.* a $HSC_2H_4OCH_2OC_2H_4OC_2H_4S$ unit will contribute to the mass of a fragment ion in the same way as a $HSC_2H_4OC_2H_4OCH_2OC_2H_4S$ unit. The occurrence of several variant mers within an LP sample is rare: fig.3.1 shows that the major species present correspond to the ideal LP (Series A) or with a single variant within the chain (Series B–D).

(iii) Fragment ions do not show the presence of an extra proton originating from the NH_4^+ group, but rather terminate in a –SH group.

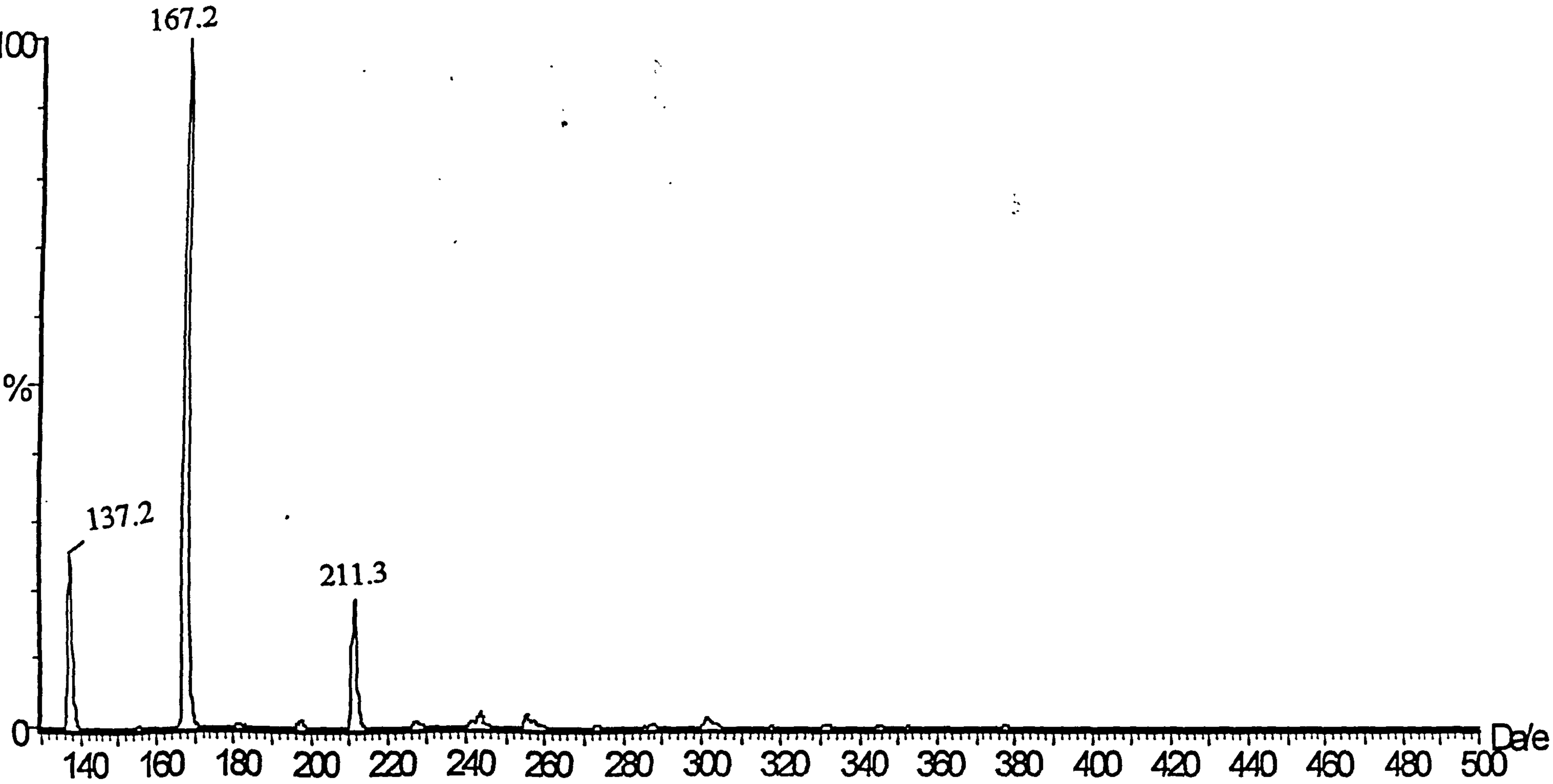

Fig.3.10: Precursor ion spectrum of ion with *m/z* 137.2 derived from the CID of LP-1400C.

Precursor ion experiments were carried out on selected fragment ions obtained by CID of LP–1400C. Thus fig.3.10 reveals that the ion with *m/z* 137.2 originates from the 167.2 fragment, which has been detected in the various series A–H following CID. The production of the *m/z* 137.2 ion from $HSC_2H_4OCH_2OC_2H_4S^+$ (*m/z* 167.1) signifies the loss of 30 Da which can be due only to elimination of formaldehyde. This elimination parallels that of C_2H_4O units from protonated macrocyclic polyether lactones under electron impact conditions[3].

CID experiments carried out on ELP–3 (fig.3.11) indicated fragmentation to involve few pathways: fragmentation involves complete retention of the terminal epoxy group in all species detected. A scheme for the fragmentation of the ELP-3 precursor ion at *m/z* 764.4 (Series B) is shown in Table 3.7.

TABLE 3.7 Scheme for the fragmentation of ELP–3 on CID

Ion *m/z*	Assignment
764.4 (precursor)	
357.3	$\overline{OCH_2CH}CH_2SC_2H_4OCH_2OC_2H_4SSC_2H_4OCH_2OC_2H_4^+$
281.2	$\overline{O-CH_2-CH}CH_2SC_2H_4OCH_2OC_2H_4SC_2H_4OCH_2^+$
223.1 (base peak)	$\overline{O-CH_2-CH}CH_2SC_2H_4OCH_2OC_2H_4S^+$
147.0	$\overline{O-CH_2-CH}CH_2SC_2H_4OCH_2^+$
117.1	$\overline{O-CH_2-CH}CH_2SC_2H_4^+$

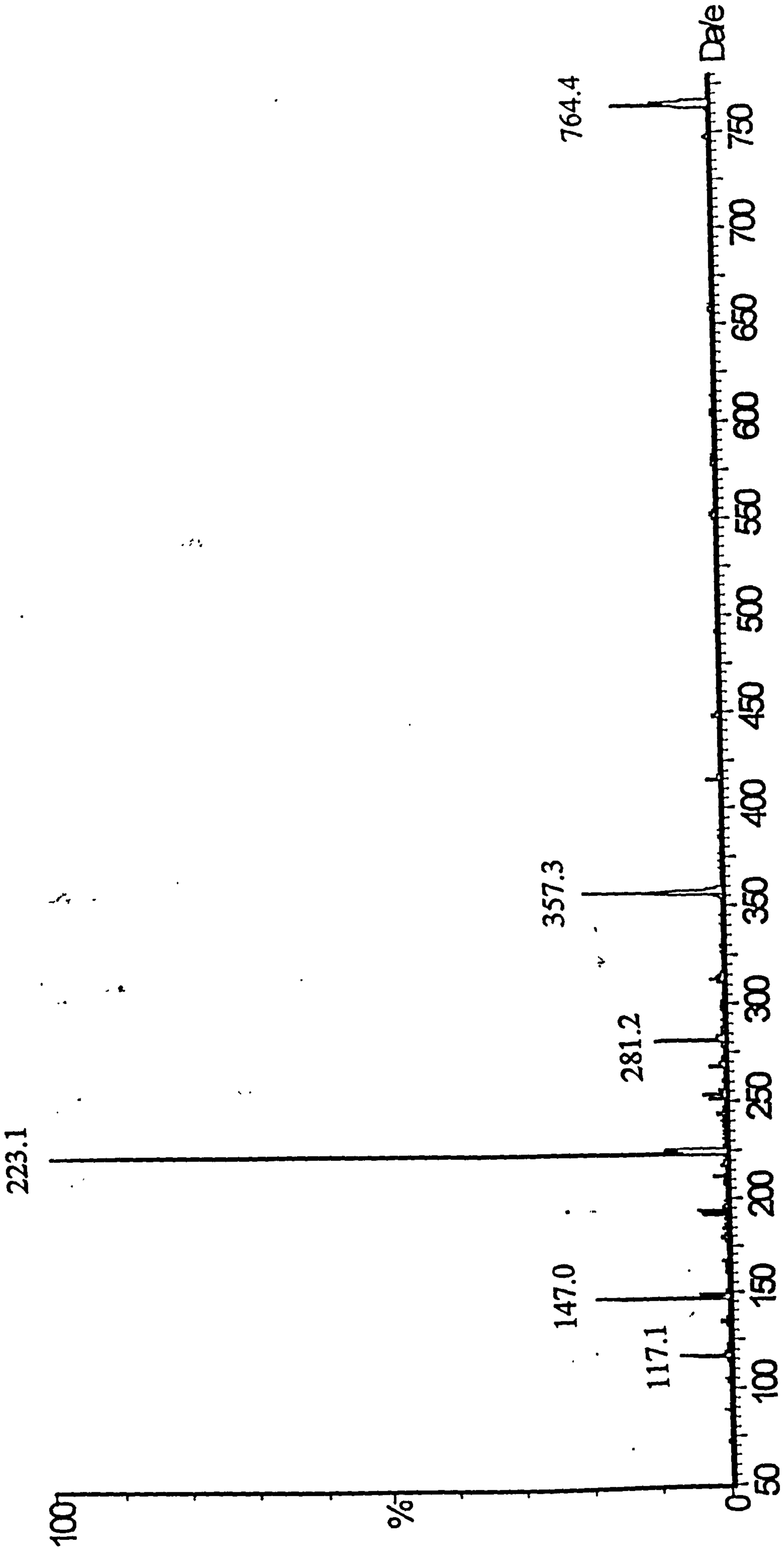

Fig.3.11: CID spectrum of *m/z* 764.4 ion from ELP-3.

3.8 ESI SPECTRA OF REACTION SYSTEMS

To investigate the possibilities of monitoring the extent of reaction when LPs undergo curing, we reacted Model Compound A with hexane–1,6–diol diacrylate (HDDA) and ran an ESI spectrum on the product without separation, see fig.3.12. A new series of peaks (Series C) appears in the spectrum attributable to the monoadduct of HDDA (RMM = 226) with the LP, *i.e.* $RSCH_2CH_2CO_2C_6H_{12}O_2CCH{=}CH_2$.

3.9 FAST ATOM BOMBARDMENT EXPERIMENTS

FAB experiments were carried out on LP 1400C by way of comparison (fig.3.13): such species as *m/z* 243, 167 and 137, which were ubiquitous in the CID/ESI spectra of various LPs, are prominent while the small fragment ions *m/z* 91 and 61 are assigned respectively to $HSC_2H_4OCH_2^+$ and $HSC_2H_4^+$.

3.10 DISCUSSION AND CONCLUSIONS

ESI has proved to be a most useful addition to the armoury of mass spectroscopic techniques applicable to the characterisation of oligomeric materials, in this case, linear polysulfides. The individual spectra are well–resolved, enabling conclusions to be reached about the distribution of mers within a given formulation, about the presence of variant mers (usually associated with additional oxymethylene or oxyethylene units or a monosulfide linkage, or some combination of these), about the identity of end–groups and about the nature and extent of simple reactions of LPs with acrylate esters.

ESI spectra offer a very direct insight into the presence of variant mers and of the end groups. Some of these features can be detected in LP oligomers by ^1H and

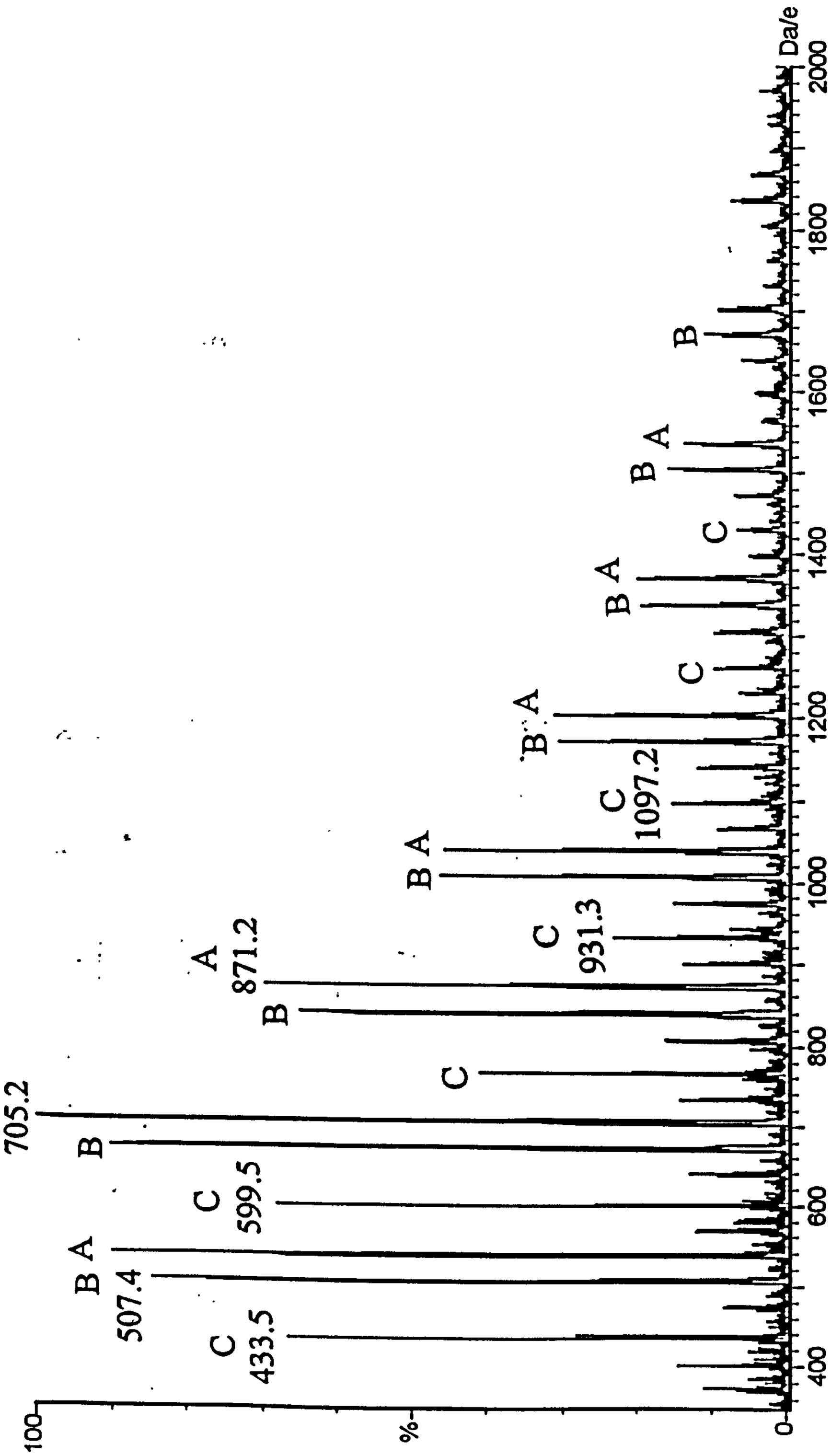

Fig.3.12: ESI spectrum of a reaction mixture of Model Compound A with hexane-1,6-diol diacrylate. Series C refers to the monoadduct of LP with diester. Mobile phase: acetone containing KI.

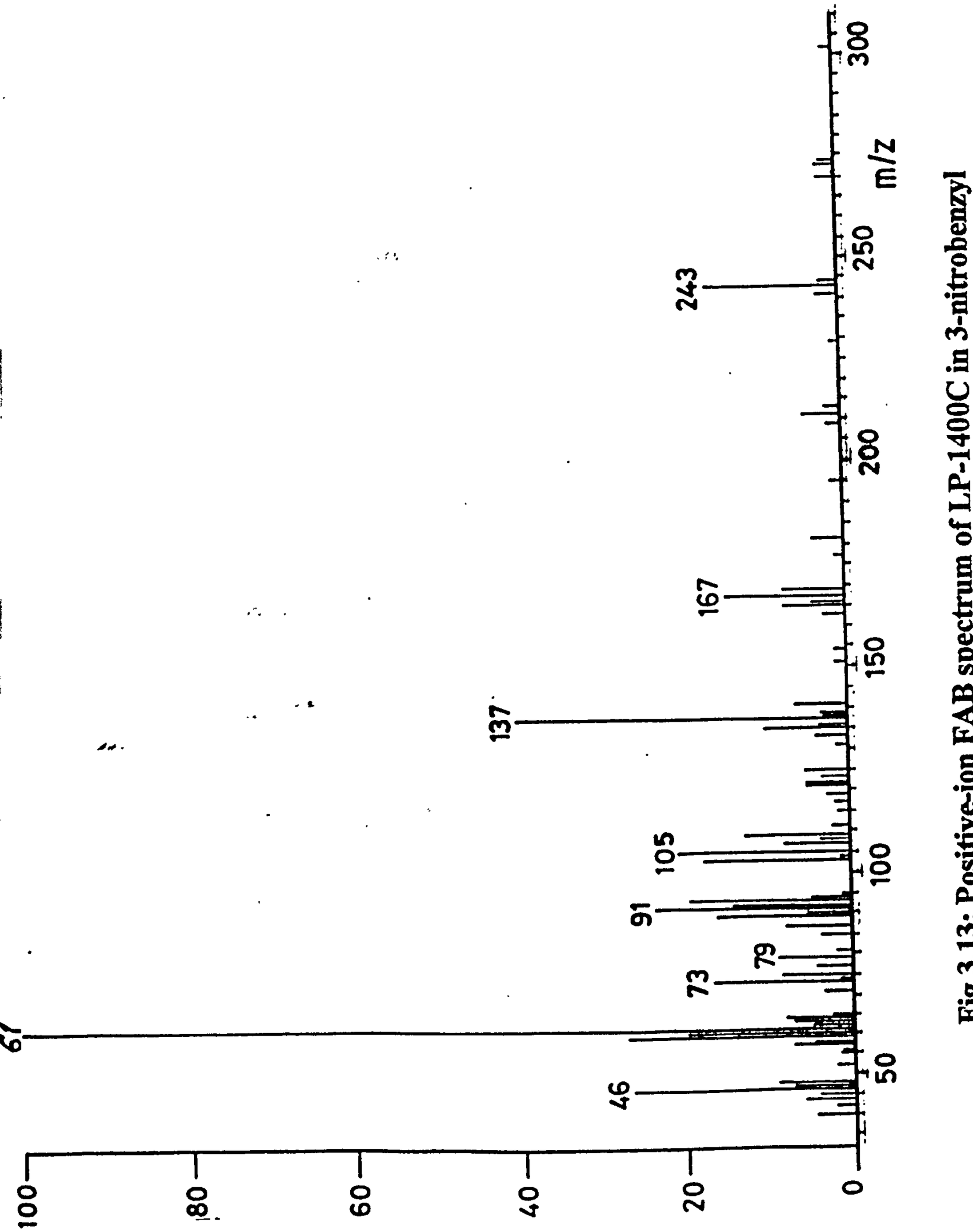

Fig.3.13: Positive-ion FAB spectrum of LP-1400C in 3-nitrobenzyl alcohol matrix.

^{13}C NMR spectroscopy, but even then, the location of an anomalous group within the chain cannot be defined as precisely as it can be from CID spectra. Infra-red spectra of LPs offer only general information about the functional groups present and cannot be used to observe the presence of additional groups such as CH_2O or C_2H_4O.

It is clear from the various ESI spectra portrayed, particularly those in fig.3.7 that while the technique provides very accurate mass information at RMM<2000, it gives a heavy bias towards the detection of low mass oligomers at the expense of those of higher mass, thus even when, as in LP-32C, the average RMM is *ca.* 4000, no peaks appear at *m/z* > 2500 and the ion abundances at *m/z* > 1800 do not reflect the abundances of oligomers present. This situation does not appear to arise from lower solubility of the high mass oligomers since changing the mobile phase offered no advantage; this could suggest that ESI discriminates against ions of higher *m/z* values and perhaps coupling a GPC column to the instrument would allow the higher oligomers to be detected as advocated by Simonsick and Prokai[4,5]. An alternative explanation is that although ESI is a very soft ionisation technique, there is still some fragmentation before detection in LPs, most likely at the weak disulfide linkage.

The most informative ESI spectra of LPs are those obtained at a cone voltage of 100 cv, using a mobile phase of acetone containing 0.5% KI, although this system does **not** lend itself to CID or precursor ion experiments, when THF/MeOH/0.5% aqueous NH_4Cl is superior.

The CID spectra of ions derived from LPs reveal relatively simple fragmentation pathways, depending on the complexity of the LP structure.

CHAPTER 3

REFERENCES

1. Lucke, H., Huthig, *Alips- Aliphatic Polysulfides. Monograph of an Elastomer.* Wepf Verlag, Basel, (1994).

2. Jasieczek, C.B., Buzy, A., Haddleton, D.M., Jennings, K.R., *Rapid Commun. Mass Spec.*, **10**, (1996) 509.

3. Podda, G.L., Corda, C., Anchisi, B., Pelli, B., Traldi, P., *Org. Mass Spectrom.*, **22**, (1987) 162.

4. Simonsick, W.J., Prokai, L., *'Abstracts 42nd ASMS Conference on Mass Spectrometry'* Chicago (1994) 515.

5. Prokai, L., Simonsick, W.J., *Rapid Commun. Mass Spectrom.*, 7, (1993) 853.

CHAPTER 4

IONS DERIVED FROM LINEAR POLYSULFIDE OLIGOMERS USING MALDI AND FIELD DESORPTION IONISATION MASS SPECTROMETRY.

4.1 INTRODUCTION

No experiments of this type have been published in the open literature, but Ludicky[1] of Morton Thiokol reported Fourier Transform (FT) mass spectra of laser desorbed commercial LPs in an internal report. The expected relative molecular mass distributions (RMMD) for LPs were not observed, with no series of peaks being observed above around 2000 Da, even for LPs of know molecular mass of above 4000. Ludicky also reports[1] that his group has been unsuccessful in obtaining MALDI spectra of LPs.

MALDI spectra have largely been devoted to fairly standard synthetic polymers such as poly(methyl methacrylate)[2-5], poly(ethylene glycol)[2,3] and polystyrene[2,3], and much the same can be said of field desorption (FD)[6-9].

Here we describe a series of essentially preliminary results on both MALDI and FD studies of several selected polysulfide oligomers.

4.2 MALDI STUDIES OF LPs

Initial studies using the generally favoured 2,5-dihydroxybenzoic acid (DHB) as the matrix, either alone or with sodium or potassium chloride as co-cation, gave no ions. Dianthrol as matrix, in combination with silver trifluoroacetate, also gave no ions from LPs.

However, the use of 9-nitroanthracene in combination with silver trifluoroacetate gave the MALDI spectrum shown in fig. 4.1 when LP-2C was used as the analyte. The principal features of this spectrum are:

i) the presence of a series of major peaks (denoted Series A) separated by 166 amu, i.e. the mass of the repeat unit.

ii) a set of minor peaks, denoted Series B, each member of which is located 32 amu below the corresponding peak in Series A. This we attribute to the presence of one unit in the entire polymer chain with one less sulfur atom.

iii) a set of minor peaks, denoted Series C, of which each member is located 44 amu above the corresponding peak in Series A. This we attribute to the presence of one unit in the entire polymer chain with one extra oxyethylene link.

iv) the RMMs of Series A do not, in contrast to the series A in the ESI spectrum of the same polymer, correspond to the RMM of the LP itself, which would be (166n + 2) + RMM of the cation.

v) the resolution of the MALDI spectra of LPs, compared to those obtained by ESI, see figs.3.1, 3.2 and 3.3, is poor in so far as virtually no peaks from other series (D,E,F, etc.) are visible.

The assignment of the peaks in fig.4.1 is less obvious compared to those found in the ESI spectra of LPs. The peak at m/z = 607 can be viewed as an 'argentated LP', i.e.

$$Ag(SC_2H_4OCH_2OC_2H_4S)_3H$$

which has an RMM of (3 x 166) + 1 + 108 = 607, and all the main peaks in the spectrum of LP-2C (fig.4.1) can be attributed to:

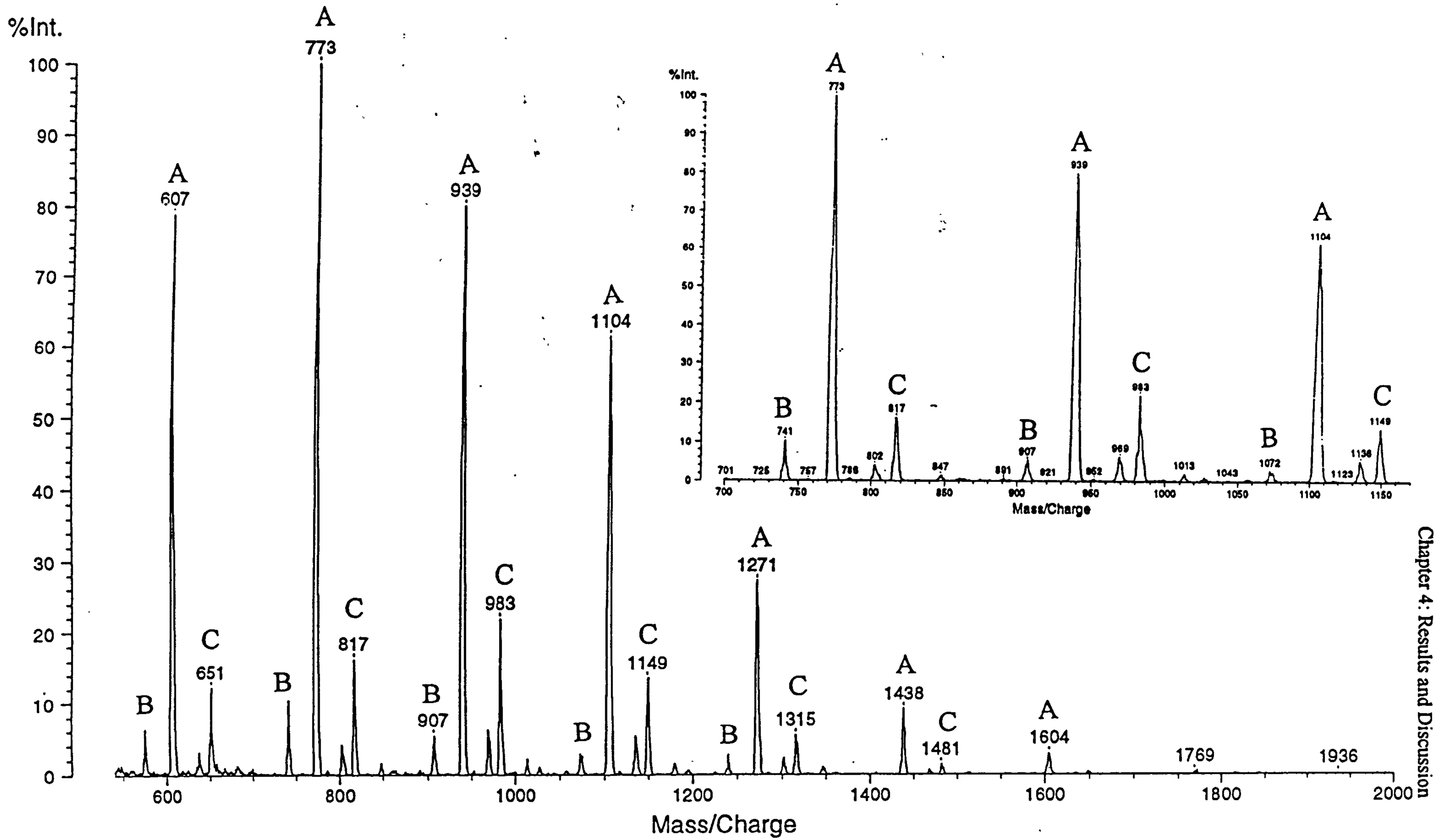

Fig. 4.1: MALDI spectrum of LP-2C with 10 µl of silver salt. Insert: expansion of spectrum in *m/z* range 700-1160 to reveal greater detail.

Series A

$Ag(SC_2H_4OCH_2OC_2H_4S)_nH$

Series B

$Ag(SC_2H_4OCH_2OC_2H_4S)_n(C_2H_4OCH_2OC_2H_4S)H$

Series C

$Ag(SC_2H_4OCH_2OC_2H_4S)_n(SC_2H_4OC_2H_4OCH_2OC_2H_4S)H$

The resolution of spectral lines was not very good and the expected isotopic splitting from ^{107}Ag and ^{109}Ag was not located (see, however, the result from ZL-2264, fig.4.3). Consequently we cannot assert confidently that the above assignments are incontrovertible: the peaks could be due to a ^{109}Ag compound of the LP with both terminal S-atoms bonded to Ag, or to a ^{107}Ag compound which is a simple adduct of Ag+ with the LP, with both hydrogen atoms intact. The result for ZL-2264 given below (see fig.4.3) clarifies this situation.

The RMMD of LP-2C is not in accord with that expected, the average RMM of this polymer is ≈ 4000 but no peaks are observed in the spectrum above 2000 amu; this result is comparable to spectra obtained by ESI (see section 3.5).

In view of the rather mediocre quality of the spectrum obtained for LP-2C using MALDI, we decided to examine LPs with fewer impurities and other LPs in their formulation.

An exceptionally pure form of LP, denoted Model A, which consists largely of just two LPs, (see fig.3.4 for ESI spectrum of this compound), gave a very clear MALDI spectrum shown in Fig.4.2, where Series A and B provide virtually the only peaks in the spectrum.

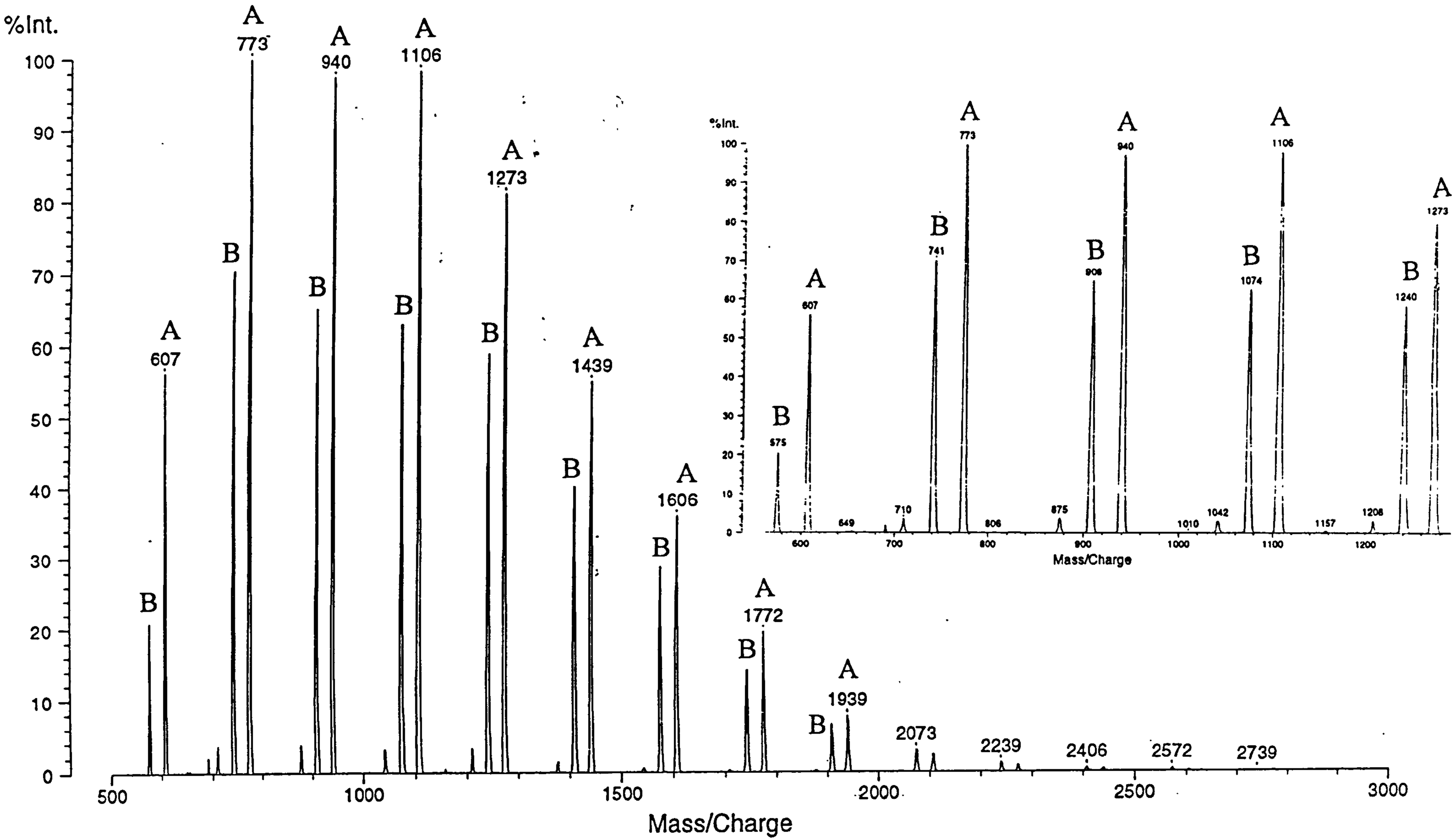

Fig. 4.2: MALDI spectrum of Model A with 10 µl of silver salt. Insert: expansion of spectrum in *m/z* range 570-1280 to reveal greater detail.

The LP denoted ZL-2264, (see fig.3.6 for ESI spectrum of this compound), which has the formal group in the repeat unit replaced by oxyethylene, also gave a very simple MALDI spectra illustrated in fig.4.3, with peaks in the series separated by the RMM of the repeat unit (180 amu), which are the analogues of Series A and B in the normally structured LPs. Under high resolution, the individual peaks showed a doublet splitting of 2 amu, which supports strongly an assignment to the species $Ag(SC_2H_4OCH_2OC_2H_4S)_n$. The only silver isotopes of significant abundance are 107 (51.84%) and 109 (48.16%) which explains the existence of the doublet feature on the inset of fig.4.3. The main peaks arising in this spectrum can therefore be assigned to a ^{109}Ag compound of LP with <u>both</u> terminal S-atoms bonded to the Ag i.e. $^{109}Ag(SC_2H_4OCH_2OC_2H_4S)_n$, while the shoulder peak at 2 amu less can be attributed to $^{107}Ag(SC_2H_4OCH_2OC_2H_4S)_n$.

We also attempted to obtain MALDI spectra for ELP-3 (an epoxy-terminated LP, see fig.3.5 for ESI spectrum) and heavily degraded samples of Model A and other LP pre-polymers but no ions were observed, making MALDI an inefficient technique for studying degradation reactions in LP-type polymers. It appears that a species obtained by a slight change in the LP structure will yield no ion peaks, which explains while series D,E,F etc. clearly visible in the ESI spectra of LPs are not visible in their MALDI spectra, and the -14 amu series clearly seen in the ESI spectrum of heavily UV-degraded Model A (fig.5.16) is also undetected by MALDI.

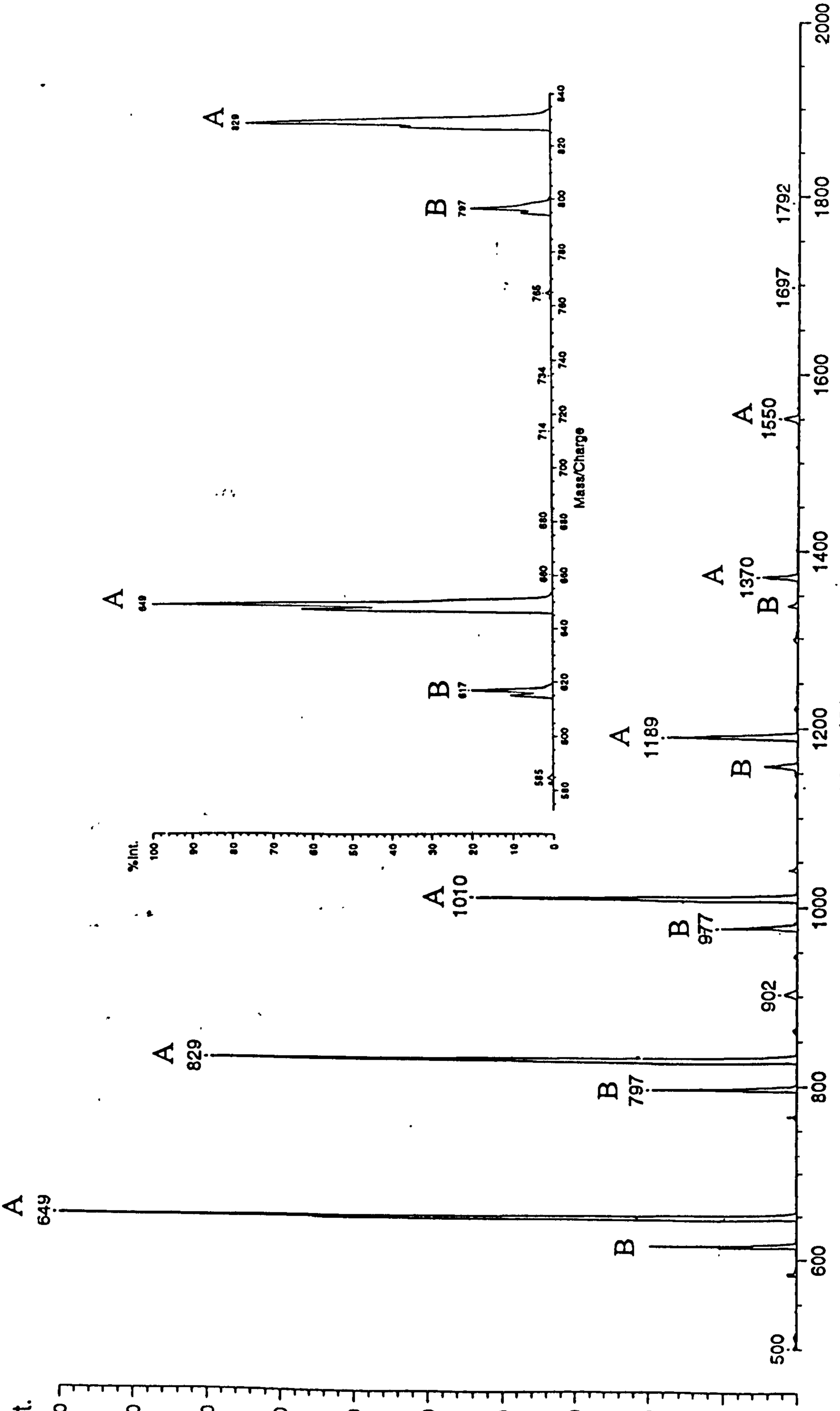

Fig. 4.3: MALDI spectrum of ZL-2264 with 10 µl of silver salt. Inset: expansion of spectrum in *m/z* range 560-840 to reveal greater detail.

4.3 THE APPEARANCE OF SILVER SULFIDE CLUSTERS IN MALDI EXPERIMENTS ON LINEAR POLYSULFIDES

An unexpected observation was that, under certain experimental conditions, the MALDI spectra of LPs changed completely from those shown in fig.4.1 and fig.4.2 to ones resembling that shown in fig.4.4. This consisted of a set of peaks separated not by the usual 166 amu associated with the LP repeat unit, but rather a series separated by 248 amu. That this figure has no relation to the LP repeat unit was confirmed by an experiment with ZL-2264 where the peak separation was, once again, 248 amu, see fig.4.4. This phenomen we attribute to the formation of clusters of Ag_2S species, formed chemically either during the sample preparation or during the laser irradiation of the matrix sample once prepared.

Taking the most abundant peak in the spectrum, i.e. that at *m/z* 1596, we can see that this is not an integral number of Ag_2S units. The peak at *m/z* 649 is that present in the 'normal' MALDI spectra of ZL-2264 and is due to $^{109}Ag(SC_2H_4OC_2H_4OC_2H_4S)_3$; however the next higher member is conspicuous by its absence. It seems that the main series has a formula of the type $[(Ag_2S)_n(X)]+$ where X represents some other fragment derived from an LP or its silver adduct. While the peak at *m/z* 1100 amu is clearly a member of this series, the next lowest member should be at *m/z* 852 amu, which is only of rather weak abundance, as is that of the next lowest member at *m/z* 604 amu.

This latter peak could be due to the cluster Ag_5S_2+ or $Ag+(Ag_2S)_2$ which has an RMM of 604, and the series in general is of the formula $(Ag_2S)_nAg+$. This would generate peaks at the following masses:

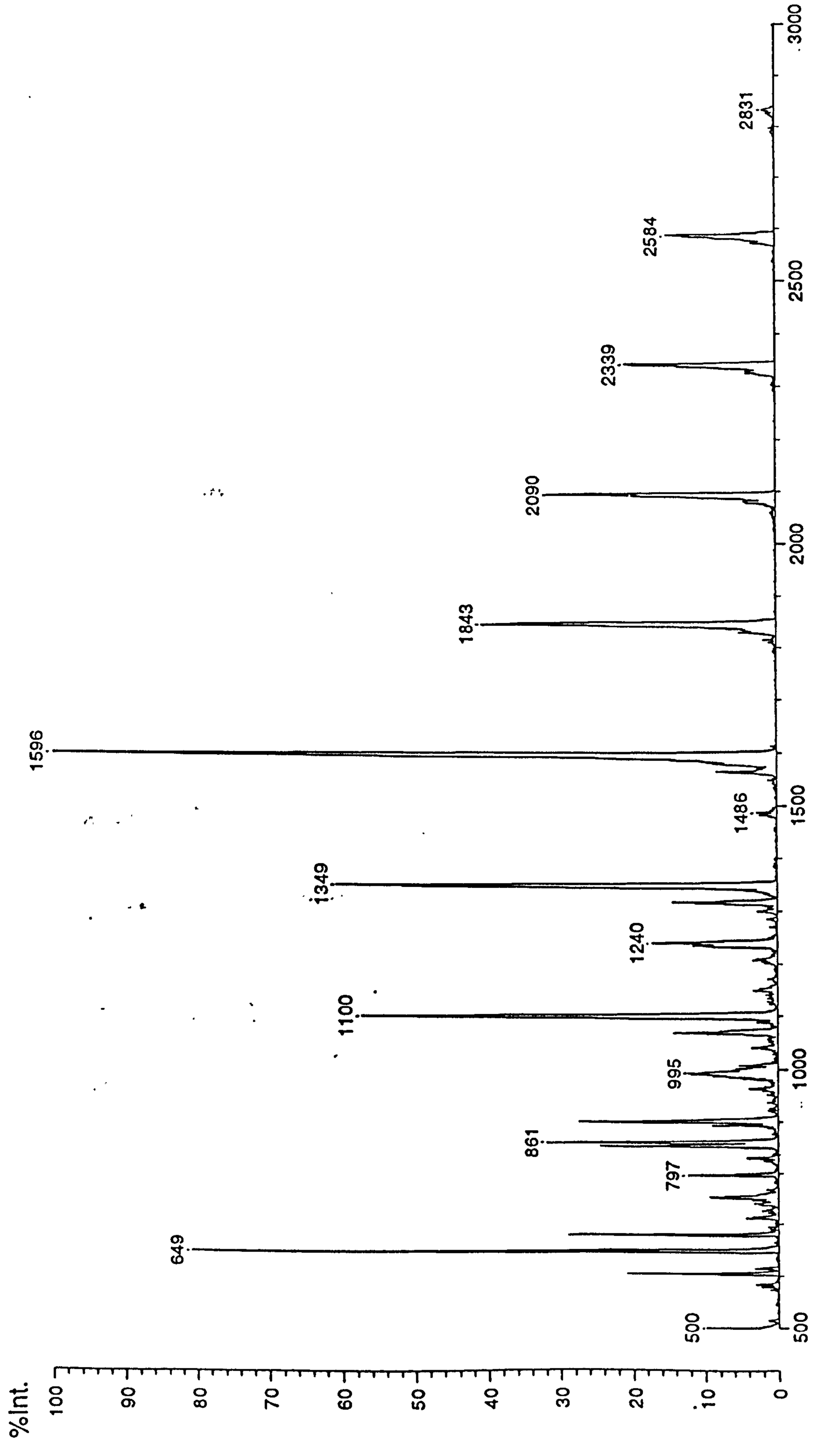

Fig. 4.4: MALDI spectrum of ZL-2264 with 200 µl of silver salt.

	m/z	*m/z* observed
$Ag(Ag_2S)+$	356	
$Ag(Ag_2S)_2+$	604	604
$Ag(Ag_2S)_3+$	852	852
$Ag(Ag_2S)_4+$	1100	1100
$Ag(Ag_2S)_5+$	1348	1349
$Ag(Ag_2S)_6+$	1596	1596
$Ag(Ag_2S)_7+$	1844	1843
$Ag(Ag_2S)_8+$	2092	2090
$Ag(Ag_2S)_9+$	2340	2339
$Ag(Ag_2S)_{10}+$	2588	2584
$Ag(Ag_2S)_{11}+$	2836	2831

Evidently the very strong Ag-S bond is the determining factor in producing these clusters from silver salts on reacting with the sulfur atoms of an LP. In accordance with this view, we found that the development of spectra like those in Fig.4.4 were promoted by:

i) high levels of Ag salt in the matrix formulation,

ii) high laser powers

iii) when the analyte/silver samples were left for a relatively long time prior to laser irradiation.

The main conclusion to be drawn from these experiments is that the experimental conditions must be carefully selected to preclude the occurrence of this

type of cluster chemistry when dealing with sulfur-containing compounds using a silver-containing matrix.

4.4 FIELD DESORPTION EXPERIMENTS WITH LINEAR POLYSULFIDE OLIGOMERS

The spectrum obtained by field desorption (FD) of LP-1400C, shown in fig.4.5, reveals the presence of the usual series as encountered in the ESI experiments, (see fig.3.1 for ESI spectrum of LP-1400C). It is instructive to compare the peaks in fig.4.5 with those in fig.3.1. All the Series A-G detected in the ESI experiment are also manifest in the FD spectra, but no addition information could be discerned. As in the ESI and MALDI experiments, the RMMD of the LP is not in accord with that expected, the most intense peak in the FD spectrum is at 500 amu, which represents only two repeat units, whereas the expected 'average' number of repeat units for LP-1400C is 7. There is a conspicuous absence of peaks above *m/z* 1330.5, which points once again to the deficiency of these soft ionisation techniques in recording molecular masses of LPs, i.e. the heavier components of a mixture of oligomers are simply "lost".

4.5 DISCUSSION AND CONCLUSIONS

We have been successful in obtaining spectra of LPs using matrix assisted laser desorption ionisation time-of-flight mass spectrometry, (MALDI-TOF-MS); although these spectra are well resolved and exhibit a separation between peaks of 166 Da, the molecular weight of the repeat unit, they are not as informative as spectra obtained by ESI-MS owing to their poorer spectral quality.

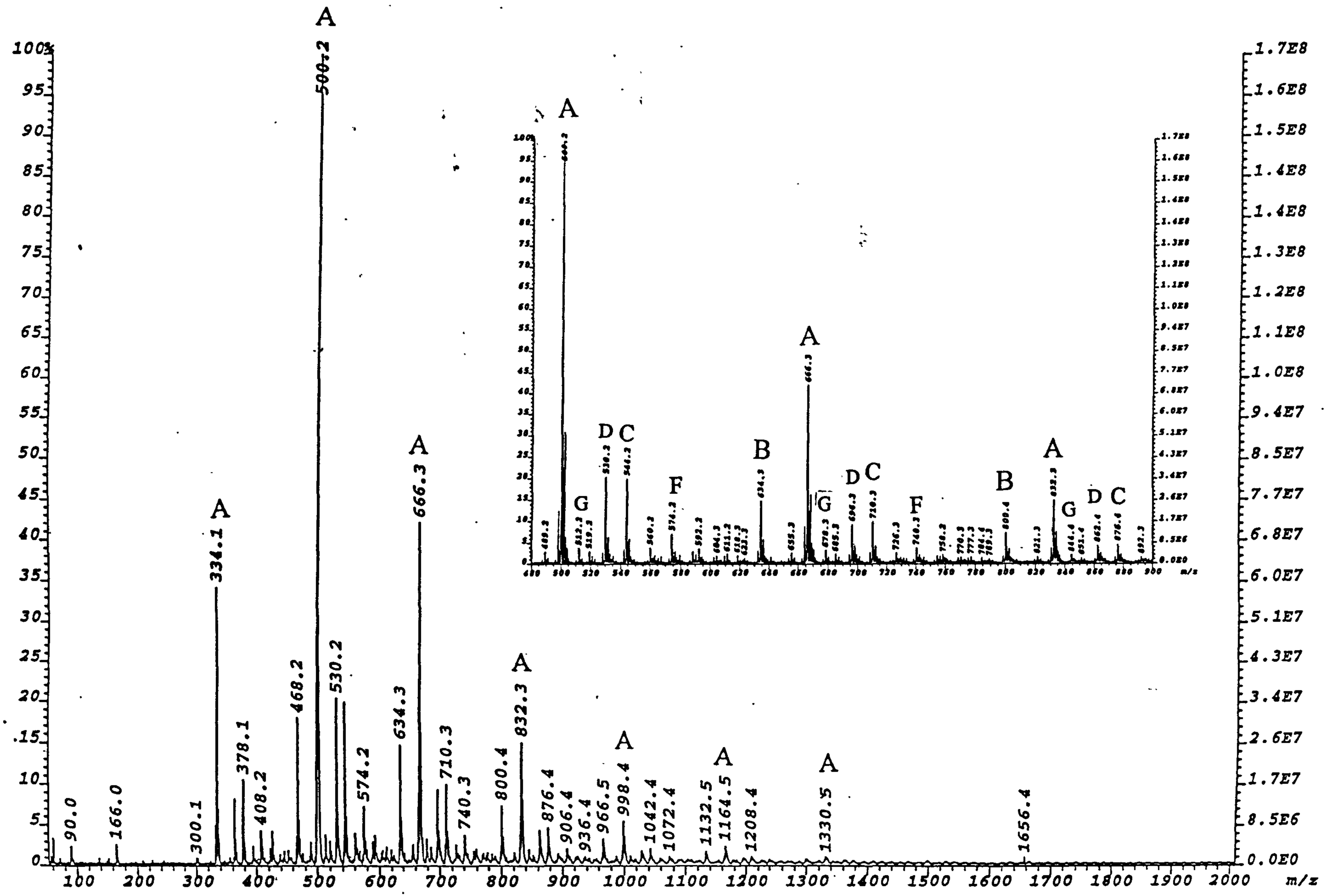

Fig. 4.5: Field desorption (FD) spectrum of LP-1400C. Insert: expansion of spectrum in m/z range 480-900 to reveal

The method of sample preparation is critical in obtaining a reasonable MALDI spectrum; matrices such as DHB and dianthrol were unable to yield LP ions even when co-cations such as sodium, potassium or silver were added. The only matrix system that has been successful for LP samples to date is 9-nitroanthracene with silver trifluoroacetate and even then, the analyte/silver mixture has to be left to stand for at least 4 hours before a spectrum could be obtained; a reasonable explanation for this is the silver cation requires time to react with the thiol groups in the LP. We also had a complication in the formation of silver clusters $[Ag(Ag_2S)_n]+$ especially under the following experiment conditions:

i) high levels of Ag salt in the matrix formulation,

ii) high laser powers

iii) when the analyte/silver samples were left for a relatively long time prior to laser irradiation.

The correct molecular mass distribution for LPs is not obtained, with low mass oligomers being detected at the expense of high mass oligomers. Possible explanations for this are:

i) there is a bias for the detector to favour the detection of low mass oligomers, especially in very polydisperse samples, as with commercial LPs.

ii) the samples undergo fragmentation during ionisation, most likely at the weak disulfide linkage, and

iii) only low mass oligomers undergo ionisation into the gas phase.

Fractionation of an LP sample using a GPC column prior to MALDI-TOF-MS analysis may lead to high mass oligomers being detected using this technique, and hence the calculation of accurate molecular mass information for this class of

polymers; this approach has been applied successfully by Montaudo et al.[10] for various polydisperse samples.

We have also been able to obtain MALDI spectra for model A and Zl-2264, but we have been unsuccessful in obtaining spectra of the epoxy terminated ELP-3 or the necessarily more complex degraded LP samples using MALDI-TOF-MS, whereas ESI-MS gave very useful data on the degradation process. It appears that a slight change in the LP structure will yield no ion peaks, which explains while series D,E,F etc. clearly visible in the ESI spectra of LPs are not apparent in their MALDI spectra.

Field desorption mass spectrometry (FD-MS) has also been successful in characterising LP samples, but this technique is less generally accessible and much more time-consuming than either ESI-MS or MALDI-TOF-MS, and a true representation of RMMD for LP-type polymers is still not observed using FD.

CHAPTER 4

REFERENCES

1. Ludicky, R., In-house Report, Morton Thiokol, (February 1995).
2. Bahr, U., Deppe, A., Karas, M., Hillenkamp, F., Giessmann, U., *J. Anal. Chem.*, **64**, (1992) 2866.
3. Corless, S., Tetler, L.W., Parr, V., Wood, D., '*Abstracts 42nd ASMS Conference on Mass Spectrometry*' Chicago (1994) 515.
4. Pasch, H., Gores, F., *Polymer*, **36**, (1995) 1999.
5. Maloney, D.R., Hunt, K.H., Lloyd, P.M., Muir, A.V.G., Richards, S.N., Derrick, P.J., Haddleton, D.M., *J. Chem. Soc., Chem. Commun.*,(1995) 561.
6. McCrae, C.E., Derrick, P.J., *Org. Mass Spectrom.*, **18**, (1983) 323.
7. Matsuo, T., Matsuda, H., Katakuse, I., *Anal. Chem.*, **51**, (1979) 1329.
8. Rollins, K., Scrivens, J.H., Taylor, M.J., Major, H., *Rapid Commum. Mass Spectrom.*, **4**, (1990) 355.
9. Craig, A.C., Derrick, P.J., *J. Chem. Soc, Chem. Commun.*, (1985) 891.
10. Montaudo, G., Garozzo, D., Montaudo, M.S., Puglisi, C., Samperi. F., *Macromolecules*, **28**, (1995) 7983.

CHAPTER 5

PHOTO- AND THERMAL DEGRADATION OF LP PRE-POLYMERS

5.1 PRELIMINARY PHOTODEGRADATION STUDIES OF LP PRE-POLYMERS BY IR SPECTROSCOPY

Photolysis experiments for all ten pre-polymers listed in table 2.2 were performed using the unfiltered output from a 350 W air-cooled xenon lamp. The IR spectrum of a thin LP film on a single NaCl disc was obtained. The sample was then mounted horizontally onto the exit port of the xenon lamp, as illustrated schematically in Fig. 5.1, and irradiated for up to 20 hours. IR spectra were obtained after various periods of time, e.g. 4 h, 8 h etc., to monitor any changes occurring. Under these conditions the radiation wavelengths used would induce both direct photolytic and photo-oxidative reactions.

Fig 5.1: Layout of apparatus

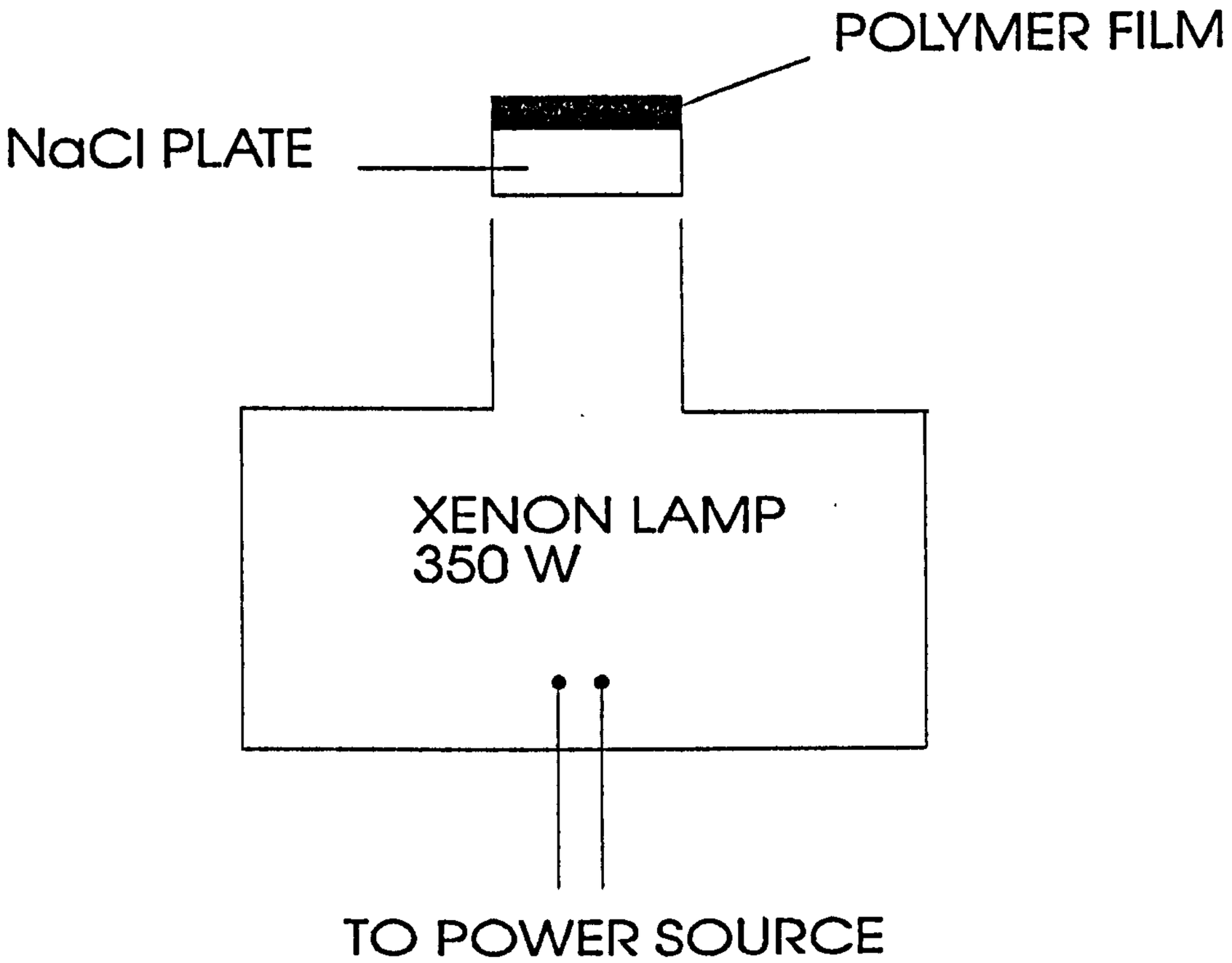

This type of experiment was repeated using a thin film of LP-32C sandwiched between two NaCl plates, to test whether restricting the supply of oxygen to the polymer affects the rate of degradation.

Typical spectral changes are illustrated in fig.5.2, from which it is apparent that the major discernible change is the development of strong absorptions in the carbonyl region, (1726 and 1689 cm^{-1}). A secondary feature is the growth of a broad, weak band in the O-H region. The location of the C=O group did not depend on the nature of the LP, (see Table 5.1).

Fig. 5.2- Spectrum showing the development of C=O and O-H frequencies in LP-980C following 20 h UV irradiation with a xenon lamp.

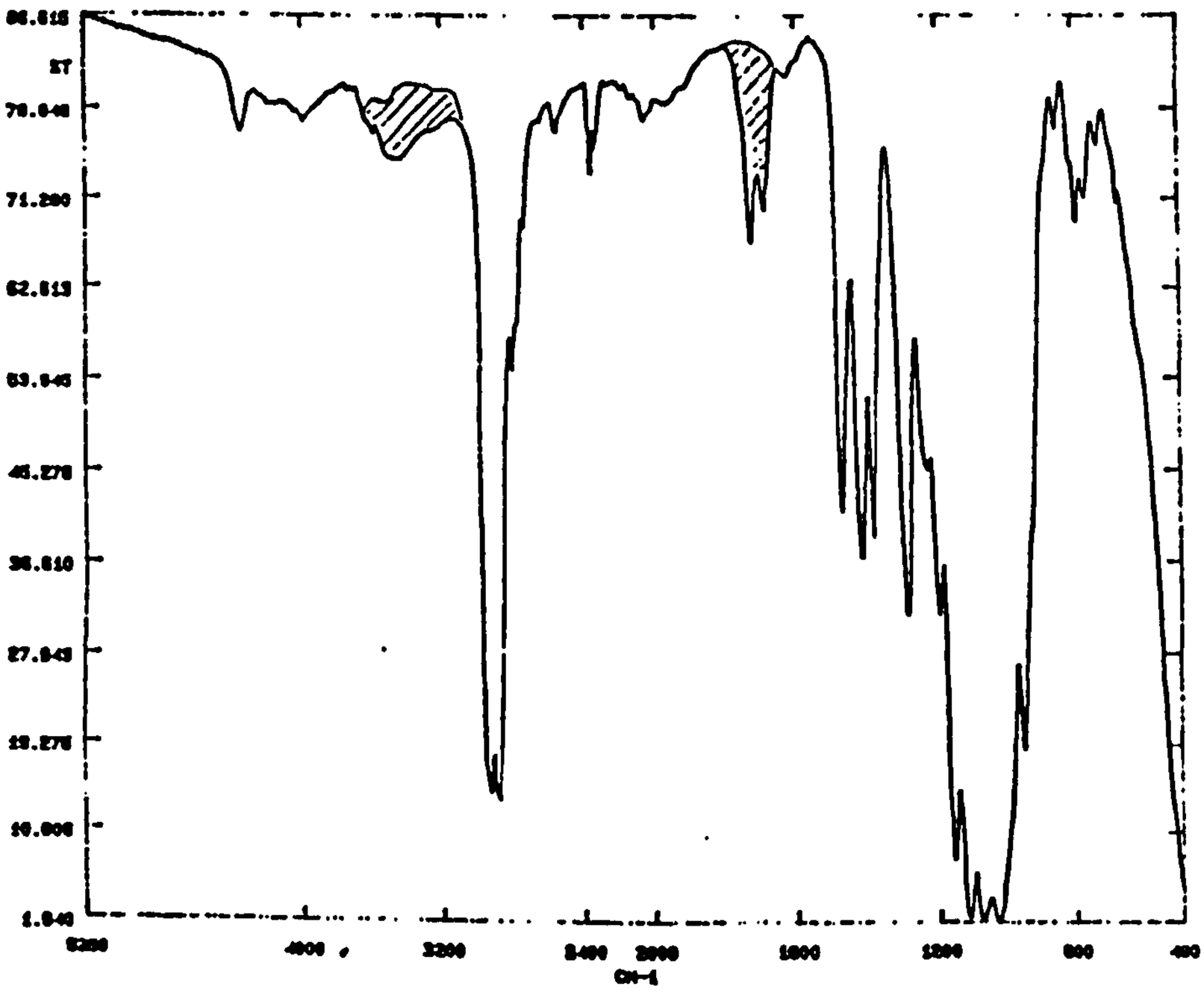

TABLE 5.1:- Comparison of ν(C=O) frequencies for pre-polymers as developed during photo-irradiation.

LP code n°	1st peak ν/cm^{-1} (± 2 cm^{-1})	2nd peak ν/cm^{-1} (± 2 cm^{-1})
1400C	1725	1687
33	1726	1688
3	1725	1689
980C	1726	1688
977C	1727	1690
541C	1726	1689
12C	1726	1689
32C	1726	Unlisted
2C	1726	1692
31	1726	1685

The kinetic curves for the growth of the C=O frequencies are illustrated in fig. 5.3 and 5.4.

In general, the development is linear for both bands at 1726 cm^{-1} and 1689 cm^{-1}, but in some instances there is evidence for a reduction in the rate of development at longer times, see fig. 5.4. This behaviour parallels that of polypropylene[1,2].

Comparison of the slopes of the linear sections of these kinetic growth curves is made in Table 5.2.

Fig.5.3 :- Profile showing the growth of carbonyl peaks during UV irradiation of LP-1400C

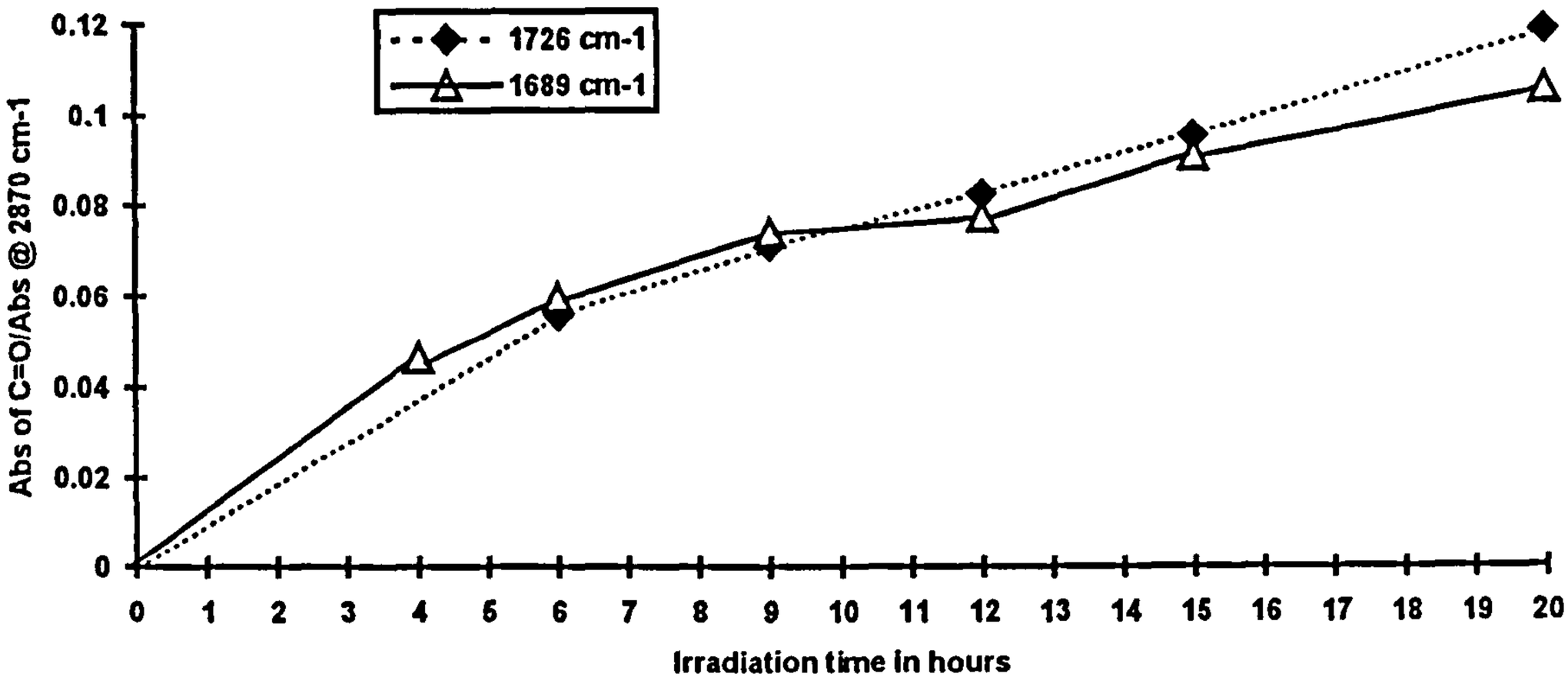

Fig. 5.4: Profile showing the growth of carbonyl peaks during UV irradiation of LP-980C

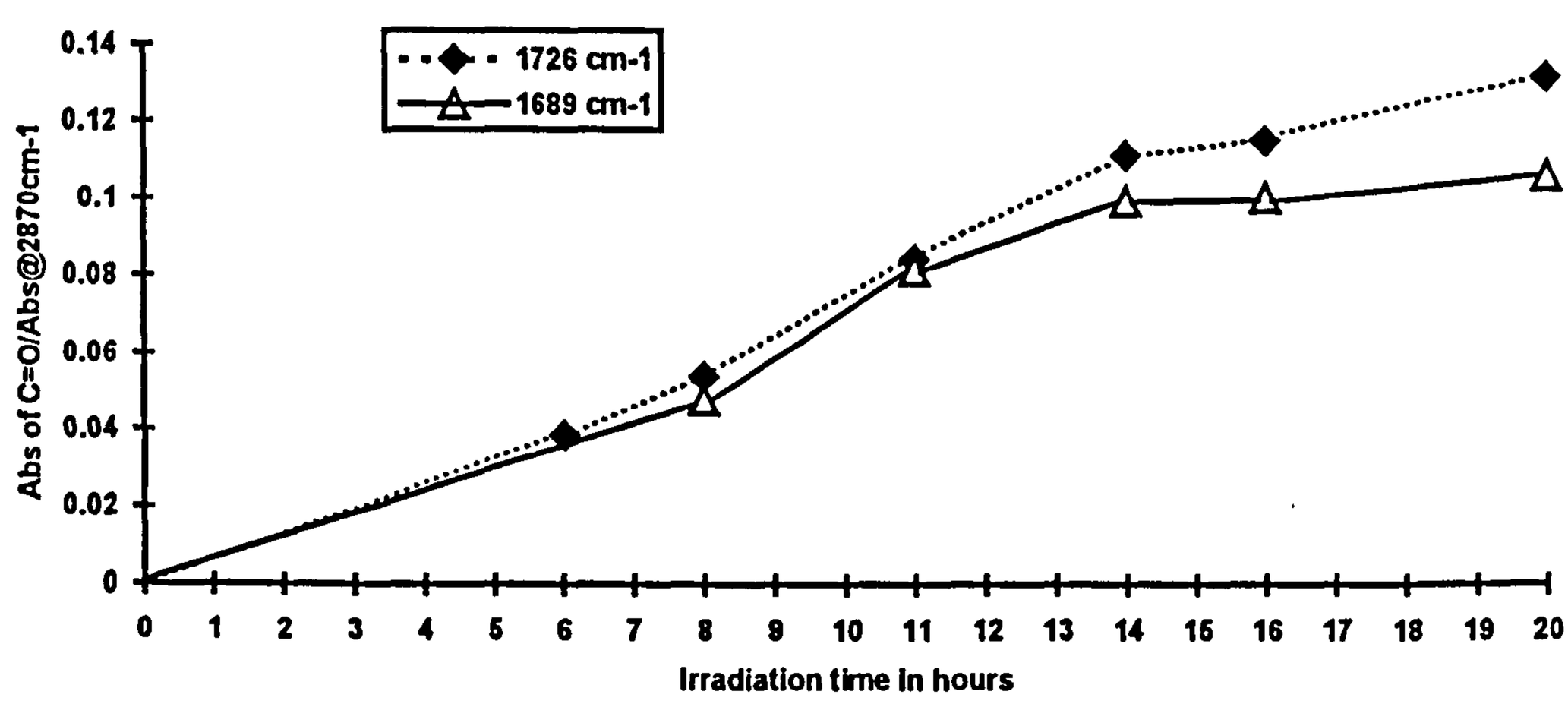

TABLE 5.2:- Comparison of initial slopes obtained for the development of carbonyl frequencies.

LP code nº	$\Delta Abs_{1726}/\Delta t$ / 10^{-6} s^{-1}	$\Delta Abs_{1689}/\Delta t$ / 10^{-6} s^{-1}	Comments
1400C	1.23	0.89	**1726:** 7 points **1689:** 6 points Straight line graphs obtained from 6 to 20 h.
33	4.38	2.68	**1726:** 4 points Slope calculated from 11 and 20 h. **1689:** 6 points Slope calculated from 6 to 20 h. Both graphs are initially linear but begin to plateau with time.
3	1.43	1.59	**1726:** 1 point only Slope calculated by plotting line through origin. **1689:** 6 points Straight line graph obtained from 9 to 20 h.
980C	1.83	1.30	**1726:** 7 points Slope calculated from 6 to 20 h. **1689:** 7 points Slope calculated from 8 to 20 h. Both graphs are initially linear but begin to plateau with time.
977C	1.77	1.46	**1726:** 5 points Straight line graph obtained from 4.5 to 20 h. **1689:** 7 points Straight line graph obtained from 6.5 to 20 h.
541C	3.63	2.36	**1726:** 5 points Straight line graph obtained from 6 to 20 h. **1689:** 7 points Straight line graph obtained from 4 to 14 h.
12C	2.78	1.72	**1726:** 2 points Slope calculated from 16 to 20 h. **1689:** 7 points Slope calculated from 5 to 20 h.
32C	7.50	No points	**1726:** 9 points Straight line graph obtained from 4 to 16 h.
2C	4.51	1.85	**1726:** 5 points Slope calculated from 8 to 20 h. **1689:** 2 points Slope calculated from 5 to 20 h.
31	2.75	1.53	**1726:** 5 points Slope calculated from 8 to 20 h. **1689:** 6 points Slope calculated from 8 to 20 h. Both graphs are initially linear but begin to plateau with time.
32C (Limited O_2)	0.84	No points	**1726:** 8 points Slope calculated from 24.5 to 54 h.

Restriction of the supply of oxygen to the sample, by placing a second NaCl disc over the liquid film, showed the development of the carbonyl band to be considerably reduced, see fig.5.5. The rate of growth of ν(C=O) is evidently heavily dependent on the availability of oxygen.

Fig.5.5: Graph showing the effect of oxygen supply on the time dependence of the development of peak at 1726 cm^{-1}

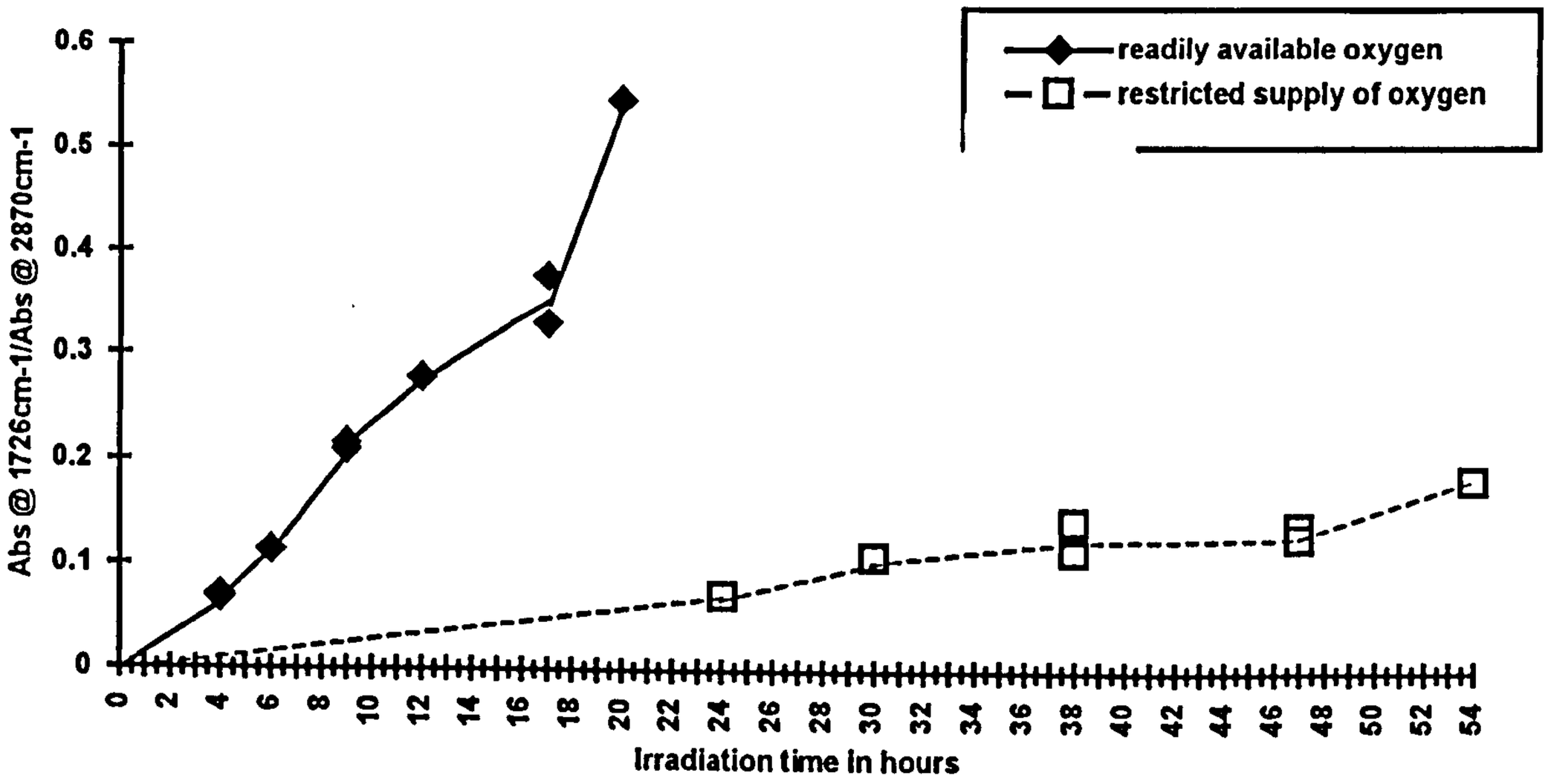

Attempts to observe the S=O group frequency in the photo-oxidised LPs were frustrated by the overlap of ν(S=O), (1000 to 1055 cm^{-1} in DMSO), with skeletal bands of the LP.

5.2 DEGRADATION STUDIES OF LP PRE-POLYMERS BY GPC

All ten LPs listed in Table 2.2 were irradiated in the UV_B 'Weatherometer' for extensive periods, i.e. of up to 3000 hours, and investigated alongside the corresponding unirradiated polymer as a control. GPC measurements indicate that UV photolysis of LPs produces a broadening of RMMD, see fig. 5.6, with a particularly significant increase in Mw, i.e. there is a considerable development of longer-chain species.

LP samples exposed to temperatures of up to 150°C for extensive periods also exhibited a similar broadening of the RMMD.

Fig. 5.6 Plot to show UV-induced changes observed in RMMD for LP-32C

KEY:
A - Before exposure
B - After 2835 h UV_B exposure

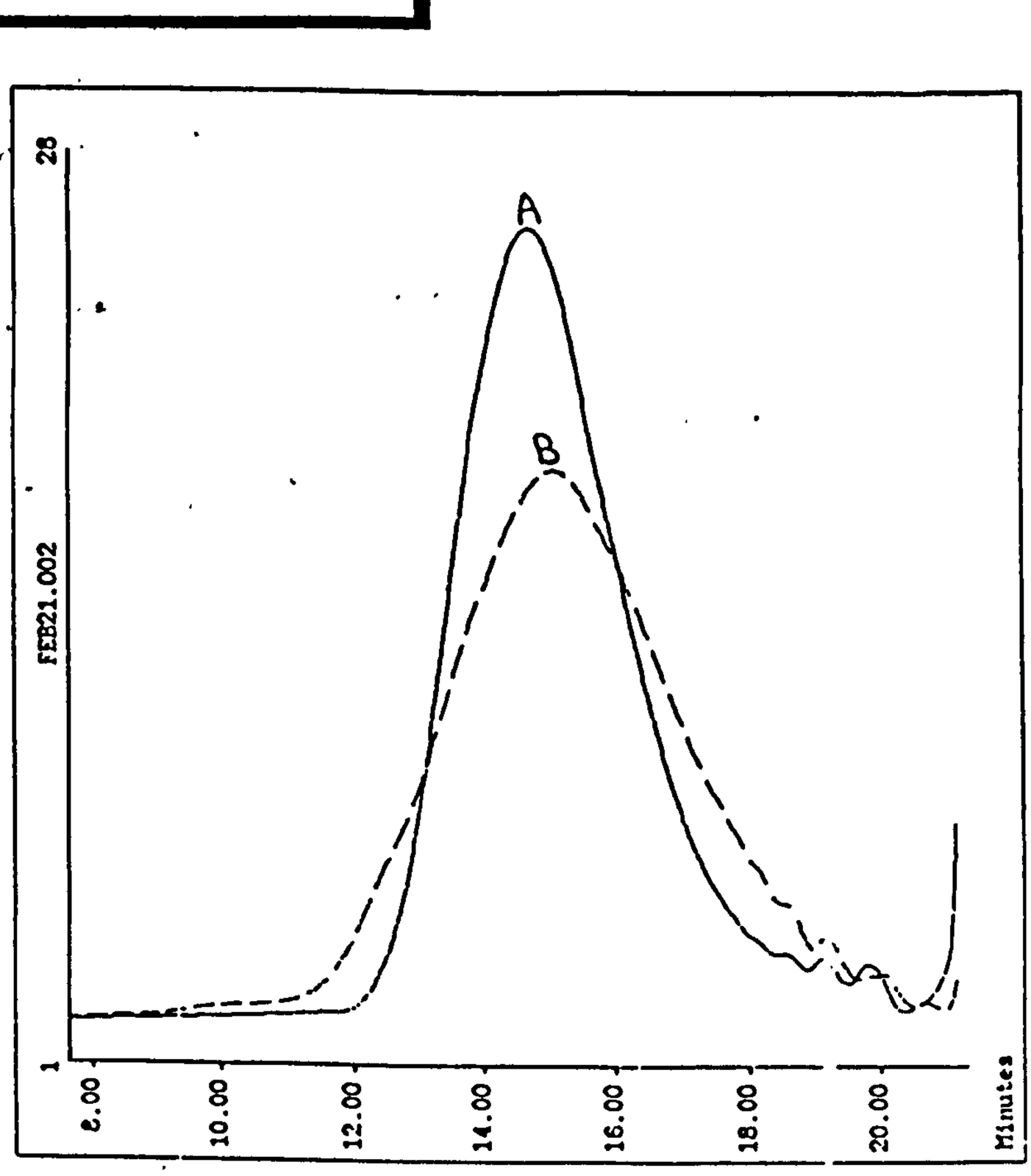

5.3 PHOTODEGRADATION STUDIES OF BULK SAMPLES OF LP PRE-POLYMERS UNDER UV_B IRRADIATION BY IR SPECTROSCOPY.

All ten LPs listed in table 2.2 were irradiated in the UV_B 'Weatherometer' in the following ways:-

i). a restricted supply of oxygen, where samples were irradiated in sealed quartz tubes.

ii). in a plentiful supply of oxygen, where samples were irradiated in 1 cm NMR tubes containing a large 'head' of air and the stoppers were removed and replaced regularly.

After prolonged UV exposure, (≈ 5000 hours), ^{1}H, ^{13}C NMR and IR spectra were recorded for each LP.

Typical IR spectra are illustrated in figs. 5.7 and 5.8.

Evidently these IR spectra show that the availability of air to the pre-polymer results in the formation of C=O and O-H bonds, and hence rapid degradation occurs.

The IR, ^{1}H and ^{13}C NMR spectra for pre-polymeric samples in a restricted supply of air remain barely altered after 5205.5 hours of exposure in the UV_B 'Weatherometer'. This implies that a supply of air is necessary to procure the carbonyl development pathway. Hence, photodegradation in LP pre-polymers must occur via an autoxidative mechanism.

The ^{1}H and ^{13}C NMR spectra for LP pre-polymer samples irradiated in freely available air have undergone major changes and are very complex, see figs.5.9 and 5.10. One of the most prominent changes is the disappearance of the thiol group, (represented

by the triplet at ≈ 1.56 ppm in ^{1}H spectra and ≈ 24.5 ppm in ^{13}C spectra), due to oxidation. Also, there is the presence of new peaks within the ^{1}H and ^{13}C NMR spectra which relate to carbonyl formation within these samples. The positions of these carbonyl frequencies are summarised in table 5.3. Many other new peaks are present in the ^{1}H and ^{13}C NMR spectra; most of these are probably due to oxidative products, but remain unassigned.

Fig. 5.7: Spectrum showing the development of O-H and C=O frequencies in LP-2C after 4820.5 hours UV irradiation in a plentiful supply of oxygen.

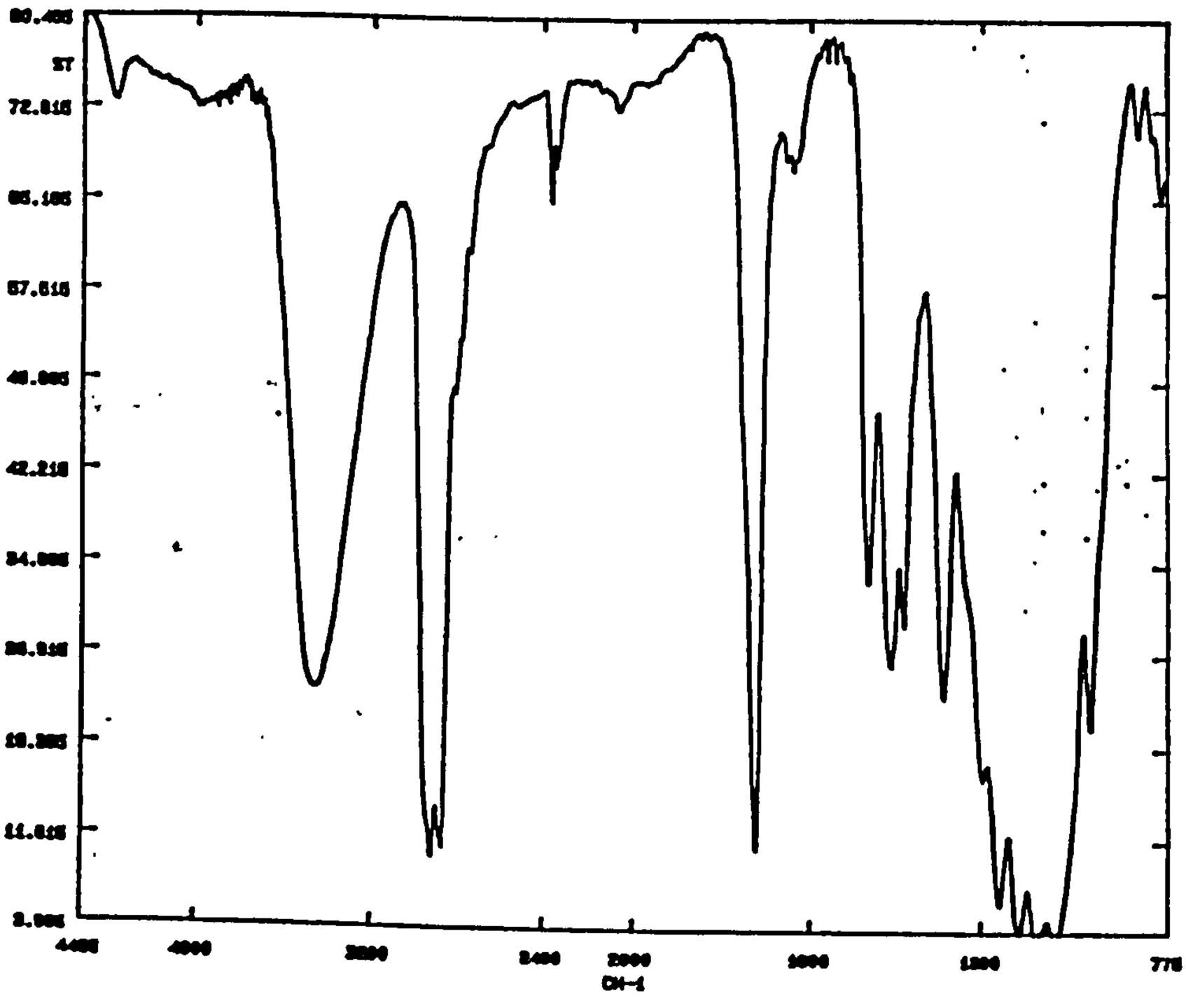

Fig. 5.8: Spectrum of LP-2C after 5205.5 hours UV irradiation in a limited supply of oxygen.

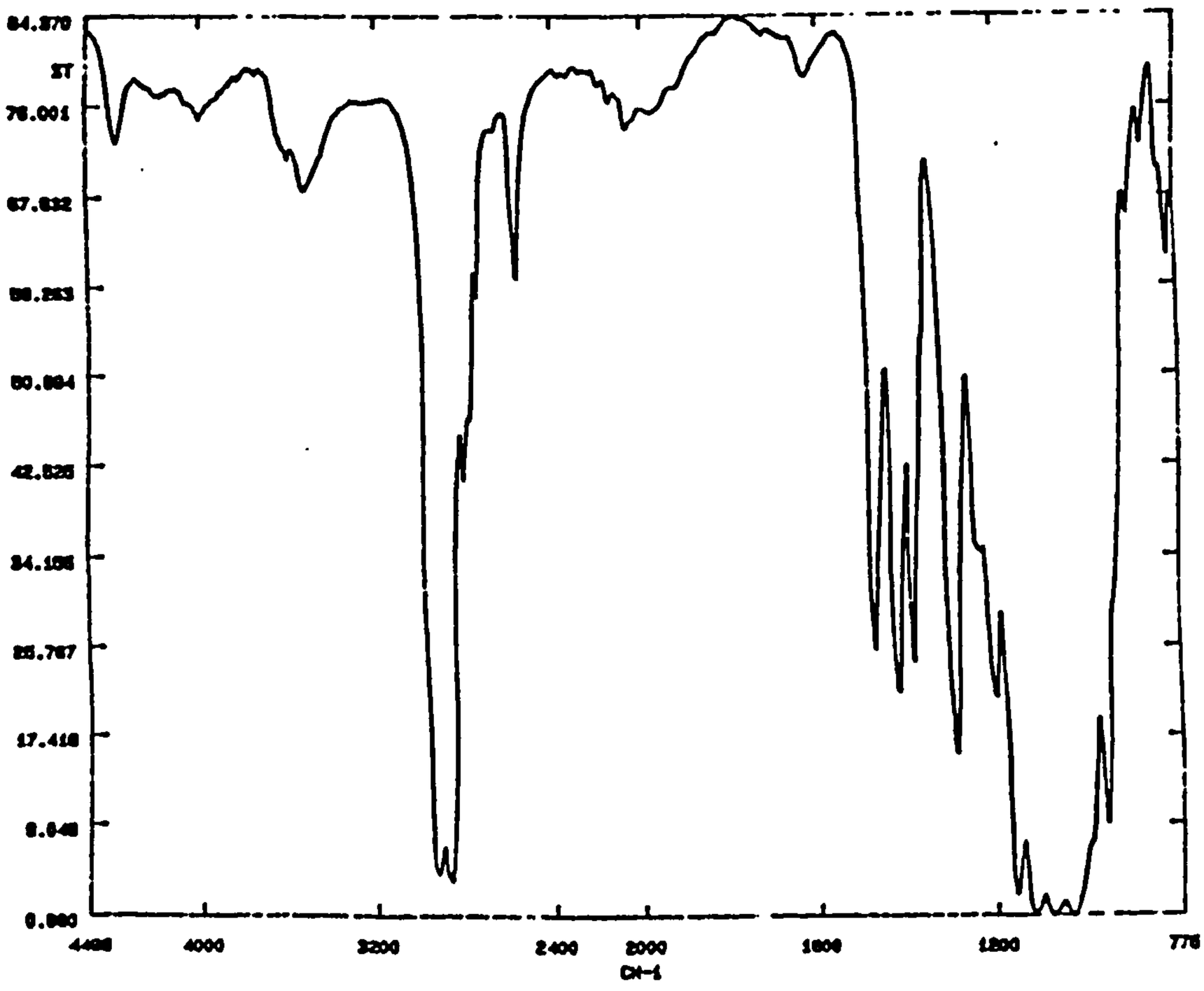

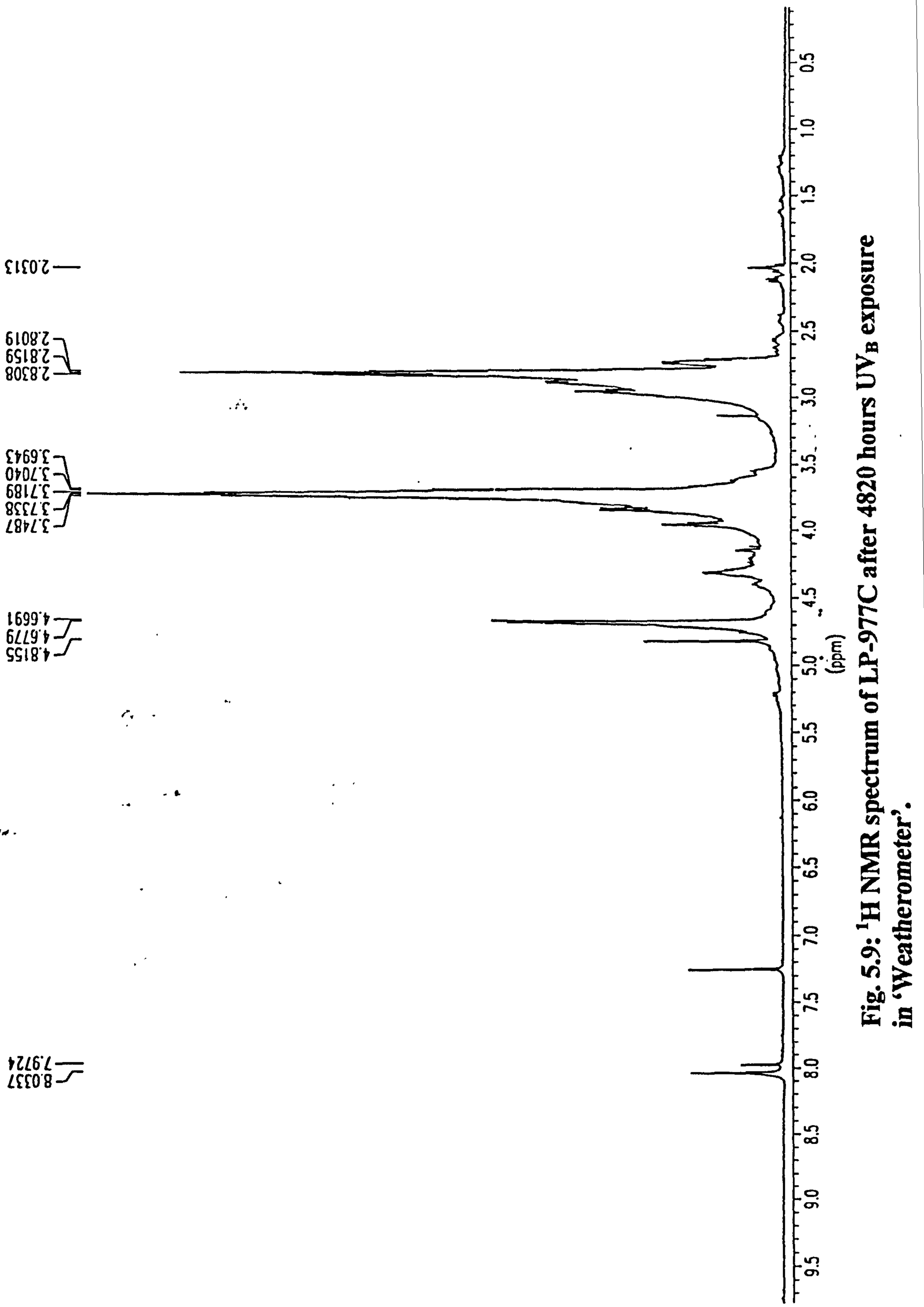

Fig. 5.9: ^{1}H NMR spectrum of LP-977C after 4820 hours UV_B exposure in 'Weatherometer'.

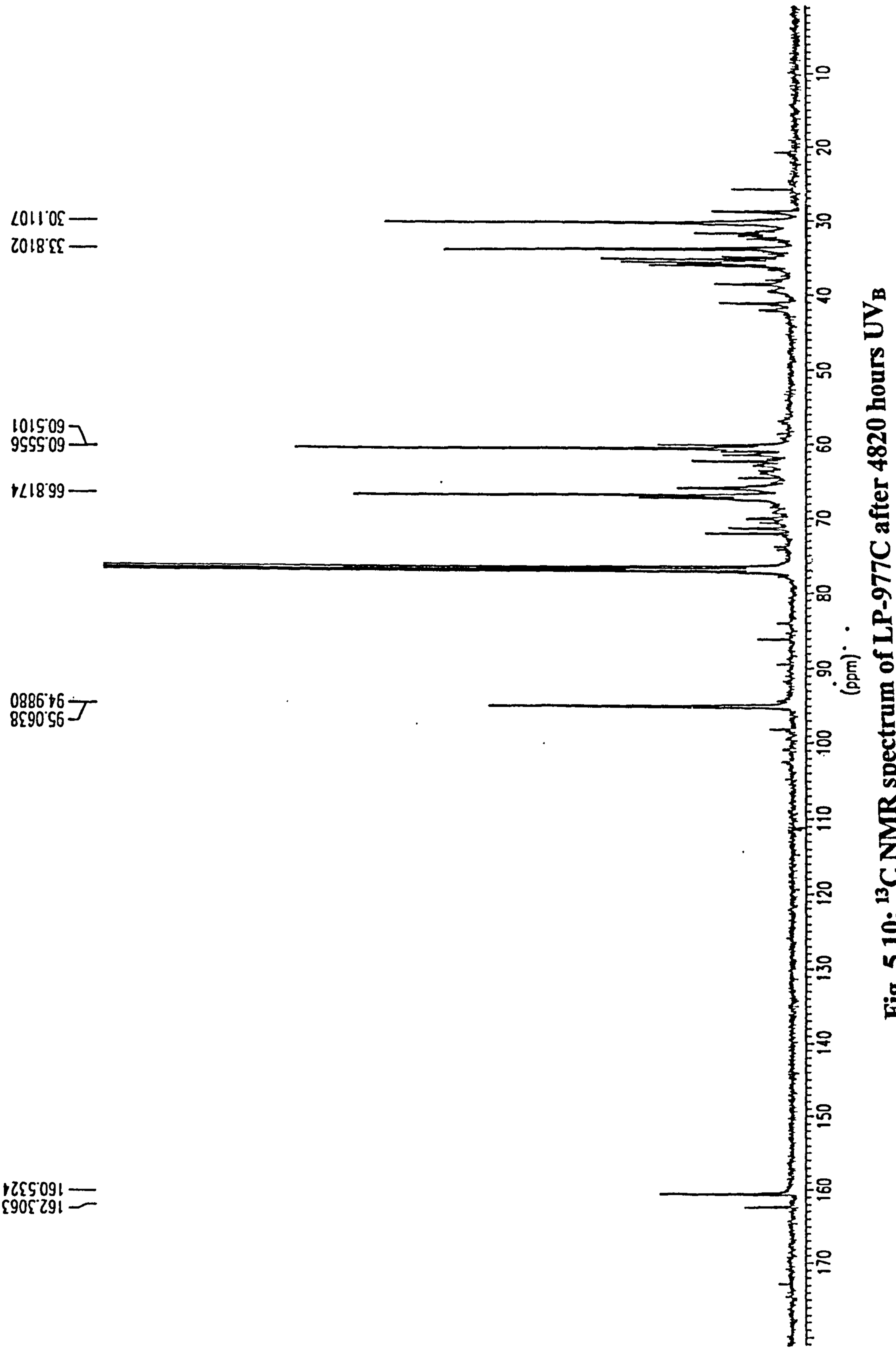

Fig. 5.10: ^{13}C NMR spectrum of LP-977C after 4820 hours UV$_B$ exposure in 'Weatherometer'.

Table 5.3: Carbonyl frequencies in heavily degraded pre-polymer samples.

LP	IR peaks (cm^{-1})	^{1}H NMR (ppm)	^{13}C NMR (ppm)
LP-1400C	1723	8.02 7.95	160.49 162.02
LP-2C	1723	8.02 7.95	160.50 162.07
LP-12C	1723	8.02 7.94	160.38
LP-980C	1723	----------	160.39
LP-3	1723	8.03	160.49
LP-32C	1723	----------	160.41
LP-31C	1723	8.03 7.95	160.43 161.54
LP-33	1723	8.02 7.95	160.42
LP-541C	1723	8.03 7.94	160.39
LP-977C	1723	8.03 7.95	160.45 161.73

5.4 CHROMATOGRAPHY EXPERIMENTS CARRIED OUT ON HEAVILY IRRADIATED LP-1400C PRE-POLYMER TO HELP IDENTIFY NEW NMR PEAKS.

TLC was carried out on heavily UV-exposed LP-1400C, (up to 6314 hours), using different solvents. From these experiments it was deduced that column chromatography could be carried out initially using chloroform as solvent, and then gradually adding progressively increasing amounts of THF, until the sample was completely removed from the column.

A column was prepared in a 10 cm^3 burette using approximately 6 cm^3 of silica gel, see fig.5.11. 0.5 g of LP-1400C dissolved in chloroform was then added and washed through using chloroform as solvent; fractions were collected. A THF / chloroform mixture was then used as eluting solvent, followed in turn by pure THF. The last few fractions were collected using methanol as solvent to ensure that all the sample had been removed from the column.

The solvent from the various fractions was removed using a rotary evaporator and the residues were dissolved in $CDCl_3$. Each solution was then placed in a NMR tube and ^1H spectra were obtained.

Chromatography was only partially successful in that although separation was achieved, the ^1H NMR spectrum for each fraction was almost identical to that of the LP obtained before separation. Only the ^1H NMR spectrum for fraction 3 was slightly simplified. This indicates that column chromatography had merely separated different molecular weight fractions with the same basic structure. The ^1H NMR spectrum of the original material showed poor resolution, but the early fractions of the separated sample

show a vast improvement in resolution, with the disappearance of the terminal thiol groups after prolonged UV exposure; this could be taken as indicating that some cyclic molecules are eliminated during the photo-degradation process.

Fig. 5.11: Overview of column.

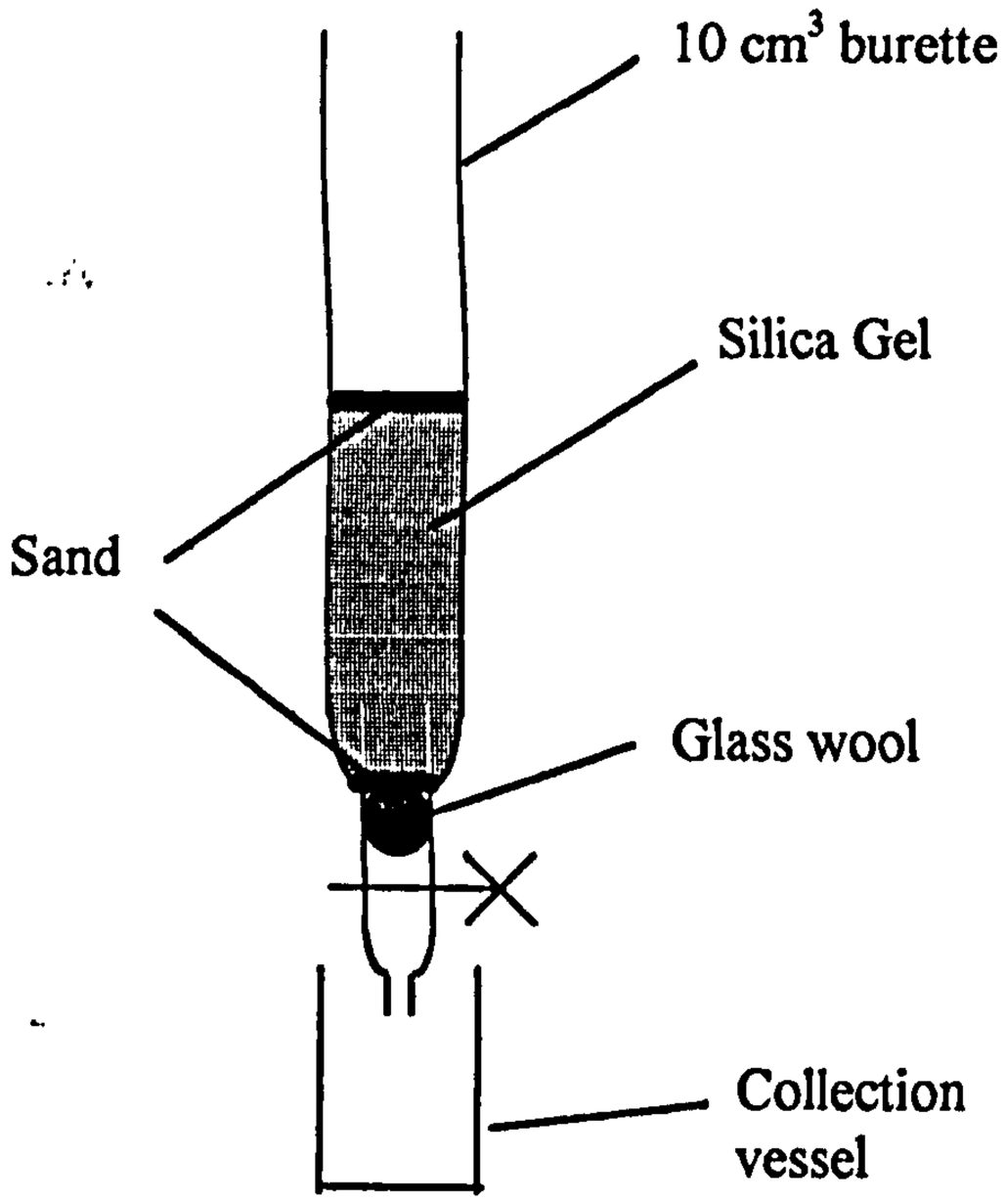

5.5 BULK THERMAL DEGRADATION STUDIES OF LP PRE- POLYMERS BY IR SPECTROSCOPY.

The LP pre-polymer listed in table 2.2 were exposed to a temperature of 100^0C for up to 200 hours, with an unrestricted supply of oxygen available to the samples. After heating, the appearance, smell and viscosity of the samples had altered dramatically. The IR spectra of these extensively heated samples showed the development of O-H and C=O frequencies, a typical example being shown in fig.5.12.

Fig.5.12: IR spectrum showing O-H and C=O frequencies in LP-980C after 200 hours at 100^0C

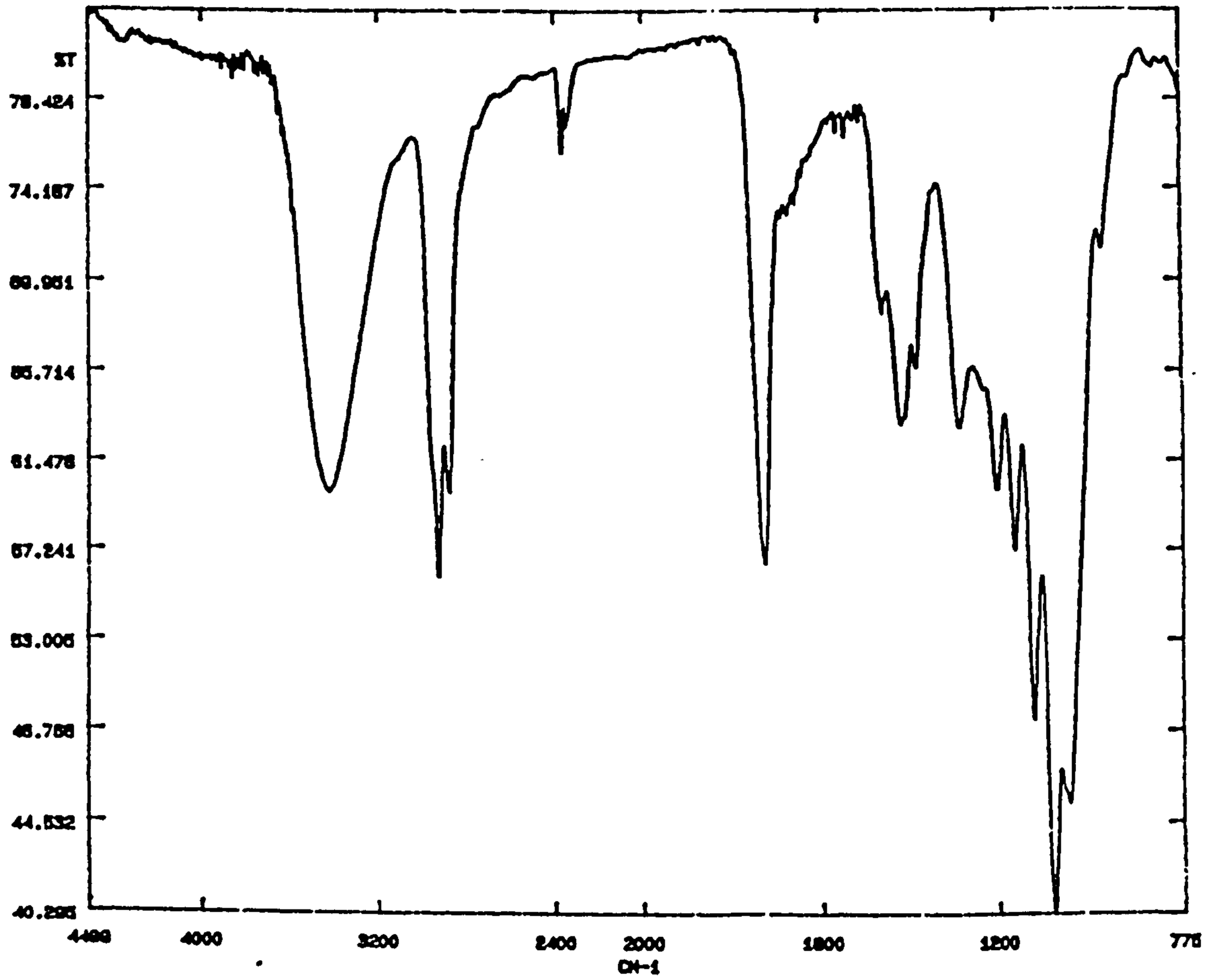

GPC traces obtained for thermally degraded pre-polymer samples showed a broadening in the RMMD, similar to that found for UV exposed samples, see section 5.2.

The thermally degraded pre-polymer samples also show similar changes in their ^{1}H and ^{13}C NMR spectra as those for pre-polymers treated to extensive periods of UV irradiation, see section 5.3 and figs.5.9 and 5.10. Again, the major changes are the disappearance of the thiol group and the presence of new peaks at approximately 8 ppm and 160 ppm in the ^{1}H and ^{13}C NMR spectra respectively, which relate to the formation

of carbonyls. It can therefore be assumed that both the thermal and photo-degradation processes of LP pre-polymer occur via a similar mechanism in the presence of oxygen.

5.6 2-D NMR EXPERIMENT ON HEAVILY UV-EXPOSED PRE-POLYMER SAMPLE.

A 2-D NMR spectrum on a heavily photodegraded sample of LP-977C, (after approximately 4820 hours UV_B exposure under oxygen), was obtained, see fig.5.13. This spectrum confirmed that the peak at approximately 8 ppm in the ^{1}H NMR spectra of both the thermal and UV-exposed pre-polymers is related to the peak found at approximately 160 ppm in the ^{13}C NMR spectra.

These NMR carbonyl peaks and the band seen at 1723 cm^{-1} in the IR spectra can therefore be assigned to the formation of a formate ester. Support for this assignment comes from degradation studies of poly(propylene oxide)[3-5] and poly(ethylene oxide)[4] carried out by Lemaire et al.[4] Griffiths et al.[3] and Barton et al.[5] This is most likely produced via a free radical mechanism, which is common for many of similar structured linear polymers such as polyethene[6], poly(ethylene oxide)[4] and poly(propylene oxide)[3-5].

5.7 EXPERIMENT TO ANALYSE VOLATILES PRODUCED WHEN A PRE-POLYMER SAMPLE UNDERGOES UV IRRADIATION.

A small amount of LP-977C was placed into each of three quartz tubes. The tubes were sealed using an air-tight "Suba" seal. One sample was then flushed with oxygen for 30 mins, see fig.5.14, another was flushed with nitrogen, while the other remained under an air atmosphere. The rubber Suba seal was then protected by covering

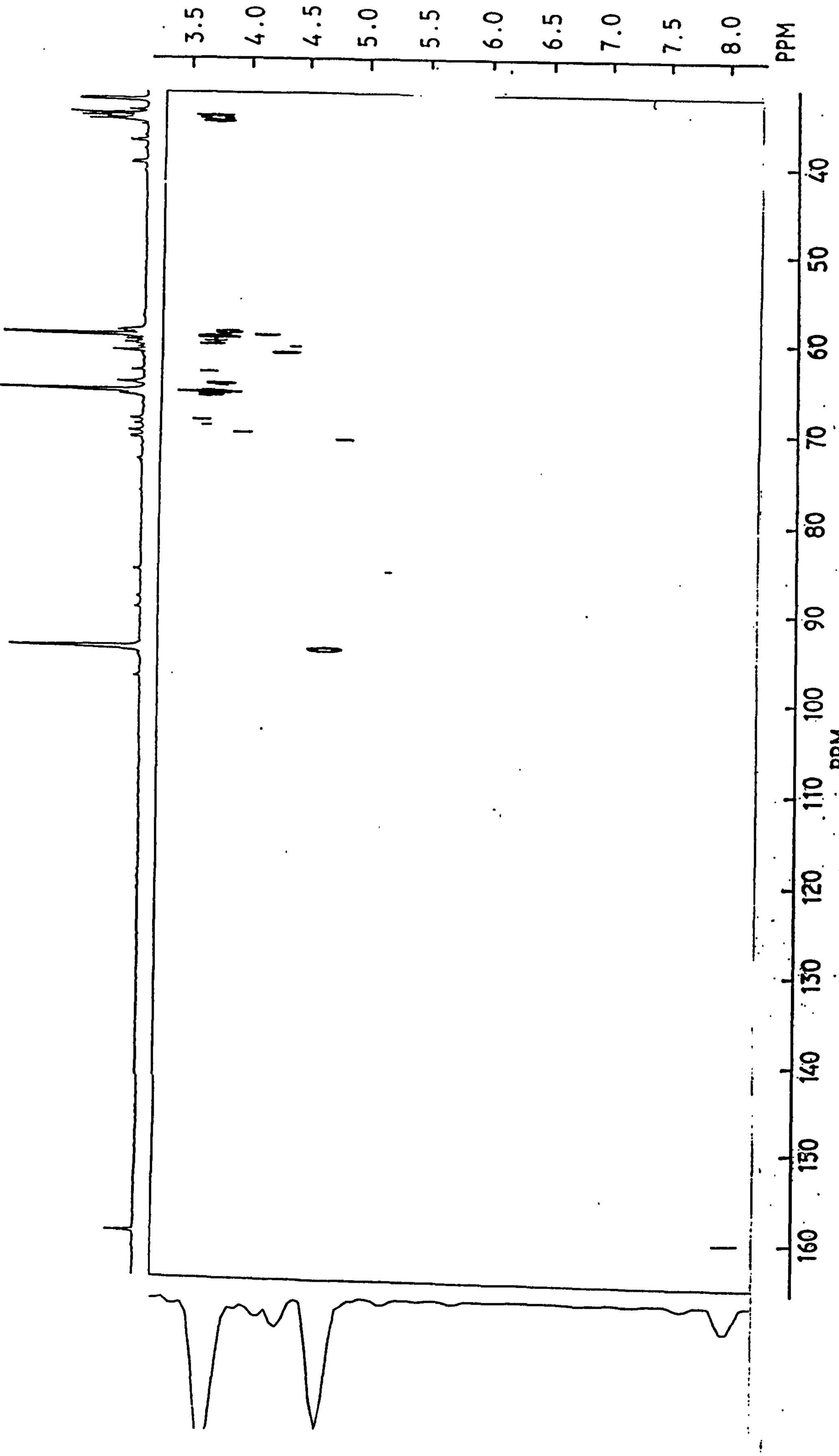

Fig. 5.13: 2-D NMR spectrum of LP-977C after 4820 hours UV_B exposure in 'Weatherometer'.

with aluminium foil and these samples were placed in the UV_B "Weatherometer" for approximately 5000 hours. The sample tubes clearly showed the release of a brown gas, which was extremely dense in the sample tube under oxygen, again indicating that oxygen has a crucial role in the photodegradation mechanism for these compounds.

GC-MS was performed on the "head-space" gas above the polymer sample, but the spectra obtained were uninformative, indicating major peaks at masses 18, 28, 32, 44 which correspond to H_2O, N_2 or CO, O_2 and CO_2, i.e. those expected for an air atmosphere. IR, GPC, ^1H and ^{13}C NMR spectra were also obtained on the degraded polymer sample at the bottom of the tube. The sample under oxygen clearly showed the development of carbonyl bands in IR and NMR spectra, and the spectra obtained were very similar to figs. 5.7, 5.9 and 5.10. However, the spectra of the sample under nitrogen remained barely altered from those originally obtained for LP-977C, again indicating that the formation of a formate ester must occur via an aerobic mechanism, i.e. a photo-oxidative route.

Fig.5.14: Overview of sample tube containing pre-polymer

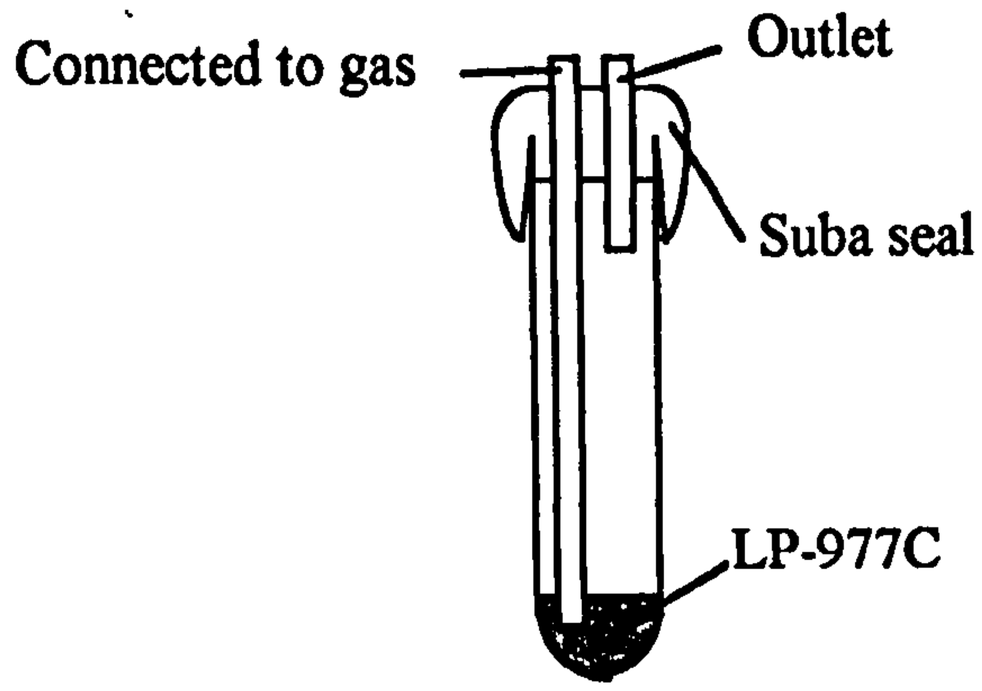

5.8 ELECTROSPRAY MASS SPECTROMETRY STUDIES OF THERMALLY- AND PHOTO- DEGRADED PRE-POLYMERS.

Pre-polymer samples, heavily degraded either by UV or by heat treatment, were analysed using ESI-MS and a typical spectrum is illustrated in fig.5.15. The resultant spectra obtained for degraded pre-polymer samples were extremely complex, which is to be expected considering the number of series present in the original materials, see section 3.1. To simplify this intrinsically complex situation, degradation studies were carried out using ESI-MS of the purified pre-polymer, Model A, (ESI-MS spectrum see fig 3.4 section 3.1). Any changes in the structure of Model A due to degradation should be visible in the ESI-MS spectrum in the form of new peaks arising at different masses, but each new series should still be separated by 166 Da, the mass of the mer unit.

Three types of method were used to degrade the pre-polymer Model A,

i) UV exposure,

ii) heating at 80^{o}C,

iii) heating at 140^{o}C;

all were carried out in the presence of oxygen. A typical ESI-MS spectrum for the UV-degraded pre-polymer is illustrated in fig.5.16. The most notable feature in the spectra of heavily UV-exposed pre-polymer samples, (exposure time in the region of thousands of hours), is the presence of the original A and B series (see section 3.1, fig.3.4), and the appearance of new series at masses corresponding to A and B series less 14 amu, and 30 amu, and plus 76 amu.

Analyses of these UV-exposed samples by GPC, IR and ^{1}H and ^{13}C NMR were also performed. The IR spectra obtained showed the disappearance of the SH band at

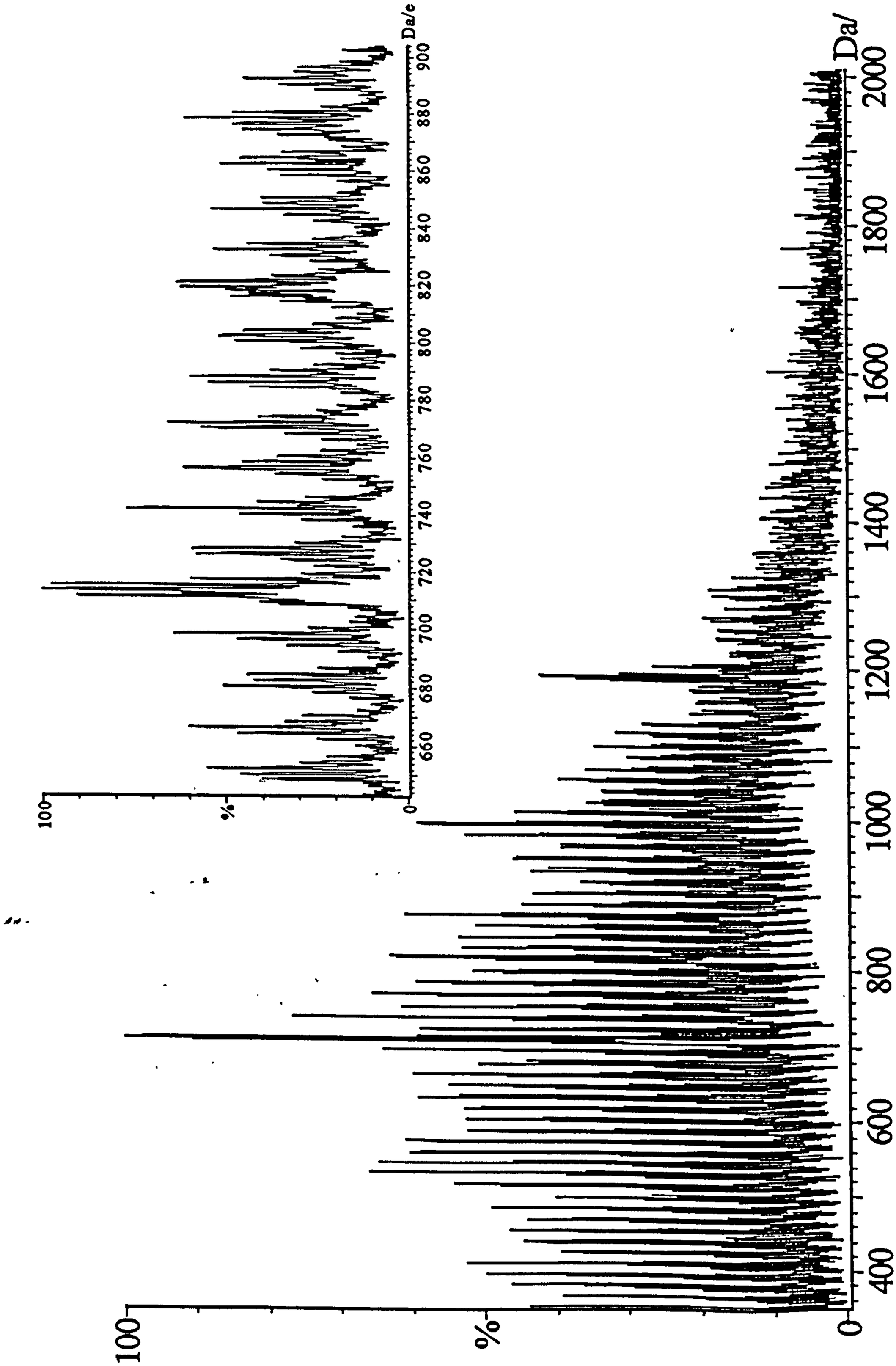

Fig. 5.15: ESI-MS spectrum of LP-977C after 2500 hours UV_B exposure in 'Weatherometer'. Mobile phase THF/MeOH containing 0.5 % aqueous NH_4Cl.

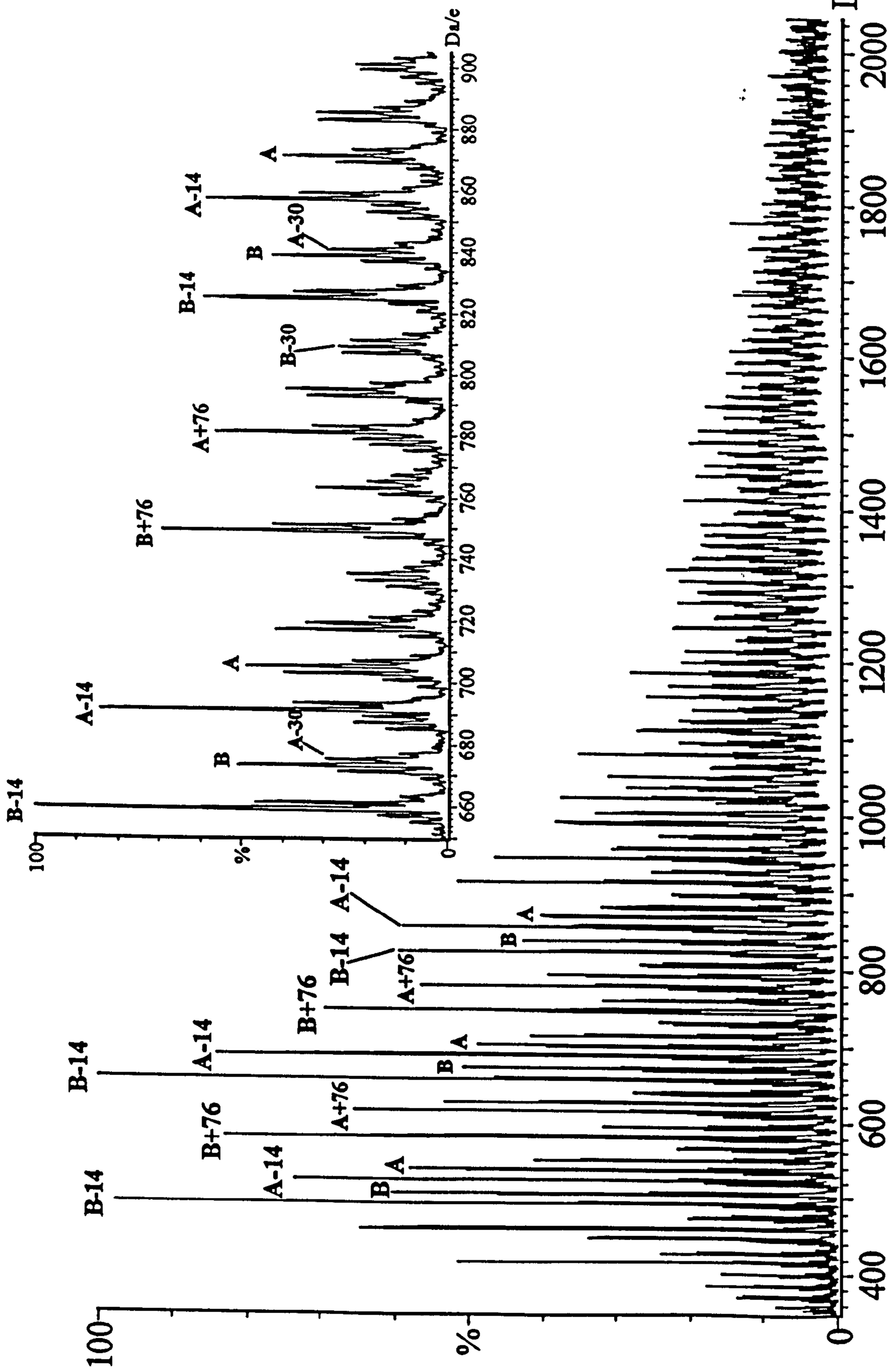

Fig. 5.16: ESI-MS spectrum of Model A after 5150 hours exposure in 'Weatherometer'. Mobile phase: acetone containing KI.

2560 cm^{-1}, the appearance of a broad band in the O-H region at approximately 3490 cm^{-1} and the development of a C=O peak at 1725 cm^{-1}. GPC analysis showed a broadening in RMMD and a huge increase in polydispersity.

^{1}H NMR spectra showed the disappearance of the terminal SH groups and the appearance of a new peak at approximately 8 ppm. The ^{13}C NMR spectra again showed the disappearance of SH and also the appearance of two new peaks at approximately 41 and 60 ppm, see fig.5.17.

Model A pre-polymer samples heated at 140°C for hundreds of hours gave rise to ESI-MS spectra similar to those obtained for the UV-exposed samples, see fig.5.16, indicating a similar degradation route. The original A and B series are still present, accompanied by the appearance of the new series: A, B -14 amu, and A, B +76 amu, and there is also evidence for the A, B -30 amu series, although the latter peaks are of very low intensity.

The IR spectra for the thermalised samples show the development of a broad band in the O-H region, a small C=O development and the disappearance of the SH band. The GPC traces again show a broadening in RMMD on exposure to heat with an increase in polydispersity. ^{1}H and ^{13}C NMR spectra show the disappearance of the terminal SH groups; there is no evidence for C=O in these NMR spectra but the IR spectra indicated only a small development at 1725 cm^{-1}, and there are two new peaks in the ^{13}C NMR spectra at 41 and 60 ppm, see fig.5.17.

Pre-polymer samples heated at 80°C for up to 1175 hours showed very little difference from the original sample. The ESI-MS spectra were virtually identical to that

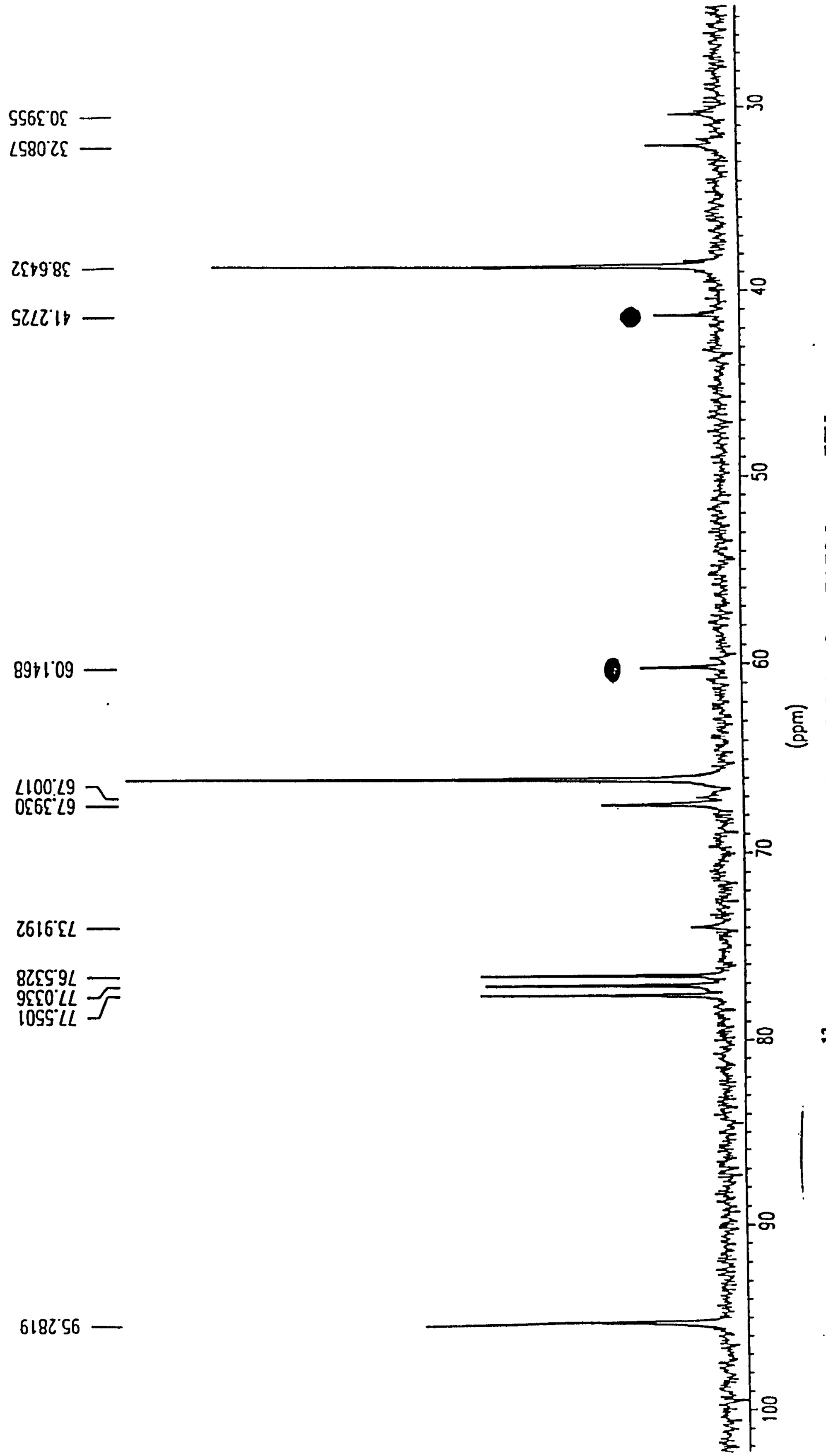

Fig. 5.17: ^{13}C NMR spectrum of Model A after 5150 hours UV_B exposure in 'Weatherometer'.

illustrated in fig.3.4, except that there was a small, but clear development with a A, B +76 amu series. The IR spectra also showed no discernible changes, with no development of O-H or C=O bands, and the peak at 2560 cm^{-1} assigned to SH was still present. The GPC traces show a broadening in RMMD on exposure under these conditions. ^{1}H and ^{13}C NMR spectra also show no change from those obtained for Model A originally. Both show that the SH terminal groups are still present, that no new peaks can be observed at 41 and 60 ppm in ^{13}C NMR spectra, and that there is no evidence for C=O formation. It therefore appears that polysulfide pre-polymers are relatively stable at 80°C, even for over a thousand hours.

The A, B -14 amu series seen in the spectra of UV- and thermally- degraded pre-polymers at 140°C can be assigned to the formation of:

$$\mathbf{HO\text{-}C_2H_4\text{-}S(\text{-}S\text{-}C_2H_4\text{-}O\text{-}CH_2\text{-}O\text{-}\ C_2H_4\text{-}S\text{-})_{n\text{-}1}\ S\text{-}\ C_2H_4\text{-}OH}$$

which is produced from the hydrolysis of the two formal links[7] by the following reaction.

$$R\text{-}O\text{-}CH_2\text{-}O\text{-}R + H_2O \longrightarrow 2\ R\text{-}OH + CH_2O \quad \text{.....(1)}$$

In more detail, the sequence of processes is as follows:

$$H(\sim SSC_2H_4OCH_2OC_2H_4SSC_2H_4OCH_2OC_2H_4SS\sim)H$$

$$\downarrow \quad \text{Pre-polymer}$$

$$H(\sim SSC_2H_4OCH_2OC_2H_4SSC_2H_4OCH_2OH + HOC_2H_4SS\sim)H$$

$$\downarrow \quad \text{Further hydrolysis at second formal link.}$$

$$\sim SSC_2H_4OCH_2OC_2H_4SSC_2H_4OH + HOCH_2OH + HOC_2H_4SS\sim$$

formaldehyde hydrate

$$\downarrow \quad \text{Further hydrolysis at a further formal link.}$$

$$HOC_2H_4S(SC_2H_4OCH_2OC_2H_4\text{-}S)_nSC_2H_4OH + \text{etc.}$$

Considering the RMM of this component of the degraded pre-polymer:

$$RMM = (2 \times 77) + n.166 = 154 + 166n$$

$$RMM\ LP\ (Series\ A) = (2 \times 1) + (n + 1)166 = 2 + 166n + 166$$

$$\Delta(RMM) = 2 + 166n + 166 - 154 - 166n = 14\ amu$$

Thus, each peak in the series based on $HOC_2H_4S(SC_2H_4OCH_2OC_2H_4\text{-}S)_nSC_2H_4OH$ will appear at 14 amu below the corresponding peak in the Series A due to the pre-polymer, i.e. at A -14 amu, (or at B-14 amu if the polymer chain contains a random monosulfide linkage).

To confirm this assignment, the IR, ^1H and ^{13}C NMR spectra all demonstrate the disappearance of the SH terminal groups, the IR spectra also show the development of O-H, while the new peaks at 41 and 60 ppm in the ^{13}C NMR spectra also confirm the assignment, since these peaks were observed in the ^{13}C spectrum for bis-(2-hydroxyethyl)disulfide, i.e. $(HOCH_2CH_2)_2S_2$[8].

The A, B +76 amu series can be explained by the reaction of the disulfide link in the A, B -14 amu series above with formaldehyde by either of the following reactions[7].

$$R\text{-}S\text{-}S\text{-}H + CH_2O \longrightarrow 2\ R\text{-}SH + CO \quad .....(2)$$

$$R\text{-}S\text{-}S\text{-}H + CH_2O + H_2O \longrightarrow 2\ R\text{-}SH + HCO_2H \quad .....(3)$$

which produces the following structure:

$$\mathbf{HO\text{-}C_2H_4\text{-}S(\text{-}S\text{-}C_2H_4\text{-}O\text{-}CH_2\text{-}O\text{-}\ C_2H_4\text{-}S\text{-})_nH}$$

Considering the RMM of this structure:

$$RMM = 77 + 166n + 1 = 78 + 166n$$

$$\text{RMM LP (Series A)} = (2x1) + 166n = 2 + 166n$$

$$\Delta(\text{RMM}) = 78 + 166n - 166n - 2 = 76 \text{ amu}$$

i.e. the peak corresponding to each value of n in the spectrum of this series will appear at 76 amu higher than the corresponding peak in the spectrum of the LP Model A.

A major problem concerning assignments of peaks in the ESI-MS of the degraded pre-polymer is the strong peaks located at masses identical to those found with Series A despite the fact that, according to the IR and NMR spectra, the material is devoid of thiol groups. Evidently a molecule of mass fitting to Series A must be formed which contains no SH groups. One candidate is the species formed by the reaction of the SH groups of $HOC_2H_4S(SC_2H_4OCH_2OC_2H_4S)_nH$ with formaldehyde:

$$2\ \text{R-SH} + CH_2O \longrightarrow \text{R-S-}CH_2\text{-S-R} + H_2O \quad \ldots\ldots\ldots\ldots(4)$$

where R-S-CH_2-S-R is, more fully,

$$\mathbf{HO\text{-}C_2H_4\text{-}S(\text{-}S\text{-}C_2H_4\text{-}O\text{-}CH_2\text{-}O\text{-}C_2H_4\text{-}S\text{-})_nCH_2(\text{-}S\text{-}C_2H_4\text{-}O\text{-}CH_2\text{-}O\text{-}C_2H_4\text{-}S\text{-})_mS\text{-}C_2H_4\text{-}OH}$$

This species has an RMM as follows:

$$77 + 166n + 14 + 166m + 77 = 166(m + n + 1)$$

which will appear at the same peak position in the mass spectrum as Model A pre-polymer. The overall scheme of the above reactions is illustrated in fig.5.18.

The final series of mass spectral peaks needing consideration is that located at A - 30 amu. Various candidates have been considered as responsible for this series. The simple loss of a CH_2O unit from the chain of Model A seems attractive but does not agree with the very clear absence of an SH group in the NMR spectra. This implies the

$$R\text{-}O\text{-}CH_2\text{-}O\text{-}R + H_2O \longrightarrow 2\ R\text{-}OH + CH_2O \quad (1)$$

$$R\text{-}S\text{-}S\text{-}R + CH_2O \longrightarrow 2\ R\text{-}SH + CO \quad (2)$$

$$R\text{-}S\text{-}S\text{-}R + CH_2O + H_2O \longrightarrow 2\ R\text{-}SH + CH_2O_2 \quad (3)$$

$$2\ R\text{-}SH + CH_2O \longrightarrow R\text{-}S\text{-}CH_2\text{-}S\text{-}R + H_2O \quad (4)$$

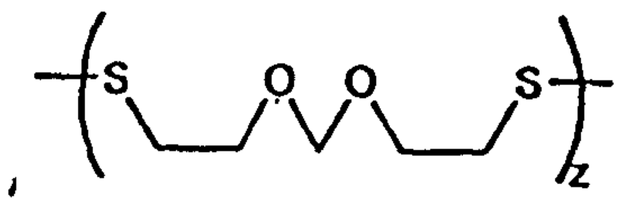

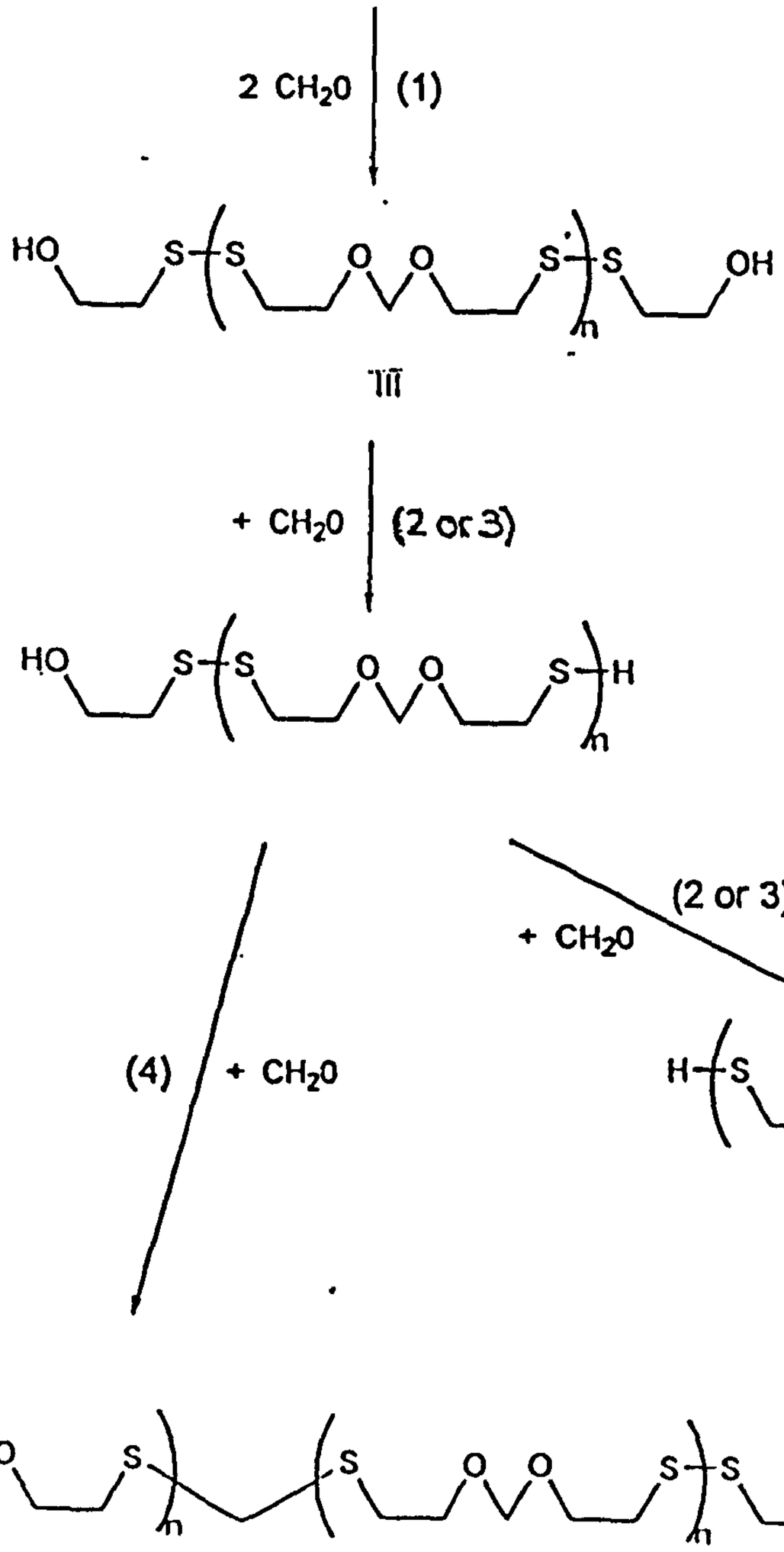

Fig. 5.18: Overall scheme of hydrolysis for LP pre-polymers.

product (denoted A_{-30}) must either feature terminal hydroxy groups or be cyclic. Possibilities are as follows:

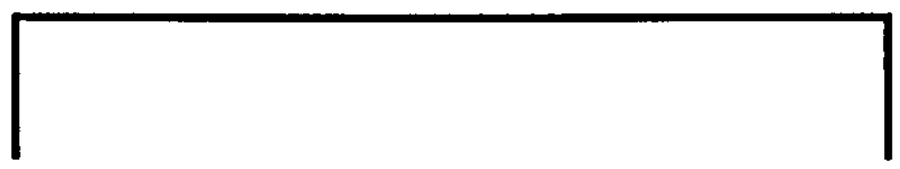

$S(SC_2H_4OCH_2OC_2H_4S)_nSC_2H_4OCH_2O$

$$RMM = 166n + 138$$

$$RMM\ LP\ (Series\ A) = (2 \times 1) + (n + 1)166 = 2 + 166n + 166$$

$$\Delta(RMM) = 166n + 2 + 166 - 166n - 138 = 30\ amu$$

or

$$HOC_2H_4S(SC_2H_4OCH_2OC_2H_4S)_nSC_2H_5$$

$$RMM = 77 + 61 + 166n$$

$$RMM\ LP\ (Series\ A) = (2 \times 1) + (n + 1)166 = 2 + 166n + 166$$

$$\Delta(RMM) = 166n + 2 + 166 - 166n - 61 - 77 = 30\ amu$$

Thus, each peak in the series based on the above structures will appear at 30 amu below the corresponding peak in the Series A due to the pre-polymer, i.e. at A -30 amu.

The cyclic structure given above contains an -O-S-S- junction which is unknown in any stable compound and is therefore very unlikely to be responsible for the A_{-30} series. The ethyl-terminated structure is certain to be stable, but the arguments against such an assignment are powerful, viz.

i) there is no obvious mechanism to produce a terminal ethyl group,

ii) the proton NMR spectrum of the photolysate shows no trace of an ethyl group.

Additional degradation experiments using the pre-polymer ZL-2264, were carried out to provide further evidence for the proposed scheme in fig.5.18. Again three methods of degradation was utilised, UV exposure, heating at 80°C and heating at 140°C. ESI-MS, IR, GPC, ^{1}H and ^{13}C NMR spectra were obtained for each sample following degradation.

In heavily UV-exposed samples, no discernible changes could be seen. One sample of ZL-2264 exposed to UV_B in the 'Weatherometer' for 2640 hours, gave rise to an ESI-MS spectra identical to that of the starting material, see section 3.3 fig.3.6. The GPC, IR and NMR are also unchanged from that obtained for the unexposed material. The same results were also obtained for heat exposed samples; ZL-2264 samples heated at 80°C and 140° C for 860 hours did not undergo any spectral changes. Therefore ZL-2264 appears to be far more stable than the normally structured LP pre-polymers. Only one sample of ZL-2264, heated at 140°C for 1130 hours, showed any signs of degradation, these being the appearance of a new series in the ESI-MS spectra of A,B +60 amu, and the appearance of a broad weak band in the O-H region in the IR spectrum.

These results, pointing to a greatly improved photo- and thermal stability of ZL-2264 compared to "normal" LPs, offer confirmation of the scheme illustrated in fig.5.18 for LP pre-polymer degradation. This scheme depends critically on the presence of the formal linkage in the pre-polymer as the initial site of hydrolysis to produce free formaldehyde, which then further attacks the disulfide linkages. The variation in the repeat unit of ZL-2264 of replacing the CH_2O linkage with C_2H_4O, eliminates any

possibility of the formation of formaldehyde by this reaction, therefore making degradation by this route impossible. We view this as a key finding in the present search for means of extending the lifetimes of polymers based on LPs.

5.9 DISCUSSION AND CONCLUSIONS

The key observations emerging from the results described in the preceding pages are as follows:

i) UV photolysis or pyrolysis of LP pre-polymers in the presence of air or oxygen results in the development of carbonyl groups detectable by IR and NMR spectroscopy. These arise as a result of a conventional free radical mechanism of autoxidation.

ii) 2-D NMR studies, and the highly characteristic field positions of the NMR resonances, show the carbonyl group to be due to a formate ester.

iii) ESI-MS studies of degraded LP pre-polymers show that, in parallel with the degradation route involving oxygenation of a methylene group demonstrated by IR and NMR studies, there is a hydrolysis mechanism involving initial cleavage of the formal group to release formaldehyde, followed by secondary reactions to give other products detected in the ESI-MS spectrum of the photolysate/pyrolysate.

iv) The extremely slow degradation by UV or heat of the pre-polymer ZL-2264 which has no formal group.

An overall, simplified scheme of degradation can thus be formulated: Fig.5.19

Fig.5.19 Overall scheme of degradation of thermally or UV-irradiated LP featuring duality of mechanism.

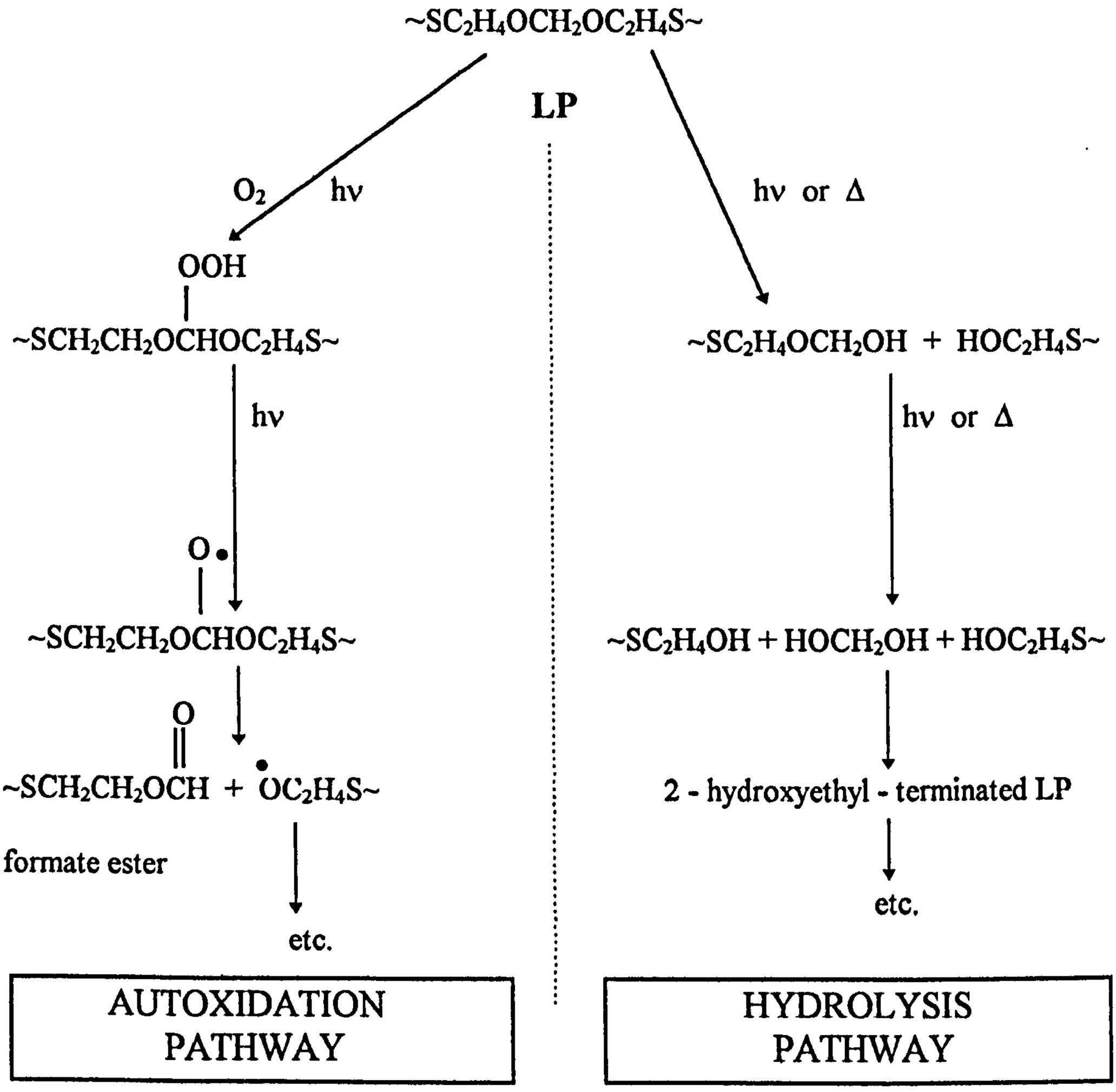

The photo-oxidative pathway finds many parallels in polymer degradation studies, the closest being those of poly(ethylene oxide)[4] and poly(propylene oxide)[3-5], where attack at C-H adjacent to the ether oxygen atom leads to a hydroperoxide and hence an alkoxyl radical followed by scission to give a formate or, from poly(propylene oxide), an acetate as well, viz:

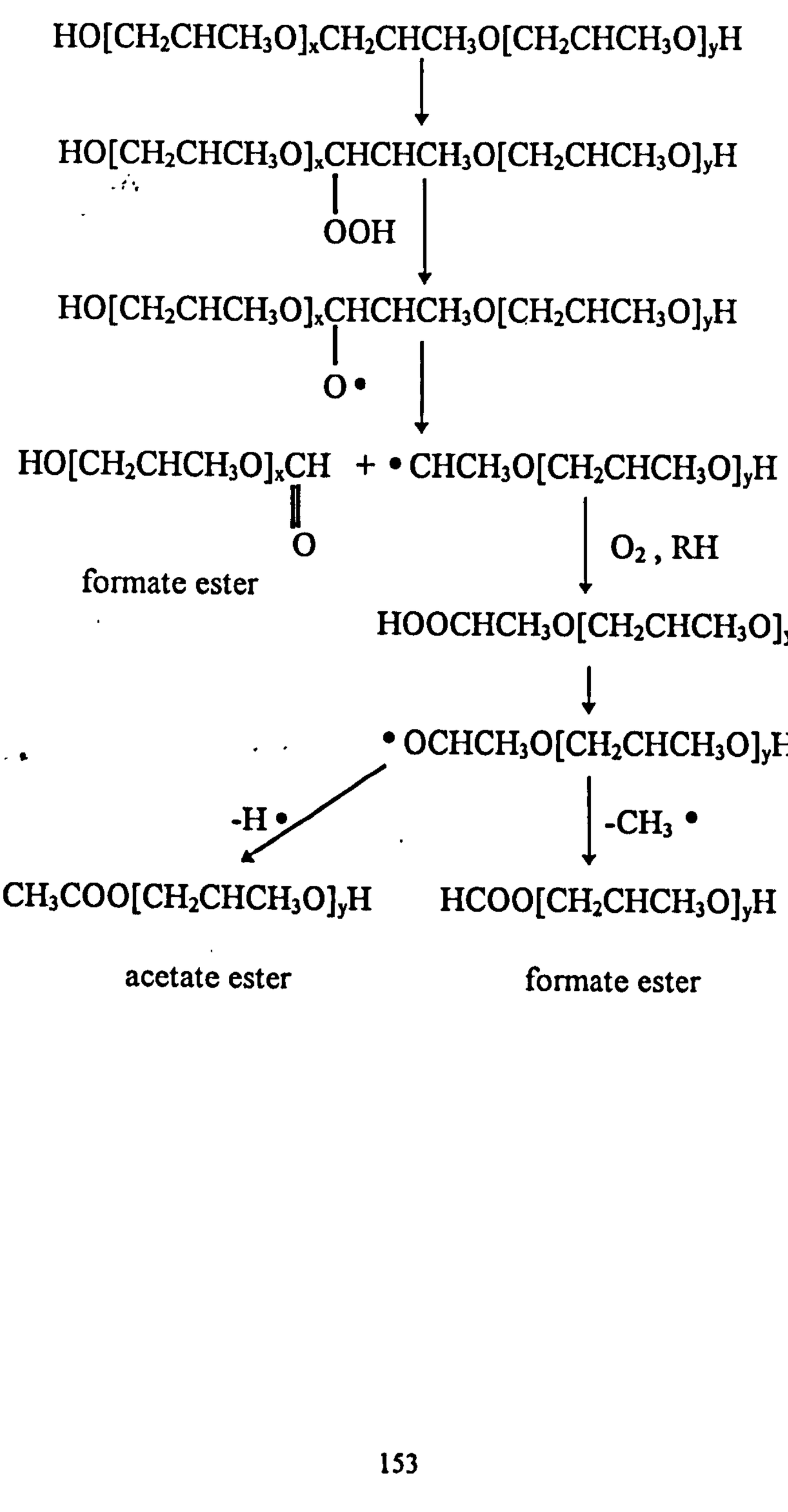

The formate ester is most probably derived from two pathways, namely:

i) via the tertiary carbon centres as proposed by Griffiths et al.[3] and

ii) via the secondary carbon atom as indicated by Lemaire et al.[4]

since the level of branching agent present in the pre-polymer appears to have little effect on the rate of degradation.

Support for our assignment of the IR band at 1725 cm^{-1} to a formate ester comes from other similar assignments e.g. by Griffiths et al.[3], Barton[5], and Lemaire et al.[4]

The results from NMR studies of degraded pre-polymers and the 2-D NMR spectrum of the photolysate also closely mirror those of Griffiths et al[3], Barton et al.[5] Lemaire et al.[4]

The hydrolysis mechanism has been widely accepted as a principal route for degradation of LPs, both cured and as pre-polymers. The development of ^{13}C NMR peaks due to $S\underline{C}H_2CH_2OH$ and $SCH_2\underline{C}H_2OH$ at 41 ppm and 60 ppm respectively finds support from model compound studies of bis-(2-hydroxyethyl)disulfide[8] which yielded ^{13}C resonances at 40 ppm and 59.4 ppm.

The stability of ZL-2264 as compared to all other LPs points to the critical role of the formal groups as the locus of initial degradation.

As regards the relative role of the two pathways given in fig.5.19, the relatively high intensity of peaks in the ESI-MS spectra of the degraded samples attributable to hydrolysed species, as opposed to oxidised species, indicates that, at least as regards pre-polymers, the hydrolysis pathway is dominant. Interestingly, we shall show in chapters 6

and 7 that in the photodegradation of LP polymers cured with MnO_2 (but not t-BuOOH), the photo-oxidative route is much more significant.

In summary, the results of this chapter indicate the duality of the mechanism advocated by Rosenthal and Berenbaum[7], show that the hydrolysis mechanism is the more significant for pre-polymers, and demonstrate the need to deploy more than one analytical approach to the solution of the mechanism of polysulfide degradation, which is so mechanistically rich and diverse.

CHAPTER 5

REFERENCES

1. Adams, J.H., *J. Polym. Sci.*, **8**, (1972) 1279.
2. Ranby, B., Rabek J.F., *Photodegradation, Photo-oxidation and Photostabilization.* Wiley Interscience, London. (1975).
3. Griffiths, P.J.F., Hughes, J.H., Park, G.S., *Eur. Polym. J*, **29**, (1993) 437.
4. Lemaire, J., Gauvin, P., Sallet, D., *Makromol. Chem*, **188**, (1987) 1815.
5. Barton, Z., Kemp. T.J., Buzy, A., Jennings, K.R., *Polymer*, **36**, (1995) 4927.
6. Grassie, N., Scott, G., *Polymer Degradation and Stabilisation,* Cambridge University Press, Cambridge. (1985).
7. Rosenthal, N.A., Berenbaum M.B., *Thermal Degradation of Ethyl Formal Polysulfide Polymers.* In-house report for Thiokol Chemical Corporation.
8. Scrivens, G., D.Phil. thesis, *An EPR Investigation into the Catalytic Oxidation of Thiols by Peroxides,* University of York, (1995).

CHAPTER 6

STUDY OF PHOTODEGRADATION OF CURED-LP FILMS USING INFRA-RED SPECTROSCOPY.

6.1 PRELIMINARY EXPERIMENTS USING 350 W XENON LAMP

Initial results were obtained for LP-977C and LP-980C by curing a thin film on a single NaCl disc. Two levels of MnO_2 were used namely *ca.* 10% and 5% by weight. The samples were irradiated in the same manner as the pre-polymers, (see section 5.1). IR spectra were obtained at intervals throughout the irradiation. A typical IR spectrum is illustrated in fig. 6.1.

Fig. 6.1: Spectrum showing the development of C=O frequencies in LP-980C with MnO_2 loading of 10%, after 20 h UV irradiation using xenon lamp.

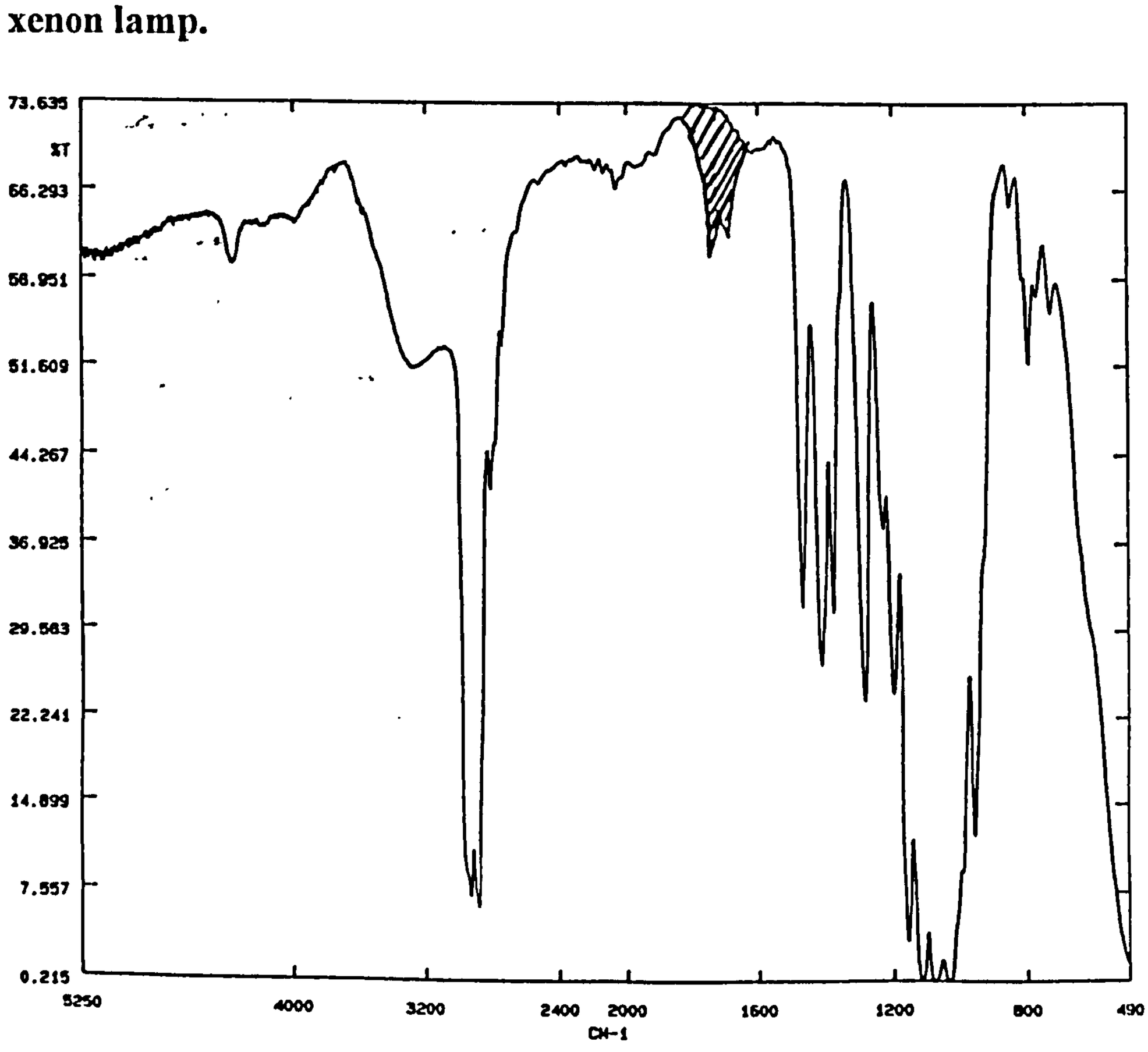

The growth kinetics of C=O absorption are rather similar to those of a liquid film, and the rates of growth are not dissimilar, see fig. 6.2, implying a common mechanism of photo-oxidation.

6.2 EXPERIMENT TO ASCERTAIN WHETHER FILM THICKNESS AFFECTS THE RATE OF PHOTODEGRADATION

LP-977C films of varying thickness were cured using *ca.* 2% MnO_2 and mounted onto cardboard, as in fig. 6.3.

Fig. 6.3: Overview of mounted cured polymer film.

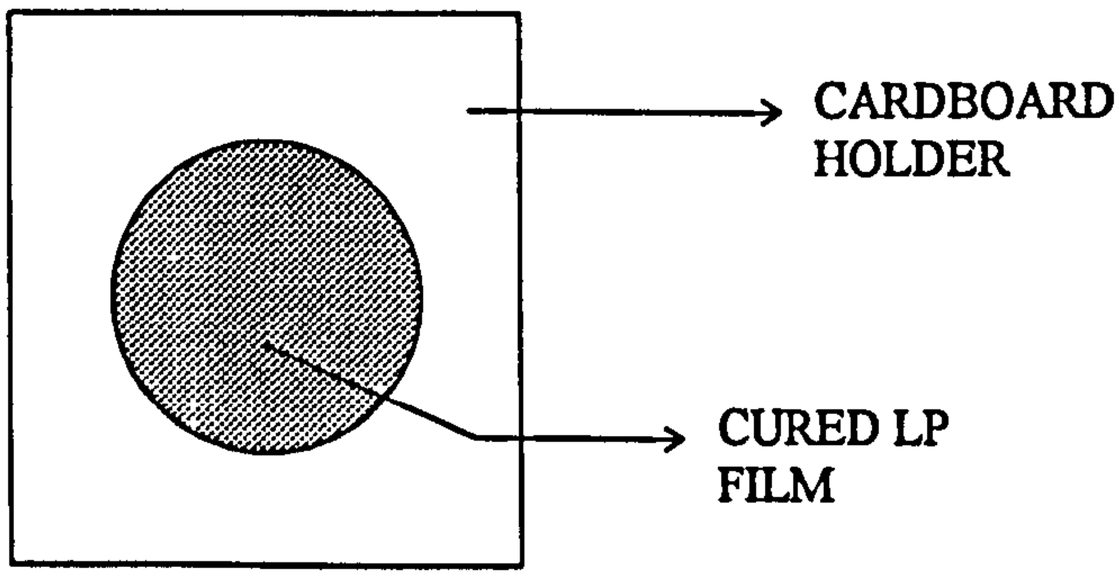

These were irradiated using the UV_B Weatherometer for approximately 1200 hours with IR spectra being obtained at intervals throughout the irradiation. Fig. 6.4. shows that the thinner films develop carbonyl groups much faster than thicker films, as would be expected from their relatively greater permeability to oxygen.

Fig. 6.2: Profile of growth of 1726 cm^{-1} peak for LP-980C and LP-977C with and without MnO_2 (10%).

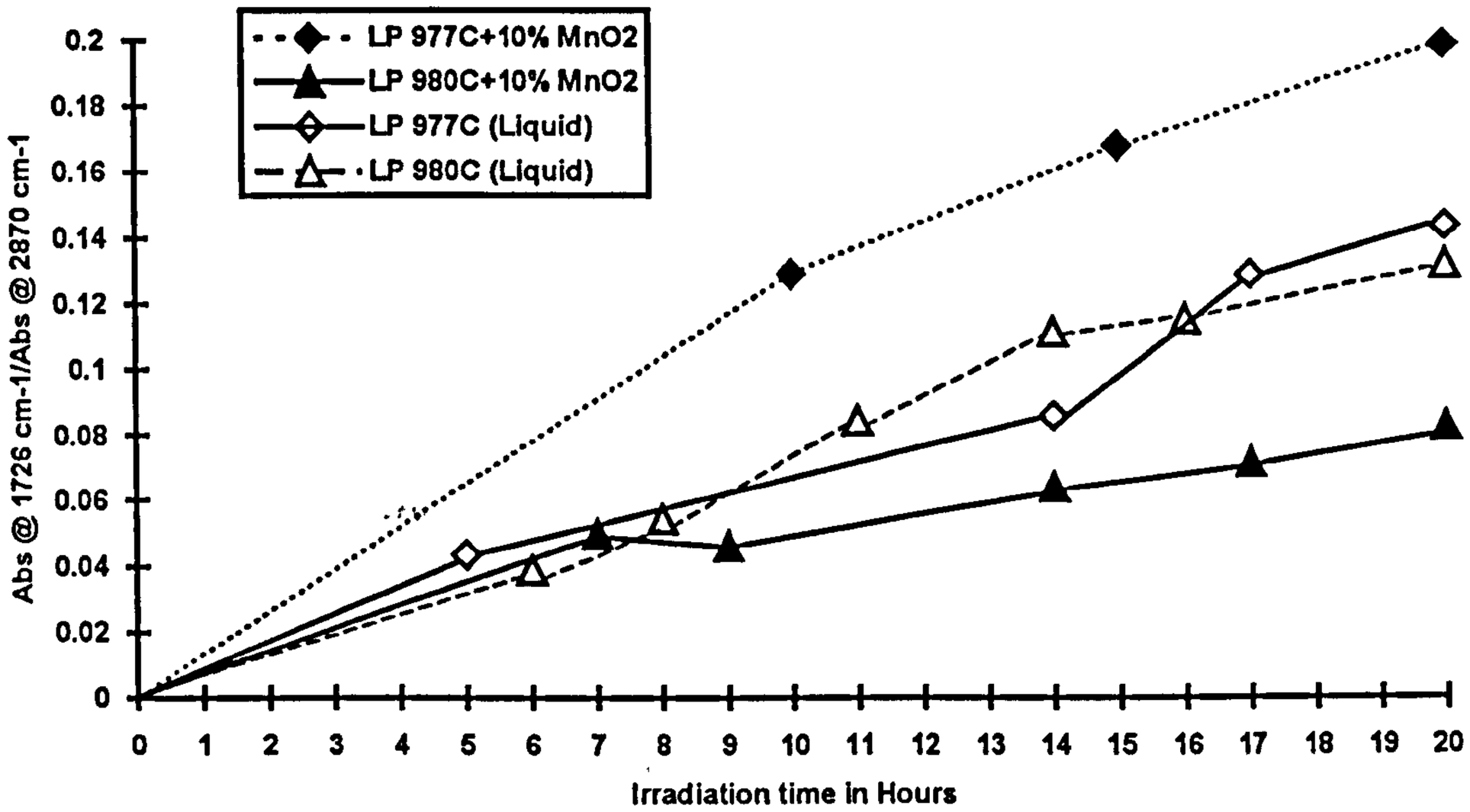

Fig 6.4: Profile of growth of carbonyl peaks in cured LP-977C films of varying thickness (with a constant *ca.* 2% of MnO_2), following UV irradiation in 'Weatherometer'.

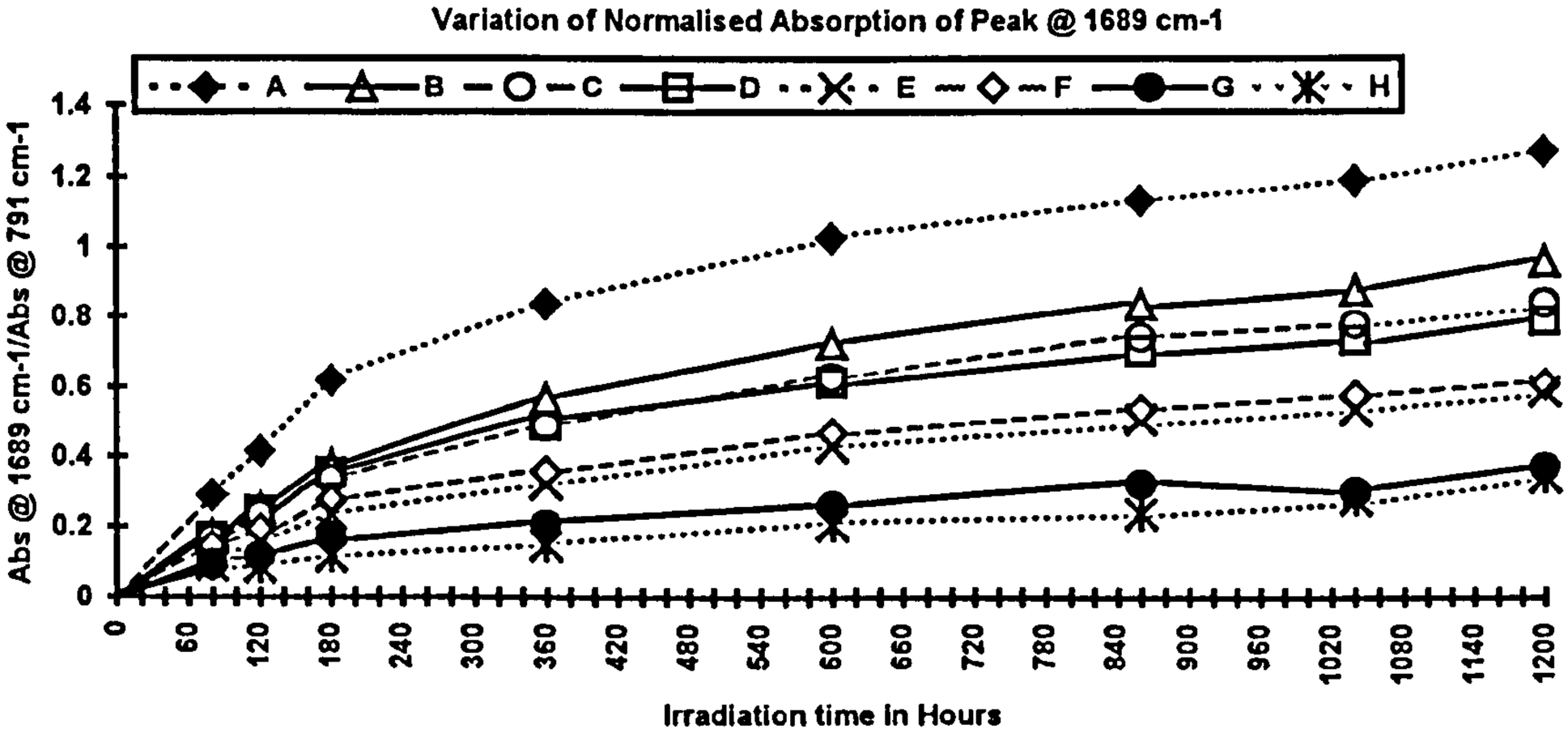

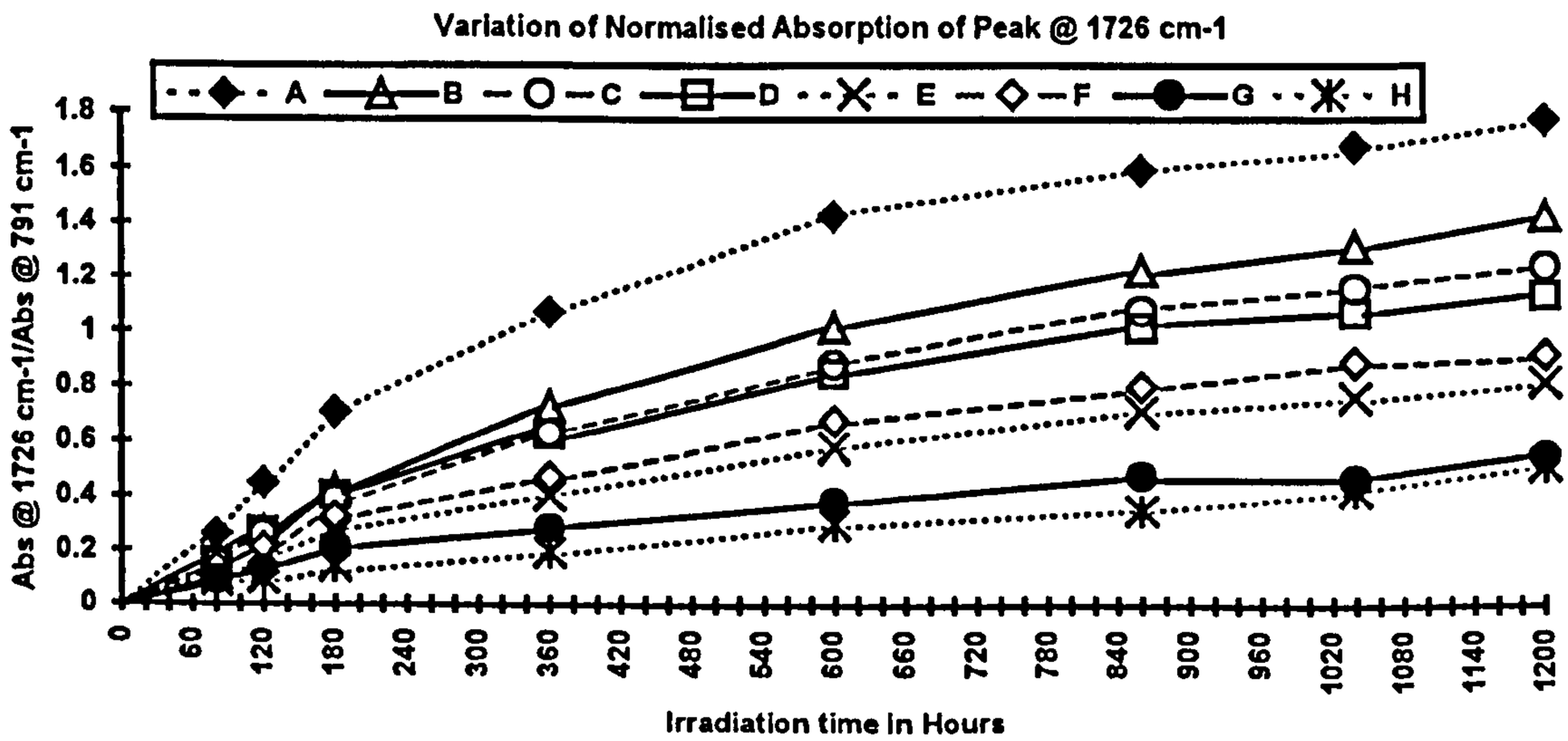

NB Samples increase in thickness from A to H, i.e. Sample A is the thinnest film.

6.3 EXPERIMENTS TO CONTROL FILM THICKNESS

The experiment described in the previous section showed degradation to be faster in the thinner films and therefore films of similar thickness are required in making comparative studies. Since IR transmission is the simplest method for following UV degradation, thin films (≈ 1 mm) of approximately constant thickness are required to obtain reasonable spectra. Various attempts using Carrimed and Microtome devices and plastic spacers were made to cast thin films of reproducible thickness but with little success.

The best possible method we had for having some control over film thickness was to compare the IR absorption at various reference peaks, e.g. 791 cm^{-1}, and to select films from a considerable number of samples which showed comparable absorption. This approach was adopted for all the following thin film experiments.

6.4 EXPERIMENT TO ASCERTAIN WHETHER MnO_2 LOADING AFFECTS THE RATE OF PHOTODEGRADATION

LPs 977C, 980C, 32C and 2C were selected for study. Thin films of each LP were cured using three levels of MnO_2 loading, i.e. *ca.* 7%, 5% and 2% by weight. These films were mounted onto cardboard, (see fig 6.3), and their IR spectra were obtained; only those of comparable thickness were utilised. The films were then irradiated in the UV_B 'Weatherometer' for approximately 2000 hours, with IR spectra being obtained at regular periods throughout the irradiation. A typical IR spectrum obtained during these film experiments is shown in fig. 6.5.

Evidently the cured films undergo a similar photo-oxidative degradation to the liquid films as indicated by the measured value of ν(C=O), see table 6.1.

Fig. 6.5. Spectrum showing the development of C=O and O-H frequencies in LP-980C with a MnO_2 loading of 2%, after 1890 h UV irradiation using 'Weatherometer'.

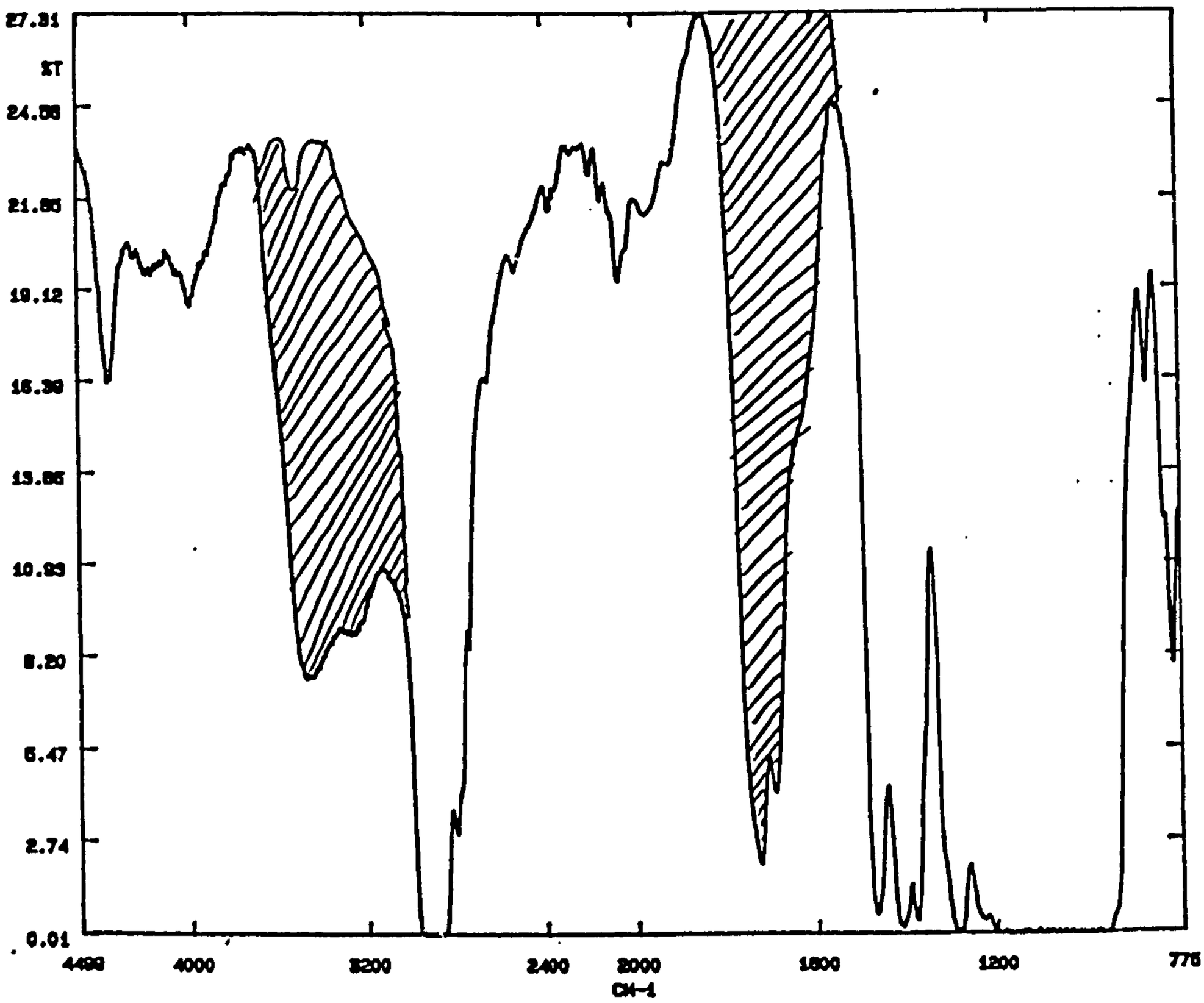

TABLE 6.1 Comparison of ν(C=O) frequencies for MnO_2 -cured LP films

LP code nº	% MnO_2	1st peak ν/cm^{-1} (± 2 cm^{-1})	2nd peak ν/cm^{-1} (± 2 cm^{-1})
977C	10 7 5 2	1726 1726 1726 1726	1685 1687 1687 1688
980C	10 7 5 2	1725 1726 1726 1725	1686 1687 1687 1687
2C	7 5 2	1726 1726 1725	1687 1687 1687
32C	7 5 2	1726 1726 1726	1686 1686 1688

The ν(C=O) is evidently virtually independent of the LP utilised and the loading of MnO_2. Moreover, variation in the LP structure has no great effect on the *rate* of photodegradation of the cured film.

Fig. 6.6. illustrates a trend for C=O development to be reduced when higher MnO_2 loadings are used to cure the LP.

Fig 6.6: Profile of growth of carbonyl peaks in cured LP-980C films with varying quantities of MnO_2, following UV irradiation in 'Weatherometer'

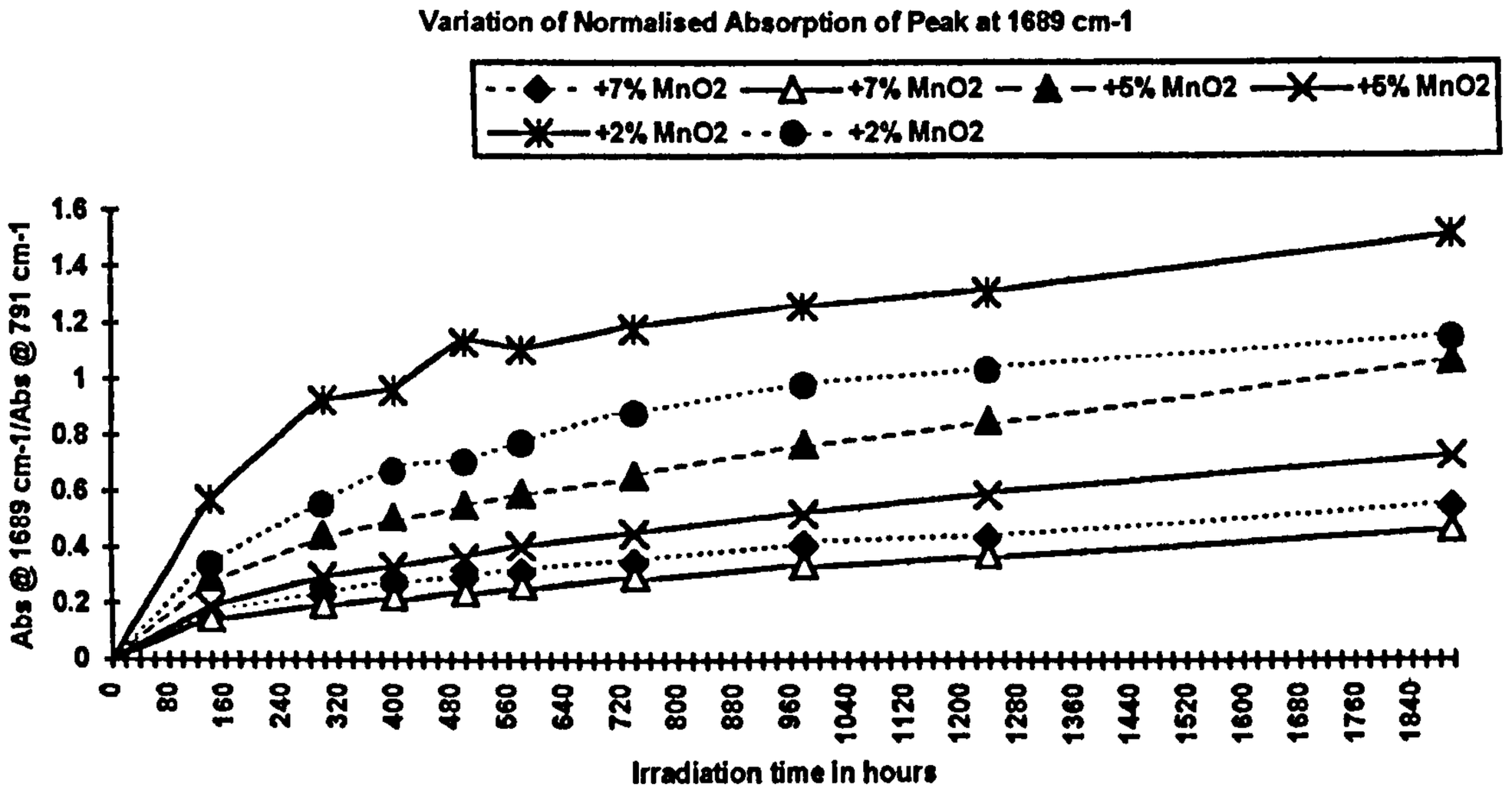

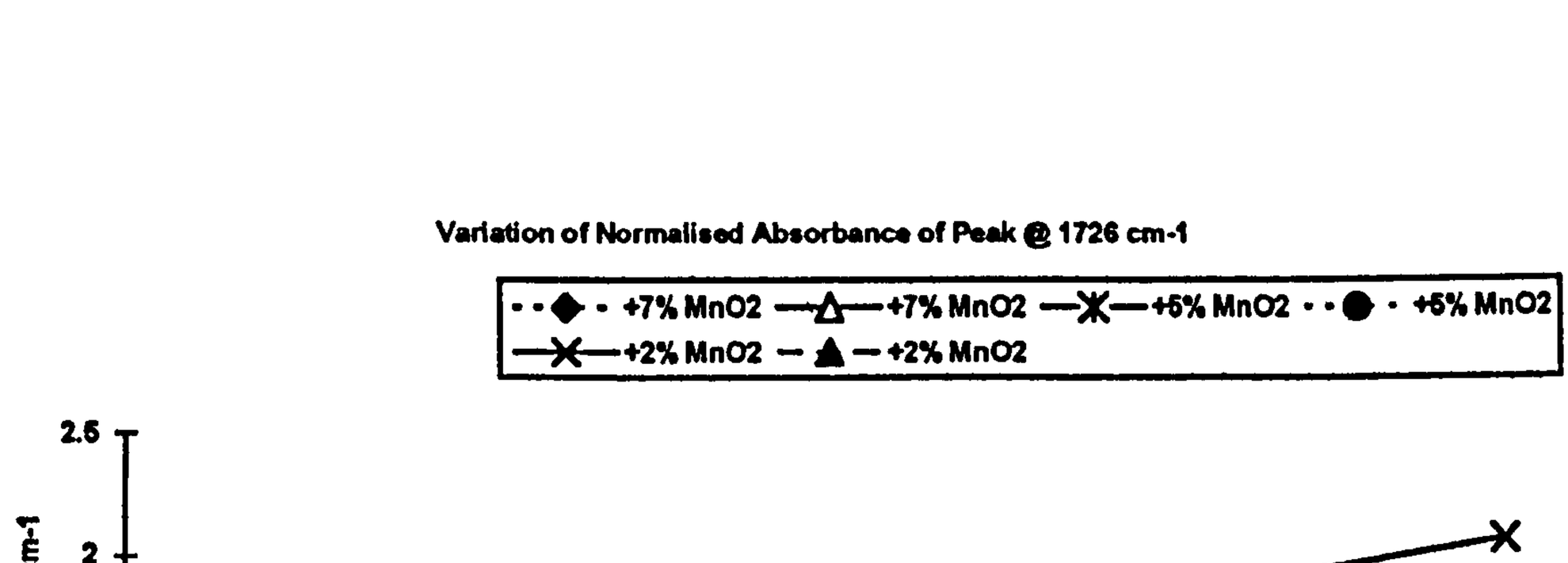

The role of the MnO_2 is one which might have been expected to be significant in the photo-degradative process. Even TiO_2 powder is known, under UV irradiation, to attack surrounding organic molecules, including polymers, by a process of oxidation[1,2], and MnO_2 is a much stronger oxidant than TiO_2. However, we find that the presence of MnO_2 does <u>not</u> greatly affect the photodegradation rate: it appears that the light absorption and scattering affects of MnO_2 more than offset any photo-oxidative role it might play. MnO_2 could also function by decomposing hydroperoxides or by scavenging radicals or electrons.

6.5 EXPERIMENT TO ASCERTAIN WHETHER AN INCREASE IN TEMPERATURE AFFECTS THE RATE OF CARBONYL GROUP DEVELOPMENT IN FILMS

Since the chamber in the UV_B Weatherometer operates at approximately 50°C and the xenon lamp also gives out considerable heat, it was important to assess whether increase in temperature has a bearing on C=O development. This assessment was carried out by exposing a cured film of LP-980C with *ca.* 7% MnO_2 loading to a temperature of *ca.* 80°C for 168 hours. Since <u>no</u> development of carbonyl absorption was apparent it can be concluded that any small temperature rise which might occur during UV irradiation of thin films is insignificant as regards photo-oxidative degradation.

6.6 TO ASCERTAIN THE EFFECTS OF PHOTODEGRADING A CURED LP ON A SILICA SURFACE.

Since IR transmission spectroscopy is the simplest method for following UV degradation of LPs, thin discs of silica, (microscope cover slips), were examined as

potential supports for IR spectroscopic examination between 4500 and 1550 cm^{-1}, and a matched pair obtained. These silica discs do not transmit IR radiation below certain wave numbers, (≈ 1500 cm^{-1}), but it is possible to monitor the development of carbonyl groups in a coating on the silica.

The LP-curative system chosen for examination was LP-977C with a MnO_2 loading of *ca.* 10%. A thin film of LP was cured on a silica disc and this was mounted onto cardboard, see fig. 6.7 and an IR spectrum was obtained prior to irradiation.

Fig. 6.7: Overview of mounted film on microscope slide

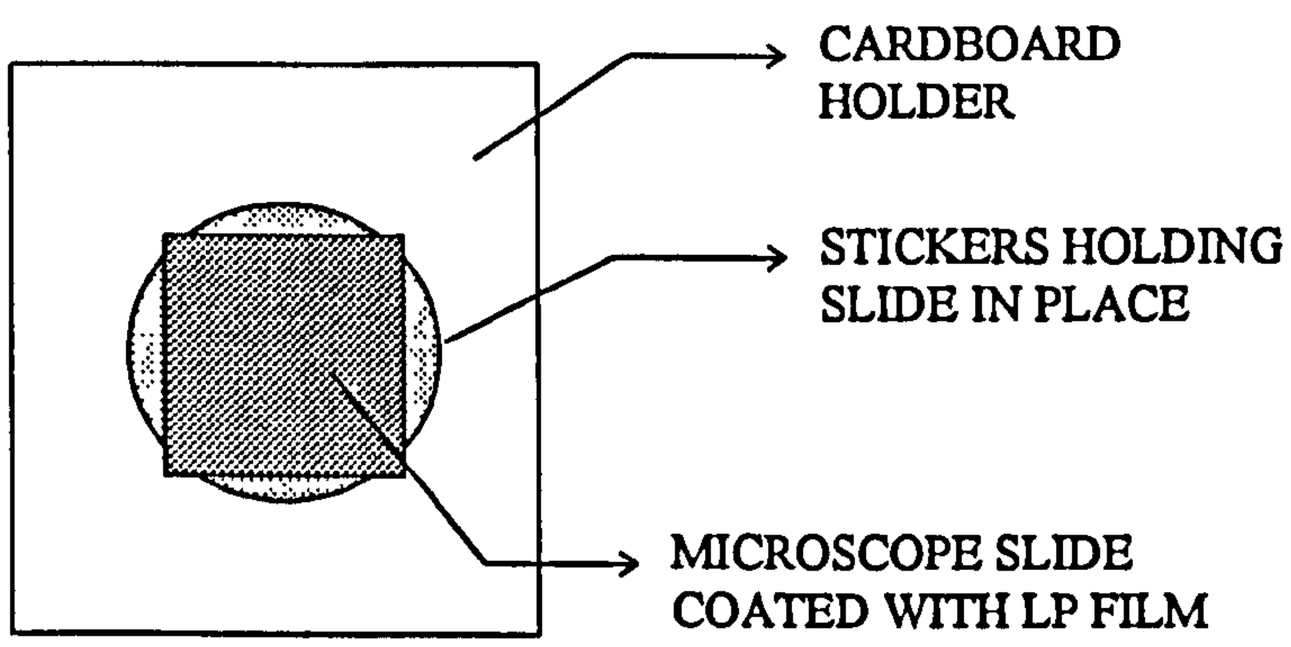

The film was then irradiated *through the silica* for up to 155 h using the 350 W xenon lamp. IR spectra were obtained at intervals throughout the irradiation, using the matched silica slide as reference. This type of experiment was repeated, but with the radiation entering the sample with the LP film *facing* the lamp, to assess whether passing the UV through the silica reduces the rate of degradation. A typical IR spectrum is illustrated in fig 6.8.

From the growth kinetics of C=O absorption, see fig. 6.9, it can be concluded that the rate of development of C=O for the LP film facing the lamp is not dissimilar to that of the film irradiated through the glass. It was originally expected that passing UV through glass might slow the degradation of the film considerably, firstly because

of light absorption/scattering effects and secondly because of the reduced access to atmostpheric oxygen.

Fig. 6.8: Spectrum showing development of C=O frequencies in LP-977C with a MnO_2 loading of 10%, after 155 h UV irradiation through silica using xenon lamp.

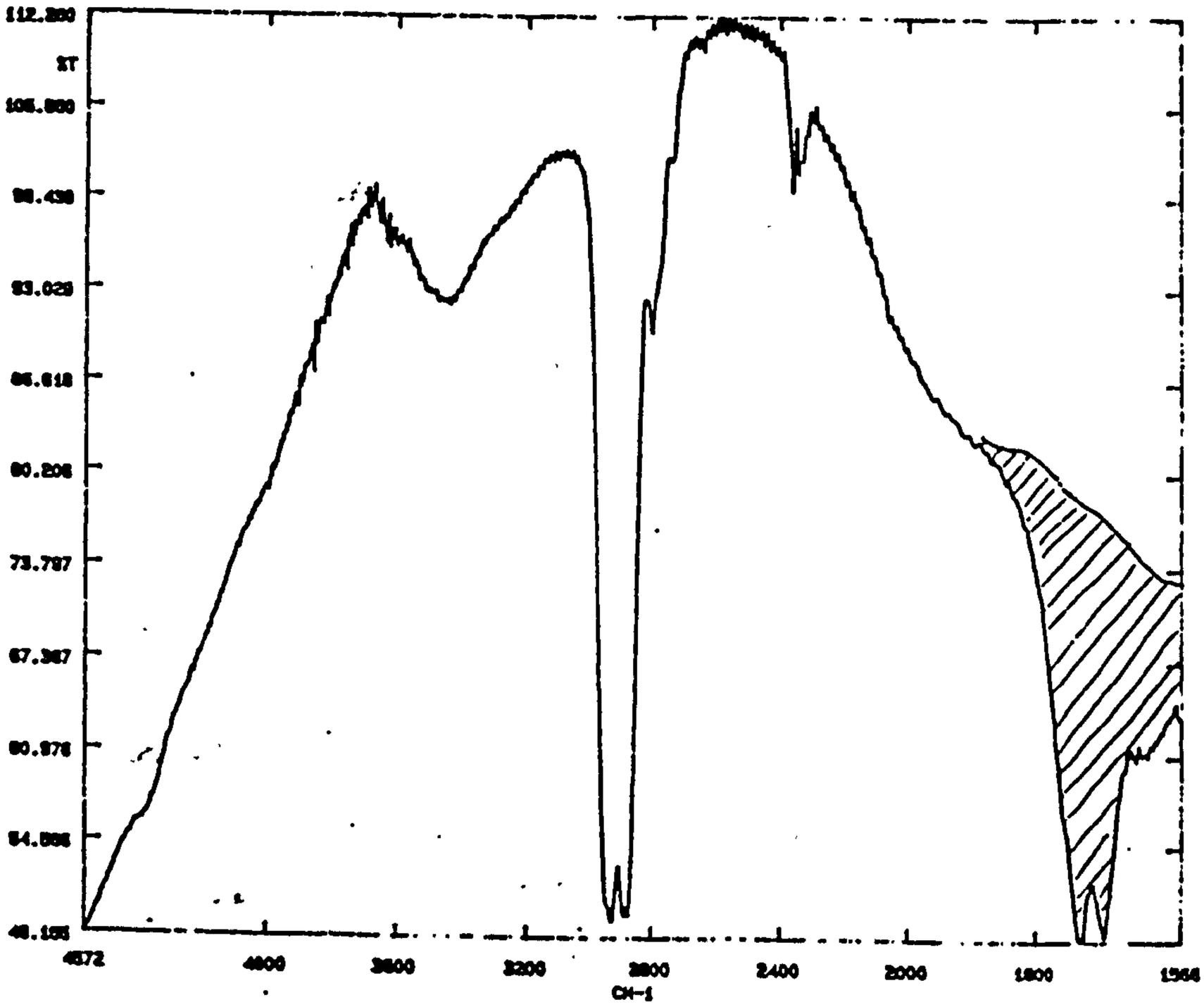

Fig. 6.9: Profile of the development of C=O frequencies in LP-977C with a MnO_2 loading of 10% , coated on a silica disc, after 155 h UV irradiation using xenon lamp.

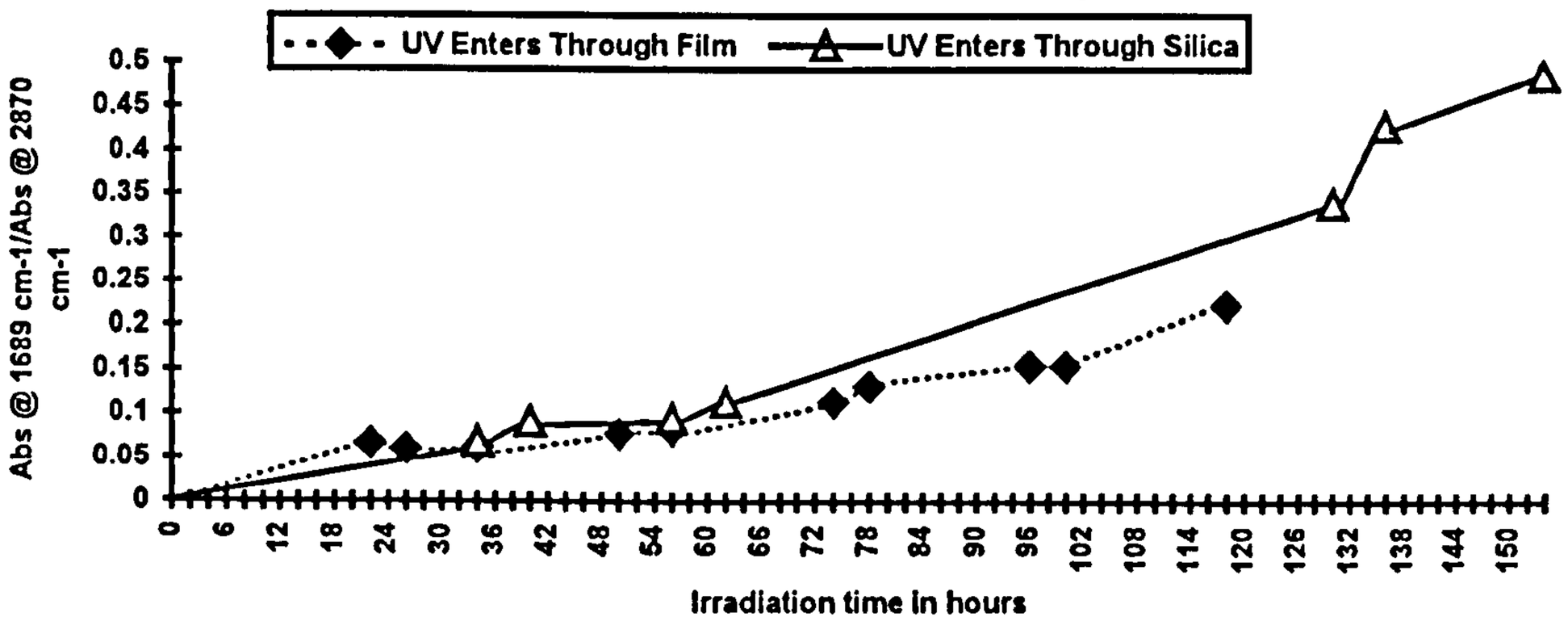

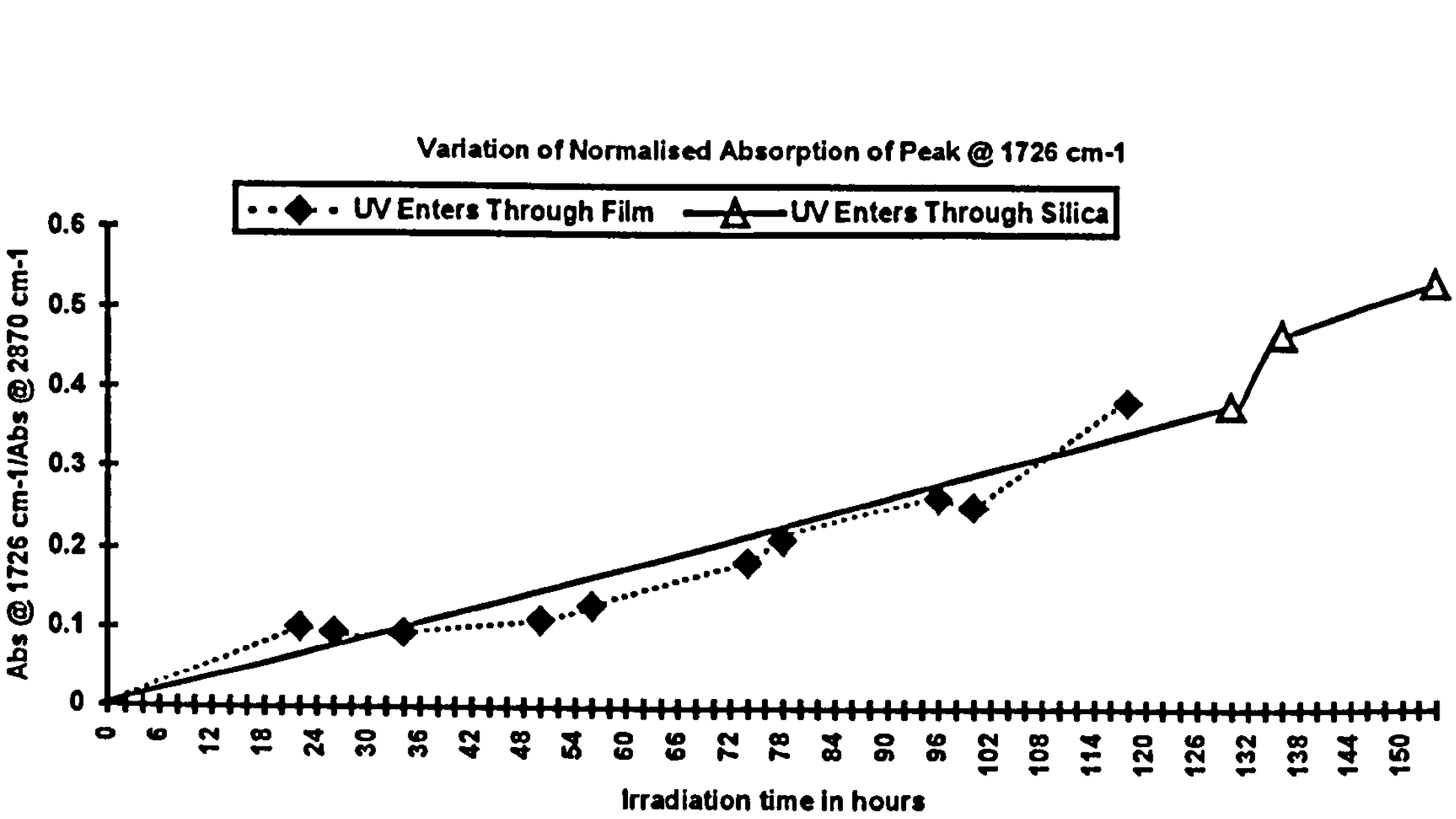

6.7 EXPERIMENT TO ASSESS THE EFFECT OF THE PRESENCE OF TERTIARY CARBON ATOMS IN THE LP ON THE RATE OF DEGRADATION.

Experiments performed so far have indicated that variation in LP structure has no measurable effect on the rate of photodegradation. LPs 2C and 12C were selected for comparison because LP-2C contains 10 times more branching agent than LP-12C. Thin films of both LPs, were cured using *ca.* 5% MnO_2, and irradiated using the UV_B 'Weatherometer' for up to 1900 hours.

Tertiary carbon atoms are generally accepted as being more vulnerable to attack by O_2 and free radicals and since LP-2C contains a higher level of branching agent, it inevitably has more tertiary carbon centres present in its backbone. The kinetic curves for the growth of the respective C=O frequencies are illustrated in fig. 6.10.

Within the rather high level of irreproducibility, the rate of degradation appears to be virtually independent of the number of tertiary carbons represented by the level of branching agent, present in the LP; if anything the rate of degradation is slightly slower in the LP-2C films. There appears then to be little difference in the rate of attack of O_2 at hydrogen atoms located on secondary and tertiary carbon atoms.

Fig. 6.10: Profile of growth of carbonyl peaks in MnO_2 - cured LP-12C and LP-2C following UV irradiation in 'Weatherometer'.

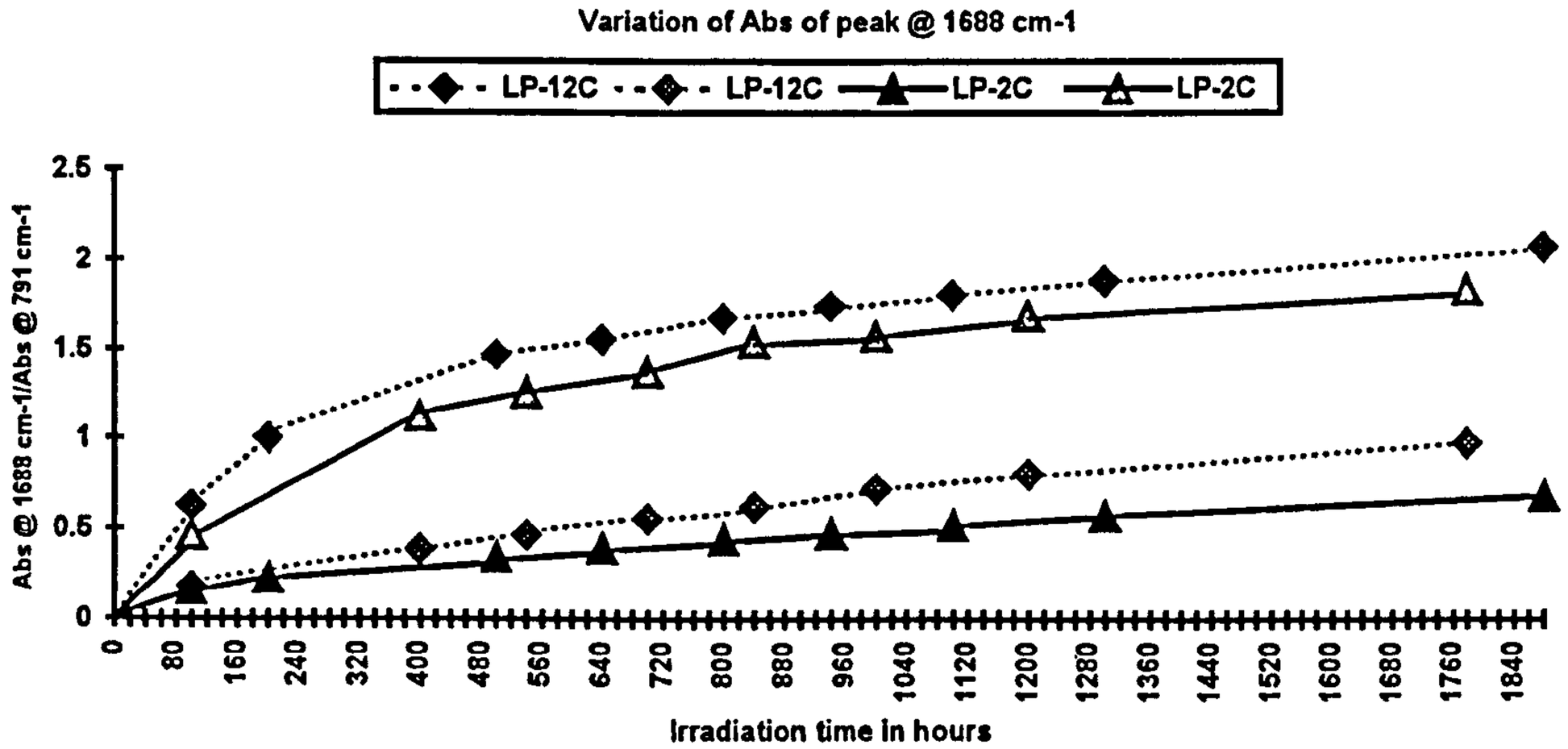

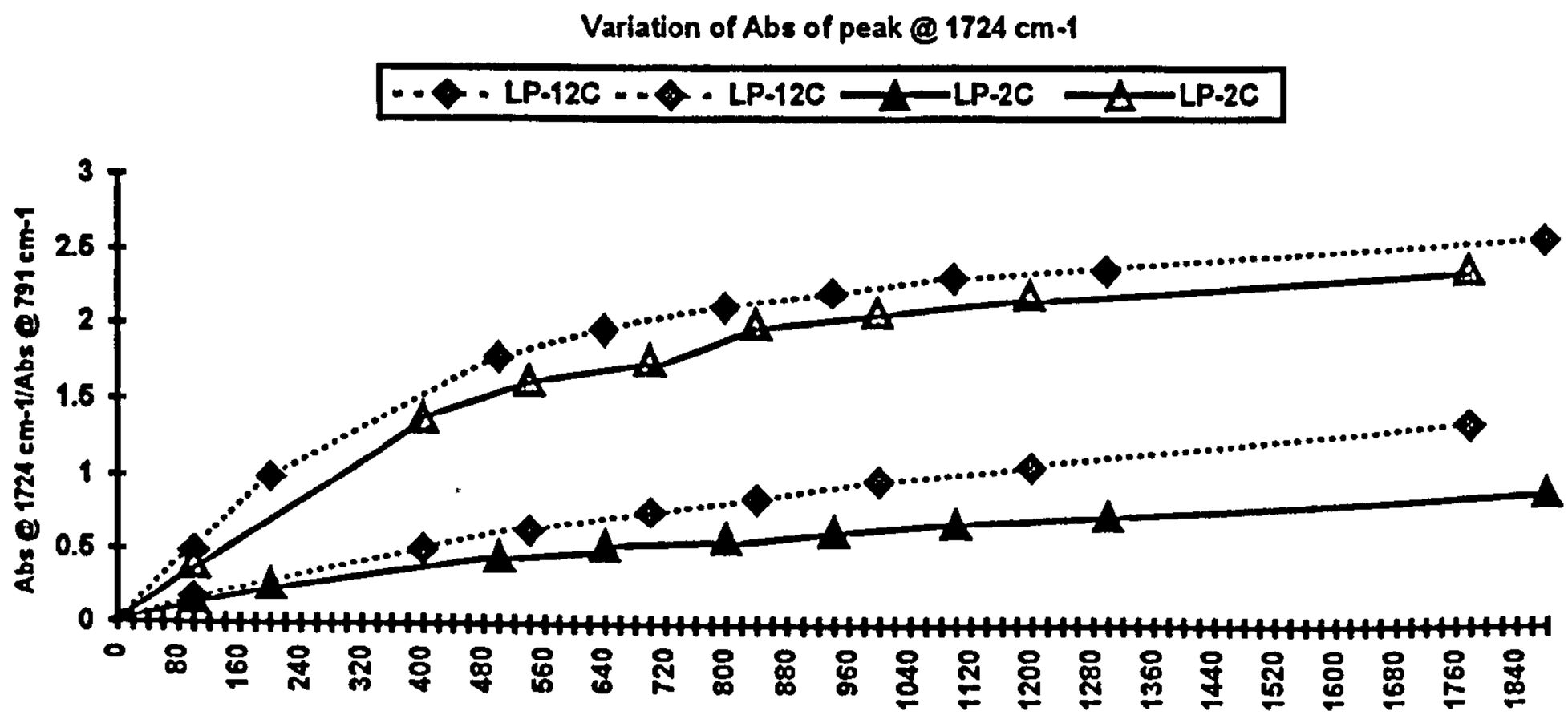

6.8 THE RELATIVE EFFECTS OF UV_A AND UV_B RADIATION IN PHOTODEGRADATION

An experiment was carried out to compare the effects of UV_A and UV_B irradiation on the rate of photodegradation of MnO_2-cured LP films. Two films of LP-977C with MnO_2 loading of *ca.* 5% were selected. One sample was irradiated in the UV_B 'Weatherometer' and the other using the UV_A chamber for up to 1400 hours.

From the kinetic growth curve for the peak at ≈1726 cm^{-1}, see fig. 6.11, it can be deduced that the rate of C=O development is approximately 20% faster when the films are irradiated using the UV_B as opposed to UV_A 'Weatherometers'.

Fig 6.11: Profile of growth of 1726 cm^{-1} peak for MnO_2-cured LP films using i) UV_A ii) UV_B irradiation.

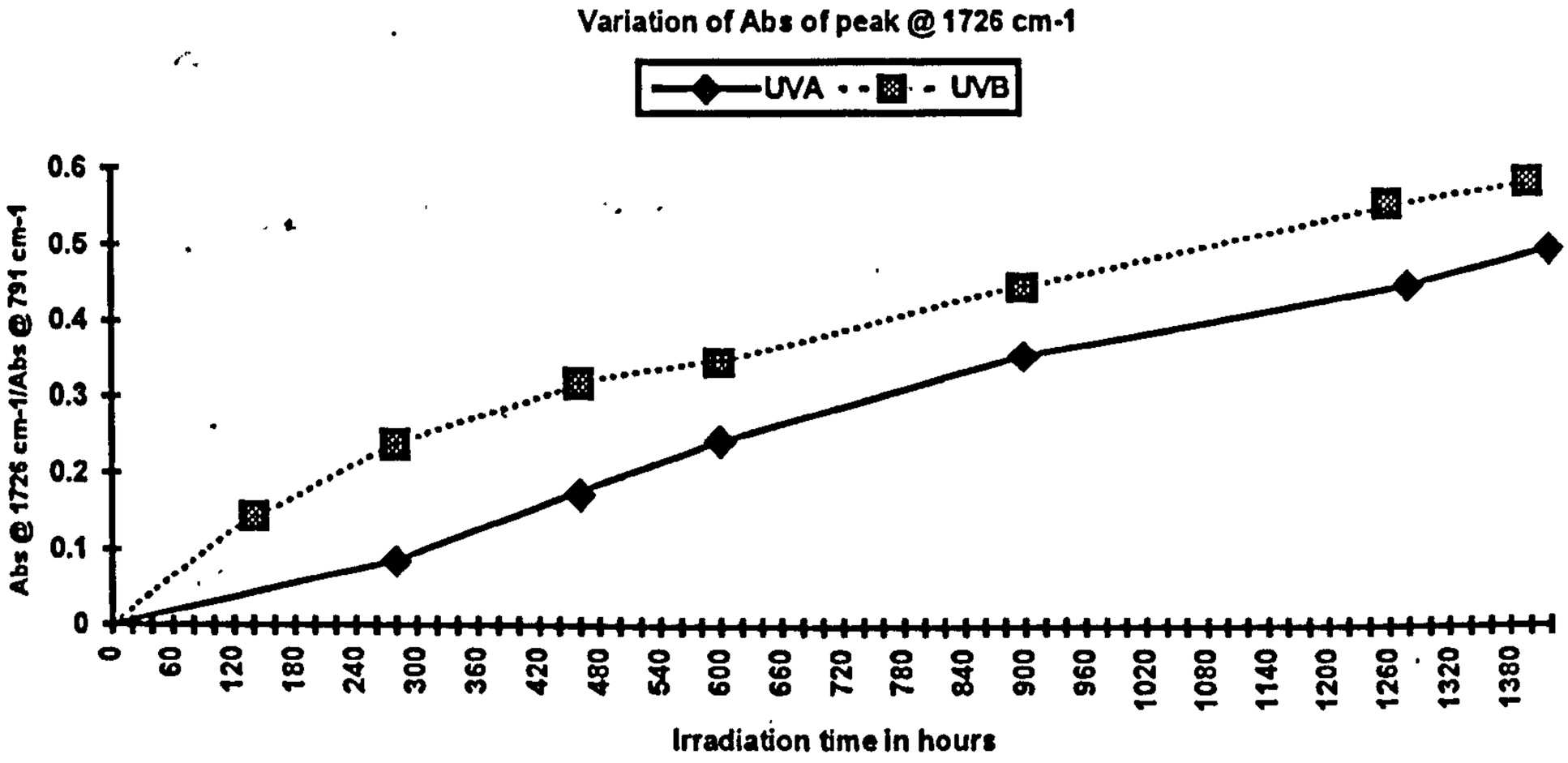

6.9 EXPERIMENT TO ASSESS EFFECT OF CARBON BLACK (ELFLEX 415) ON THE RATE OF PHOTODEGRADATION.

Carbon black, (Elflex 415), is used widely in sealant formations as a black pigment which possibly retards degradation. Morton International add 0.6 parts per hundred rubber, (phr), to insulated glass sealants to obtain the classic black colour. Therefore it was important to assess the effect of addition of carbon black on the photodegradation rate of LPs.

Films of LP-977C were made up with *ca.* 0, 0.2, 0.6 and 1% Elflex 415 and irradiated in the UV_B Weatherometer.

From the kinetic growth curves obtained for peaks at 1724 cm^{-1} and 1688 cm^{-1}, see fig. 6.12, it can be concluded that carbon black effectively retards carbonyl development at levels of 1 and 0.6 phr, while at 0.2 phr only marginal protection is achieved.

6.10 EXPERIMENTS TO ASSESS EFFECT OF ADHESION PROMOTER (A187) ON RATE OF DEGRADATION.

Films of LP-977C cured with *ca.* 5% MnO_2 were prepared containing *ca.* 0, 1 and 3% A187 and irradiated in the UV_B Weatherometer. All films containing the additive undergo a similar photo-oxidative degradation to the control cured film, the principal effect of photolysis being the development of C=O frequencies at *ca.* 1724 cm^{-1} and 1688 cm^{-1} and a weak broad band in the O-H region.

From the kinetic growth curves obtained for peaks at 1724 cm^{-1} and 1688 cm^{-1}, see fig. 6.13, it can be concluded that adding 3% A187 increases the formation of carbonyl species in MnO_2-cured LP films to a small extent.

Fig. 6.12: Profile of growth of carbonyl peaks in MnO_2-cured LP-977C films with varying levels of carbon black, following UV irradiation in UV_B 'Weatherometer'.

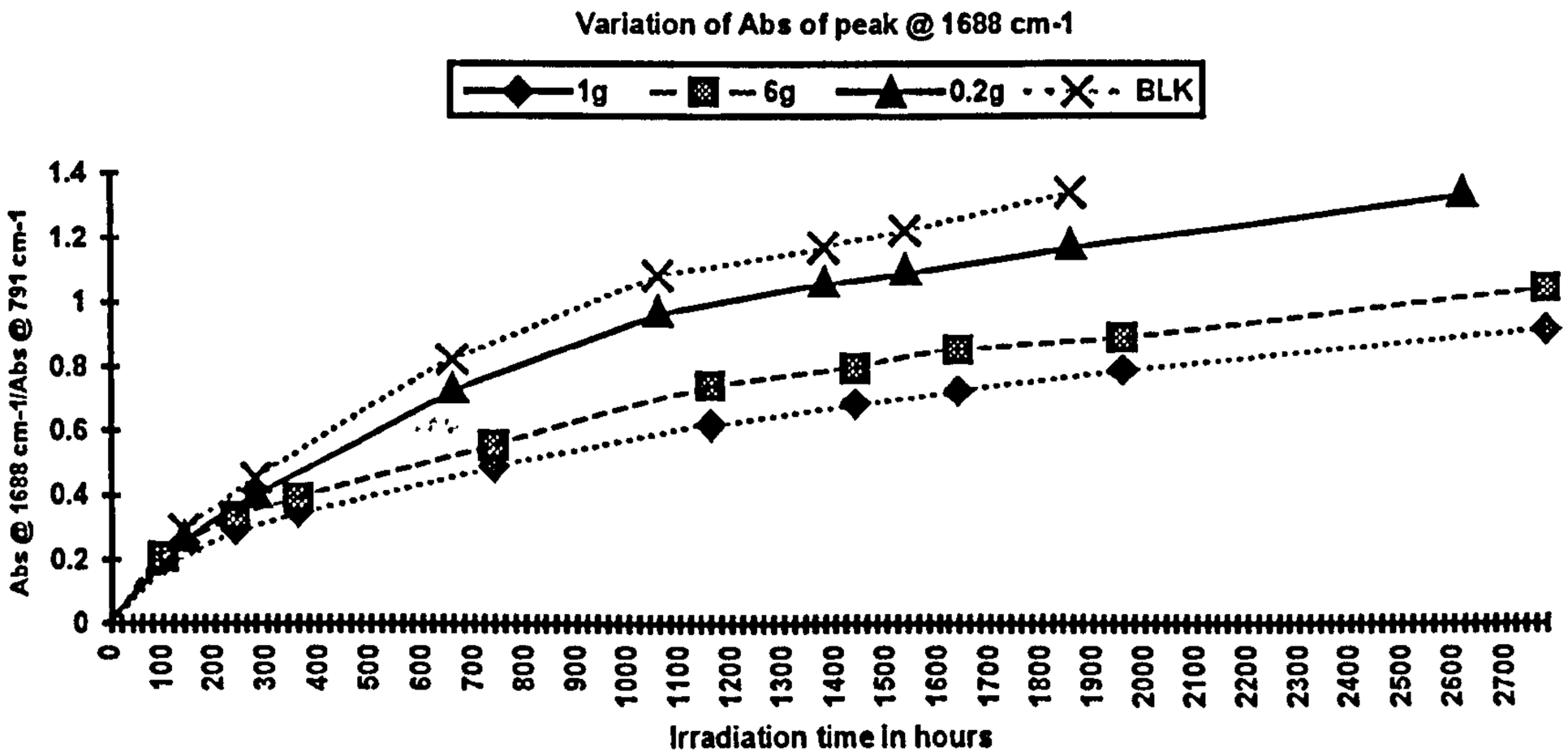

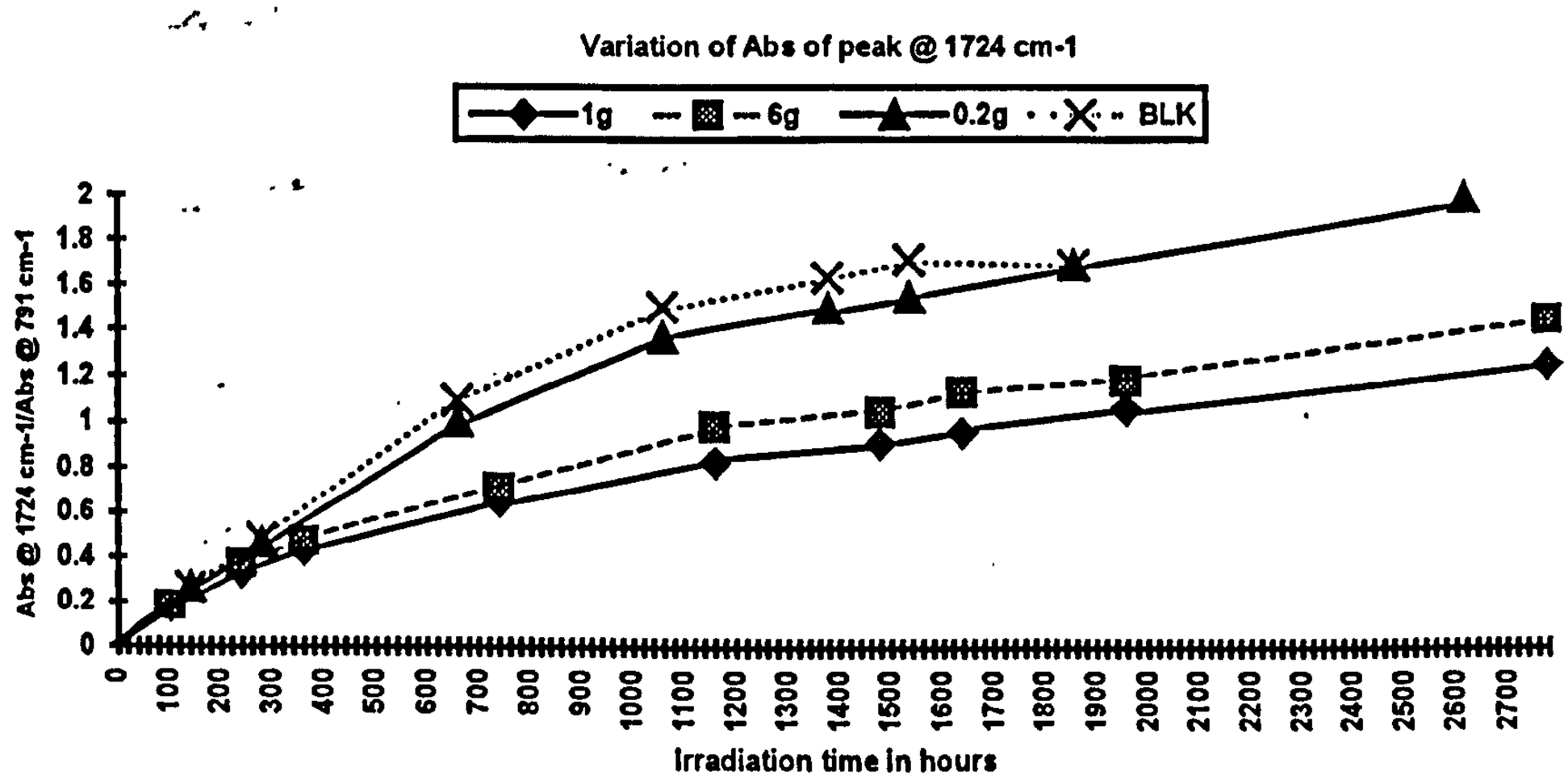

Fig. 6.13: Profile of growth of carbonyl peaks in MnO_2-cured LP-977C films with varying levels of A187 following UV irradiation in UV_B 'Weatherometer'.

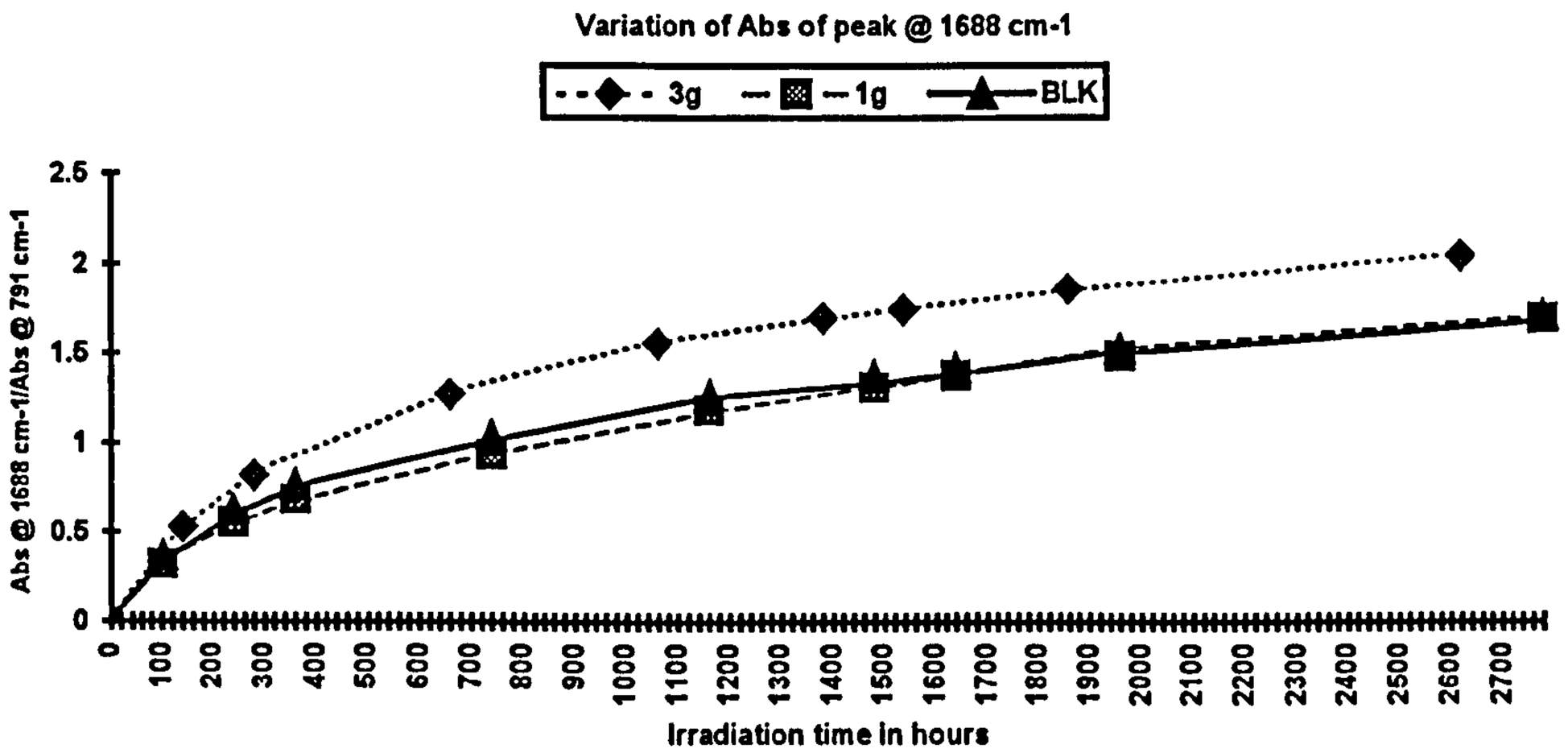

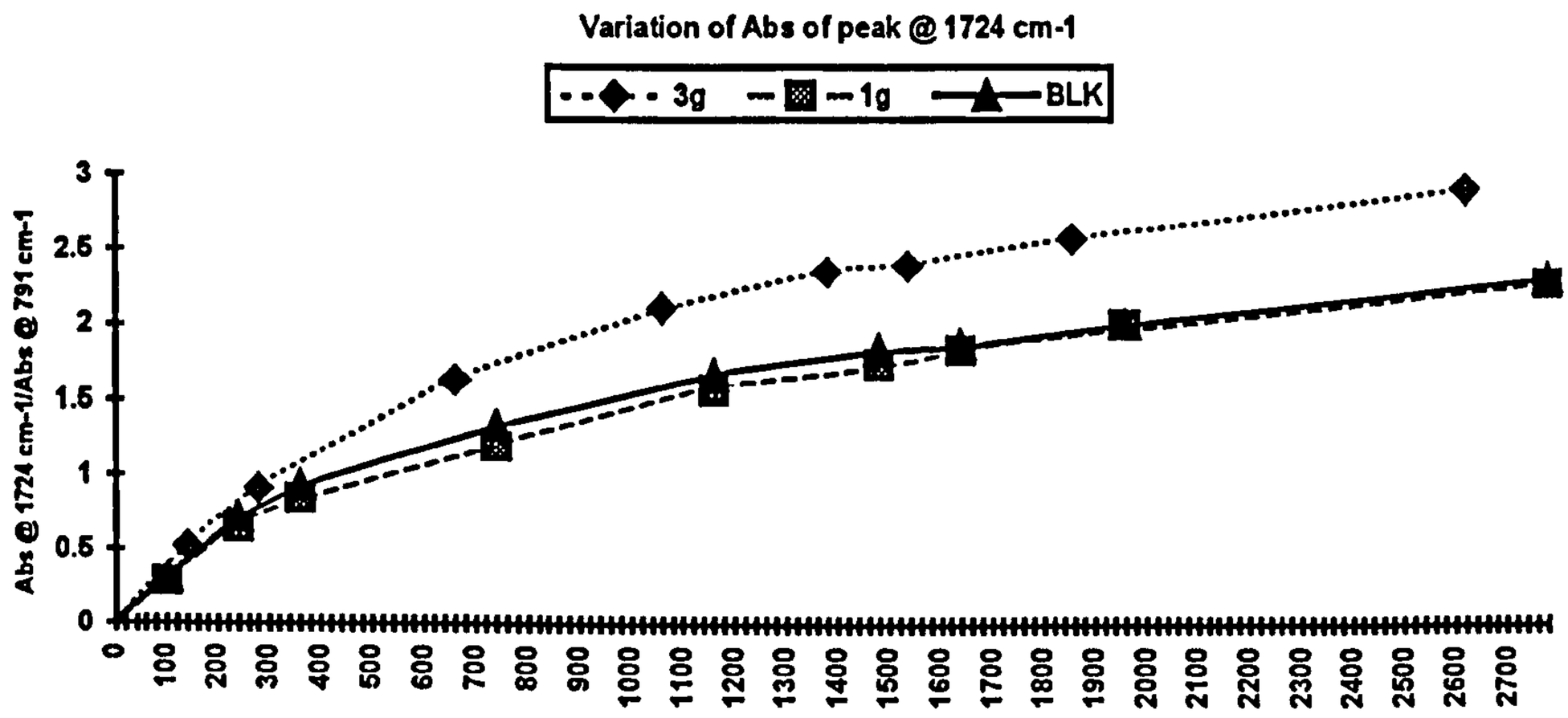

6.11 EXPERIMENT TO ASSESS EFFECT OF THE ACCELERATOR TETRAMETHYLTHIURAM DISULFIDE (TMTD) ON RATE OF DEGRADATION.

TMTD is often added in small quantities to LP sealants to accelerate curing.

Films of LP-977C with *ca.* 5% MnO_2 were cured containing *ca.* 0, 0.2 and 0.5% TMTD and irradiated in the UV_B Weatherometer.

From the kinetic growth curves for peaks at 1724 cm^{-1} and 1683 cm^{-1}, see fig. 6.14, it can be deduced that a small quantity of TMTD, i.e. 0.5 or 0.25 phr, retards the formation of carbonyl species in MnO_2 -cured LP films to a small extent.

Fig. 6.14: Profile of growth of carbonyl peaks in MnO_2 - cured LP-977C films with varying levels of TMTD, following UV irradiation in UV_B 'Weatherometer'.

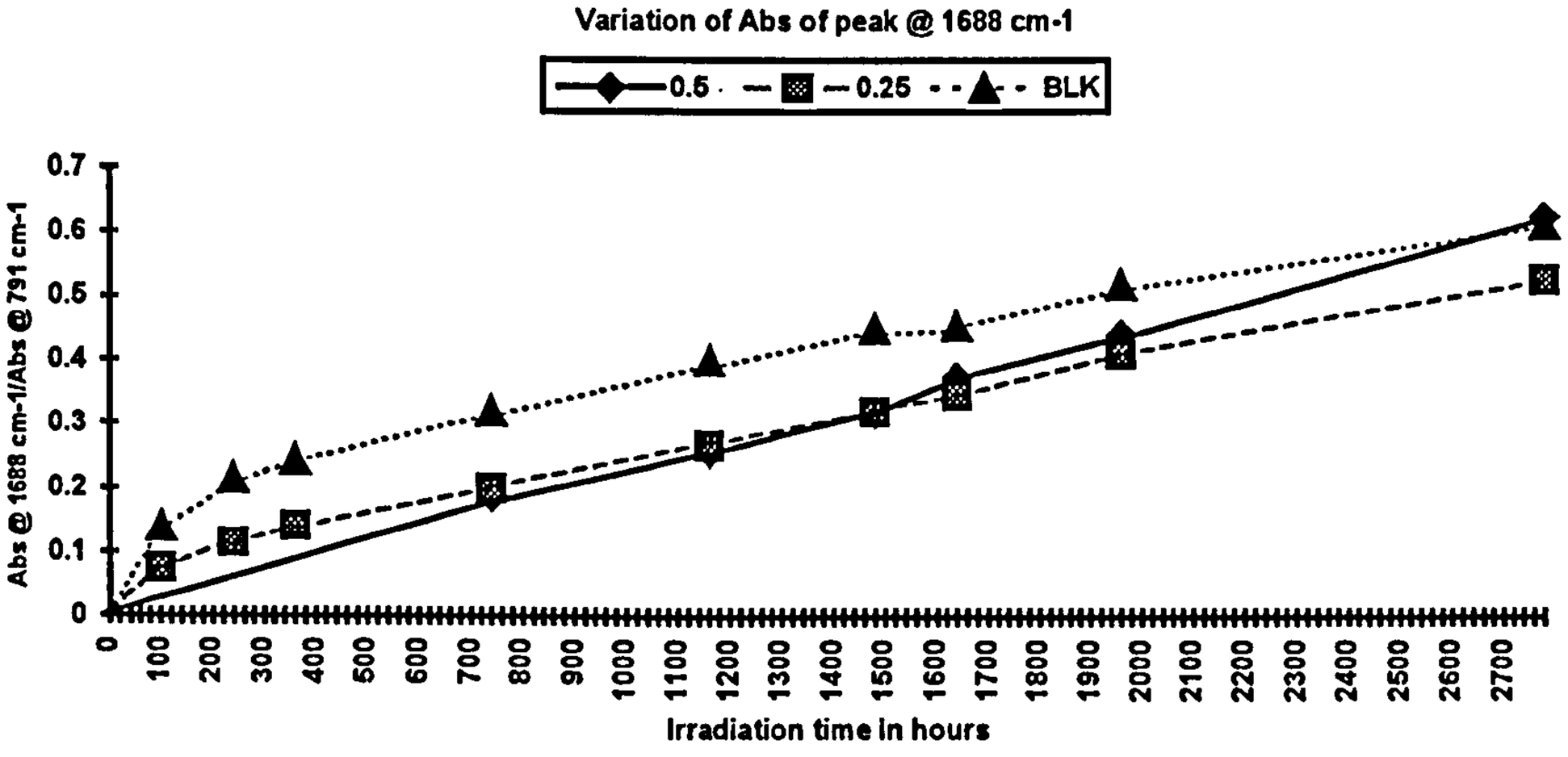

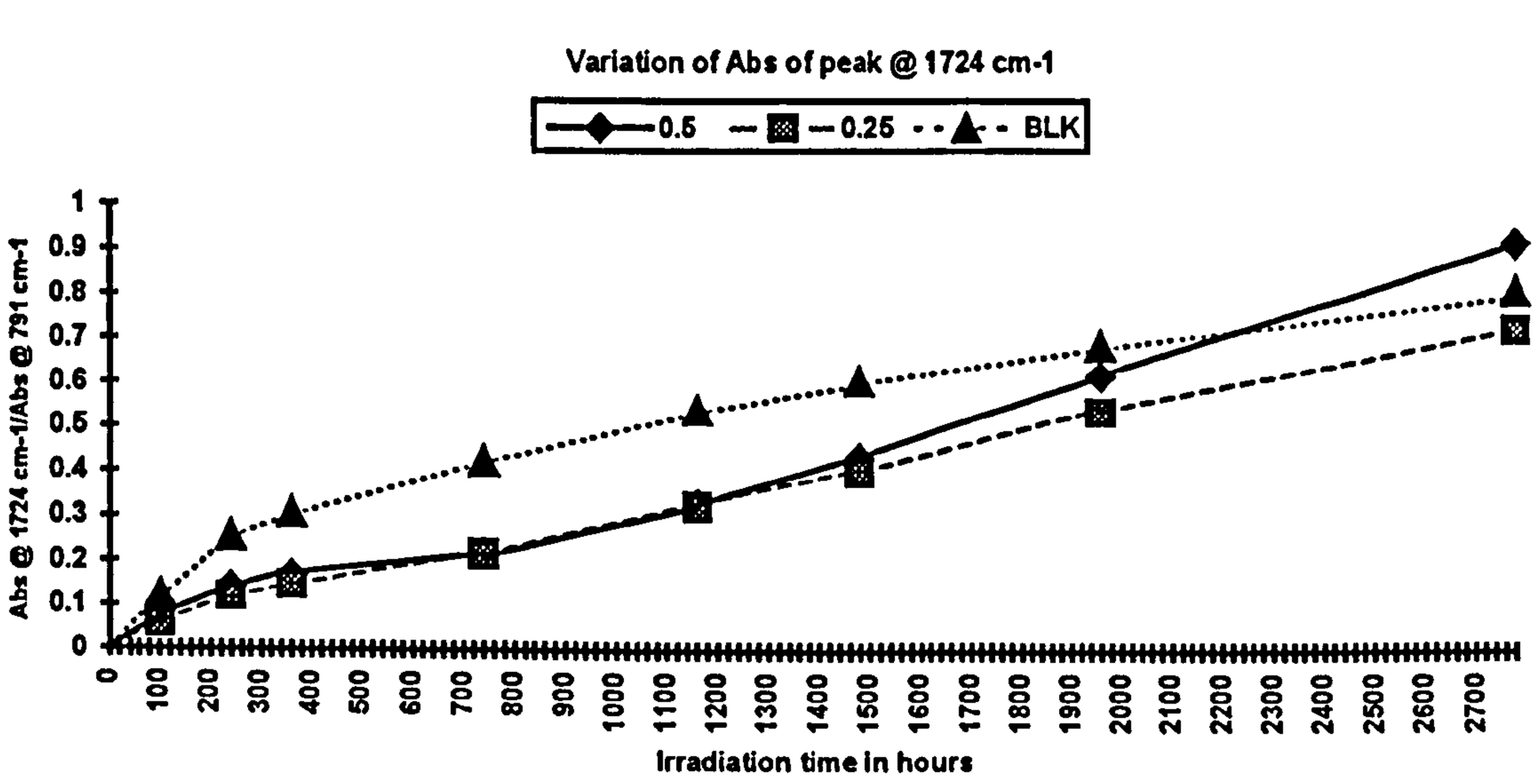

6.12 PHOTODEGRADATION OF LPs CURED USING ALTERNATIVE CURATIVES

LPs 977C, 980C, 32C and 2C were selected for study and cured using:

a) sodium perborate

b) t-butyl hydroperoxide, TBHP.

The amount of curative required was calculated according to the thiol content in the LP. To the sodium perborate-cured samples, 3 phr of 0.5M NaOH was added to accelerate the rate of cure, while for the TBHP-cured samples, 1 pph of tributylamine was used. The films were irradiated in the UV_B 'Weatherometer' for approximately 2800 hours and IR spectra were obtained periodically throughout the experiment.

Typical IR spectra are illustrated in figs. 6.15 and 6.16 of these photodegraded films.

Evidently the $NaBO_3$-cured films undergo a similar photo-oxidative degradation to MnO_2-cured films, the principal effect of photolysis being the development of C=O frequencies at *ca.* 1724 cm^{-1} and 1688 cm^{-1}, (*cf.* MnO_2-cured films at *ca.* 1726 and 1689 cm^{-1}), and a weak broad band in the O-H region.

The position of ν(C=O) is evidently independent of the LP utilised, as can be seen from table 6.2.

The kinetic curves for the growth of ν(C=O) absorptions, see fig. 6.17, are rather similar to those obtained for MnO_2-cured films.

Variation in the LP structure appears to have little effect on the rate of photodegradation of the cured film. Any minor differences are most probably due to variations in film thickness, with the thinnest degrading fastest.

Fig 6.15: Spectrum shows the development of O-H and C=O frequencies in LP-980C with $NaBO_3$ as curative after 2793.4 hours UV_B irradiation using the 'Weatherometer'

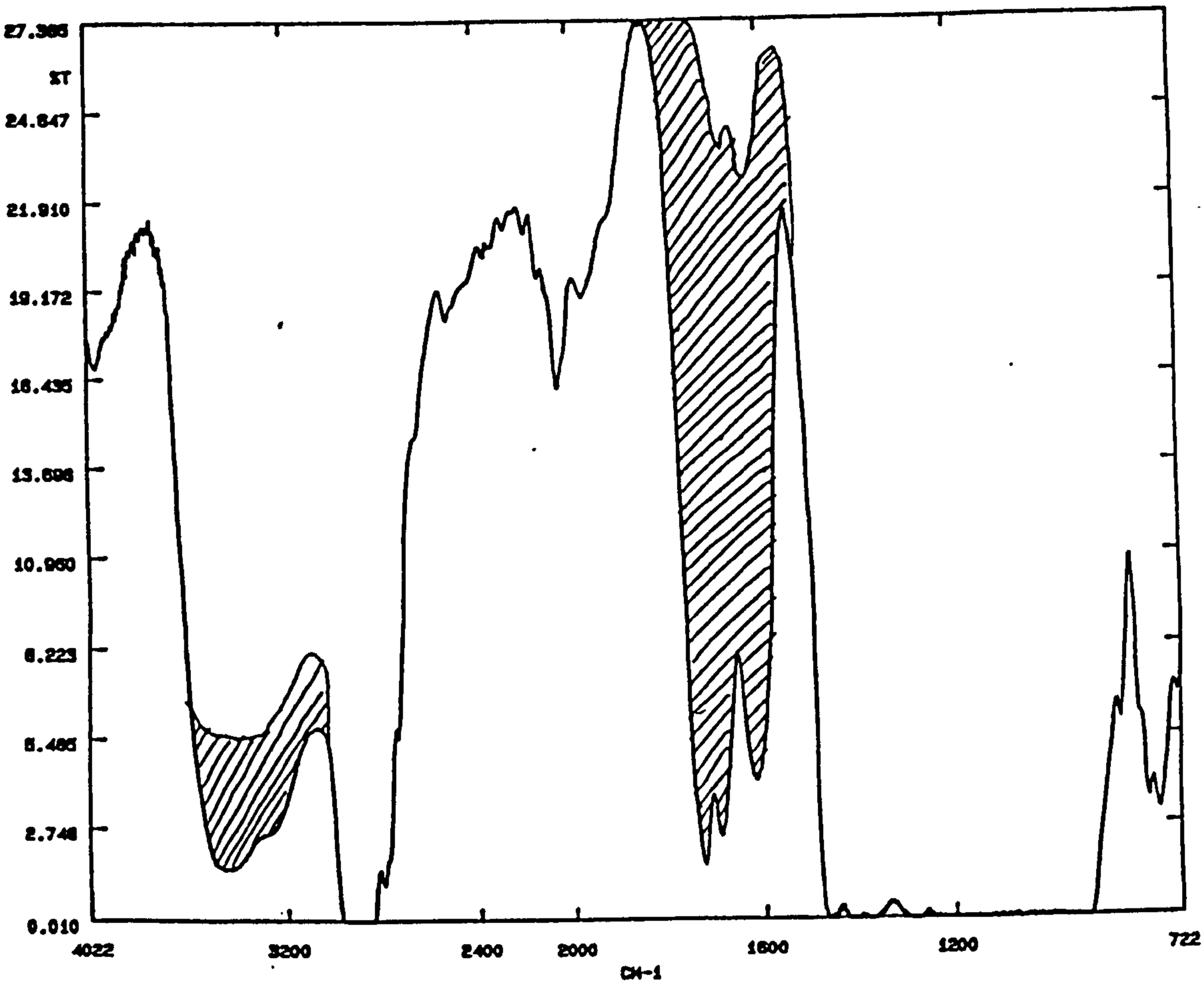

Fig 6.16 Spectra showing the development of O-H and C=O frequencies in LP-977C with TBHP as curative after a) 484.3 hours and b) 2468.9 hours UV_B irradiation using 'Weatherometer'.

a)

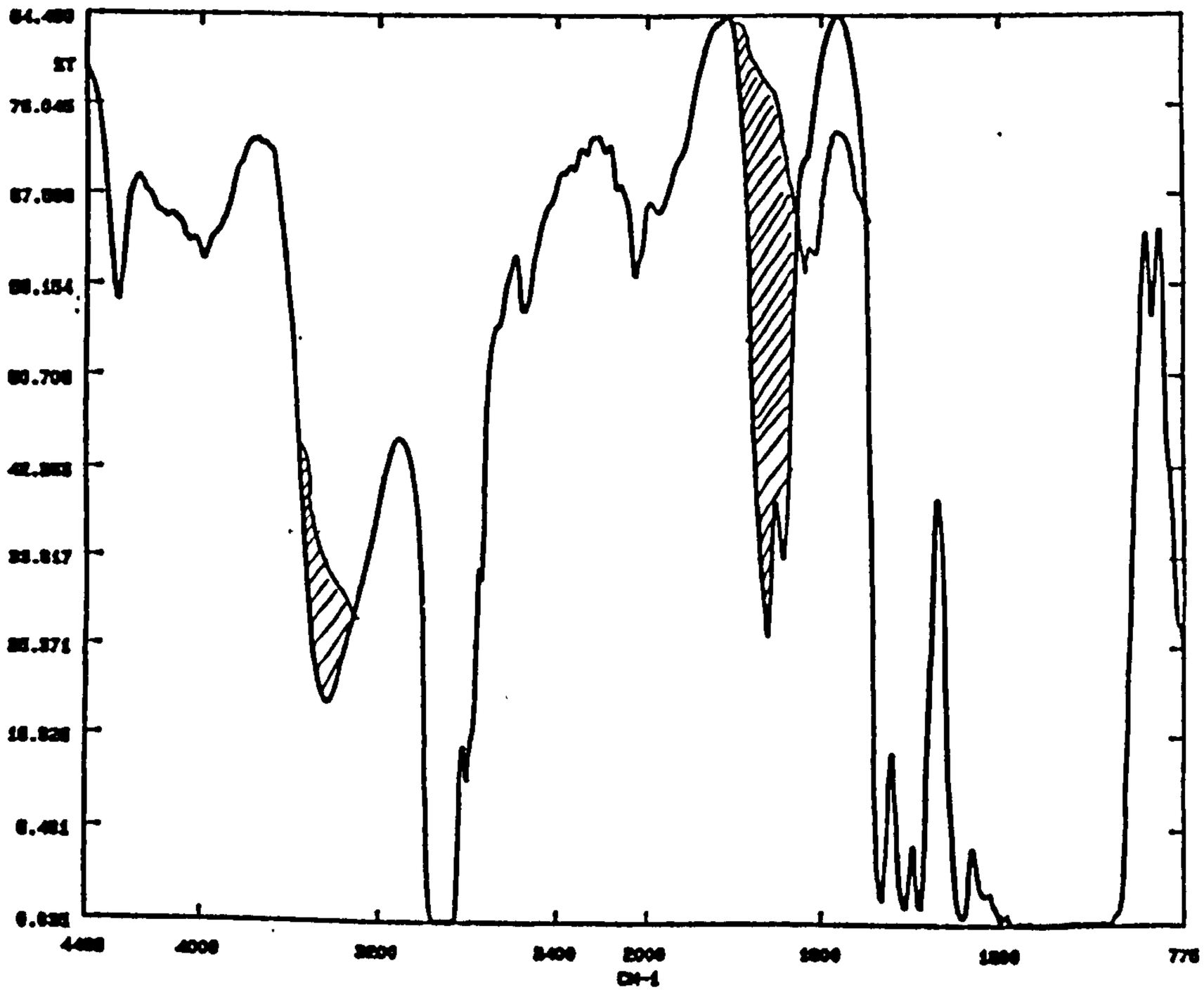

b)

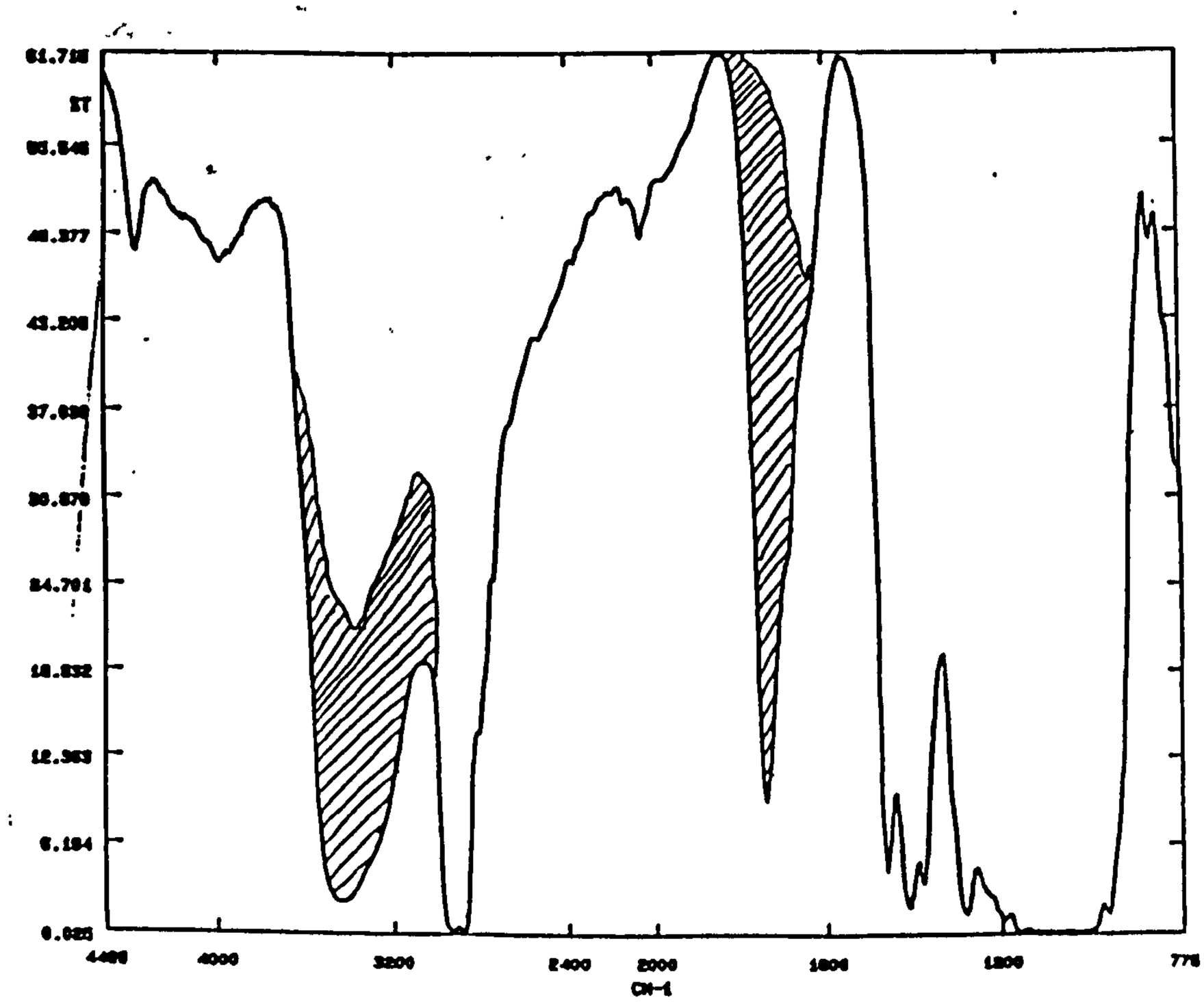

TABLE 6.2 Table to compare position of ν(C=O) in $NaBO_3$-cured LP films.

LP Code N°	%$NaBO_3$	1st Peak ν/cm^{-1} (± 2cm^{-1})	2nd Peak ν/cm^{-1} (± 2cm^{-1})
977C	5	1724	1688
980C	5	1724	1688
2C	2.75	1724	1688
32C	2.75	1724	1687

The TBHP-cured films initially undergo a similar photo-oxidative degradation to $NaBO_3$- and MnO_2-cured films, developing two peaks in the C=O region at 1724 cm^{-1} and 1687 cm^{-1} but after extensive UV exposure, (500 hours plus), a single peak between 1741 - 1737 cm^{-1} develops.

TBHP-cured films appear to be more susceptible to photodegradation than films prepared with the other curatives investigated, with 75% of films undergoing failure after 816 hours of exposure.

The growth kinetics of C=O absorption are initially similar to those for MnO_2- and $NaBO_3$-cured films, see fig. 6.18, but these became less reproducible after long exposures, (< 800 hours), when films began to exhibit complete or partial failure.

Fig 6.17: Profile of growth of carbonyl peaks in $NaBO_3$-cured LP films following UV irradiation in 'Weatherometer'.

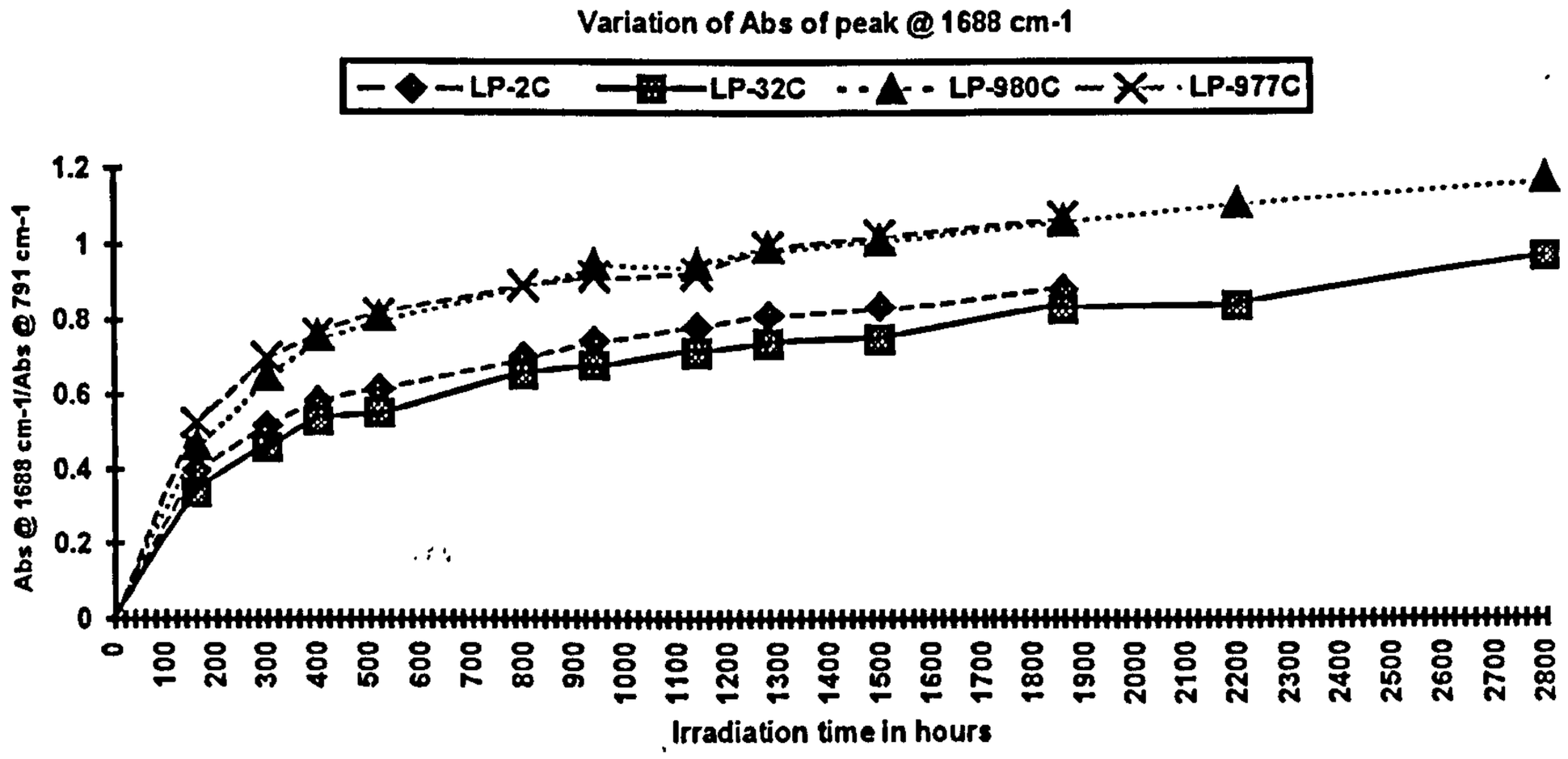

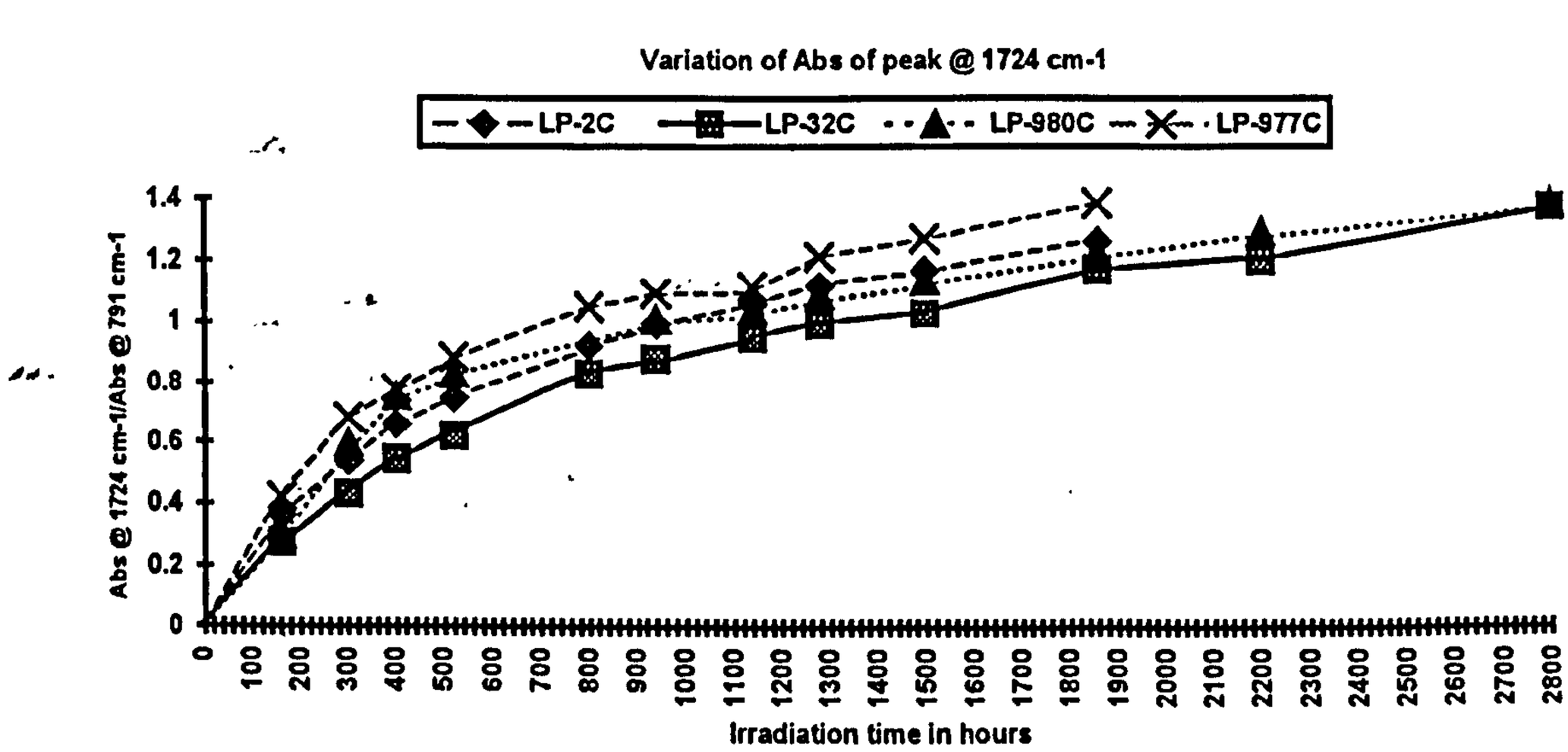

Fig 6.18: Profile of growth of carbonyl peaks in TBHP-cured LP films following UV irradiation in UV_B 'Weatherometer'.

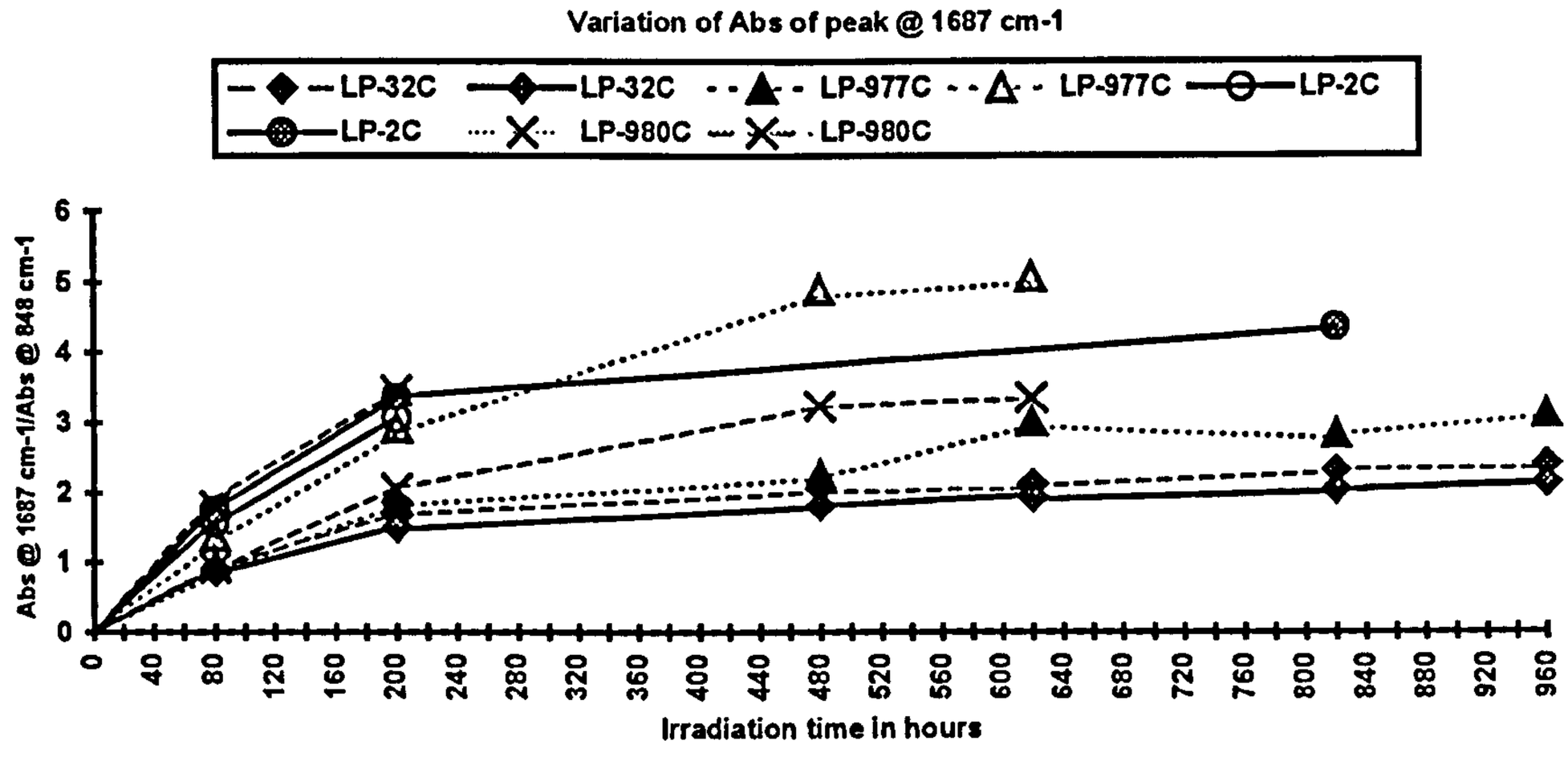

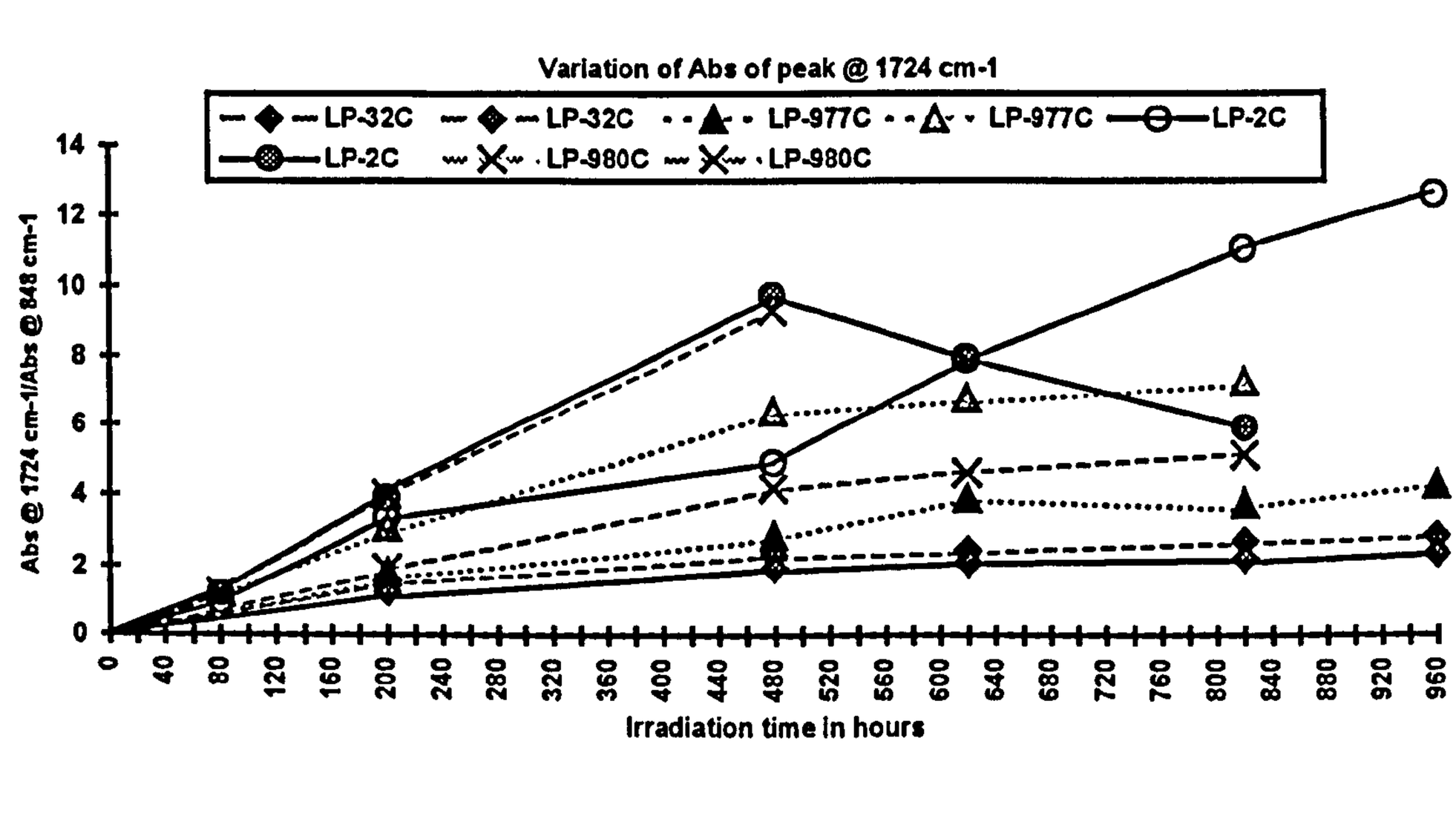

Again there is no evidence to suggest that variation in the LP structure has any effect on the rate of photodegradation.

Extending the range of LP-curatives does not affect the growth of C=O groups during photo-oxidation. Kinetic growth curves obtained for $NaBO_3$-cured LP films follow the same trend as those obtained for MnO_2, while the growth curves for TBHP-cured films were similar initially although less reproducible in the later stages.

It appears that the photodegradation mechanism of cured LP films is virtually independent of the curative used. It thus seems unlikely that the metal centres of the curatives themselves, e.g. Mn, B, are acting as sites for photodegradation, e.g. by a redox mechanism, and it is most probably the main functional groups in the polymer which are attacked directly. The relatively slower rates of failure of LP-films cured with MnO_2 is probably due to its acting as a light filter.

6.13 PHOTOGRAPHS OF UV - EXPOSED AND NON - EXPOSED FILMS

Because the deterioration of LP - polymer films after UV exposure is visible to the naked eye due to the formation of cracks, a range of LP-polymer films cured with MnO_2, TBHP and $NaBO_3$ were photographed before and after exposure to UV for up to 800 hours. Evidence for deterioration is clearly apparent, as illustrated in figs. 6.19, 6.20 and 6.21.

TBHP- and $NaBO_3$-cured films appear to be much more susceptible to UV irradiation than those cured with MnO_2; thus many such films exhibit complete or partial failure at relatively short exposure times compared to MnO_2-cured films.

Fig: 6.19a: Photographs of MnO_2-cured LP films before exposure.

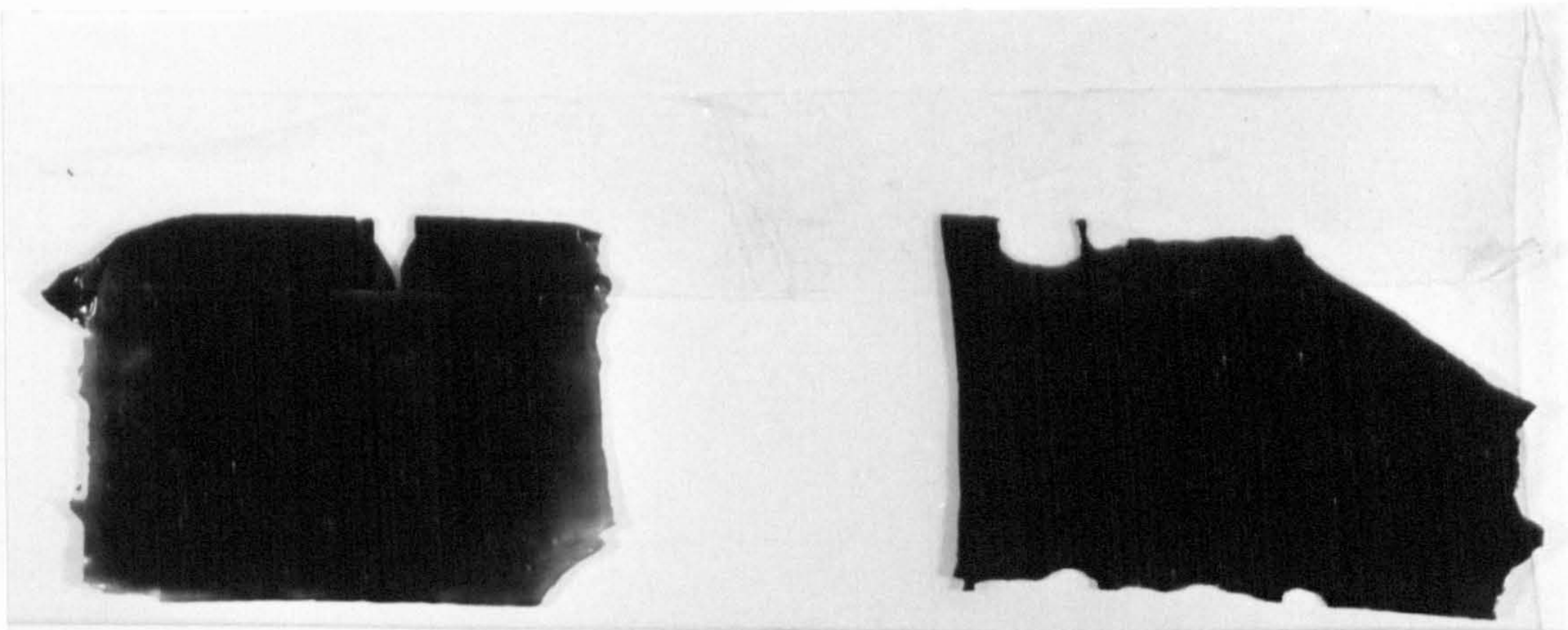

THIN FILM
BEFORE PHOTOLYSIS
LP-2C = 9.9832 g
MnO_2 = 0.2013 g

FILM BEFORE
PHOTOLYSIS
LP-2C = 10.0065 g
MnO_2 = 0.5003 g

THICK FILM BEFORE
PHOTOLYSIS
LP-32C = 9.9885 g
MnO_2 = 0.5006 g

THIN FILM BEFORE
PHOTOLYSIS
LP-32C = 10.0115 g
MnO_2 = 0.1992 g

Fig 6.19b: Photographs of MnO_2-cured LP films after UV exposure.

THIN FILM AFTER 797 h
EXPOSURE TO UV_B
LP-2C = 9.9832 g
MnO_2 = 0.2013 g

FILM AFTER 797 h
EXPOSURE TO UV_B.
LP-2C = 10.0065 g
MnO_2 = 0.5003 g

THICK FILM AFTER 797 h
EXPOSURE TO UV_B.
LP-32C = 9.9885 g
MnO_2 = 0.5006 g

THIN FILM AFTER 797 h
EXPOSURE TO UV_B.
LP-32C = 10.0115 g
MnO_2 = 0.1992 g

Fig 6.20a: Photographs of $NaBO_3$-cured LP films before exposure.

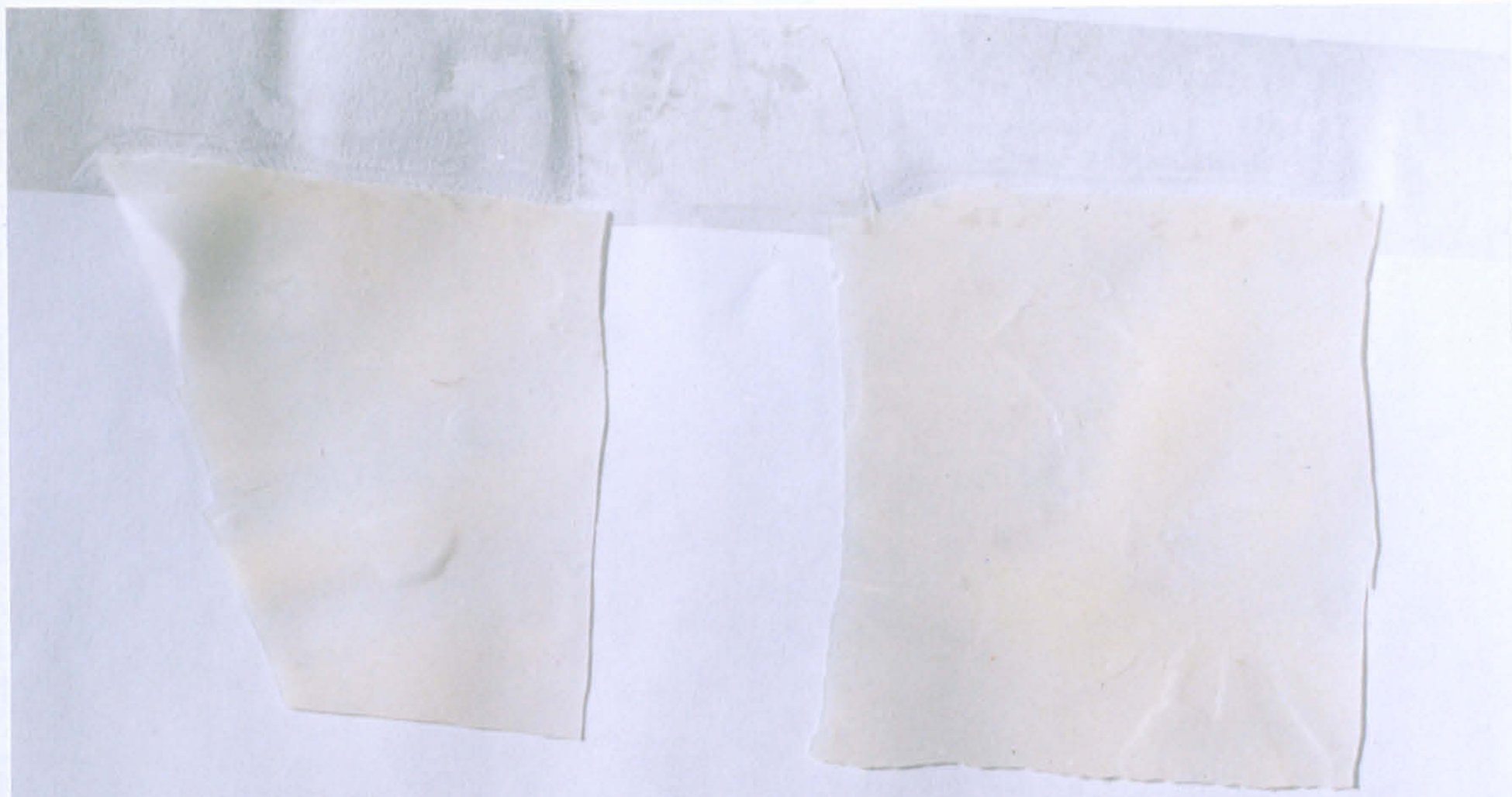

FILM BEFORE PHOTOLYSIS
LP-32C = 100 g
$NaBO_3$ = 2.75 g
(NaOH (0.5 M)) = 3 g

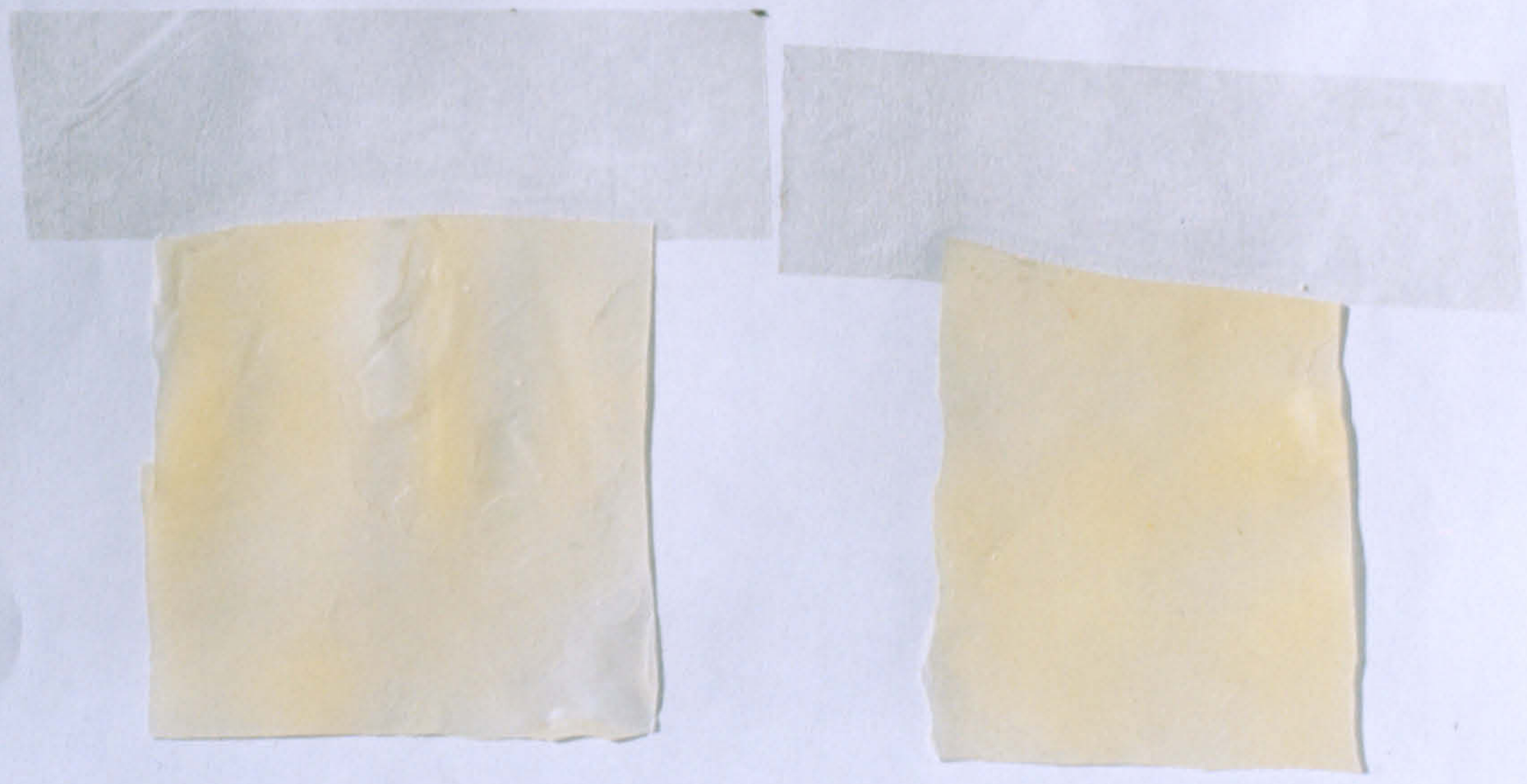

FILM BEFORE PHOTOLYSIS
LP-2C = 100 g
$NaBO_3$ = 2.75 g
(NaOH (0.5 M)) = 3 g

Fig 6.20b: Photographs of $NaBO_3$-cured LP films after UV exposure.

Fig 6.21a: Photographs of TBHP-cured LP films before exposure

Fig 6.21b: Photographs of TBHP-cured LP films after UV exposure

FILM AFTER 743 h
EXPOSURE TO UV_B
TBHP = 100 g
LP-2C = 7.7 g
(Triethanolamine - 1 g)

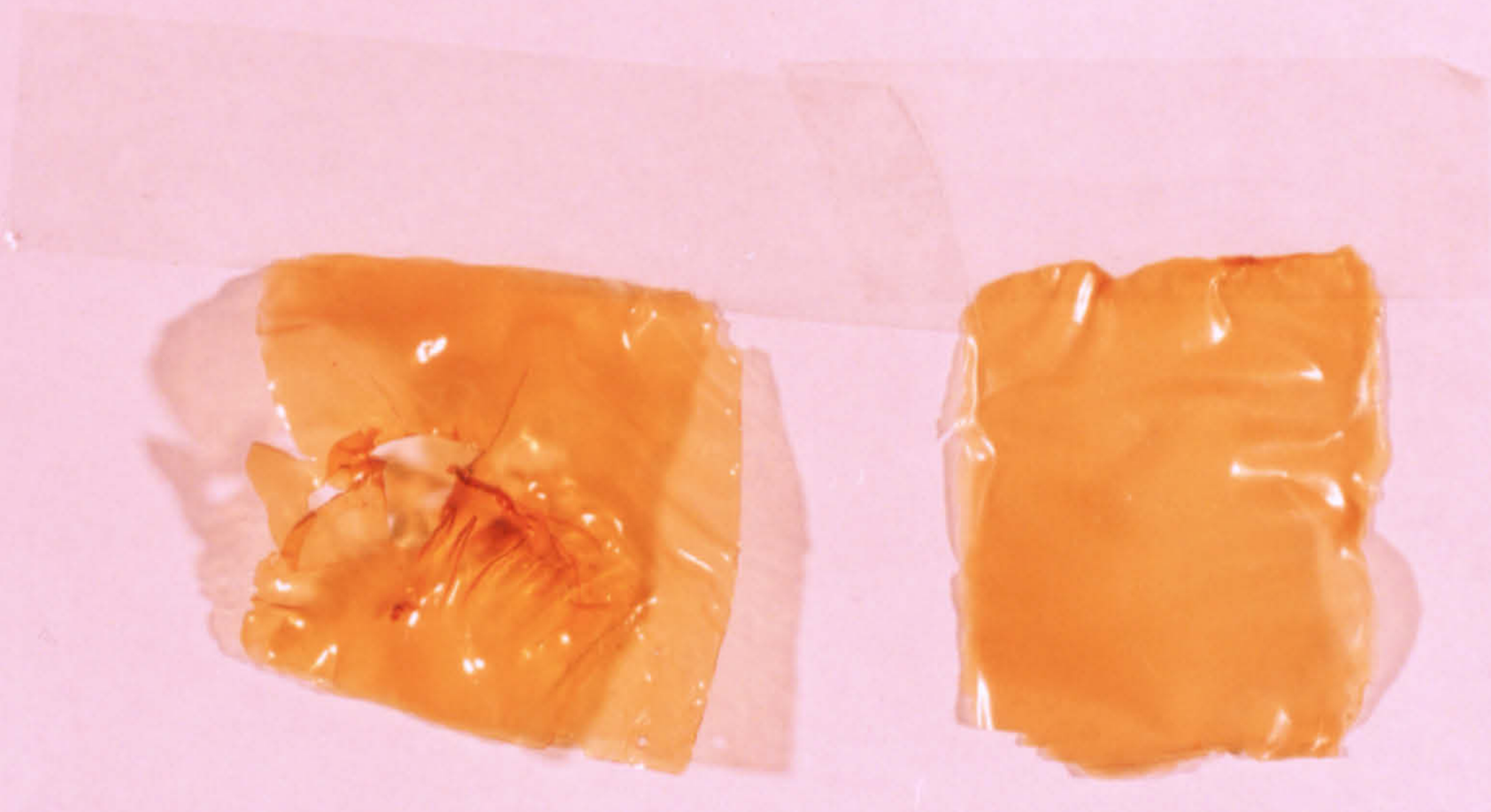

FILM AFTER 743 h
EXPOSURE TO UV_B
TBHP = 6.8 g
LP-32C = 100 g
(Triethanolamine - 1 g)

6.14 OPTICAL MICROSCOPIC EXAMINATION OF LP FILMS BEFORE AND AFTER PHOTODEGRADATION

Photographs were taken of LP films cured using TBHP, MnO_2 and $NaBO_3$ using an optical microscope, before and after UV exposure.

The dramatic change in surface morphology of these films following UV exposure can be seen in fig. 6.22. These photographs show that TBHP-cured LP films exhibit a liquid-like appearance after prolonged exposure whereas MnO_2-and $NaBO_3$-cured films exhibit a grainy texture.

6.15 EFFECT OF ADDING CARBON BLACK TO LP FILMS CURED WITH VARIOUS AGENTS.

A series of LP-977C films containing a constant level of carbon black, (0.6 phr), were prepared using $NaBO_3$, TBHP and MnO_2 as curatives. These samples were then irradiated in the UV_B 'Weatherometer' for up to 2800 hours.

From the kinetic growth curves of C=O absorption illustrated in fig. 6.23, it is clear that a relatively very rapid failure was observed in films cured using TBHP while the degradation rates of MnO_2-and $NaBO_3$-cured films were not dissimilar. TBHP curing therefore appears to confer less stability to UV irradiation than curing with $NaBO_3$ or MnO_2.

Fig. 6.22a: Surface morphology photograph of TBHP-cured film before UV exposure.

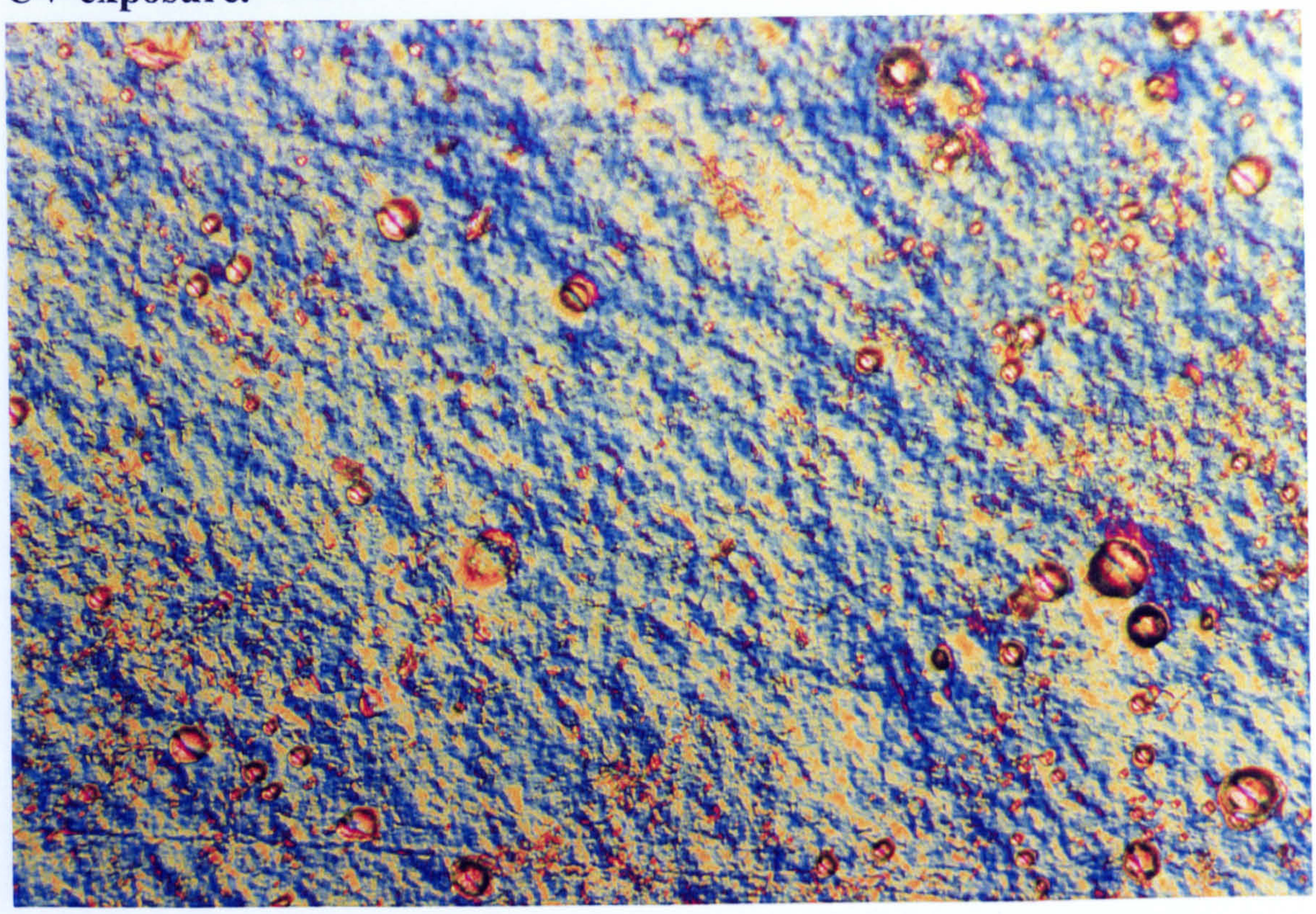

Fig. 6.22b: Surface morphology photograph of TBHP-cured film after UV exposure.

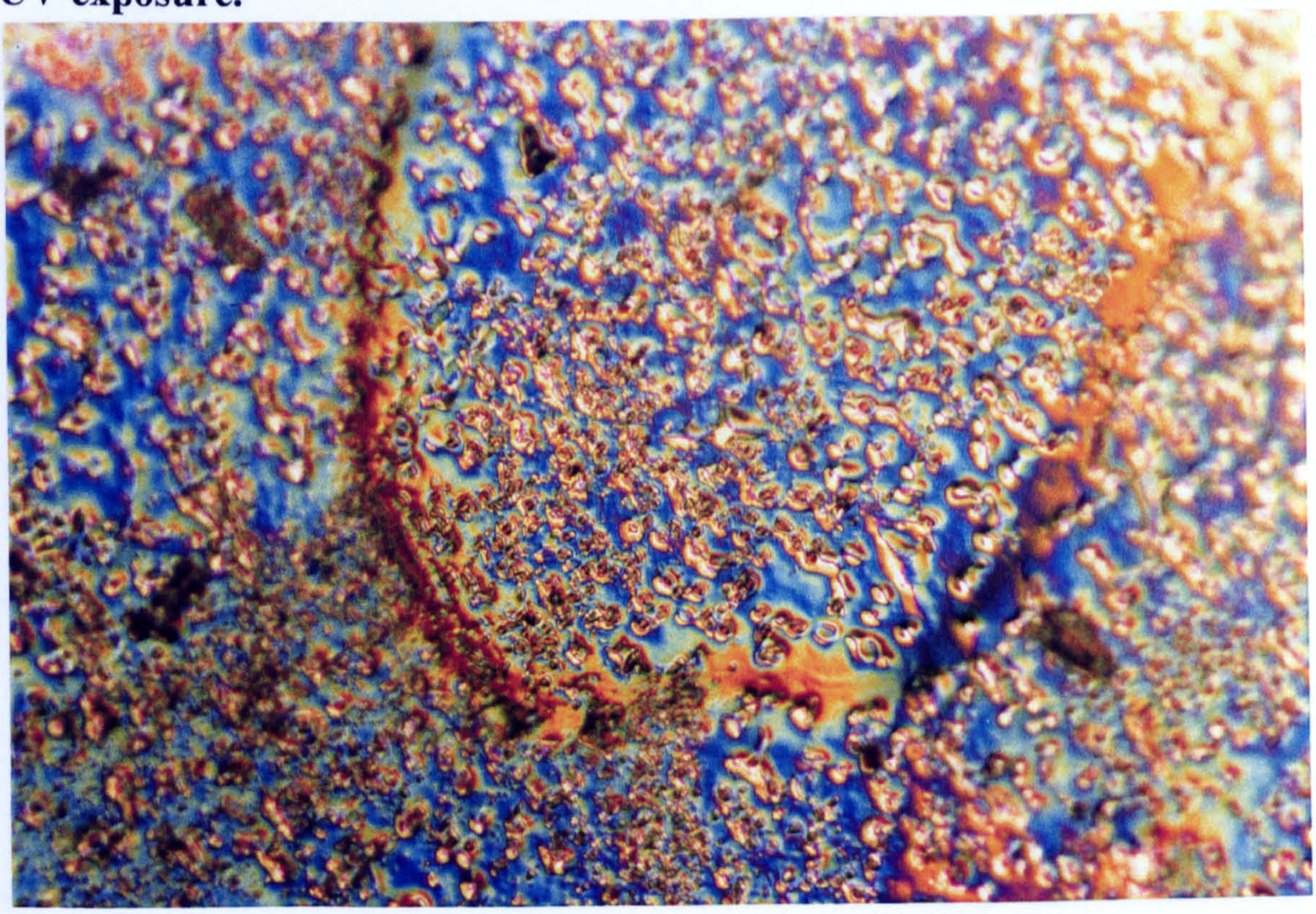

Fig. 6.22c: Surface morphology photograph of $NaBO_3$-cured film before UV exposure.

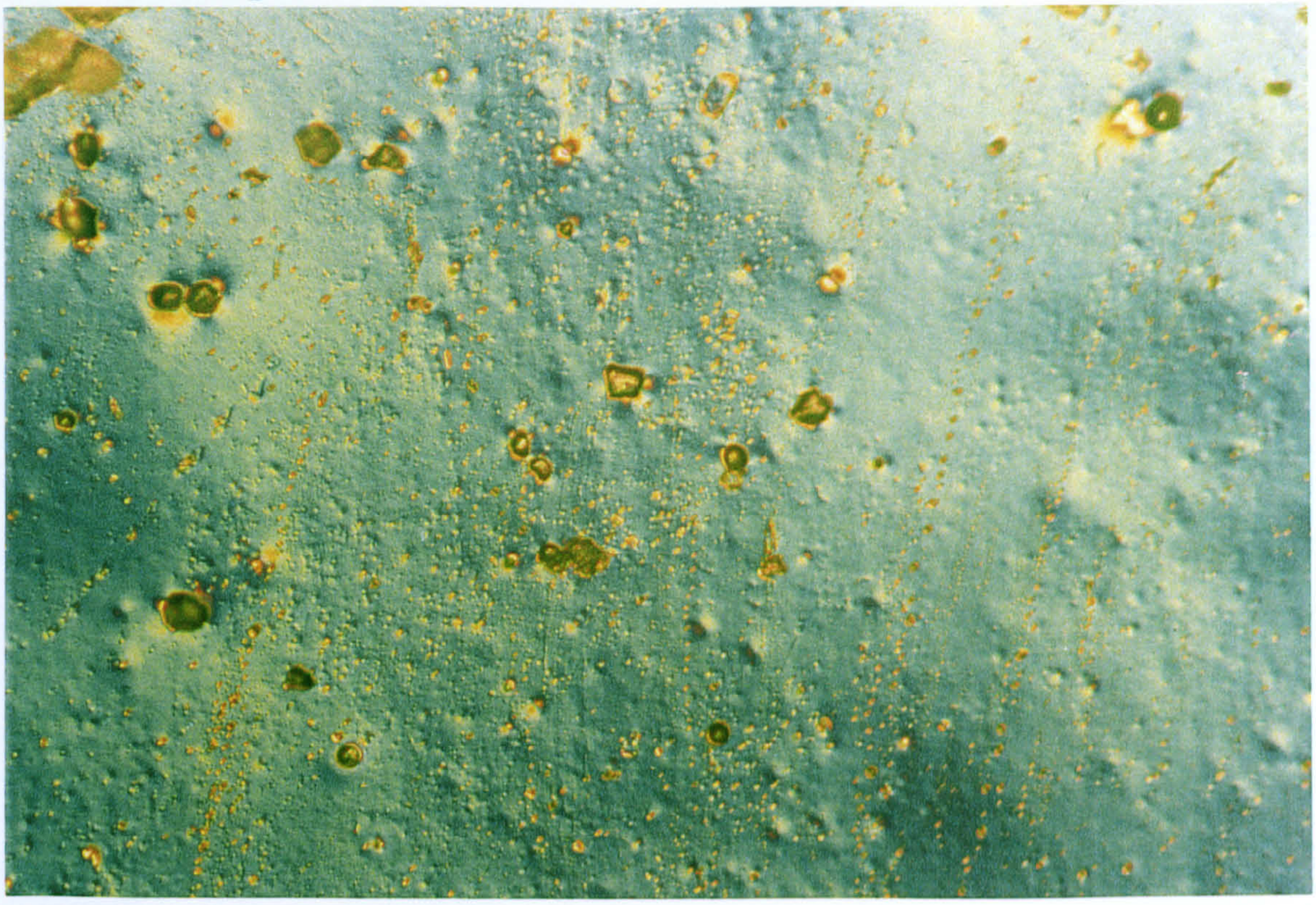

Fig. 6.22d: Surface morphology photograph of $NaBO_3$-cured film after UV exposure.

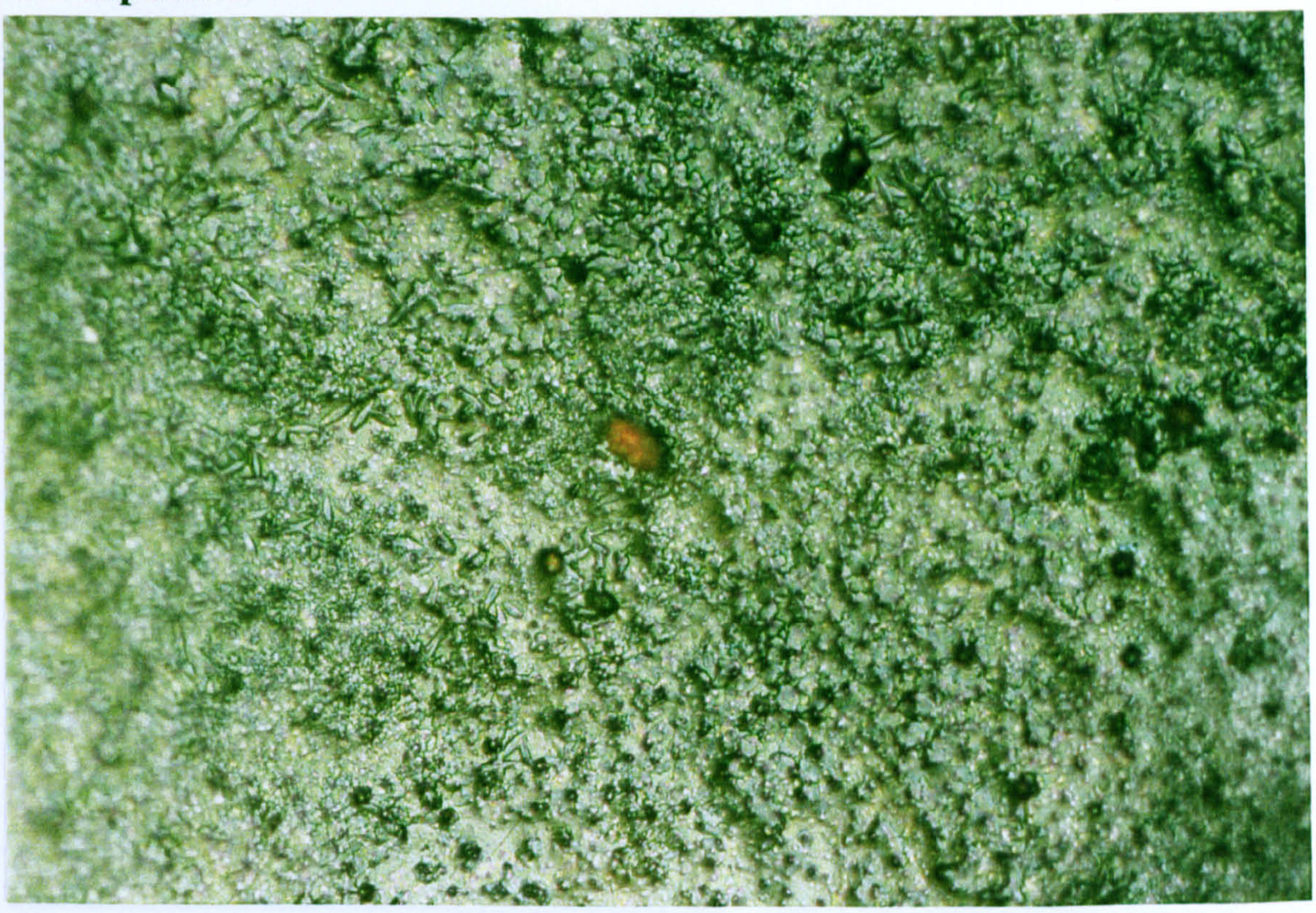

Fig. 6.22e: Surface morphology photograph of MnO_2-cured film before UV exposure.

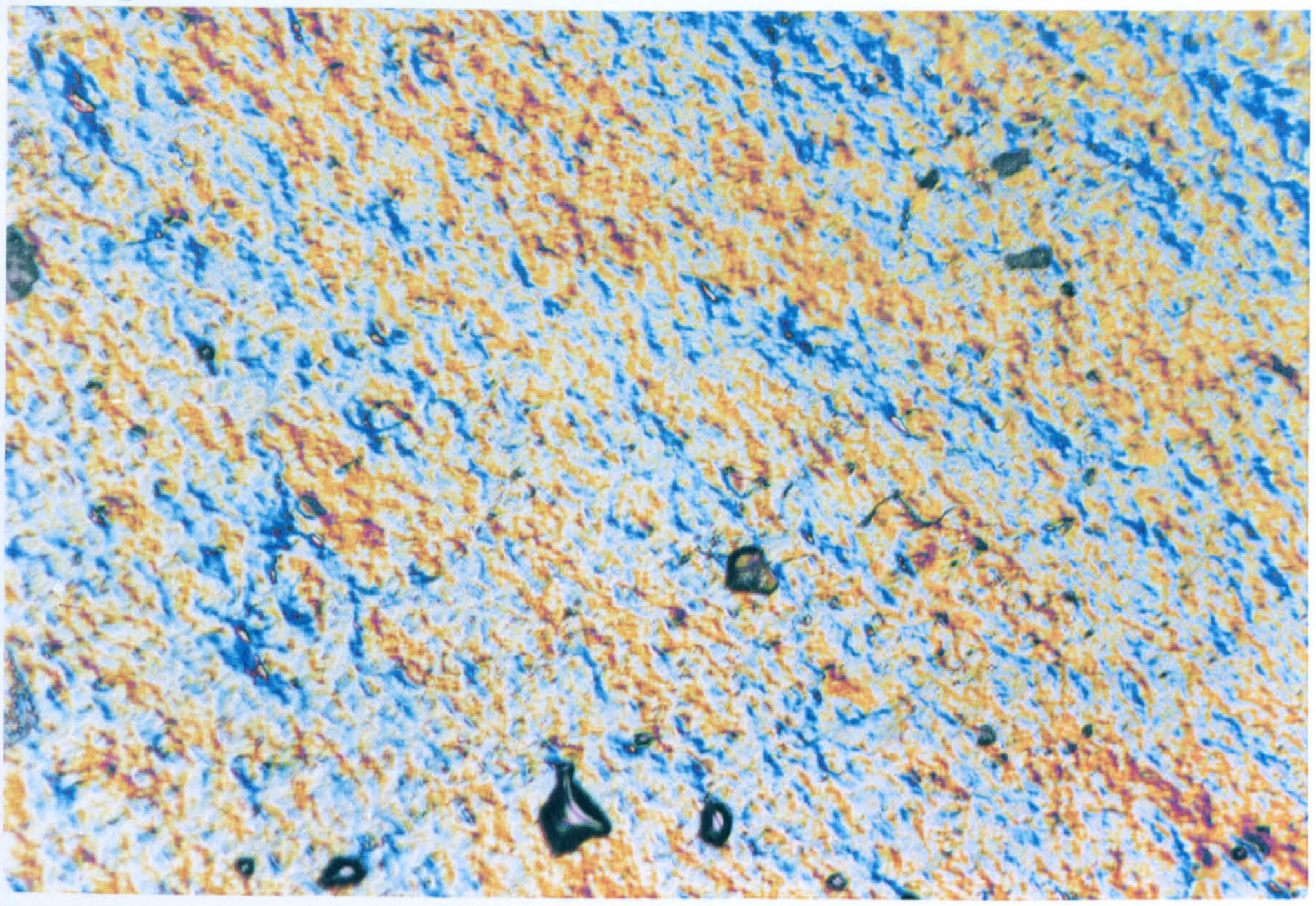

Fig. 6.22f: Surface morphology photograph of MnO_2-cured film after UV exposure.

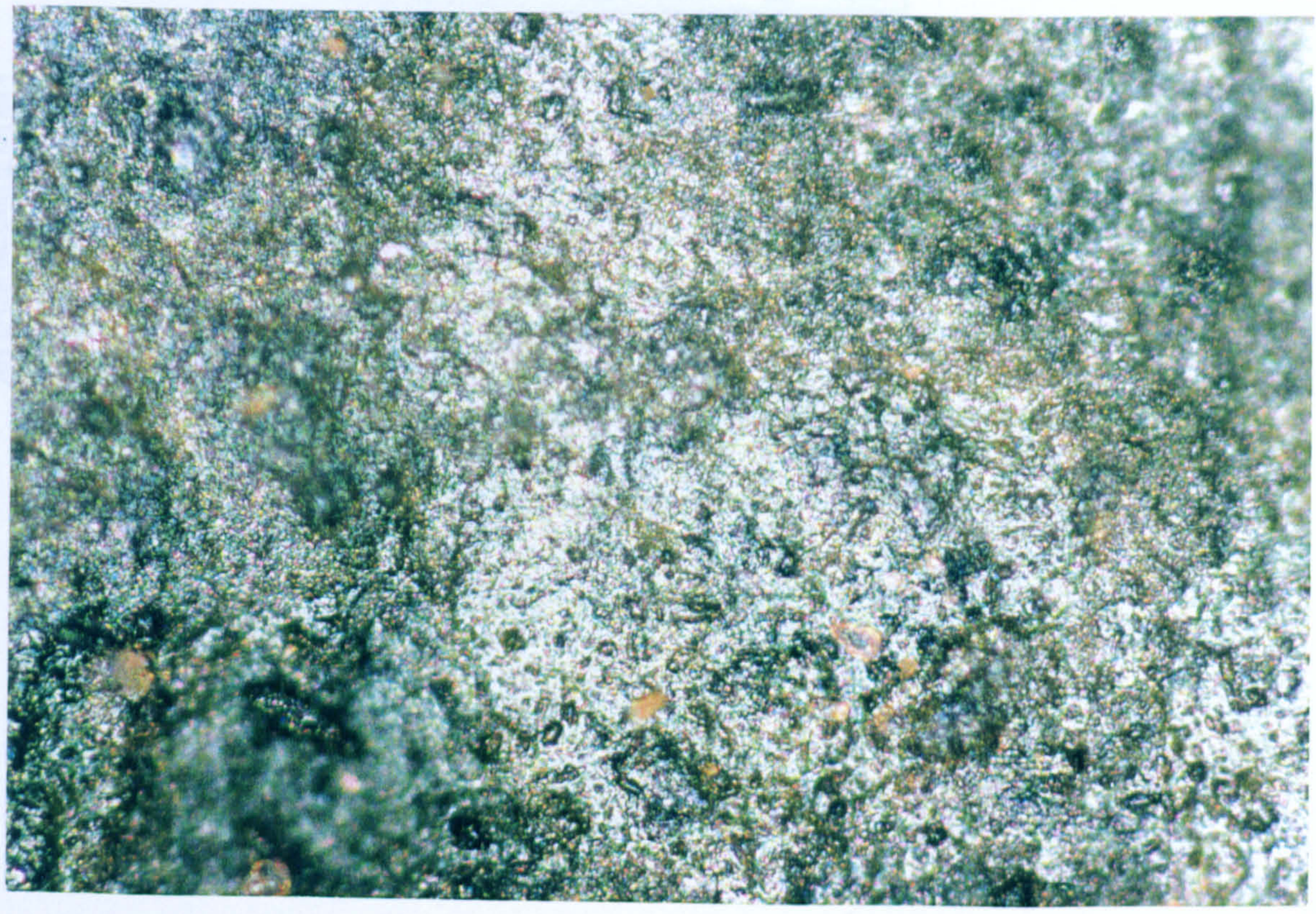

Fig 6.23: Profile of growth of carbonyl peaks with various cured LP-977C films with constant carbon black content, but cured with different curatives, following UV_B irradiation in 'Weatherometer'.

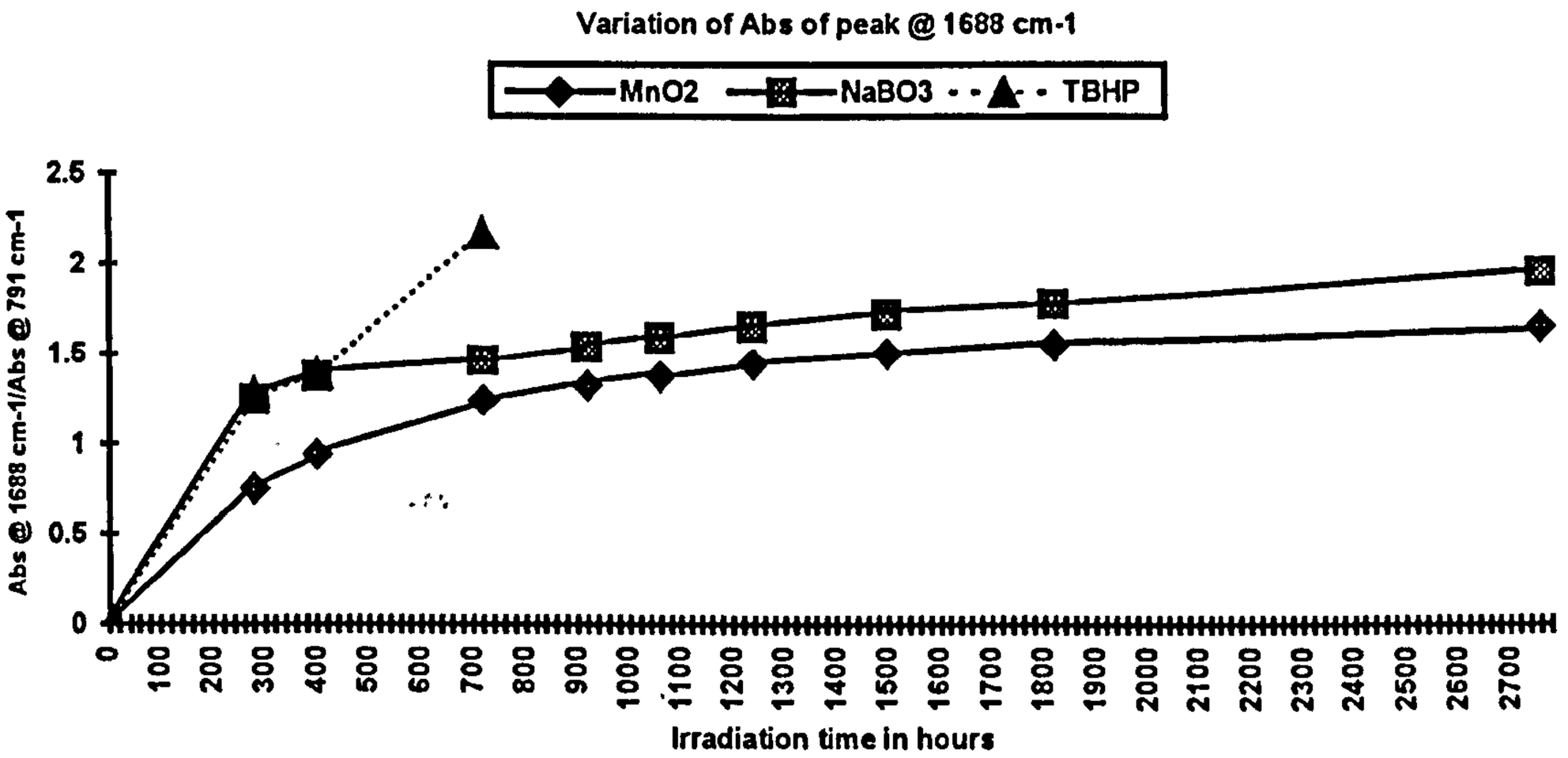

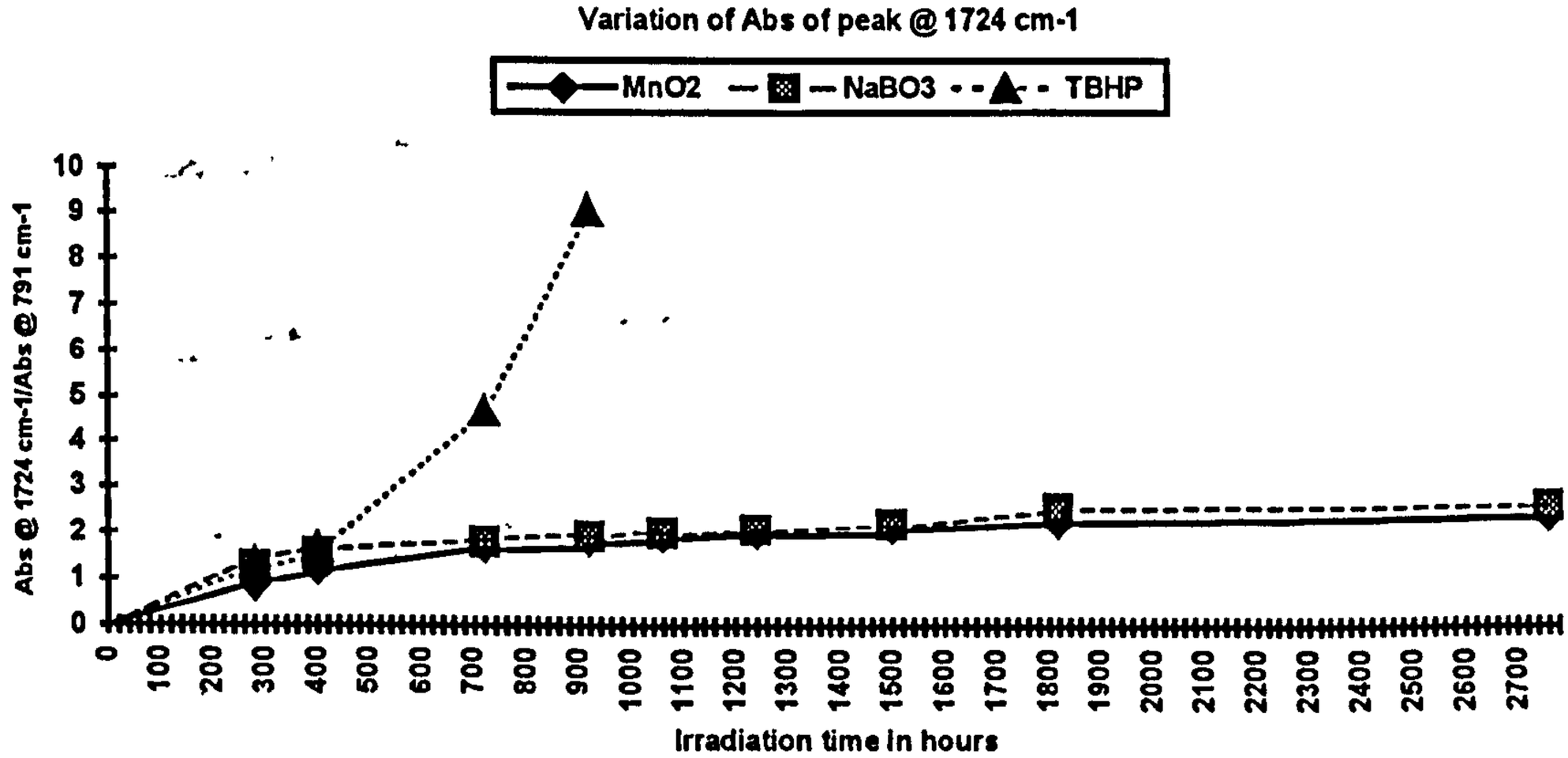

6.16 EFFECT OF VARYING TBHP LEVEL IN LP-977C-CURED FILMS

Films containing various levels of TBHP, i.e. 12, 10, 8 and 6 phr, were prepared and irradiated in the UV_B 'Weatherometer' for up to 1800 hours. FTIR spectra were obtained at various intervals throughout the experiments. From the kinetic growth curves obtained for peaks at 1724 cm^{-1} and 1685 cm^{-1}, see fig 6.24, it can be concluded that the level of TBHP used to cure LP-977C has little effect on the rate of carbonyl development within the irradiated films. The highest TBHP level shows only a slight increase in the rate of degradation.

Fig. 6.24: Profile of growth of carbonyl peaks in LP-977C films cured with varying levels of TBHP following UV_B irradiation in 'Weatherometer'

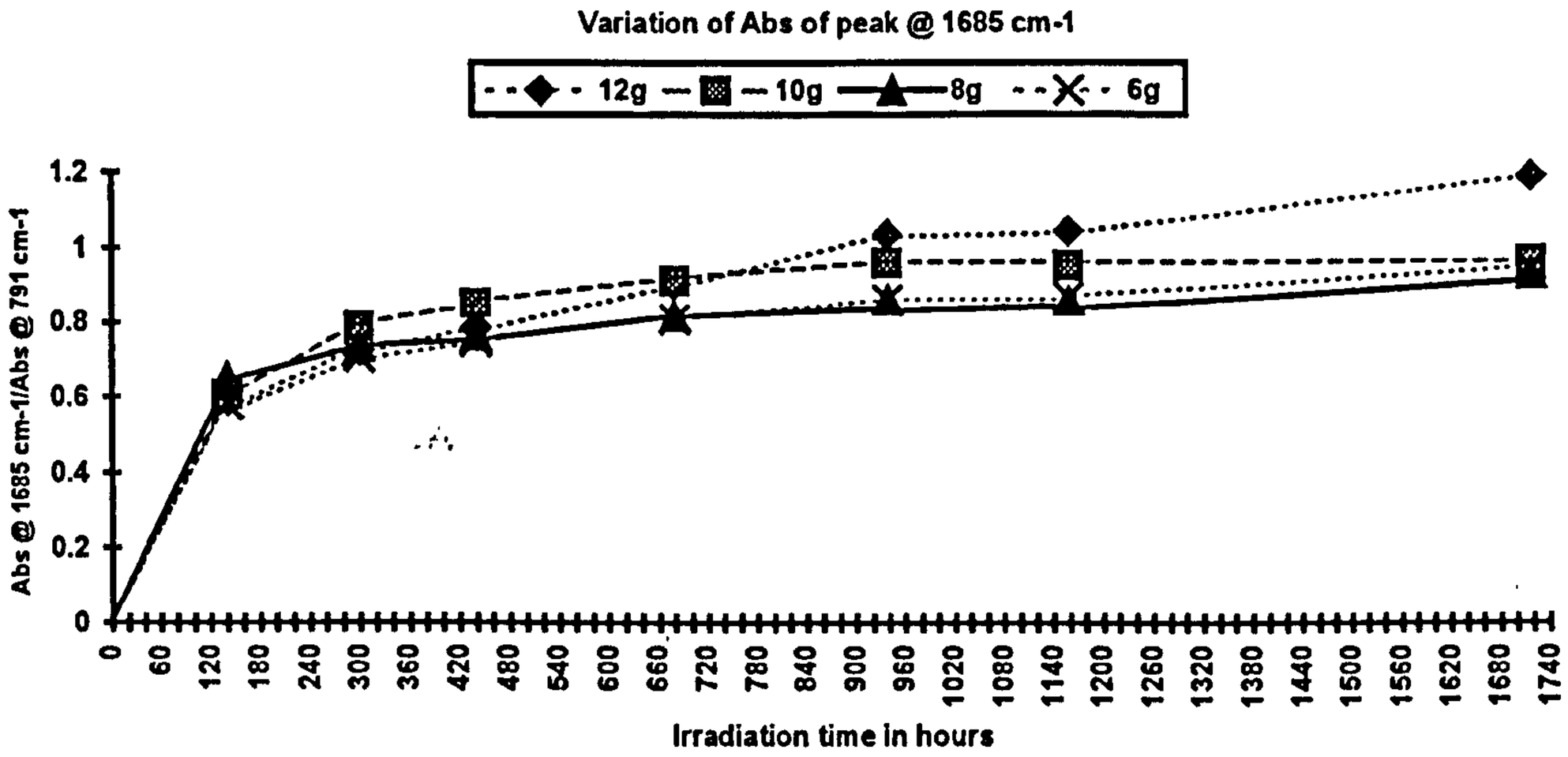

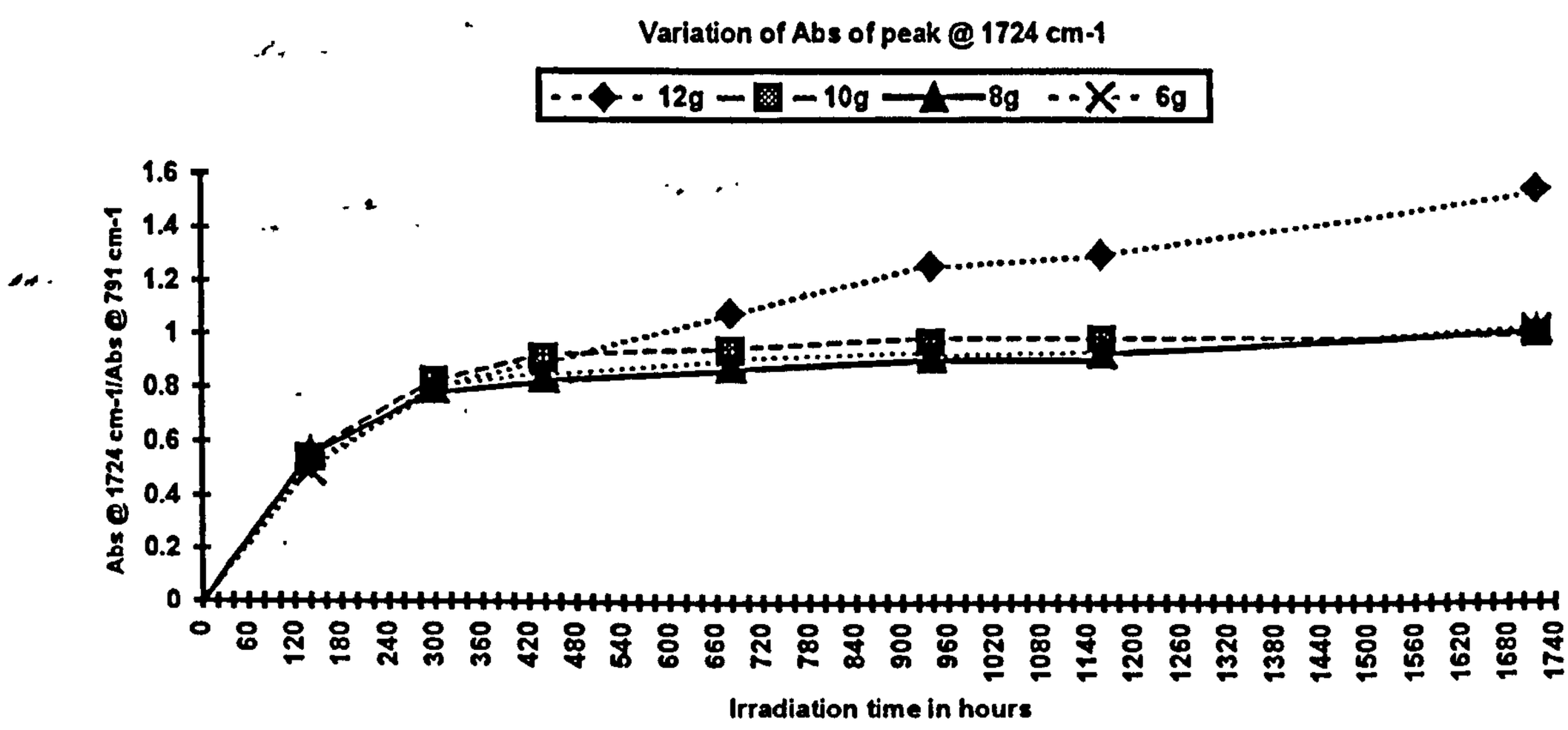

6.17 EFFECT OF USING $CuCl_2$ / KI AS A POTENTIAL INHIBITOR SYSTEM FOR LP PHOTODEGRADATION.

During the 19th Conference on "Polymer Degradation and Stabilisation" at the University of Sussex in September 1994, a presentation[3] showed convincing evidence that a combination of KI/$CuCl_2$ acts as an effective stabilising system for PVC. An experiment was therefore carried out using FTIR to assess whether this combination would inhibit photodegradation in LP samples.

A series of LP-977C films containing

i. $CuCl_2$ 0.02 phr

ii. KI 0.2 phr

iii. $CuCl_2$ / KI 0.02 / 0.2 phr

iv. No additives

were prepared and cured using *ca.* 5% MnO_2. These samples were irradiated in the UV_B 'Weatherometer' for up to 2160 hours. FTIR spectra were obtained periodically throughout the irradiation to assess the rate of carbonyl development within the films.

From the carbonyl growth curves illustrated in fig. 6.25, it can be seen that this inhibitor system is ineffective for LP systems. If anything the incorporation of metal salts into the polymer appears to increase the rate of carbonyl formation. This result is not really surprising since metal impurities in polymers are thought to catalyse the formation of peroxides and hydroperoxides, leading to degradation. Whatever repair mechanism operates in irradiated PVC films does not do so in LPs.

Fig. 6.25:- Profile of growth of carbonyl peaks in MnO_2-cured LP-977C films using $Cu(II)Cl_2$ and KI as inhibitor following UV_B irradiation in 'Weatherometer'.

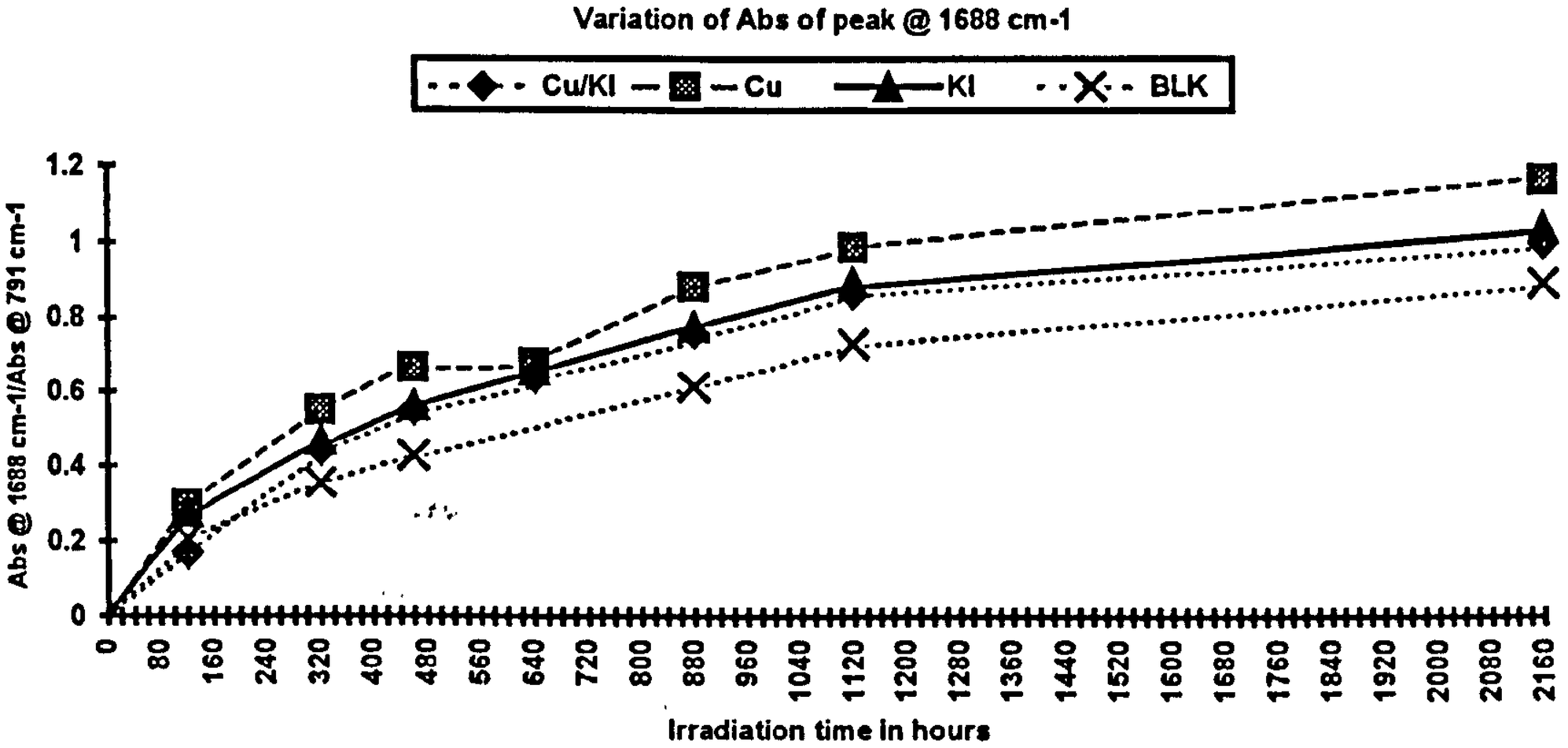

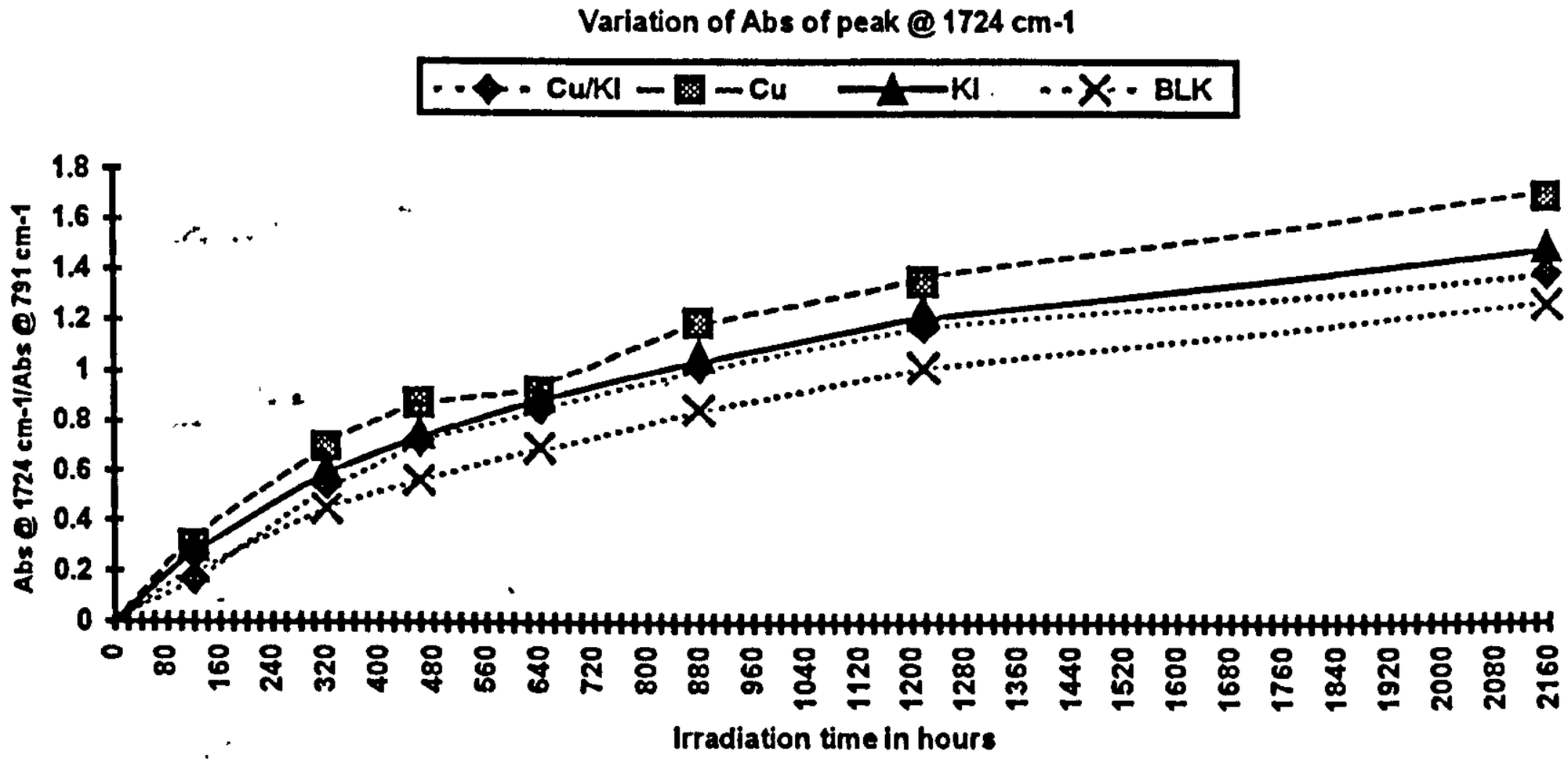

6.18 EFFECTS OF USING TINUVINS 1130 AND 292 AS POTENTIAL INHIBITORS FOR LP PHOTODEGRADATION.

A series of LP-977C films containing 1 phr of Tinuvin were prepared and cured using *ca.* 5% MnO_2.

These samples were irradiated in the UV_B 'Weatherometer' for up to 1700 hours. FTIR spectra were obtained periodically throughout the experiment to assess the rate of degradation registered by carbonyl formation within the films.

From the kinetic growth curves illustrated in fig 6.26, it can be concluded that although Tinuvin 1130 has no real effect in retarding the photodegradation rate in the LP films, Tinuvin 292 clearly shows some ability to reduce the rate of C=O development.

6.19 EXPERIMENTS TO ASSESS THE LEVEL OF TINUVIN 292 REQUIRED TO REDUCE LP PHOTODEGRADATION.

A series of LP-977C films containing 0.5, 1, 2 and 4 phr of Tinuvin 292 were prepared and cured using *ca.* 5% MnO_2. These samples, together with a blank control were irradiated in the UV_B 'Weatherometer' for up to 1700 hours. FTIR spectra were obtained at various periods throughout the experiment to assess the rate of degradation by carbonyl formation within the films.

From the kinetic growth curves for the development of C=O peak at 1730 cm^{-1}, it can be concluded that the optimum level of Tinuvin 292 to inhibit photodegradation in an LP sample is between 0.5 and 1 phr.

Fig. 6.26: Profile of growth of carbonyl peaks in MnO_2-cured LP-977C containing Tinuvins 292 and 1130 as inhibitors, following UV irradiation in 'Weatherometer'

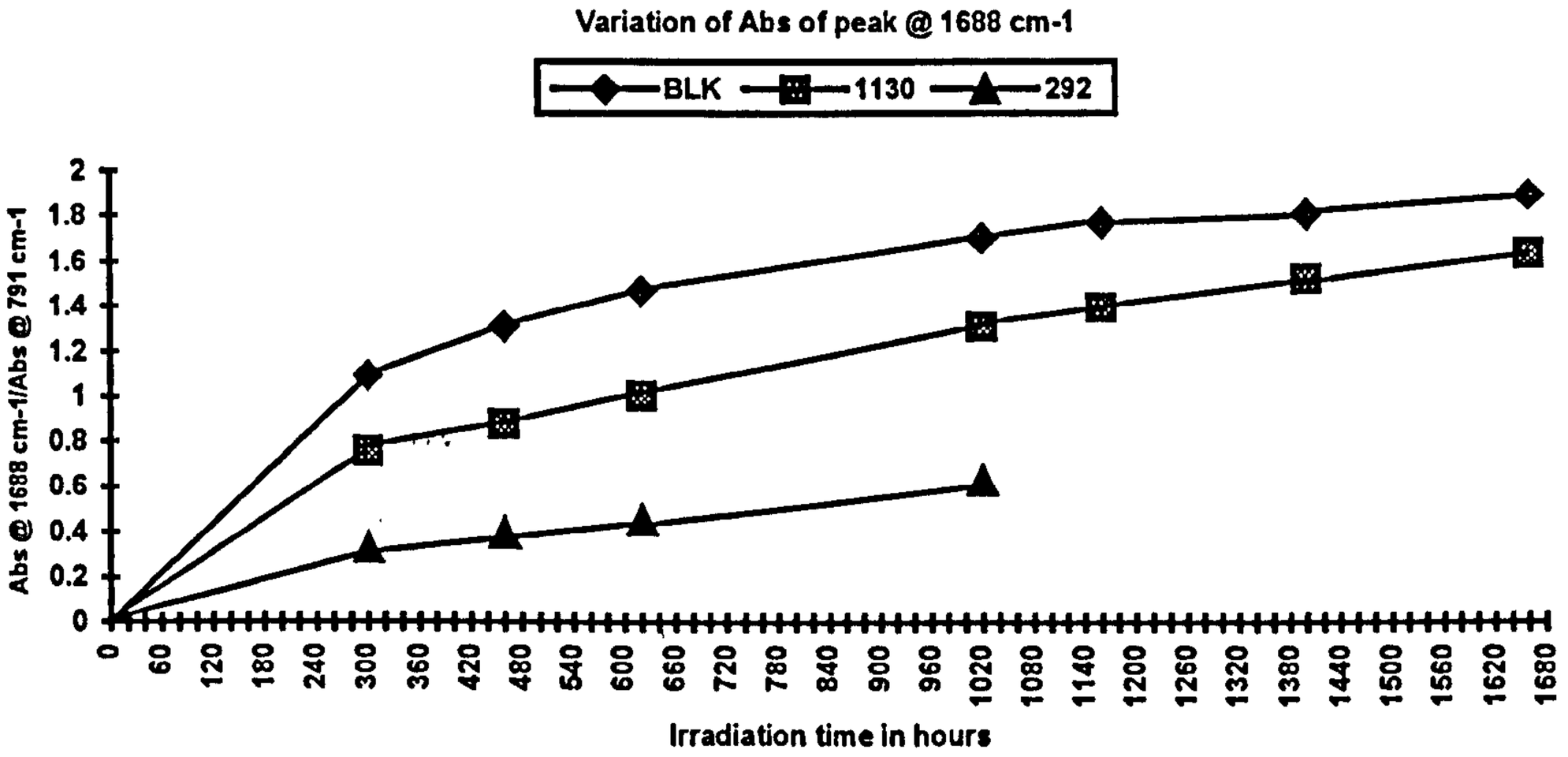

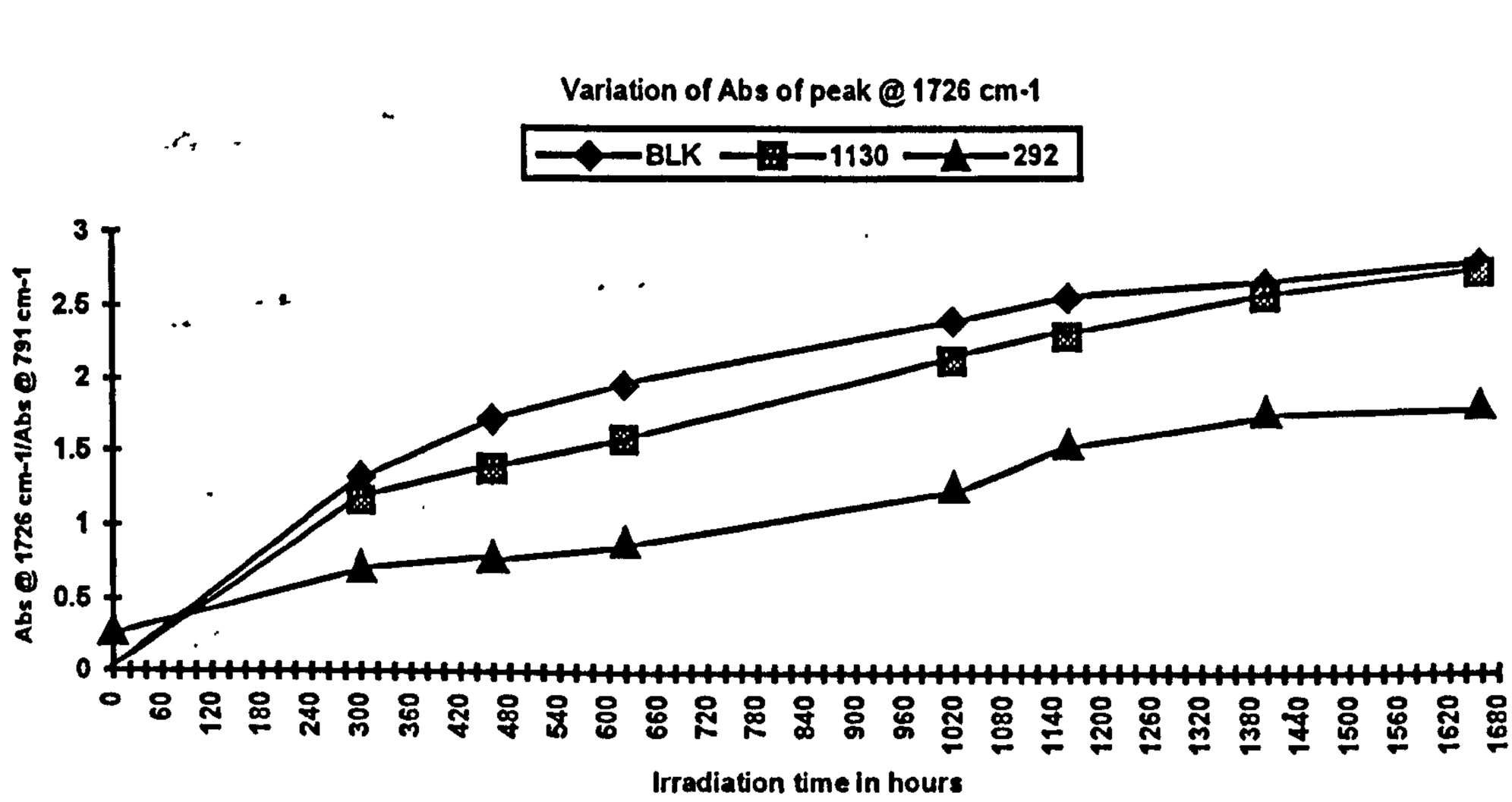

Fig 6.27: Profile of growth of carbonyl peaks in MnO_2-cured LP-977C; experiment to assess the optimum level of Tinuvin 292 to inhibit degradation following UV_B irradiation in 'Weatherometer'.

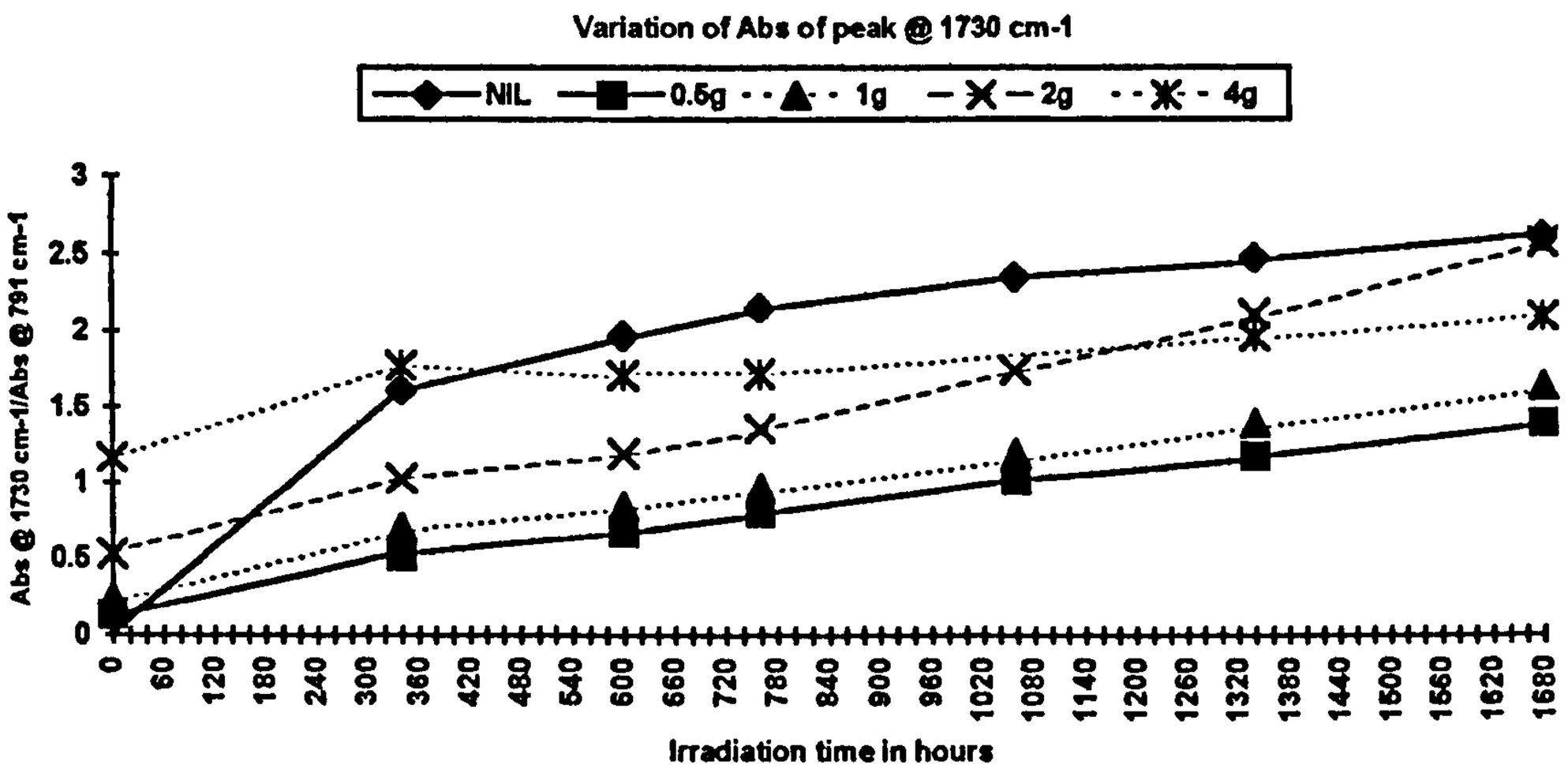

6.20 EXPERIMENTS TO ASSESS WHETHER CURED FILMS OF LP ZL-2264 PRODUCE CARBONYL BANDS WHEN EXPOSED TO UV IRRADIATION

Films of LP-2C and ZL-2264 were cured using MnO_2 and TBHP and then irradiated in the UV_B 'Weatherometer' for up to 300 hours.

The cured films of ZL-2264 undergo a similar photo-oxidative degradation to those of LP-2C, the principal effect of photolysis of ZL-2264 cured with MnO_2 being the development of C=O frequencies at *ca.* 1724 cm^{-1} and 1688 cm^{-1}, (*c.f.* LP-2C MnO_2 cured films at *ca.* 1724 cm^{-1} and 1688 cm^{-1}). As regards the TBHP-cured films, ZL-2264 gave C=O frequencies at *ca.* 1733 cm^{-1} and 1692 cm^{-1}, compared to those for 1725 cm^{-1} and 1688 cm^{-1} for LP-2C.

The rate of growth and pattern of ν(C=O) absorptions within the ZL-2264 films appear to be rather similar to those obtained for cured films of LP. Evidently, variation in the LP repeat unit, i.e. an extra CH_2 in the polymer backbone, appears to have no effect on the rate of formation of C=O within the cured films.

6.21 SOLID STATE ^{1}H NMR EXPERIMENT

In an attempt to confirm that the 1725 cm^{-1} carbonyl band seen in the UV irradiated polymer films relates to the same band assigned in the LP pre-polymer samples (cf. 1725 cm^{-1}) to a formate ester by a 2-D NMR experiment, see chapter 5.6, a cross polarisation-magic angle spinning solid state ^{1}H NMR spectrum was obtained between 5 and 9 ppm on a heavily degraded TBHP-cured LP film. The experiment was unsuccessful in achieving confirmation, however, because the necessarily weak peak at 8 ppm assigned in the liquid sample to the formate ester could not be detected above the noise level in the powdered film sample. Only a broad, weakly resolved band was obtained between 0 and 10 ppm, with proton frequencies detectable at 4.78, 3.86 and 3.03 ppm. These peaks correspond to O-$\underline{CH_2}$-O at 4.70 ppm, O-$\underline{CH_2}$-CH_2 at 3.80 and O-CH_2-$\underline{CH_2}$ -SS at 2.89 for the liquid pre-polymers.

6.22 DISCUSSION AND CONCLUSIONS

All cured LP thin film samples, irrespective of structure and curing agent, including ZL-2264 (with an extra CH_2 linkage in the repeat unit), produce a carbonyl absorption at 1725 cm^{-1} when exposed to UV irradiation. A 1725 cm^{-1} band was also found in UV-irradiated LP pre-polymer samples, (see section 5.1) which

was assigned using NMR techniques as being due to the formation of a formate ester by a free radical route, common to other degraded linear polymers of generally similar structure such as poly(propylene oxide)[4] where the formate ester is located at 1725 cm^{-1}. The use of solid state ^1H NMR (above, section 6.21) was unable to confirm that the same degradation pathway is occurring in the cured film experiments, since the NMR spectra obtained were poorly resolved and the structural detail obtained was therefore limited. Irradiated films leached in $CDCl_3$ for long periods of time also failed to produce dissolved material enabling a search for the 8 ppm peak assigned to the formate ester. Even so, the similarity in shape and position of the photoproduced carbonyl band make it highly probable that the carbonyl band developed in all polysulfide UV irradiated films is due to the same degradation pathway as the carbonyl development seen in the pre-polymer samples, i.e. a free radical route leading to the formation of a formate ester. A detailed mechanism for this reaction is illustrated in section 5.9.

Oxygen plays a crucial role in the formation of the formate ester, indicating a photo-oxidative degradation route common to most polymer degradation mechanisms. This is constant with the film thickness experiment, (see section 6.2), where the thinner films degrade faster due to their relatively greater permeability to oxygen.

Variation in LP structure has no perceptible effect on the rate of carbonyl formation; this is illustrated by comparing the photodegradation rates of MnO_2 -cured films of LP-2C and LP-12C (see section 6.7). Although the former contains ten times more branching agent than the latter, and thus contains more tertiary carbon centres in its backbone, there is virtually no difference in the rate of carbonyl production.

The rates of attack of oxygen at the hydrogen atoms located on secondary and tertiary carbon atoms appear to be similar, implying that the formate ester is derived from two pathways, namely (i) via the tertiary carbon centres as proposed by Griffiths et al.[4] and (ii) via the secondary carbon atoms as indicated in the publication by Lemaire et al.[5] for the degradation of poly(propylene oxide) and poly(ethylene oxide). This helps to confirm the mechanism proposed for the formation of formate ester in LP pre-polymers illustrated in section 5.9.

Extending the range of curatives to include MnO_2, $NaBO_3$ and TBHP does not affect the carbonyl growth during photo-oxidation, and the kinetic growth curves obtained follow a similar pattern, although films cured by the organic curative TBHP exhibit mechanical failure after relatively short exposure times. Lowering the level of TBHP used to cure the polysulfide (section 6.16) did not appear to increase the lifetime of these films.

From visual examination and the photographic evidence illustrated in sections 6.13 and 6.14, it is apparent that while the films cured with inorganic curatives develop cracks and discolour after prolonged UV exposure, the TBHP-cured films develop a brown-liquid like appearance. The latter observation indicates that photodegradation in films cured with TBHP occurs via two competing mechanisms: (i) the formation of formate ester discussed previously via a free radical route, and (ii) an acid-catalysed hydrolysis mechanism, which is discussed in detail in Chapter 7.

Because the extent of the free radical photodegradation mechanism for cured LP-films leading to carbonyl groups is virtually independent of the curative used, it is therefore unlikely that metal centres such as Mn, Pb, B and Ca, are acting as sites of degradation via a redox mechanism. It is the methylene groups within the main

functional groups of the polymer which are directly attacked by oxygen to produce the formate ester, most likely via attack at both the secondary and tertiary carbon atoms when the latter are present.

Increased loading of MnO_2 curative also appears to have an effect in reducing the extent of carbonyl formation in LP films, this curative appearing therefore to act as an efficient inhibitor of photodegradation for these systems. At higher levels, e.g. 7 parts per hundred rubber (phr), the photodegradation rate is reduced. The addition of a strong oxidant such as MnO_2 might have been expected to be significant in the overall photodegradative process of these polymers, since under UV irradiation even weak oxidising agents such as TiO_2 are known to attack surrounding organic molecules[1,2] by an oxidative mechanism. The fact that MnO_2 appears to reduce the photodegradation suggests that the black colour of the films offers this protection simply as a result of light absorption and scattering effects, which appear to offset any photo-oxidative role MnO_2 might have been expected to play.

Carbon black also efficiently retarded the photodegrative effects on LP films cured using MnO_2 (section 6.9). This was not unexpected since previous research[6,7] has shown that adding carbon black to polymer systems often protects against weathering effects; again this is most likely due to light absorption and scattering effects produced simply by the addition of a black pigment. The addition of carbon black to films cured using TBHP and $NaBO_3$, (section 6.15), also appeared to improve service lifetimes. Although the TBHP-cured films still failed at relatively short UV exposures times compared to those cured using MnO_2 and $NaBO_3$, no liquid-like appearance was produced in TBHP films protected using carbon black.

The addition of $KI/CuCl_2$[3] (section 6.17), proved to be unsuccessful in

inhibiting the production of carbonyl groups in LP films. In recent years, Tinuvin inhibitors such as 1130 and 292 have been used to help extend the service lifetimes of many polymers used in industrial applications. From section 6.18 and 6.19, it is clear that these are relatively inefficient in protecting cured films of polysulfide, Tinuvin 292 offers a slight protection to photodegradative effects at a level between 0.5 and 1 phr. The normal stabilising effects of these HALS could be partly offset by their combination with sulfur acids derived from the oxidation of LPs. Again, the sulfur acids could form sulfon amides on reaction with the nitroxyl radicals derived from the amine.

These various experiments indicate that the most efficient and economical inhibiting approaches for industrial polysulfide sealant formulations are the use of MnO_2 as curative and the addition of the pigment carbon black, at a level between 0.6 and 1 phr.

Additives such as tetramethylthiuram disulfide (TMTD) and adhesion promoter A187 have little effect on the carbonyl formation. Results from experiments in sections 6.10 and 6.11 suggest that the addition of the adhesion promoter A187 may slightly increase the photodegradation rate in the preliminary stages while the addition of the curative accelerator TMTD may have a slight retarding effect in the early stages. Neither appears to have any great influence on the polymer photodegradative mechanism as indicated by development of the dominant carbonyl band at 1724 cm^{-1}.

The effects of adding plasticiser and filler to these polymers were impossible to assess using IR spectroscopy, because these additives already display very strong absorption in the C=O region of the IR spectrum. Experiments were conducted to

assess their effects on photodegradation using DMTA, but the results derived were irreproducible and equivocal as regards drawing conclusions.

Any study of cured LP films was expected to be relatively difficult with the highly crosslinked polymeric system exhibiting solvent resistance. Only the use of IR spectroscopy to monitor the rates of carbonyl formation in LP films was able to provide useful information on the photodegradation and photostabilisation effects associated with the various curatives, additives and inhibitors.

CHAPTER 6

REFERENCES

1. Kamat, P.V., *Chem.Rev.*, **93**, (1993) 267.

2. Allen. N.S., Edge. M., Bellobono, I.R., Selli. E. *Current Trends In Polymer Photochemistry,* Ellis Horwood. London. (1995) 238-254.

3. Janssen, K., Gijsman, P., Tummers. D., *Polymer Degradation and Stability,* **49**, (1995) 127.

4. Griffiths, P.J.F., Hughes, J.G., Park, G.S. *Eur. Polym. J.*, **29**, (1993) 437.

5. Lemaire, J., Gauvin, P., Sallet, D., *Makromol. Chem,* **188**, (1987) 1815.

6. Turley, R.S., Brent Strong, A., *J. Adv. Mater.,* April (1994) 53.

7. Mwila, J., Miraftab, M., Horrocks, A.R., *Polymer Degradation and Stability,* **44**, (1994) 351.

CHAPTER 7

PHOTO- AND THERMAL DEGRADATION OF CURED LP BLOCKS

An unusual phenomenon was observed whereby LPs cured in the form of cast blocks using tertiary butyl hydroperoxide (TBHP) decomposed under heat or UV irradiation to produce a liquid exudate which appeared at the surface as droplets. A series of experiments on cured polymer blocks was therefore carried out to identify the nature of this exudate and hence the degradation process occurring.

7.1 THERMAL DEGRADATION AT 140^0 C OF TBHP-CURED LP BLOCKS.

Since ESI-MS was to be employed in the study of the production of this liquid exudate, the purified pre-polymer, Model A, of simple structure (for ESI-MS spectrum see fig.3.4 section 3.1) was used for these experiments. Any changes in the structure of the original LP arising as a result of degradation should be visible in the ESI-MS spectrum in the form of new peaks at different masses, but each new series should still be separated by 166 Da, the mass of the repeat unit. Two levels of TBHP were investigated:

i) high levels of TBHP whereby one mole of TBHP is present for each mole of thiol.

ii) low levels of TBHP whereby one mole of TBHP is present for two moles of thiol.

Each polymer block was then placed into a glass vial and exposed in the presence of air to a temperature of 140^0 C. After only 115 hours exposure, both blocks had

completely transformed to a polymeric liquid. Samples of these exuded liquids were taken at various time intervals throughout the experiment and examined using ESI-MS, IR, GPC, ^{1}H and ^{13}C NMR.

The amount of TBHP used in the curing reaction of the pre-polymer Model A appeared to have no effect on the rate of thermal degradation.

ESI-MS spectra obtained for all samples exposed to 140^{0} C for up to 310 hours are virtually identical. A typical ESI-MS spectrum of these exudates is illustrated in fig.7.1. The most notable features in these spectra are the presence of the original A and B series (see section 3.1, fig.3.4), and the appearance of new series at masses corresponding to the A and B series less 14 amu and 30 amu; a series A-2 amu is also prominent. There is also evidence for the existence of a new series at A,B +76 amu, although these latter peaks are of very low intensity.

The IR spectra obtained for these exudates showed the development of a broad band in the O-H region and a C=O peak at 1724 cm^{-1}. There was no peak at $\approx$ 2560 cm^{-1} which would indicate the regeneration of thiol (SH). A typical IR spectrum is illustrated in fig.7.2. GPC analysis of the exudates proved to be uninformative.

^{1}H NMR spectra show the appearance of a new triplet at 0.94 ppm. There is no evidence for the development of thiol since no triplet is present at $\approx$ 1.56 ppm. There is also no development of a peak at $\approx$ 8 ppm which would relate to production of a formate ester. An example of a typical ^{1}H NMR spectrum is shown in fig.7.3.

^{13}C NMR spectra showed the appearance of two new peaks at approximately 41 and 60 ppm. There is no peak development at $\approx$ 160 ppm which would relate to

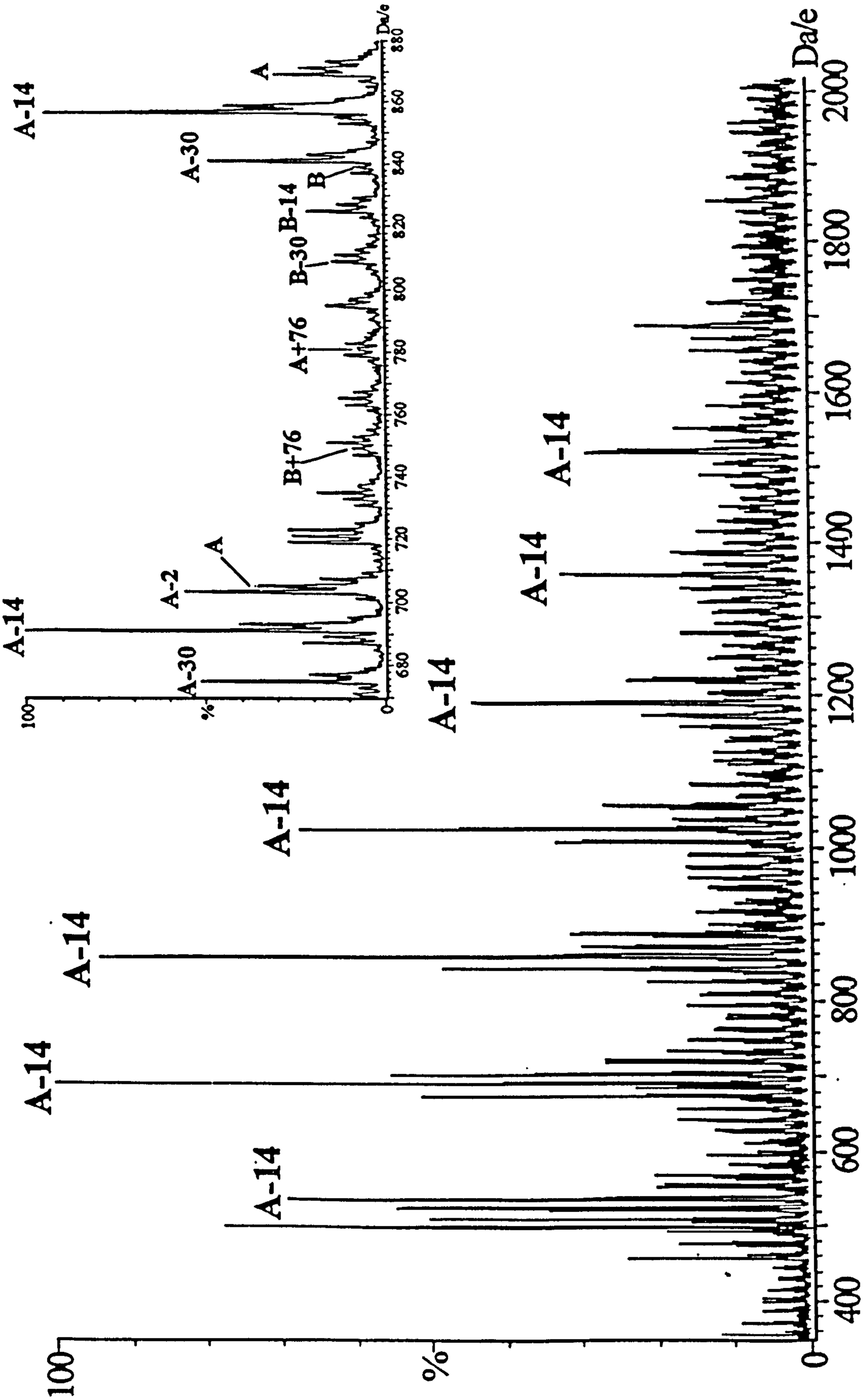

Fig. 7.1: ESI-MS spectrum of TBHP-cured LP exudate exposed to 140^0 C for 120 hours, (solvent system acetone/KI).

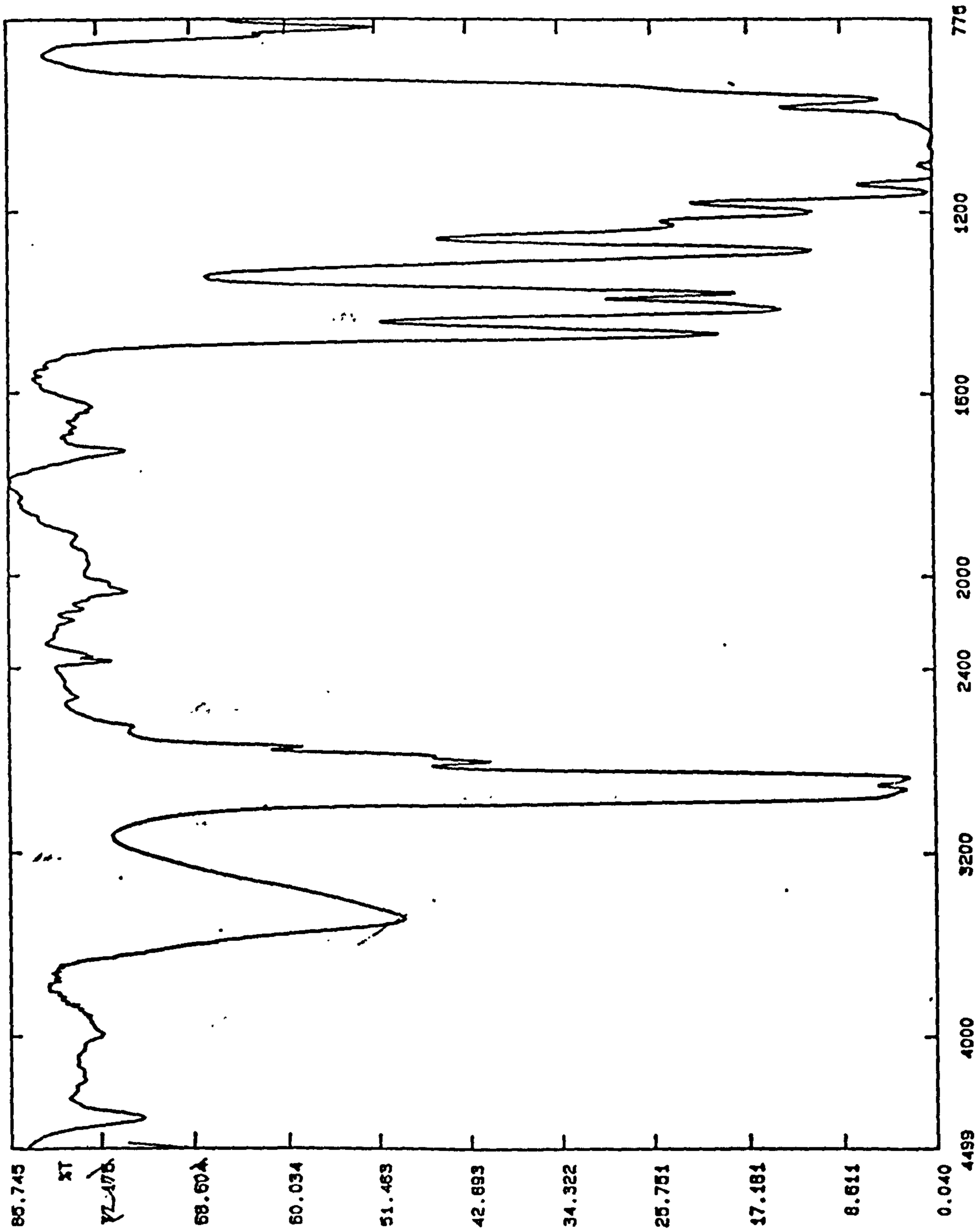

Fig. 7.2: IR spectrum of TBHP-cured LP exudate exposed to 140° C for 120 hours.

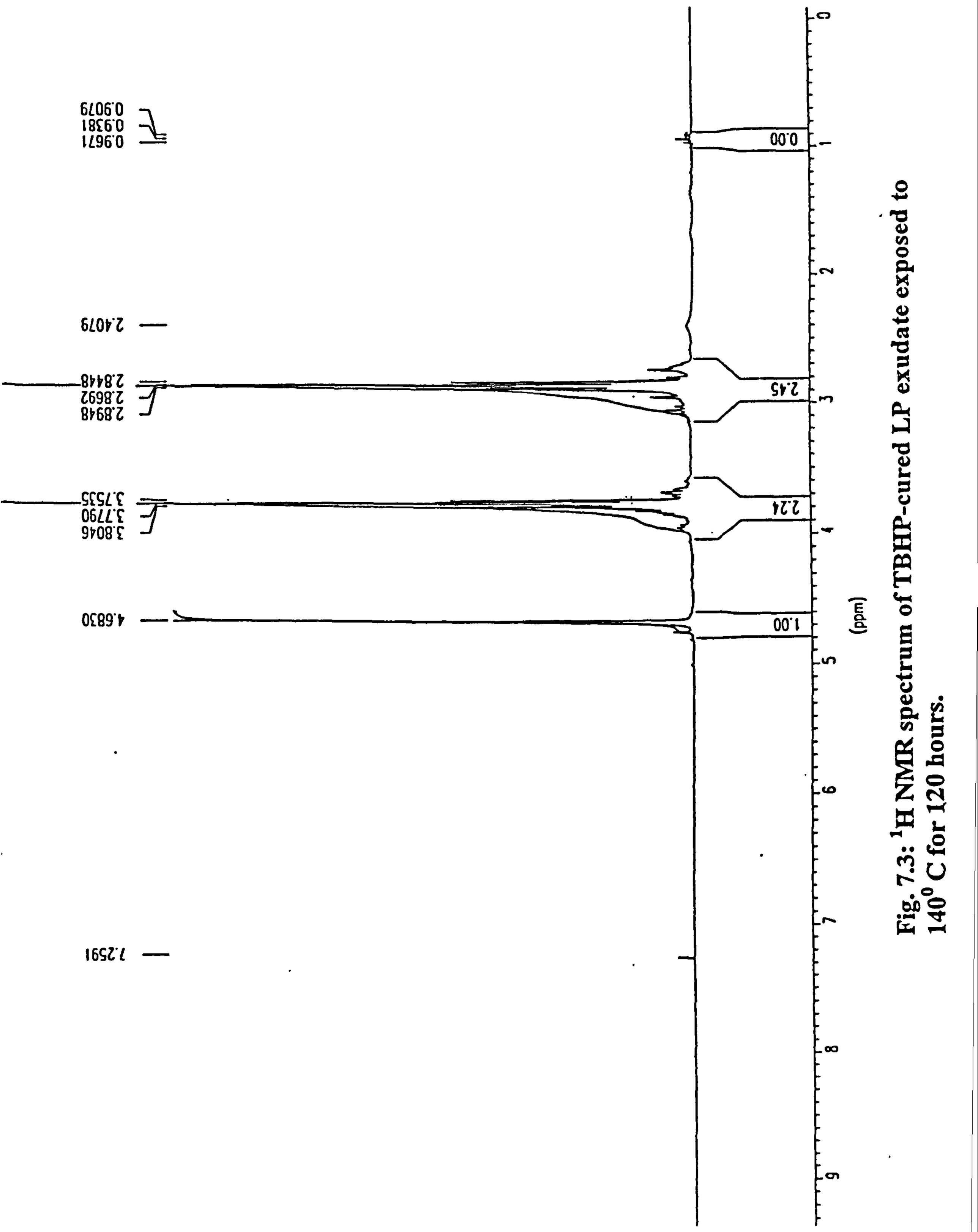

Fig. 7.3: ^{1}H NMR spectrum of TBHP-cured LP exudate exposed to 140^0 C for 120 hours.

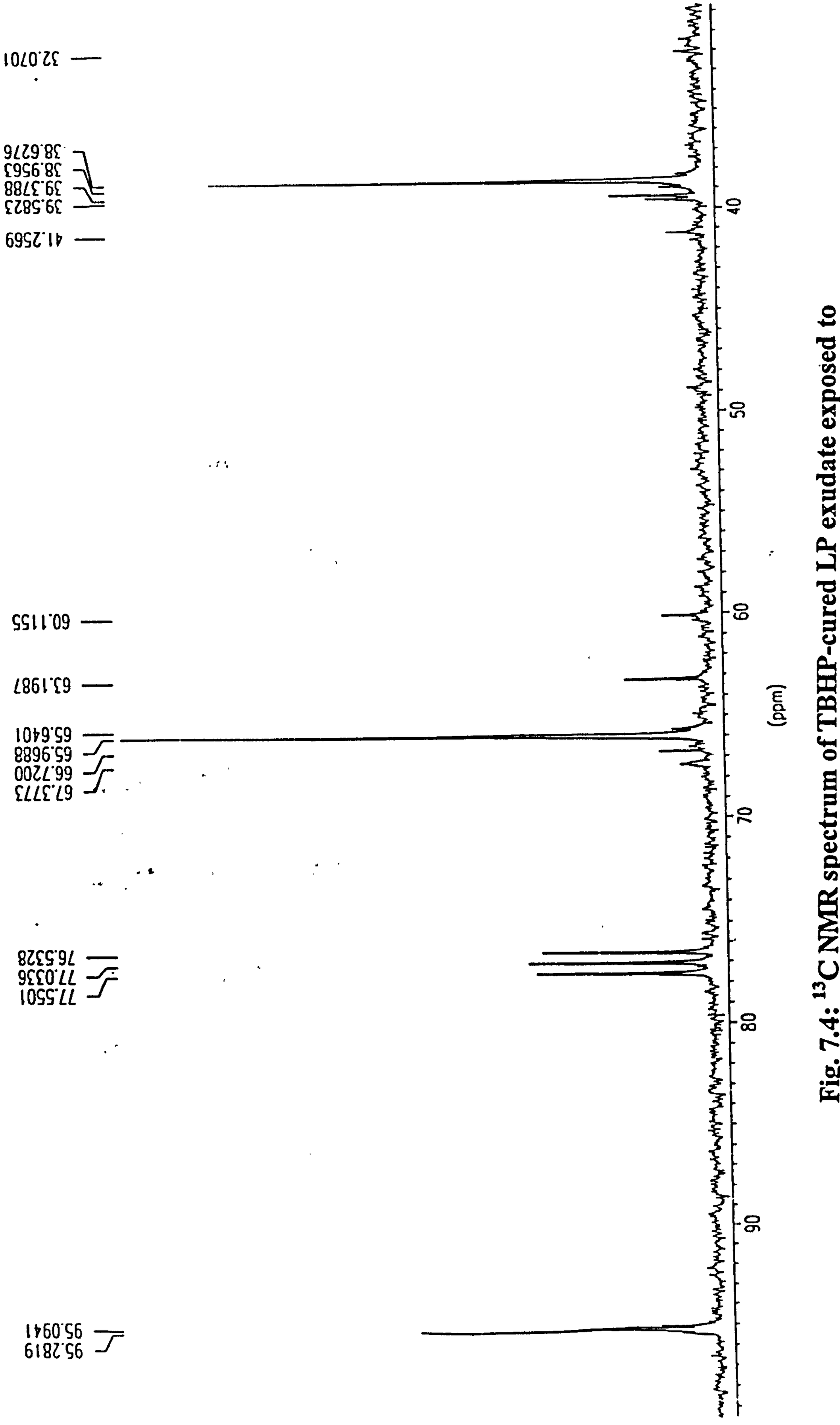

Fig. 7.4: ^{13}C NMR spectrum of TBHP-cured LP exudate exposed to 140^0 C for 120 hours.

carbonyl formation and no peak at ≈ 24.5 ppm which would have indicated the regeneration of thiol end groups. Fig.7.4 shows a typical ^{13}C NMR spectrum.

The A -14 amu series found in the ESI-MS spectra of these exudates can be assigned, on the basis of arguments presented in section 5.8, to the formation of:

$$\mathbf{HO\text{-}C_2H_4\text{-}S(\text{-}S\text{-}C_2H_4\text{-}O\text{-}CH_2\text{-}C_2H_4\text{-}S)_{n-1}S\text{-}C_2H_4\text{-}OH}$$

while the B -14 amu series can be assigned to the above structure with one less sulfur atom in one of the repeat units. This species is formed from the hydrolysis of the two neighbouring formal links[1] according to the following net reaction.

$$R\text{-}O\text{-}CH_2\text{-}O\text{-}R + H_2O \longrightarrow 2\ R\text{-}OH + CH_2O \quad \text{.....(1)}$$

A more detailed explanation for this reaction can be found in section 5.8.

Evidence for this assignment is supported by the IR and ^{13}C NMR spectra; the IR spectra show the development of O-H, while the new peaks at 41 and 60 ppm in the ^{13}C NMR spectra correspond to the existence of S-$\underline{C}H_2$-CH_2-OH and S-CH_2-$\underline{C}H_2$-OH respectively[2]. When a small quantity of MnO_2 was added to these liquid exudates, no curing reaction was observed, indicating again that the thiol end groups had been replaced by O-H terminal groups.

There is no evidence for the existence of SH end groups in the IR, ^{1}H and ^{13}C NMR spectra and therefore the liquid exudate appears to be formed via a hydrolysis pathway and <u>not</u> a depolymerisation reaction whereby the cured LP reforms the initial pre-polymer structure.

The A +76 amu series can be explained by the reaction of the disulfide link in the A -14 amu series with formaldehyde by either of the following net reactions[1]:

$$R\text{-}S\text{-}S\text{-}H + CH_2O \longrightarrow 2\ R\text{-}SH + CO \quad \text{.....(2)}$$

$$R\text{-}S\text{-}S\text{-}H + CH_2O + H_2O \longrightarrow 2\ R\text{-}SH + HCO_2H \quad \text{.....(3)}$$

which lead to the formation of:

$$HO\text{-}C_2H_4\text{-}S(\text{-}S\text{-}C_2H_4\text{-}O\text{-}CH_2\text{-}C_2H_4\text{-}S)_nH$$

A more detailed explanation for this reaction can be found in section 5.8. (The B + 76 amu series can again be assigned to the above structure with one less sulfur atom in one of the repeat units).

The original A and B series can be explained by two different pathways: if the +76 amu structure undergoes reaction 2 or 3 then the original pre-polymer would be reformed; this is highly unlikely since there is no evidence for thiol end groups in either the IR, ^{1}H or ^{13}C NMR spectra. However, an alternative pathway could proceed via the reaction of two moles of the +76 amu structure with one mole of formaldehyde by the following reaction:

$$2\ R\text{-}SH + CH_2O \longrightarrow R\text{-}S\text{-}CH_2\text{-}S\text{-}R + H_2O \quad \text{.....(4)}$$

to give the following structure:

$$HO\text{-}C_2H_4\text{-}S(\text{-}S\text{-}C_2H_4\text{-}O\text{-}CH_2\text{-}C_2H_4\text{-}S)_nCH_2(\text{-}S\text{-}C_2H_4\text{-}O\text{-}CH_2\text{-}C_2H_4\text{-}S)_mS\text{-}C_2H_4\text{-}OH$$

A more detailed explanation for this reaction can be found in section 5.8. Again, the B series can be assigned to the above structure with one repeat unit containing only one sulfur atom.

The A -2 amu structure is most probably due to the formation of cyclic molecules. The final series of mass spectral peaks needing consideration are those located at A,B -30 amu. Various candidates are considered in section 5.8 but the exact structure remains unassigned. The simple loss of CH_2O unit from the polymer chain is the obvious explanation but the absence of thiol end groups rules this out. Another possibility is an ethyl-terminated structure:

$$HO\text{-}C_2H_4\text{-}S(\text{-}S\text{-}C_2H_4\text{-}O\text{-}CH_2\text{-}C_2H_4\text{-}S)_nSC_2H_5$$

The triplet appearing at ≈ 0.94 ppm in the ^{1}H NMR spectra suggested the formation of an ethyl end group, but a decoupling experiment ruled this out; moreover, there is no obvious mechanism to explain the production of such a structure.

The development of a carbonyl band at ≈ 1724 cm^{-1} in the IR spectra of these exudates provides evidence that the competing free radical autoxidation pathway is also occurring but is far less significant in TBHP-cured LP samples whereby a hydrolysis mechanism appears to be the principal degradation route. A more detailed account of the autoxidation reaction can be found in section 5.9.

ESI-MS spectra obtained for all samples heated at 140^{0} C for 310 hours onwards are extremely complex, indicating heavy degradation, see fig.7.5, making a full interpretation difficult. All the series described above are present, confirming the hydrolysis mechanism, but there is also the presence of new peaks at different masses, with each new series separated by 166 Da, the mass of the mer unit. These correspond to series A: +16, +30, +46, +60 and +90, which most likely correspond to the formation of secondary degradation products. The IR, ^{1}H and ^{13}C NMR spectra for these samples are virtually identical to those illustrated in figs. 7.2, 7.3 and 7.4.

A sample of pre-polymer Model A cured using a high level of TBHP was prepared with the addition of ≈ 7% carbon black. This sample was heated to 140^{0} C for over 1000 hours but no liquid exudate was formed. Adding carbon black to this system therefore appears to inhibit the hydrolysis mechanism.

Additional samples using the pre-polymer ZL-2264 were cured using a high level of TBHP; even after heating at 140^{0} C for over 1000 hours no liquid exudate was formed. This result indicates a greatly improved thermal stability of ZL-2264

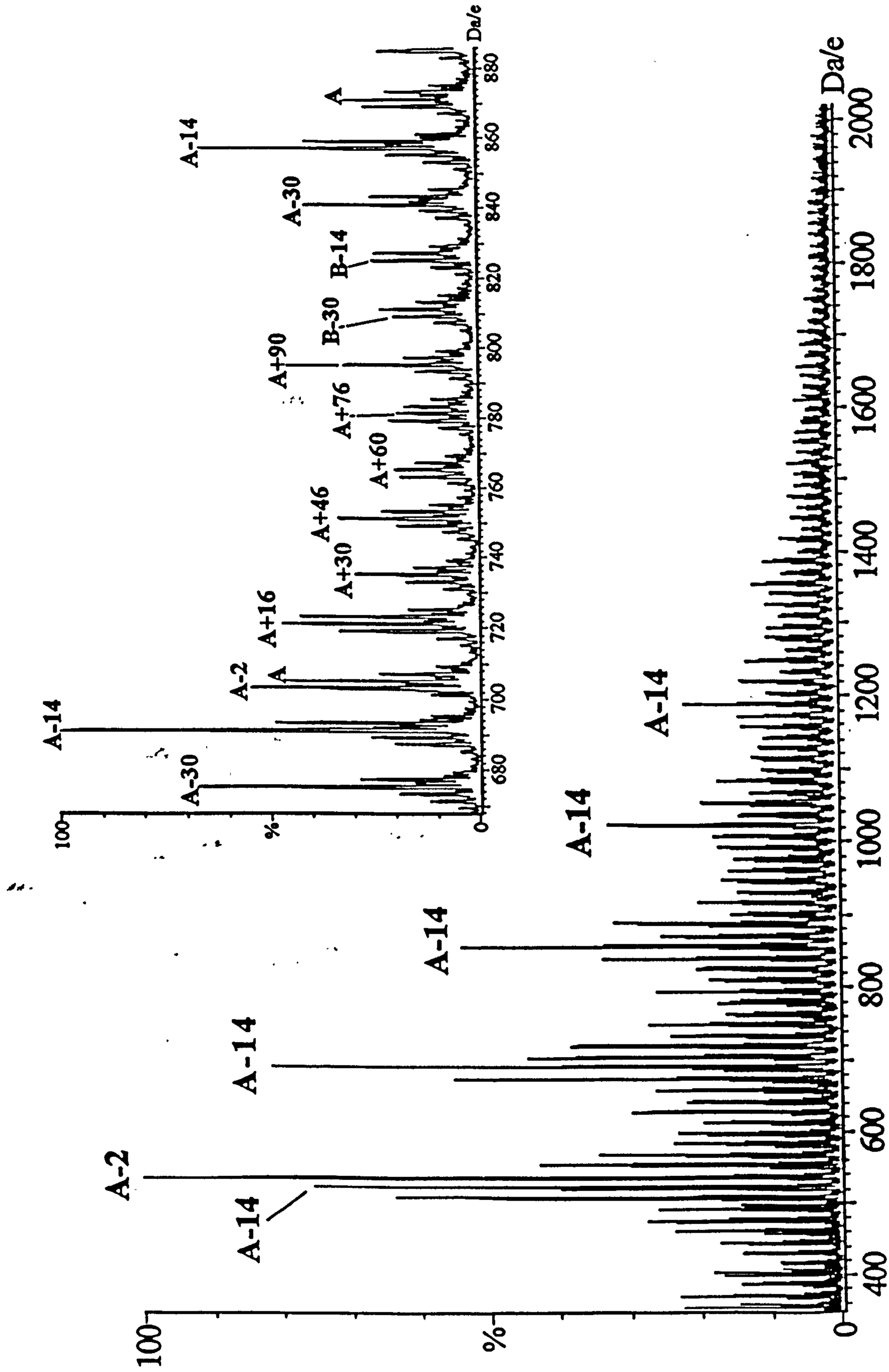

Fig. 7.5: ESI-MS spectrum of TBHP-cured LP exudate exposed to 140^0 C for 310 hours, (solvent system acetone/KI).

compared to normally structured LPs, and offers confirmation of the hydrolysis mechanism proposed above and discussed in detail in sections 5.8 and 5.9. This proposed mechanism depends on the presence of the formal linkage in the polymer chain as the initial site of hydrolysis to produce free formaldehyde, which then further attacks disulfide linkages. The variation in structure of ZL-2264, i.e. the CH_2O linkage in the repeat unit being replaced by C_2H_4O, eliminates the formation of free formaldehyde, rendering this degradation pathway impossible.

7.2 THERMAL DEGRADATION AT 80^0 C OF TBHP-CURED LP BLOCKS.

As in the previous section, samples were prepared using the purified pre-polymer, Model A, and high and low levels of TBHP. Blocks of these samples were then placed in glass vials and exposed to 80^0 C until a liquid exudate was produced. The amount of TBHP used in the curing reaction of the pre-polymer Model A appears to have no effect on the rate of thermal degradation, with both samples decomposing to a polymeric liquid after 860 hours exposure.

ESI-MS spectra obtained for all samples heated at 80^0 C for up to 1200 hours are virtually identical. The most notable features in these spectra are the presence of the original A and B series (see section 3.1, fig.3.4), and the appearance of new series at masses corresponding to the A and B series less 14 amu and 30 amu; a series A-2 amu is also prominent. There is evidence for the existence of a new series at A,B +76 amu, although these latter peaks are of very low intensity. Spectra obtained are therefore similar to that illustrated in fig.7.1.

GPC traces obtained for these samples are uninformative. IR, ^{1}H and ^{13}C NMR spectra obtained for these samples are virtually identical to those obtained for samples in section 7.1 and illustrated by figs. 7.2, 7.3 and 7.4 respectively.

The IR spectra obtained for these exudates showed the development of a broad band in the O-H region and a C=O peak at 1724 cm^{-1}. There is no peak at $\approx$ 2560 cm^{-1} which would indicate the regeneration of thiol (SH).

^{1}H NMR spectra show the appearance of a new triplet at 0.94 ppm. There is no development of a peak at $\approx$ 8 ppm relating to production of formate ester, or a triplet at $\approx$ 1.56 ppm which would indicate thiol end groups. ^{13}C NMR spectra showed the appearance of two new peaks at approximately 41 and 61 ppm. There is no peak development at $\approx$ 160 ppm relating to carbonyl formation and no peak at $\approx$ 24.5 ppm which would have indicated the regeneration of thiol end groups.

These results indicate the same hydrolysis route as for samples heated at 140^{0} C, see section 7.1, except that samples heated at 80^{0} C undergo a considerably slower rate of degradation. The development of a carbonyl band at $\approx$ 1724 cm^{-1} in the IR spectra of these exudates provides evidence that the competing free radical autoxidation pathway is also occurring, see section 5.9 for a detailed explanation of this mechanism.

An LP sample cured using a high level of TBHP and an addition of $\approx$ 7% carbon black was prepared. This sample was exposed to 80^{0} C for over 3000 hours but, as in the case of the analogous experiment at 140^{0}C, no liquid exudate was formed. Adding carbon black to this system therefore appears to inhibit the hydrolysis mechanism.

Additional samples using the pre-polymer ZL-2264 were cured using TBHP; even after heating at 80^0 C for over 3000 hours no liquid exudate was formed. This offers confirmation of the hydrolysis mechanism proposed for exudate samples in section 7.1 and discussed in detail for pre-polymers in sections 5.8 and 5.9.

7.3 PHOTODEGRADATION OF TBHP-CURED LP BLOCKS.

As in the previous sections, 7.1 and 7.2, samples were prepared using the purified pre-polymer, Model A, and high and low levels of TBHP. Blocks of these samples were then placed in glass vials and exposed to UV until a liquid exudate was produced. The amount of TBHP used in the curing reaction of the pre-polymer Model A appears to have a crucial effect on the rate of photodegradation, since no liquid exudate formed in the samples cured with the low level of TBHP, even after extensive UV-exposure of 1500 hours.

ESI-MS spectra obtained for samples cured with a high level of TBHP and exposed to UV irradiation for up to 1400 hours are extremely complex, indicating heavy degradation. They are virtually identical to the spectra obtained for heavily thermal degraded samples (310 hours plus at 140^0 C) described in section 7.1 and illustrated by fig.7.5.

The most notable features in these spectra are the presence of the original A and B series (see section 3.1, fig.3.4), and the appearance of new series at masses corresponding to the A and B series less 14 amu and 30 amu; a series A-2 amu is also prominent. There is evidence for the existence of a new series at A,B +76 amu, although these latter peaks are of very low intensity. These peaks indicate the same hydrolysis route seen in TBHP-cured samples exposed to heat see sections 7.1 and

7.2, and for extensively degraded pre-polymer samples see sections 5.8 and 5.9. There is also the existence of other series; these correspond to series A: +16, +30, +46, +60 and +90, which most likely arise from the formation of secondary degradation products.

GPC traces obtained for these samples are uninformative. ^{1}H and ^{13}C NMR spectra obtained for these samples are virtually identical to those obtained for samples in section 7.1 and 7.2, illustrated by figs.7.3 and 7.4 respectively.

The IR spectra obtained for these exudates showed the development of an intense broad band in the O-H region and an intense C=O peak at 1747 cm^{-1}, i.e. <u>not</u> at 1724 cm^{-1} as seen for thermally degraded samples in sections 7.1 and 7.2. The development of a large carbonyl band at 1747 cm^{-1} in the IR spectra of these exudates provides evidence that the competing free radical autoxidation pathway is also occurring but is much less significant than the hydrolysis pathway, see section 5.9 for a detailed explanation of these mechanisms. No carbonyl peaks were detected in the NMR spectra of these samples.

An LP sample cured using a high level of TBHP and an addition of ≈ 7% carbon black was prepared. This sample was exposed to UV irradiation for over 3000 hours but <u>no</u> liquid exudate was formed; again, carbon black therefore appears to inhibit the hydrolysis mechanism.

Additional samples using the pre-polymer ZL-2264 were cured using TBHP; even after exposure to UV irradiation for over 3000 hours <u>no</u> liquid exudate was formed. This confirms the hydrolysis mechanism which depends on the presence of the formal linkage in the polymer chain as the initial site of hydrolysis to produce free formaldehyde, which then further attacks disulfide linkages. This mechanism is

described for exudate samples in section 7.1 and discussed in detail for pre-polymers in sections 5.8 and 5.9.

7.4 DEGRADATION OF TBHP-CURED LP 'H' BLOCKS.

'H' block samples were prepared as described in section 2.3.4 using the purified pre-polymer, Model A, and a high level of TBHP. Three types of method were used to degrade these samples:

i) heating at 80^0 C

ii) heating at 140^0 C, and

iii) UV exposure.

An unusual phenomenon was noticed whereby 'H' block LP samples cured using tertiary butyl hydroperoxide (TBHP) decomposed under 140^0 C heat or UV irradiation to produce a pool of liquid at the centre of the block just under the polymer/glass interface. Samples of these liquids were taken at various time intervals throughout the experiment and examined using ESI-MS, IR, GPC, ^{1}H and ^{13}C NMR. 'H' block samples heated at 80^0 C did <u>not</u> produce this polymeric liquid even after 3000 hours exposure, indicating that these TBHP-cured LP 'H' block samples are relatively stable at temperatures up to 80^0 C.

Both UV- and heat- (140^0 C) treated samples produced a liquid exudate after only 168 hours. ESI-MS spectra obtained for all samples exposed to either UV or 140^0 C for up to 860 hours are virtually identical, and similar to that illustrated in fig. 7.1. The most notable features in these spectra are the presence of the original A and B series (see section 3.1, fig.3.4), and the appearance of new series at masses corresponding to the A and B series less 14 amu and 30 amu; a series A-2 amu is also

prominent. There is evidence for the existence of a new series at A,B +76 amu, although these latter peaks are of very low intensity.

GPC traces obtained for these samples are uninformative. IR, ^{1}H and ^{13}C NMR spectra obtained for these samples are virtually identical to those obtained for samples in section 7.1 and illustrated by figs. 7.2, 7.3 and 7.4 respectively.

The IR spectra obtained for these exudates showed the development of a broad band in the O-H region and a C=O peak at 1724 cm^{-1}. There is no peak at $\approx$ 2560 cm^{-1} which would indicate the regeneration of thiol (SH).

^{1}H NMR spectra show the appearance of a new triplet at 0.94 ppm. There is no development of a peak at $\approx$ 8 ppm relating to development of a formate ester, or a triplet at $\approx$ 1.56 ppm which would indicate thiol end groups.^{13}C NMR spectra showed the appearance of two new peaks at approximately 41 and 61 ppm. There is no peak development at $\approx$ 160 ppm relating to carbonyl formation and no peak at $\approx$ 24.5 ppm which would have indicated the regeneration of thiol end groups. These results indicate the same hydrolysis route as for sample blocks exposed to heat at 140^{0} C, 80^{0} C and UV in section 7.1, 7.2 and 7.3.

'H' block samples were prepared with an addition of $\approx$ 7% carbon black, these were then degraded by the above methods; even after extensive exposure times of 5000 hours none of these degradation methods yielded a liquid exudate. This result indicates that the hydrolysis mechanism is inhibited by the addition of carbon black to the system.

Additional 'H' block samples using the pre-polymer ZL-2264 were cured using TBHP; even after extensive UV irradiation or heating at 140^{0} C for over 3000 hours, no liquid exudate was formed. This offers confirmation of the hydrolysis

mechanism proposed for exudate samples in section 7.1 and discussed in detail for pre-polymers in sections 5.8 and 5.9.

The development of a carbonyl band at ≈ 1724 cm^{-1} in the IR spectra of these exudates provides evidence for the less significant free radical autoxidation pathway, (see section 5.9 for a detailed explanation of this mechanism).

7.5 DEGRADATION OF MnO_2- AND $NaBO_3$ -CURED LP SAMPLES.

Polymer block and 'H' block samples were prepared using MnO_2 and $NaBO_3$ as curing agents. Three types of method were used to degrade these samples:

i) heating at 80^0 C

ii) heating at 140^0 C, and

iii) UV exposure.

After extensive exposure times of 5000 hours none of these degradation methods yielded a liquid exudate in any of these samples. This result indicates that the hydrolysis mechanism which is the dominant degradation mechanism of TBHP- cured LP samples and pre-polymer samples, is relatively insignificant in LP samples cured using MnO_2 and $NaBO_3$. Chapter 6 describes the development of a carbonyl peak at ≈ 1725 cm^{-1} in the IR spectra of LP films cured using these agents; indicating that the principal degradation mechanism for LP samples cured using MnO_2 and $NaBO_3$ is the free radical autoxidation pathway, (see section 5.9 for a detailed explanation of this mechanism).

7.6 DEGRADATION OF HDDA-CURED LP SAMPLES.

Samples were prepared using the purified pre-polymer, Model A, and cured using hexane-1,6-diol diacrylate (HDDA). Blocks of these samples were then placed in glass vials and degraded by three different methods:

i) heating at 80^0 C

ii) heating at 140^0 C, and

iii) UV exposure.

Only samples heated at 140^0 C yielded a liquid exudate after approximately 300 hours exposure. Samples exposed to UV and 80^0 C did not decompose to form a polymeric liquid even after 3000 hour exposure times; indicating that acrylate-cured materials are more stable than TBHP-cured samples, but less stable than LPs cured with MnO_2 or $NaBO_3$.

Samples of the liquids obtained after exposure to 140^0 C were taken at various time intervals throughout the experiment and examined using ESI-MS, IR, GPC, ^1H and ^{13}C NMR.

The ESI-MS spectrum of Model A reacted with HDDA is illustrated in fig.3.12, (section 3.8); it is more complex than that obtained for pre-polymer Model A, (fig.3.4 section 3.1), with an additional series appearing in the spectrum attributable to the monoadduct of HDDA with the LP.

ESI-MS spectra obtained for samples exposed to 140^0 C for up to 860 hours are extremely complex and therefore difficult to analyse fully. The most prominent features in these spectra are the presence of the original A and B series (see section 3.8, fig.3.12), the appearance of new series at masses corresponding to the A and B

series less 14 amu, and series A -30 amu and series A-2 amu are also prominent. Other new peaks are hard to identify due to the complex nature of these spectra.

The IR spectra obtained for these exudates showed the development of a broad band in the O-H region and a large C=O peak at 1729 cm^{-1}. There is no peak at $\approx$ 2560 cm^{-1} which would indicate the regeneration of thiol (SH). GPC analysis of the exudates proved to be uninformative.

^{1}H NMR spectra show no evidence for the development of thiol since no triplet is present at $\approx$ 1.56 ppm. There is also no development of a peak at $\approx$ 8 ppm which would relate to production of formate ester.^{13}C NMR spectra showed the appearance of two new peaks at approximately 41 and 61 ppm. There is no peak development at $\approx$ 160 ppm which would relate to carbonyl formation and no peak at $\approx$ 24.5 ppm which would have indicated the regeneration of thiol end groups.

These results indicate the same hydrolysis route occurs in HDDA cured-LP samples degraded at 140^{0} C as in TBHP-cured samples, sections 7.1-7.4, and discussed in detail for pre-polymers in sections 5.8 and 5.9.

Another sample of pre-polymer Model A cured using HDDA was prepared with the addition of $\approx$ 7% carbon black. This sample was exposed to 140^{0} C for over 2000 hours but no liquid exudate was formed. Adding carbon black to this system therefore appears to inhibit the hydrolysis mechanism.

An additional sample using the pre-polymer ZL-2264 was cured using HDDA, but even after exposure to 140^{0} C for over 2000 hours no liquid exudate was formed. This confirms the hydrolysis mechanism which depends on the presence of the formal linkage in the polymer chain as the initial site of hydrolysis to produce free formaldehyde, which then further attacks disulfide linkages. This mechanism is

described for exudate samples in section 7.1 and discussed in detail for pre-polymers in sections 5.8 and 5.9.

'H' block samples were prepared as described in section 2.3.4 using the purified pre-polymer, Model A, and HDDA; these were then degraded by the three methods described previously. None of these 'H' block samples produced a polymeric liquid even after 3000 hours exposure, indicating that HDDA-cured LP 'H' block samples are relatively more stable than those cured using TBHP.

7.7 DISCUSSION AND CONCLUSIONS

The liquid formed when TBHP-cured LP samples are exposed to prolonged periods of UV irradiation or heat is a result of the hydrolysis mechanism described in sections 5.8 and 5.9 for pre-polymer samples, and not a simple depolymerisation reaction since there is no evidence for thiol end groups in either the IR or NMR spectra of these exudates. This degradation route involves the initial cleavage of the formal group to release formaldehyde, followed by secondary reactions to form products identified in the ESI-MS spectra of these exudates. The development of ^{13}C NMR peaks due to $S\underline{C}H_2CH_2OH$ and $SCH_2\underline{C}H_2OH$ at 41 and 60 ppm provides support for the hydrolysis mechanism.

Further evidence for this hydrolysis mechanism being the principal route of degradation in these TBHP-cured samples comes from samples prepared using ZL-2264, (which has no formal link in its chain), when <u>no</u> liquid exudate developed even after extensive exposure times. Also, exudates could not be re-cured using MnO_2, confirming that SH end groups are no longer present.

Since carbonyl bands at ≈ 1724 cm^{-1} are present in the IR spectra of these exudates, there also appears to be a competing free radical autoxidation mechanism occurring, but this is much less significant. This autoxidation pathway is common to many polymer degradation studies, the closest analogies being those of poly(propylene oxide)[3-5] and poly(ethylene oxide)[4] where attack at C-H adjacent to the ether oxygen atom leads to the formation of hydroperoxide and hence alkoxyl radical, followed by scission to produce a formate ester. Mechanisms for this free radical pathway are illustrated in section 5.9 for pre-polymer degradation.

The addition of the pigment Carbon Black appears to prevent the hydrolysis mechanism, leading to a more thermally and photochemically stable polymer system. The level of TBHP used to cure the LP appears to have no effect on the lifetime of the thermal stability of the LP, but a lower level of TBHP appears to lead to improved photostability.

TBHP-cured LPs in contact with glass, i.e. 'H' block samples, also appear to degrade principally via the hydrolysis route to yield a liquid exudate at the centre of the polymer block just below the glass/polymer interface.

HDDA-cured LP samples appear to be more stable than those samples cured using TBHP. Acrylate samples do undergo the same hydrolytic degradation mechanism as that described for TBHP samples in section 7.1 and for pre-polymers in sections 5.8 and 5.9. Carbon Black appeared to stabilise the material against this hydrolysis mechanism.

LP samples cured using MnO_2 and $NaBO_3$ as curative agents are more resilient to exposure to heat and UV. The principal route of degradation in these samples, according to the results of thin film studies described in chapter 6, appears

to be that of free radical autoxidation as described in section 5.9 for pre-polymer samples. The hydrolysis pathways appears to be inhibited by the addition of these curatives.

The results of this chapter indicate that two degradation mechanisms occur in LPs, and the nature of the curative used determines the principal pathway. The hydrolysis mechanism is clearly the most significant for TBHP-cured samples, leading to the formation of a polymeric liquid after extensive exposure to heat or UV, and this mechanism was also found to be dominant in the degradation of pre-polymers, see section 5.9. However, in MnO_2- and $NaBO_3$- cured samples the free radical autoxidation mechanism is dominant.

We have incorporated a wide range of analytical techniques to understand fully the phenomenon of the appearance of these liquid exudates since the degradation pathways of polysulfides are extremely rich and diverse. The origin of these liquid exudates appears to be hydrolysis, which agrees with the findings of Berenbaum and Rosenthal[1] in their thermal degradation study and our own results for degradation of pre-polymers described in chapter 5.

CHAPTER 7

REFERENCES

1. Rosenthal, N.A., Berenbaum M.B., *Thermal Degradation of Ethyl Formal Polysulfide Polymers.* In-house report for Thiokol Chemical Corporation

2. Scrivens, G., D.Phil. thesis, *An EPR Investigation into the Catalytic Oxidation of Thiols by Peroxides,* University of York, (1995).

3. Griffiths, P.J.F., Hughes, J.H., Park, G.S., *Eur. Polym. J,* **29**, (1993) 437.

4. Lemaire, J., Gauvin, P., Sallet, D., *Makromol. Chem,* **188**, (1987) 1815.

5. Barton, Z., Kemp. T.J., Buzy, A., Jennings, K.R., *Polymer,* **36**, (1995) 4927.

CHAPTER 8

PHOTODEGRADATION OF POLYSULFIDE POLYMERS AT THEIR INTERFACE WITH GLASS

8.1 X-RAY PHOTOELECTRON SPECTROSCOPY (XPS) OF THE SURFACES OF A RUPTURED LP-GLASS SEAL

Two 'H-Block' samples consisting of an MnO_2-cured LP construction sealant, (see section 2.3.4 and 2.3.5 for formulation and preparation), in contact with window quality glass were prepared. One sample was used as a control, while the other was UV-irradiated until the interfacial surface developed a conspicuous yellowish zone. The seals were ruptured following immersion in liquid nitrogen and the following surfaces were prepared to be analysed using XPS:

(i) A fresh glass surface as a control.

(ii) Glass surface ruptured from exposed polymer.

(iii) Unexposed polymer surface ruptured from glass.

(iv) Unexposed polymer surface from centre of bond.

Over the last two decades XPS has become an established technique for characterising the surface of polymers.[1-7] The physical basis of XPS is the interaction of a beam of x-rays (normally $Al(K_\alpha)$ or $Mg(K_\alpha)$) with a solid sample. The kinetic energy, (E_k), at which the photo-electrons leave the atom is measured using an electron energy analyser, which together with the sample and photon source is contained within an ultra high vacuum chamber.[7-9]

The characteristic binding energy (E_B) of the electron is a function of the energy level and chemical state of the element involved, and is related to the outgoing electron kinetic energy and the photon energy involved, (hν):[7-9]

$$E_B = h\nu - E_k$$

Electrons within the energy range 10 to 1500 eV travelling through a solid have a very high probability of suffering inelastic collisions and hence energy losses. Ionisation usually occurs to a depth of a few micrometers, but only electrons that originate at the surface can leave the sample without energy loss. Consequently excited electrons can escape only from a short distance beneath the surface, (2 nm or less) and the technique is accepted widely as a surface chemistry method as far as solids are concerned.[7-9]

A sample of the surface of the glass we are utilising gave the XPS spectrum shown in fig.8.1, from which characteristic electron energies can be observed from the 1s orbitals of Na, O, C, the 2p orbitals of Si, Ca, K, the 2s orbital of Si and the 3d orbital of Sn. A minor peak observed may be due to trace amounts of Cd(3d). Auger electron peaks were also found due to carbon and oxygen.

A technical complication which arose was that the glass surface, which is highly insulating, rapidly built up a positive charge, which has the effect of shifting the measured characteristic electron energies to lower values. To overcome this effect, electrons of low energy, i.e less than 100 eV, were fired at the surface to neutralise the accumulating positive charge and restore the peaks to their expected values. This 'electron flooding' brings its own problems, however, in so far as it inevitably results in the deposition of carbon on the sample surface and the consequent appearance of a

large signal due to C(1s). The amplitude of this signal thus has the effect of rendering all other signals relatively weak, even to vanishing point, see fig. 8.2.

A glass surface ruptured from a polymer-glass seal following UV-irradiation, which presents a yellow-brown aspect attributable to residual adhering degraded polymer, gave the XPS spectrum shown in fig. 8.3.

Fig. 8.1: XPS spectrum of a virgin glass surface.

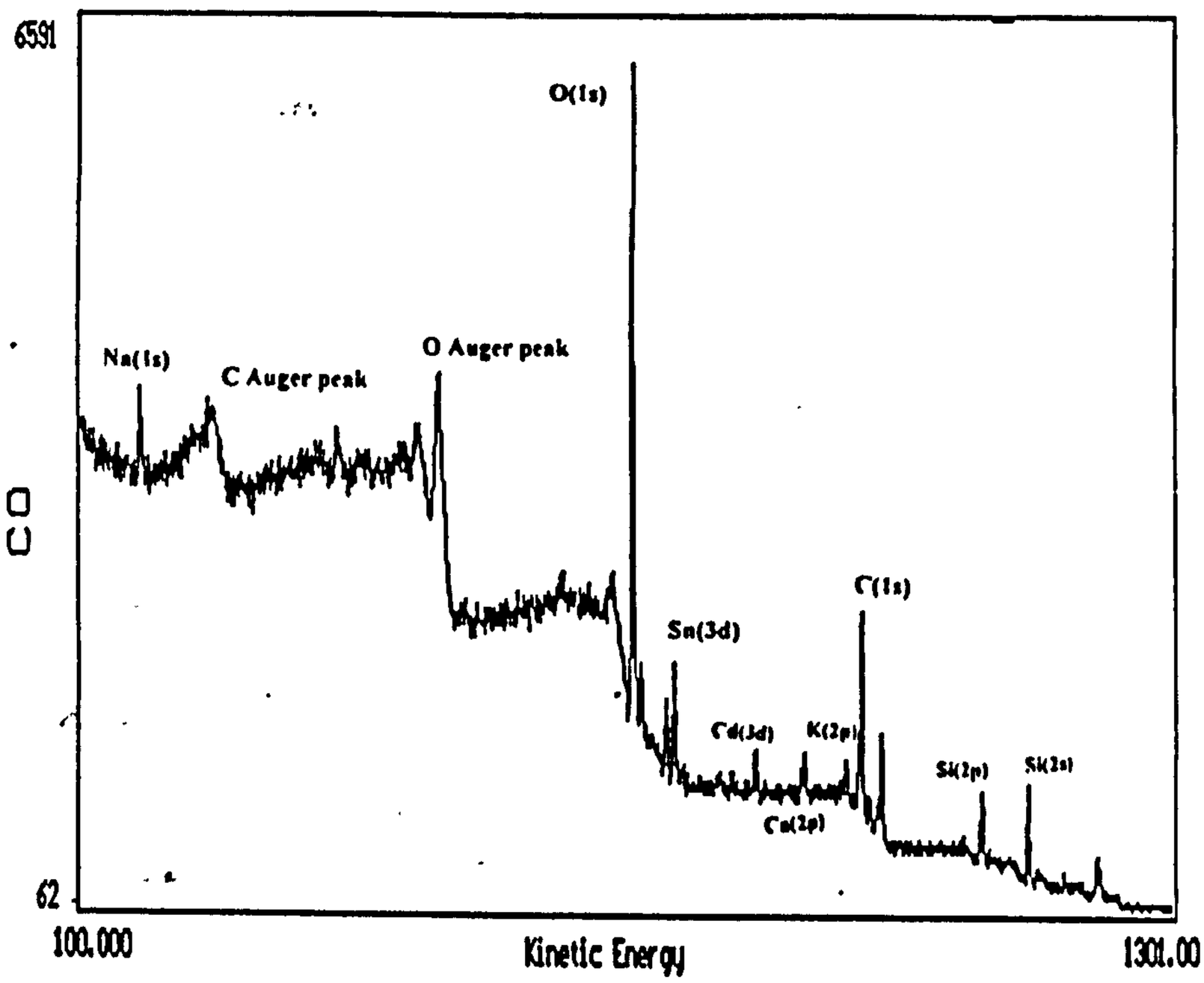

Fig. 8.2: XPS spectrum of a virgin glass surface after bombardment with low energy electrons.

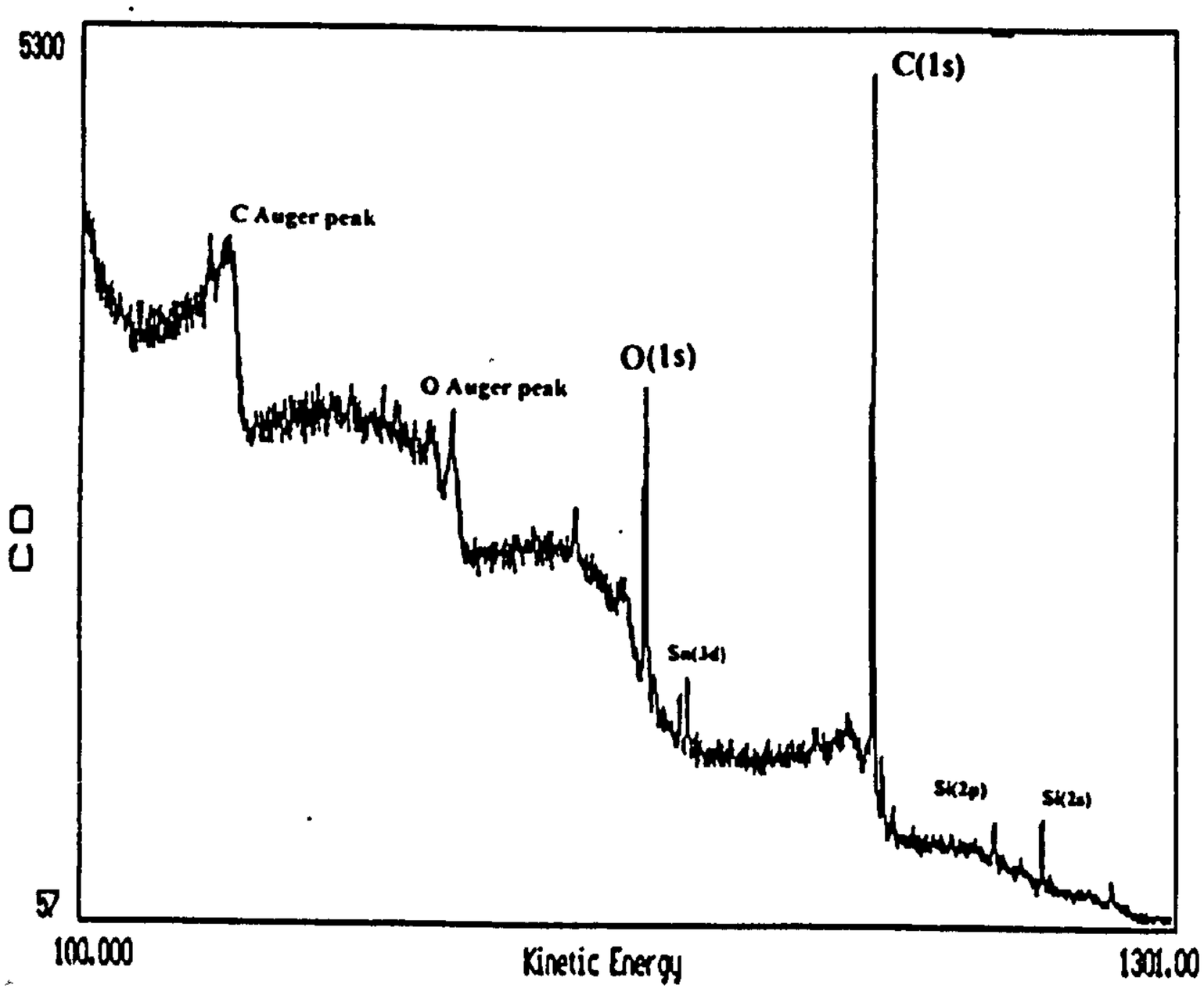

Fig. 8.3: XPS spectrum of a glass surface ruptured from exposed polymer.

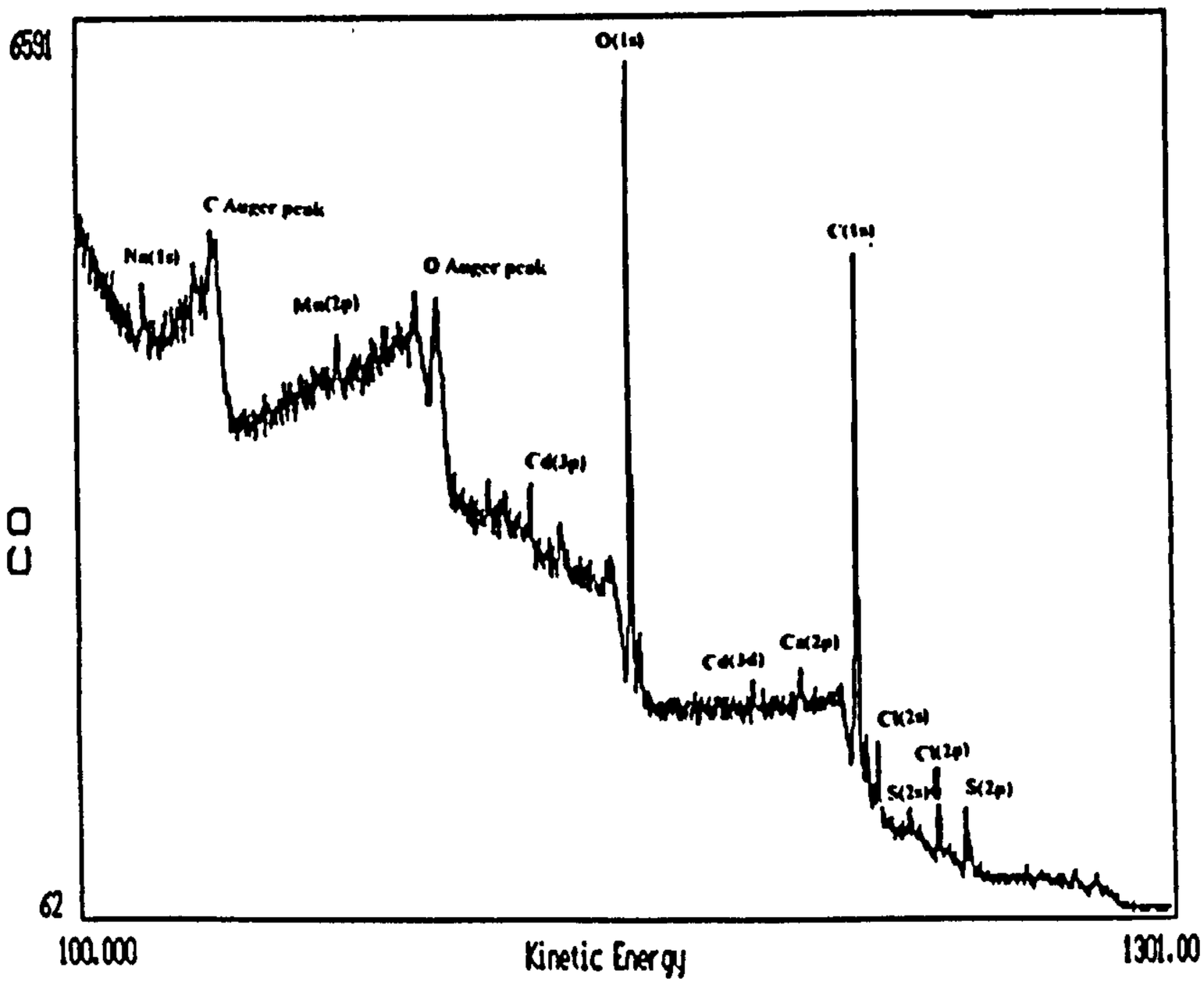

The principal peaks are due to: C(1s), O(1s), Na(1s), Cl(2s,2p), and S(2p). Minor peaks are also attributable to Mn(2p), S(2s) Ca(2p) and possibly Cd(3d,3p). Evidently, Si(2p,2s) peaks are not observed and the Na(1s) peak is much reduced; both these peaks are expected from clean glass. However, peaks typical of the polymer such as S(2s), Cl(2s) and Mn(2p) have emerged instead.

Polymer sample (iii), which was <u>not</u> exposed to UV-irradiation but simply ruptured from its seal with glass, is also highly insulating and gave the spectrum shown in fig. 8.4, which features electron peaks due to: C(1s), O(1s), Na(1s), Cl(2s,2p), S(2s,2p), Ca(2p), Mn(2p) and possibly Sn(3d). Auger peaks are due to carbon and oxygen.

Fig. 8.4: XPS spectrum of an unexposed polymer surface ruptured from glass.

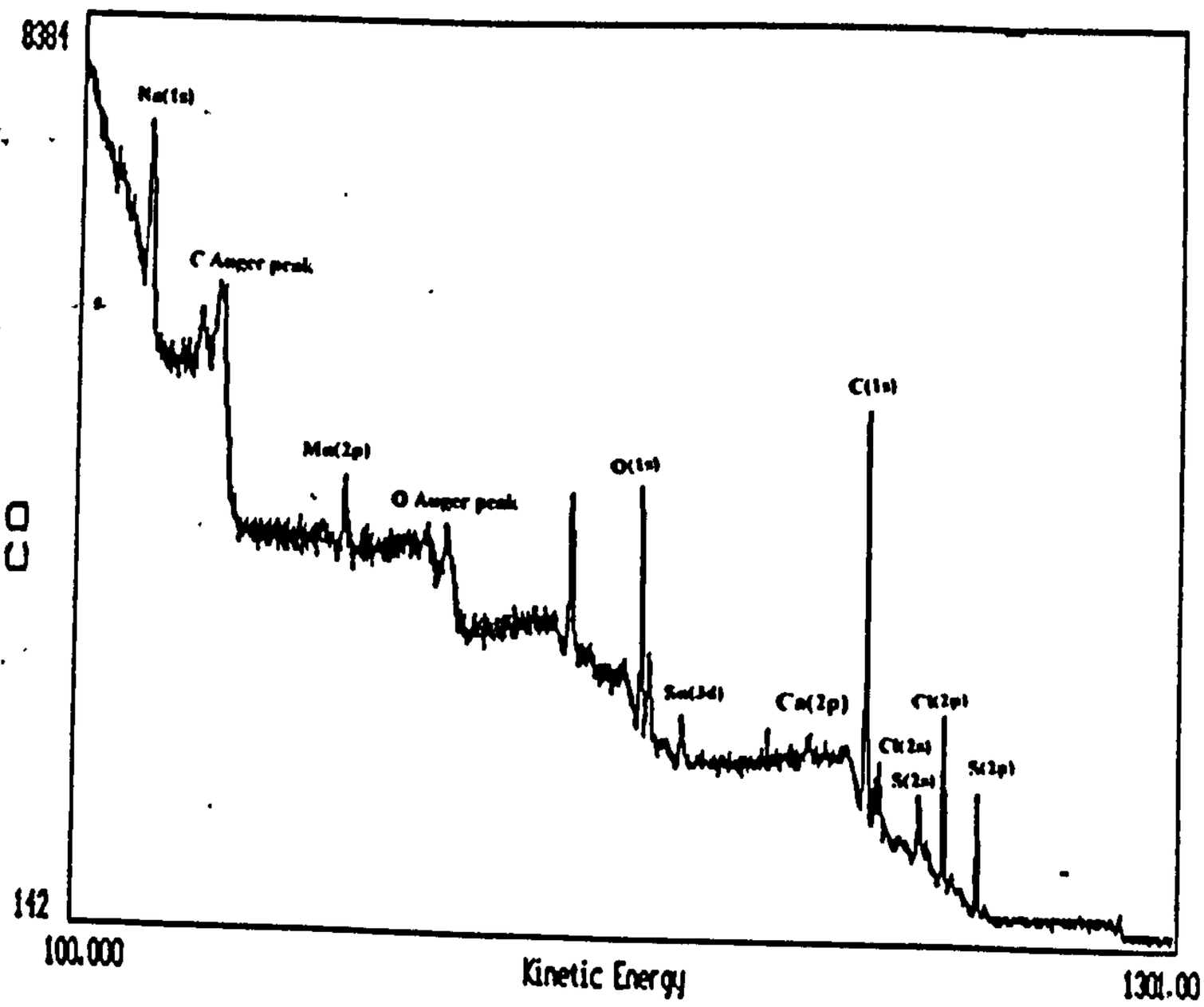

We experienced technical problems with this sample due to slow outgassing; because the polymer had a relatively high vapour pressure, the vacuum could not be reduced below 10^{-7} millibar, (which is the operational limit of the x-ray gun and analyser).

A slow scan of the C(1s) peak, see fig. 8.5, revealed only a single broad peak with no substructure. It seems that for these types of polymer sample the resolution of any chemical shift within the C(1s) range is going to be almost impossible using this type of instrument. This is associated with the build-up of positive charge during the XPS experiments, and also the radiation damage to the polymer, which make the precise measurements associated with shifts very difficult.

Polymer sample (iv), a freshly cut section of unexposed polymer, which was remote from the glass interface and is typical of the bulk of the polymer, gave the XPS spectrum shown in fig. 8.6. This shows all the peaks described for sample (iii) and also one due to F(1s).

Fig. 8.5: XPS spectrum of the C(1s) peak of an unexposed polymer surface ruptured from glass

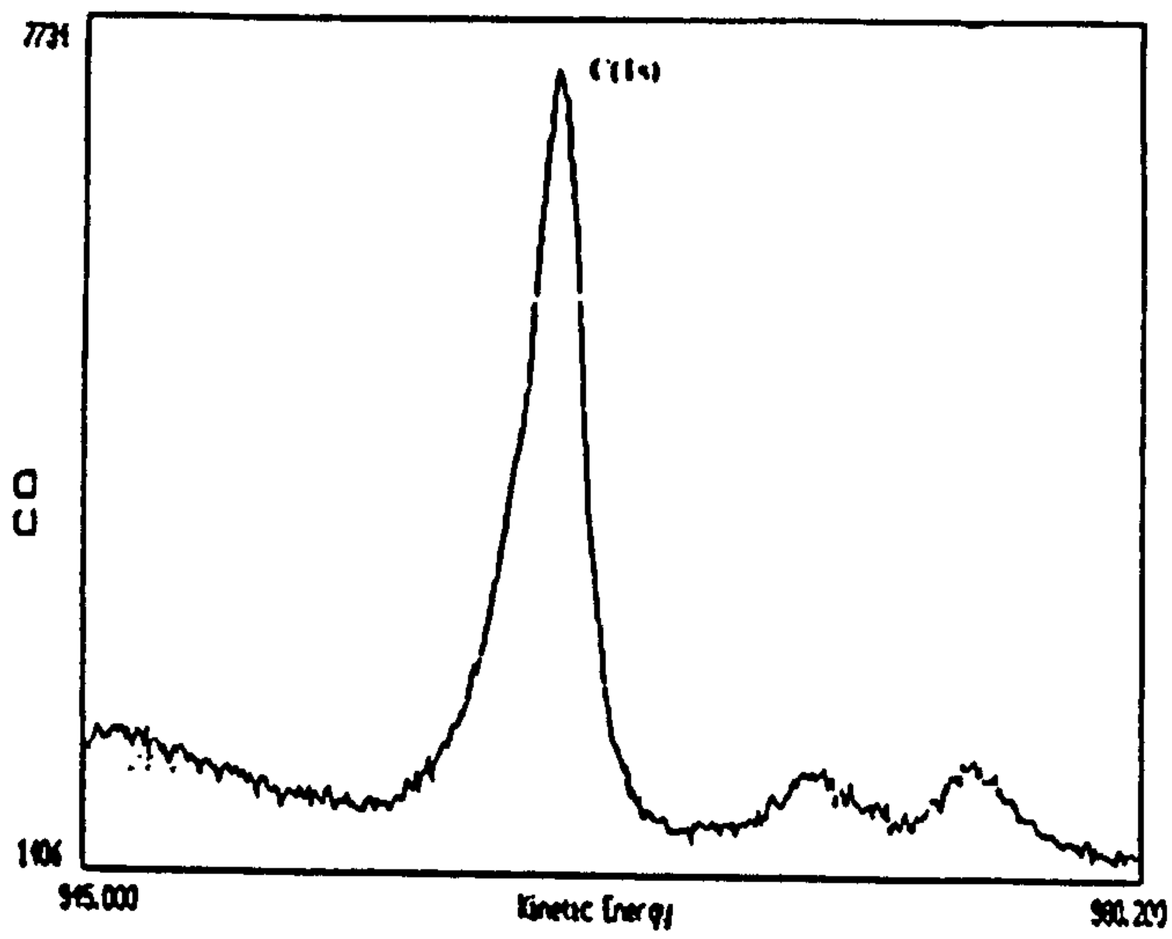

Fig. 8.6: XPS spectrum of an unexposed polymer surface taken from centre of bond.

The origins of the elements identified by XPS are summarised in Table 8.1.

Table 8.1: Origins of elements identified in XPS spectra of cured LP-glass interfaces following rupture.

Sample	Element	Origin
Glass sample ruptured from exposed polymer surface.	Carbon	Present in glass and in polymer backbone.
	Oxygen	Present in glass and in polymer backbone.
	Sodium	Present in glass.
	Calcium	Present in glass and from $CaCO_3$ filler used in sealant.
	Cadmium ?	Present in glass.
	Manganese	From MnO_2 curing agent used in sealant.
	Chlorine	From plasticiser (Cereclor 63-L)
	Sulfur	From polymer backbone.
Unexposed polymer ruptured from glass.	Carbon	Present in glass and polymer backbone.
	Oxygen	Present in glass and polymer backbone.
	Sodium	Present in glass and possible impurities in sealant.
	Chlorine	From plasticiser (Cereclor 63-L)
	Sulfur	Present in polymer backbone.
	Calcium	Present in glass and from $CaCO_3$ filler used in sealant.
	Manganese	From MnO_2 curing agent used in sealant.
	Tin	Present in glass.
Unexposed polymer surface from centre of bond.	Carbon	From polymer backbone.
	Oxygen	From polymer backbone.
	Sodium	Possibly from impurities in LP (since sodium salts are used in manufacture) or impurities in $CaCO_3$ filler.
	Calcium	From $CaCO_3$ filler used in sealant.
	Chlorine	From plasticiser (Cereclor 63-L)
	Sulfur	From polymer backbone.
	Manganese	From MnO_2 curing agent used in sealant.
	Fluorine	From fluorinated release agent used in sealant.

8.2 FTIR-ATR STUDY OF THE POLYMER SURFACE OF RUPTURED MnO_2-CURED POLYSULFIDE GLASS BONDS.

Extended photolysis of 'H-Blocks' of two sections of glass plate bonded together by a 12 mm thick layer of MnO_2-cured LP led to a readily fractured assembly, (when the adhesion promoter A187, was omitted). After the polymer-glass bond was broken, an IR spectrum of the surface was taken using attenuated total reflectance, (ATR), spectroscopy.

Comparative samples were run of unexposed material, the LP block surfaces "near" and "remote" from the light source and also a section midway across the block, (which had experienced no illumination whatsoever).

The main points to emerge from these preliminary studies are:-

i) that the fracture of the polymer-glass bond is <u>not</u> associated with the development of C=O groups.

ii) there are signs of the progressive development of a weak broad band at ≈ 1600 cm^{-1} as the seal undergoes exposure. This feature is also present, but to a reduced extent in some of the blank samples. The species most probably responsible for this peak is a formate ion; sodium formate has its very broad carbonyl band at 1580 cm^{-1}, while Lemaire et al. assigned formate ions at 1605 cm^{-1}.

A similar band is present in the LPs themselves and in the adhesion promoter, A187, which was not present in the test samples illustrated in the figures 8.7, 8.8 and 8.9.

Fig. 8.7: FTIR-ATR spectra of MnO_2-cured LP-977C surface after a) 286 hours and b) 929 hours in dark.

A)

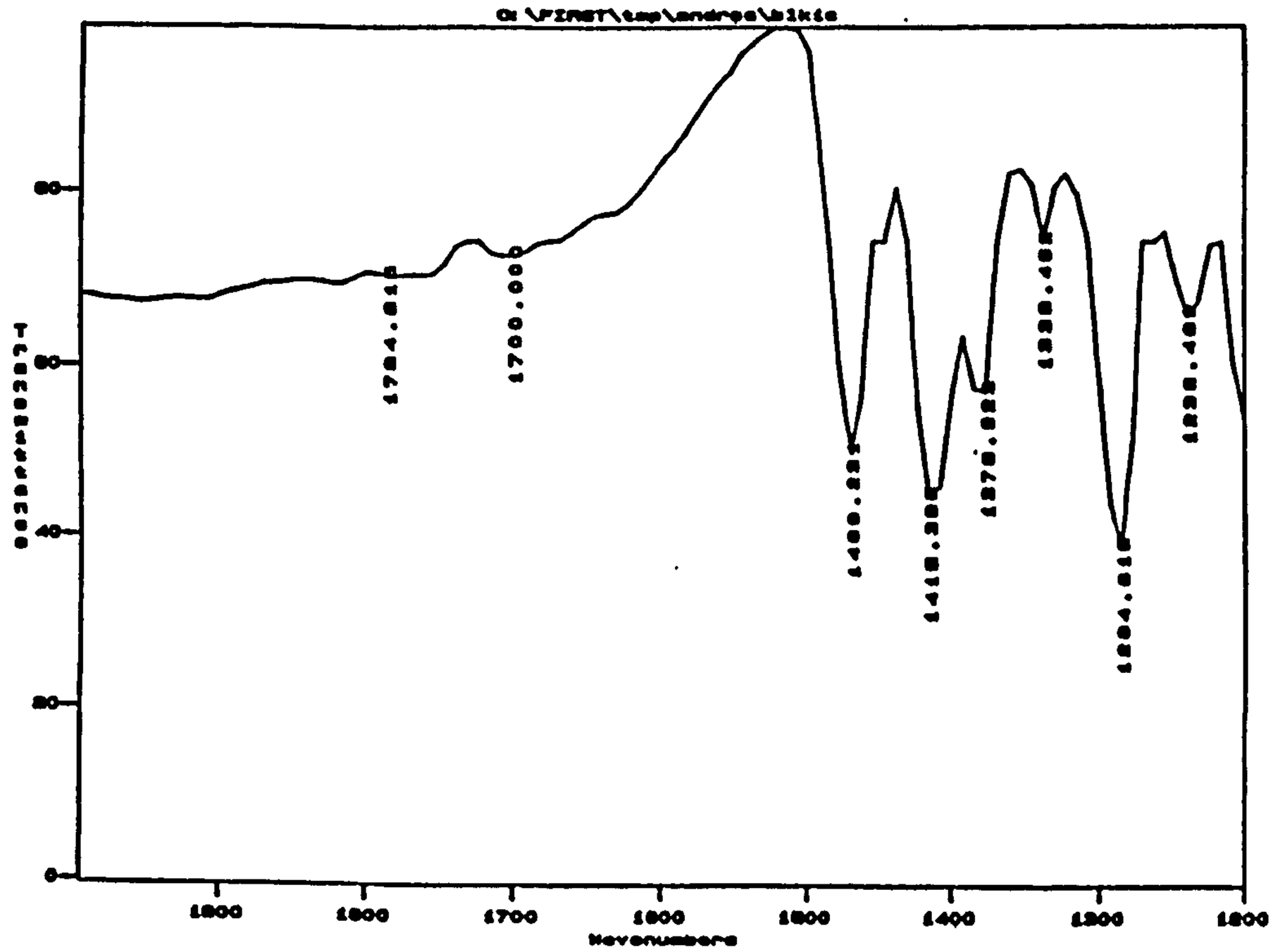

B)

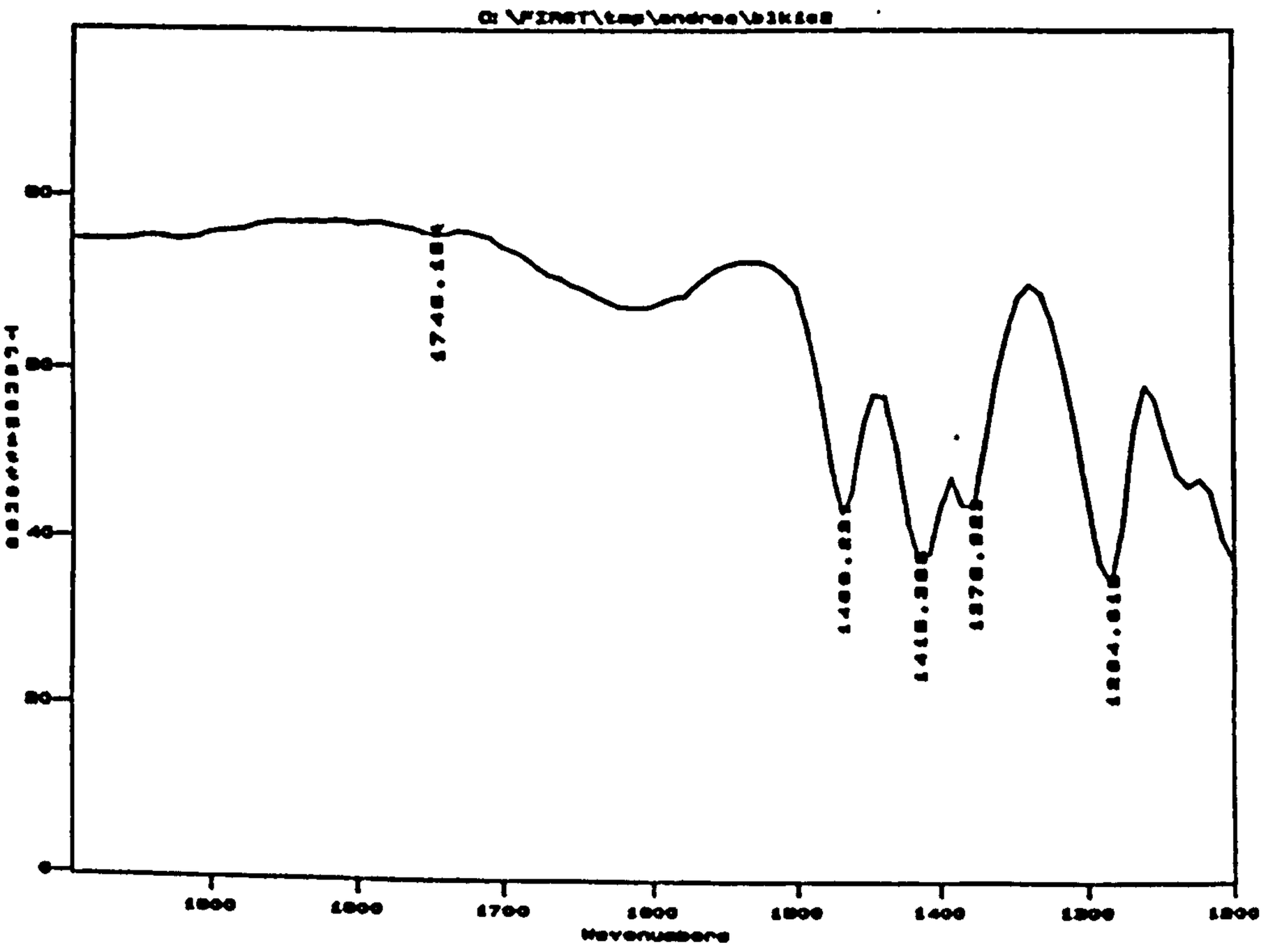

Fig. 8.8: FTIR-ATR spectra of MnO_2-cured LP-977C 'near' polymer surface after a) 286 hours and b) 929 hours exposed to UV irradiation.

A)

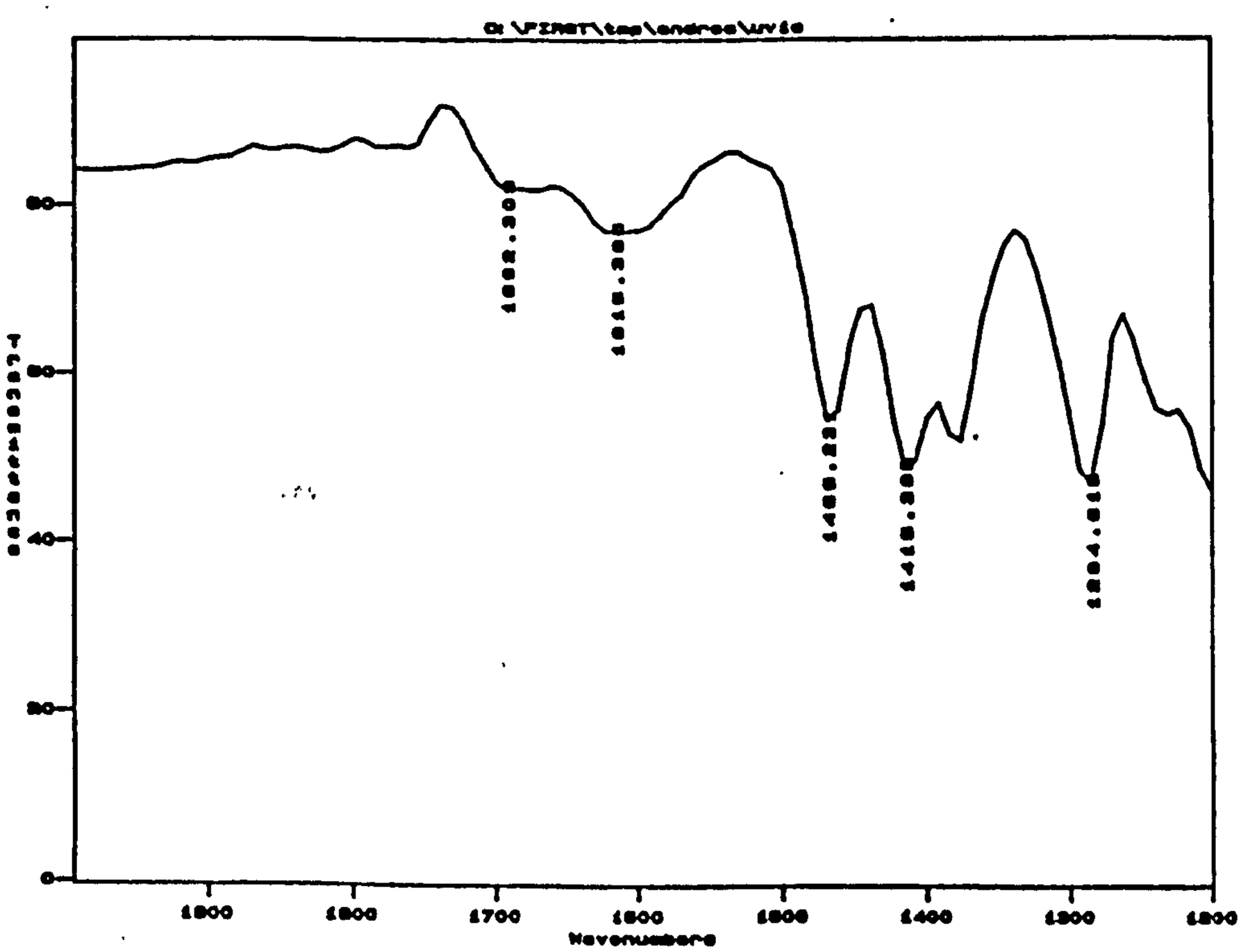

B)

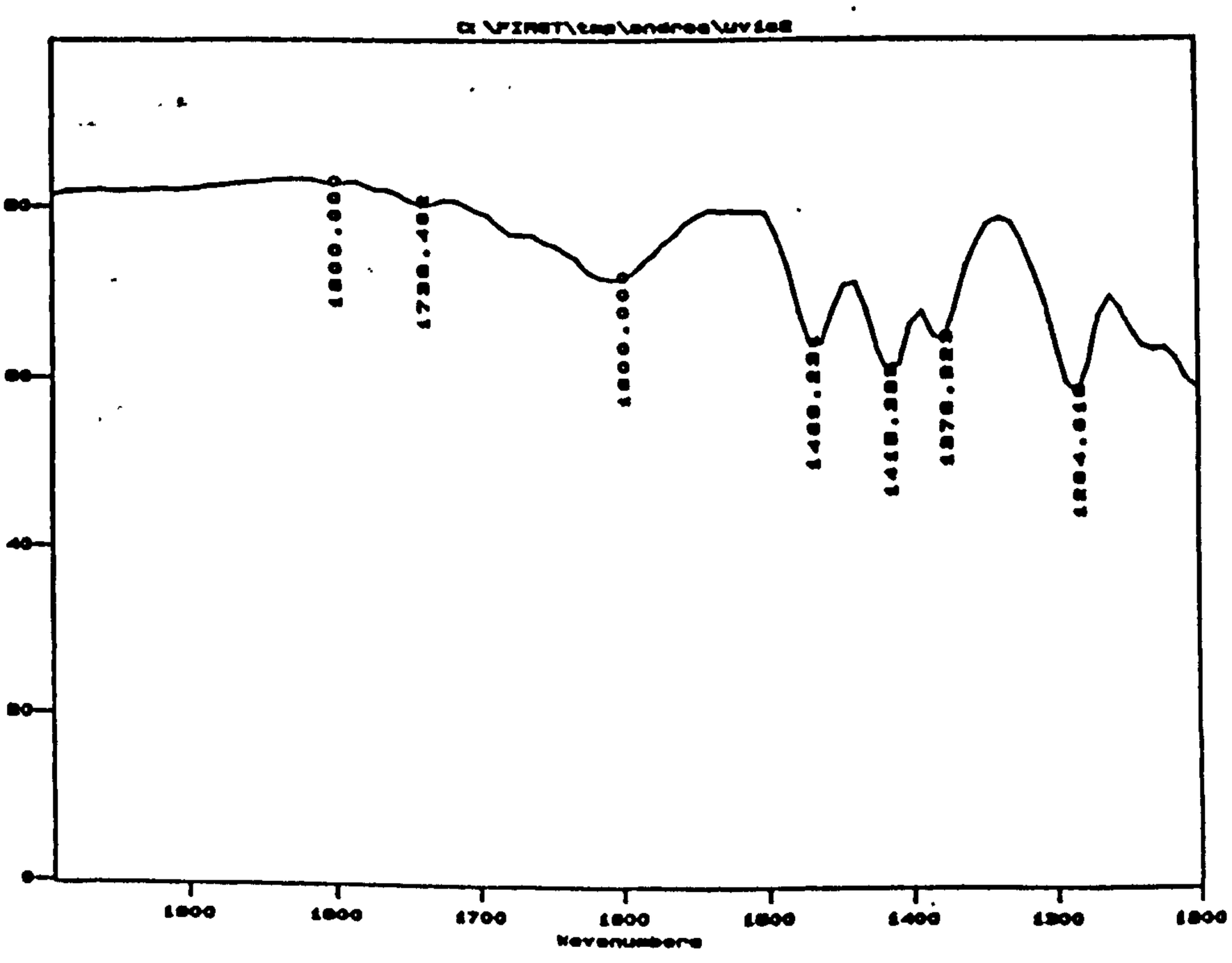

Fig. 8.9: FTIR-ATR spectra of MnO_2-cured LP-977C 'remote' polymer surface after a) 286 hours and b) 929 hours exposed to UV irradiation.

A)

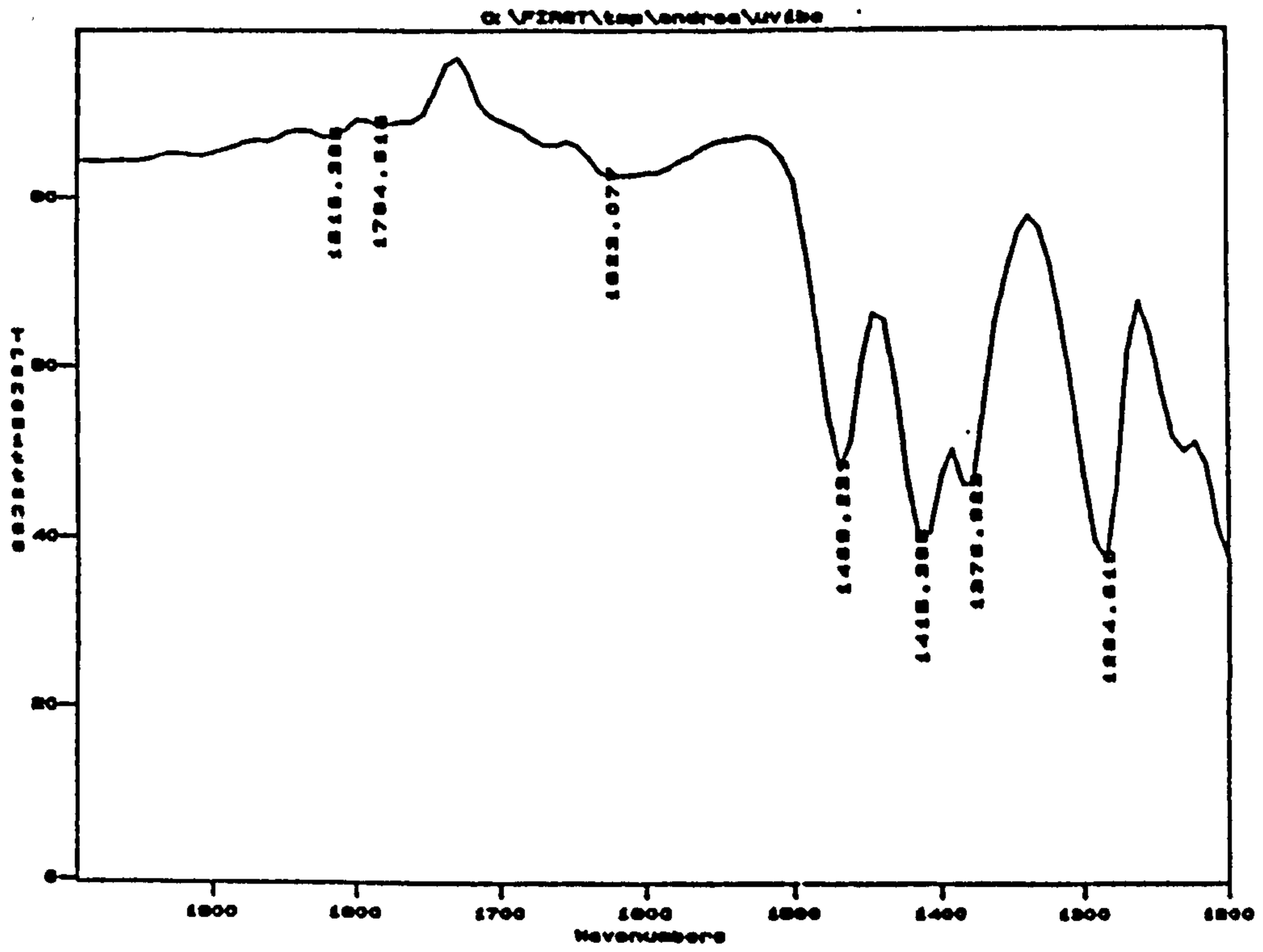

B)

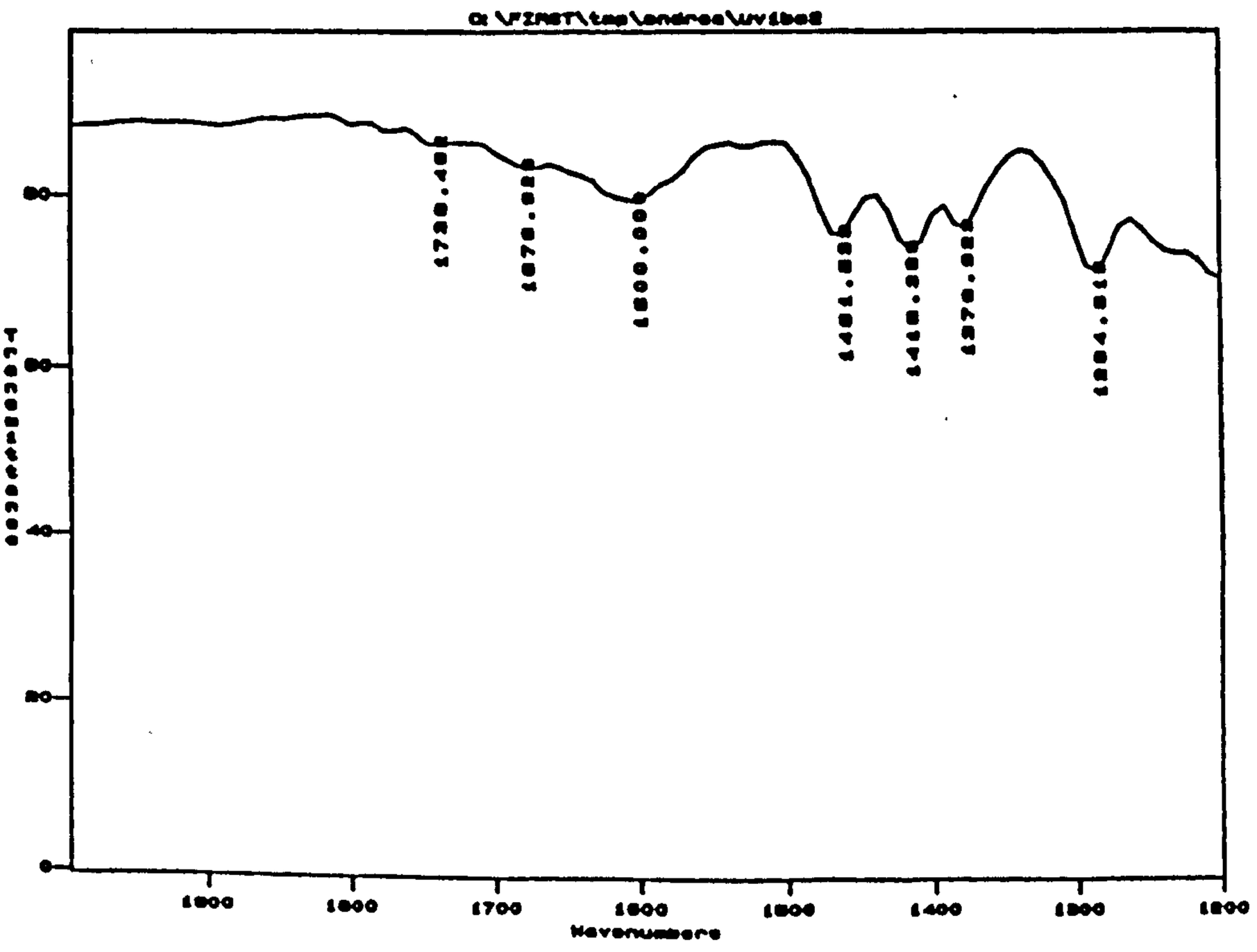

8.3 STATIC SECONDARY ION MASS SPECTROMETRY STUDIES OF LP POLYMER SURFACES.

Preliminary samples consisting of a block of MnO_2-cured LP-32C in contact with glass were prepared. One sample was used as a control, while the others were exposed to UV irradiation in the Sol-2 light box for 237 and 455 hours, when a yellow/ brown discolouration had developed at the polymer/glass interface. The seal was ruptured using liquid nitrogen and the samples were prepared for surface analysis by Static Secondary Ion Mass Spectrometry, also known as SIMS.

The spectra obtained for all three samples were closely similar; each showed a peak at every mass from 13 to 149 mass units, with very similar intensities for both the unexposed and exposed samples. It was therefore impossible to obtain any useful information on the presence of, and change in, functional groups using this technique.

8.4 RAMAN STUDIES OF LP PRE-POLYMERS AND CURED LP SURFACES

Attempts were made using the laser facility at Rutherford Appleton Laboratory to record the Raman spectra of UV-irradiated surfaces of an MnO_2-cured sample of LP-32C, which displayed different levels of intensity in the yellow/brown discolouration that forms during extensive periods of UV exposure. We were unable to obtain suitable spectra from such a surface. However, it was possible to record a Raman spectrum of LP-32C pre-polymer, as shown in fig.8.10, using the 363 nm line from an argon ion laser. The calibrate was toluene. The assignments of the major peaks in the spectrum are shown in table 8.2.

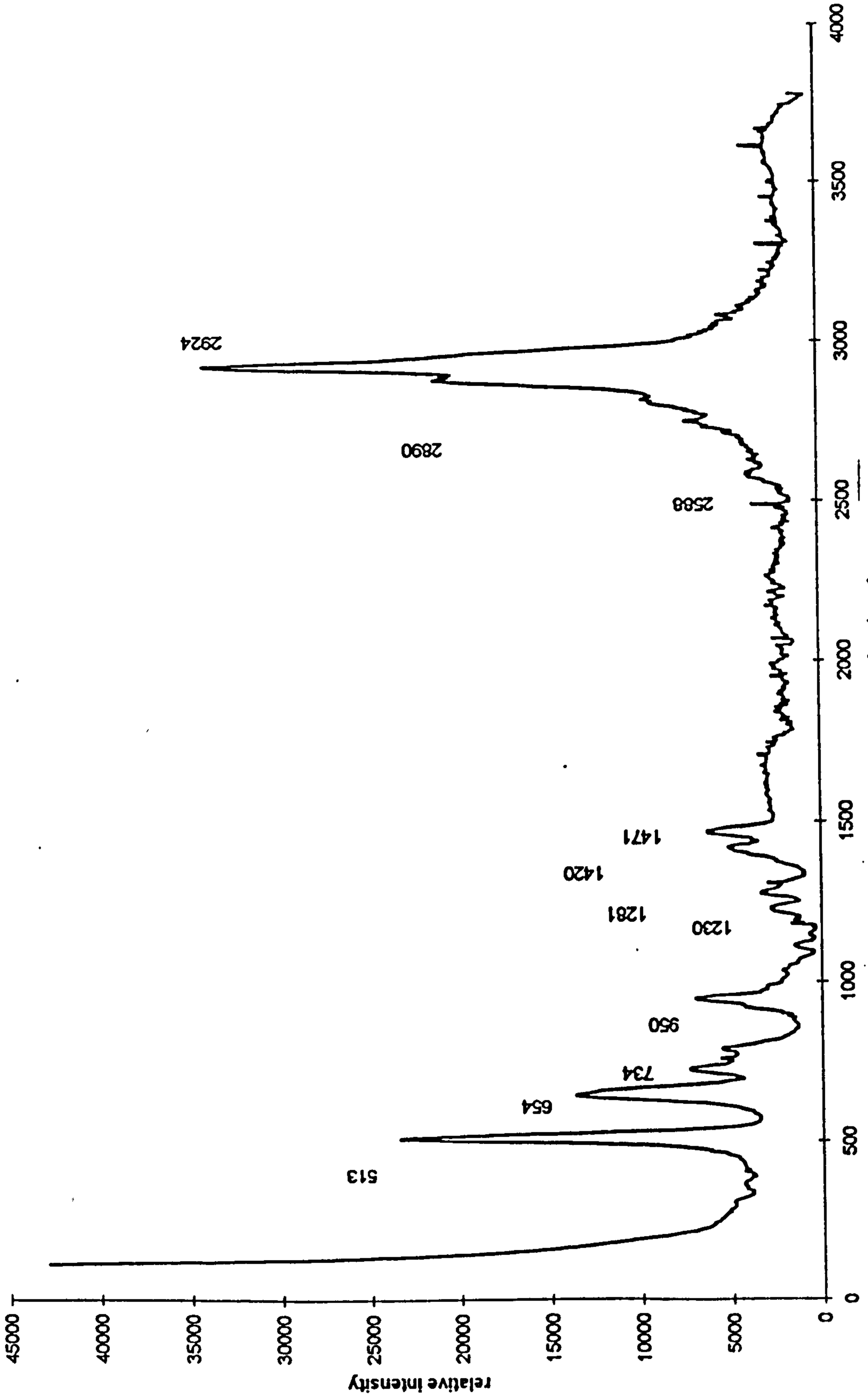

Fig. 8.10: Raman spectrum of LP-32C.

Table 8.2: Assignments of peaks in Raman spectrum of LP-32C.

Frequency / cm^{-1}	Intensity	Assignment
2924 2890	Strong	Asymmetric and symmetric CH_2 stretch. Sharp
2558	Weak	S-H stretch. Sharp.
1471	Medium	CH_2-O, CH_2 scissoring deformation. Sharp.
1420	Medium	CH_2-S, CH_2 stretch. Sharp.
513	Strong	S - S

8.5 EDAX STUDIES OF CURED LP SURFACES

Two samples consisting of a block of MnO_2-cured LP-32C in contact with glass were prepared. One sample was used as a control while the other was UV-irradiated until a yellow/brown discolouration occurred at the glass/polymer interface. The seals were ruptured by immersion in liquid nitrogen and the samples were prepared for analysis on the EDAX instrument at Shipley Ltd., Coventry.

Like the XPS studies summarised in section 8.1, the spectra obtained using EDAX were informative about the presence of elements such as sulfur, carbon and oxygen at the polymer surface, but no details could be obtained on the presence of functional groups or their conversion following UV irradiation.

8.6 ELEMENTAL ANALYSIS BY C H N ANALYSIS.

Samples were submitted for analysis of:

i) LP-32C pre-polymer,

ii) LP-32C after approximately 4800 hours UV_B exposure,

iii) an unexposed MnO_2-cured LP surface and

iv) MnO_2-cured LP surface after approximately 1000 hours UV exposure, showing a strong yellow-brown discolouration.

The analysis obtained for each sample is given in table 8.3:

Table 8.3: Elemental analysis of LP samples.

Sample	**LP-32C**	**LP-32C after 4800 h UV_B**	**MnO_2-cured LP-32C (unexposed surface)**	**MnO_2-cured LP-32C (surface exposed to UV.)**
Carbon %	36.85	36.68	33.95	33.52
Hydrogen %	6.16	6.13	5.70	5.47

From the results obtained, the elemental analysis of the pre-polymer samples appear to be almost unchanged after extensive UV_B exposure. The elemental composition of the unexposed and exposed polymer surfaces also appears to remain largely unchanged, with some slight loss of C and H (presumably as volatiles or gases). It appears therefore the surface discolouration, which is visibly apparent in the exposed sample, is not due to the migration to, or formation of inorganic complexes at the surface, which remains largely organic.

8.7 ATTEMPTED LEACHING OF MnO_2-CURED LP SURFACES

Unexposed and UV-exposed 'H' block samples of MnO_2-cured LP-32C were taken and sliced into thin layers, using a clean scalpel blade. These slices of polymer were leached for long periods of time, (up to one week), in solvents such as chloroform, THF and chloroform-d. GPC, ^{1}H NMR and FTIR analyses were then performed on these solutions.

The GPC analysis of these leached surfaces was relatively uninformative with all solutions showing a similar RMMD. The ^{1}H NMR analysis produced identical spectra independent of whether the solution was leached from an exposed or unexposed block, or the relative position within the block, i.e. the polymer at the glass surface showed the same peaks as the polymer sample taken from the centre of the bond. As with the experiment of leaching cured films, see section 6.22, it is possible that leaching failed to produce sufficient dissolved material to enable a search to be made for the 8 ppm peak assigned to the formation of formate ester under prolonged UV exposure.

FTIR analysis of chloroform-leached solutions was relatively more successful, with the appearance of a carbonyl band at 1723 cm^{-1} found in the surface layer of the UV-exposed sample. This development of a carbonyl group at a UV-exposed polysulfide/glass surface indicates that the surface reaction is due to the same degradation pathway as that leading to carbonyl group formation in the pre-polymer samples, i.e. a free radical route leading to the formation of formate ester. A detailed mechanism for this reaction is given in section 5.9.

8.8 STUDY OF YELLOW DISCOLOURATION AT EXPOSED POLYMER/GLASS INTERFACE BY FTIR

A UV-irradiated 'H' block of MnO_2-cured LP-32C was taken and the seal was ruptured by immersion in liquid nitrogen; the yellow/brown layer where discolouration had occurred, was carefully sliced away using a clean scalpel blade. This layer was then placed onto a cardboard mount and a thin-film FTIR spectrum was obtained, see fig. 8.11. This spectrum clearly shows the development of a broad band in the OH region and the development of carbonyl bands at 1723 cm^{-1} and 1688 cm^{-1}, and a broader band around 1600 cm^{-1}.

This result is quite surprising since detailed analysis of surfaces by ATR-FTIR, see section 8.2, did not show the development of carbonyl frequencies at 1723 cm^{-1} and 1688 cm^{-1}, but was only able to detect the broad band at 1600 cm^{-1}.

The band seen at 1723 cm^{-1} is again most likely to be due to the development of formate ester at the polymer/glass interface by a free radical mechanism, see section 5.9. Leaching this thin surface layer in $CDCl_3$, followed by ^1H NMR analysis on the resulting solution was unsuccessful in assisting detection of the 8 ppm peak which would have confirmed the assignment to a formate ester.

8.9 TENSILE TESTING OF MnO_2-CURED LP-32C SAMPLES EXPOSED TO UV RADIATION WITH VARIOUS LEVELS OF ADHESION PROMOTER.

When adhesion promoter, A187 was omitted from 'H' block samples, it was observed that after prolonged UV exposure at the polymer/glass interface, the polymer would strongly adhere to the glass, while those bonds containing A187

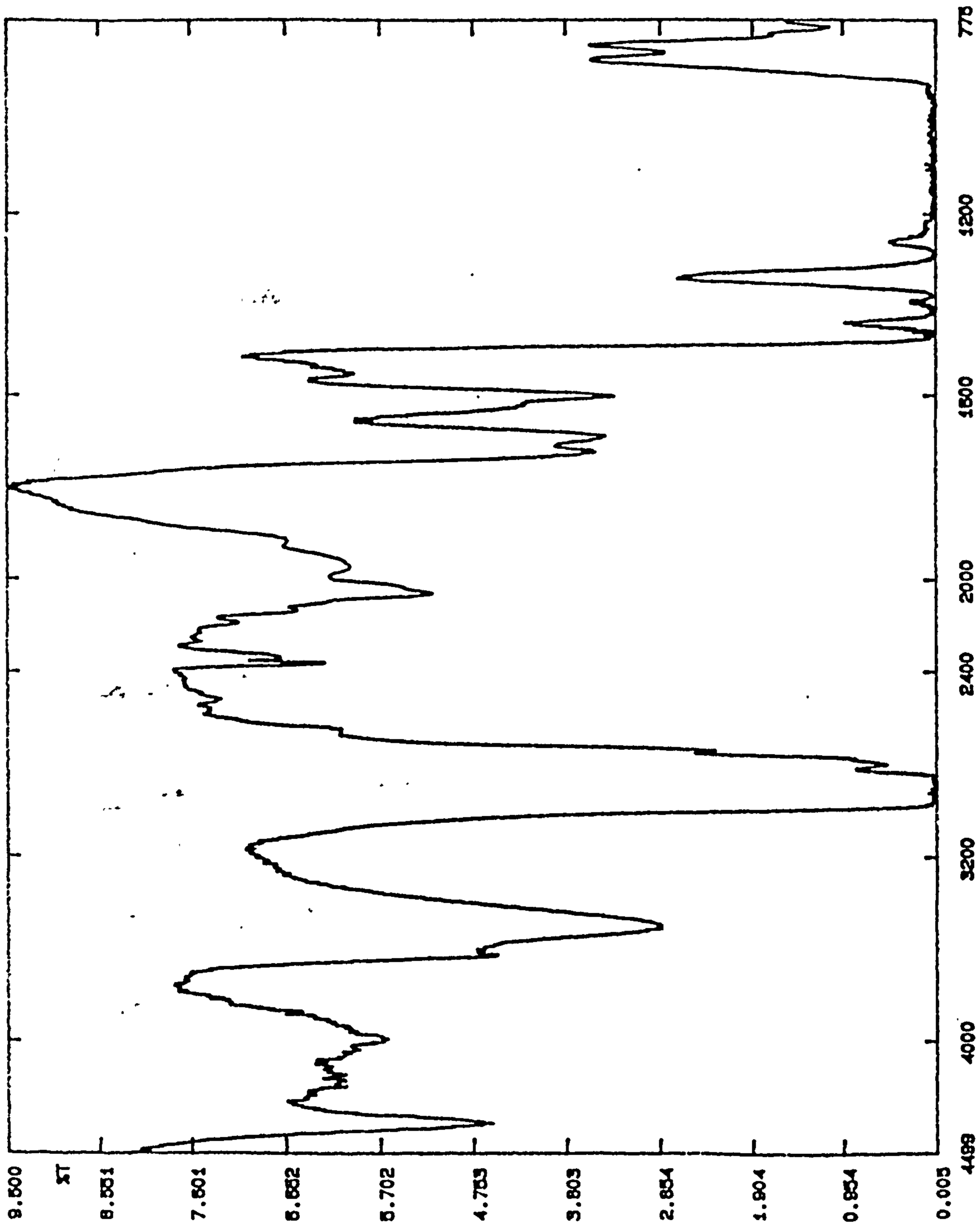

Fig. 8.11: IR spectrum of yellow/brown discolouration.

would often lose adhesion at the edges of the seal. An experiment was therefore conducted in which a range of 'H' block samples were prepared using different levels of adhesion promoter, i.e. 0, 1 and 3 phr. The tensile strengths in Newtons of the resulting bonds before exposure were then obtained for each sample.

The samples were then exposed to UV irradiation, and samples were removed at various periods of time throughout the experiment. The strength of the bond "remote" from the exposed side was firstly obtained for all three levels of adhesion promoter using the tensile tester at Morton International Laboratories. The glass on the remote side was then readhered to the polymer using Araldite, and allowed to set for 1 hour. The samples were then re-pulled on the tensile tester to obtain the tensile strengths of the UV-exposed bonds. The results obtained for these experiment are summarised in graphs in figs. 8.12, 8.13 and 8.14.

From the graphs it can clearly be concluded that improved adhesion occurs in the sample in the absence of adhesion promoter after prolonged UV-exposure; it appears therefore that UV exposure actually improves the adhesion of the polymer to the glass.

The samples with adhesion promoter present initially show a loss in adhesion properties with exposure to UV, but after around 1000 hours the samples show an increase in bond strength; the samples with 3 phr promoter still show a lower value than that obtained originally, while the samples with 1 phr show a clear improvement.

Fig. 8.12: Graph to show load in Newtons against UV exposure time in hours with no adhesion promoter present.

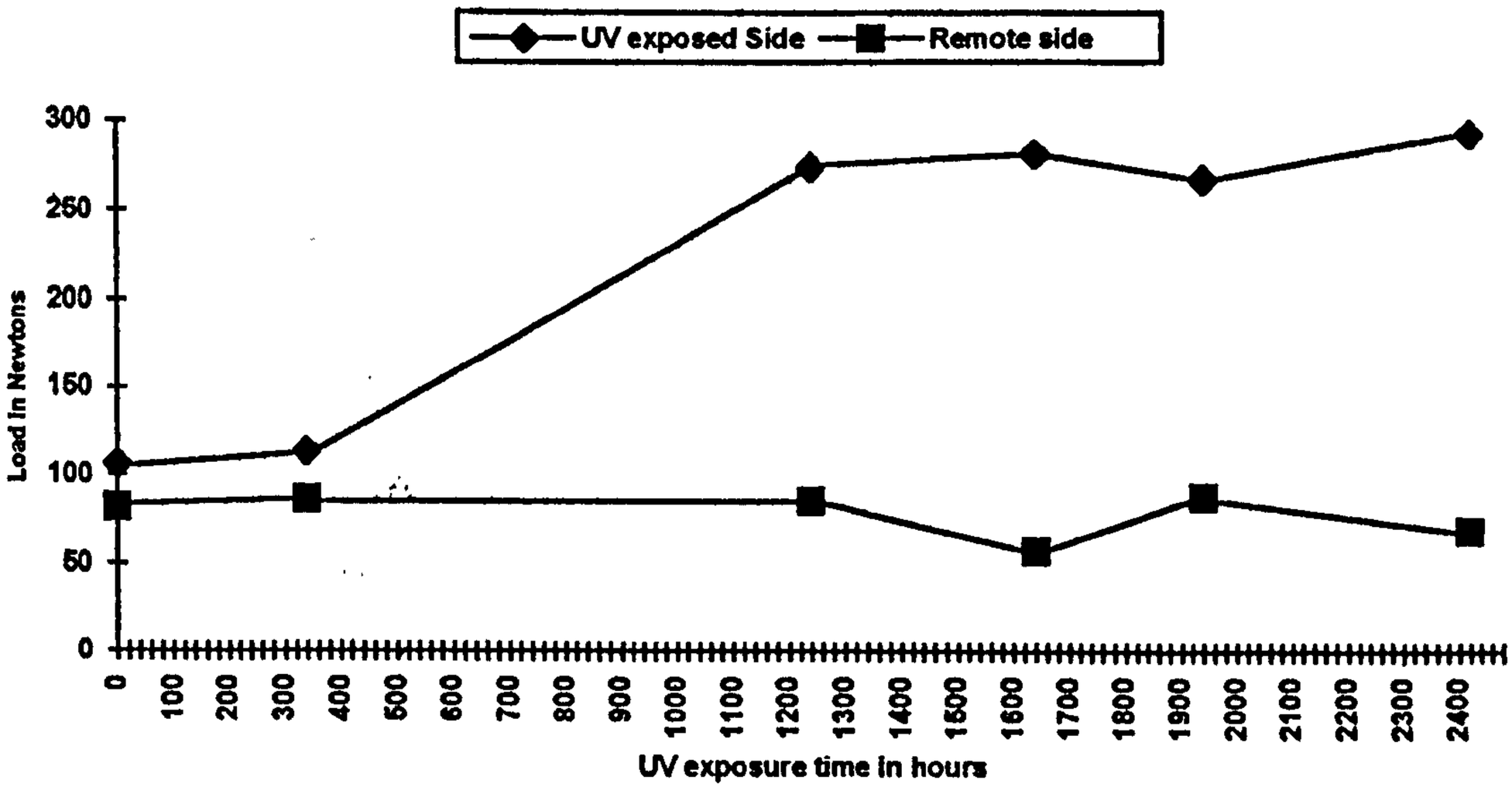

Fig. 8.13: Graph to show load in Newtons against UV exposure time in hours with 1 phr adhesion promoter present.

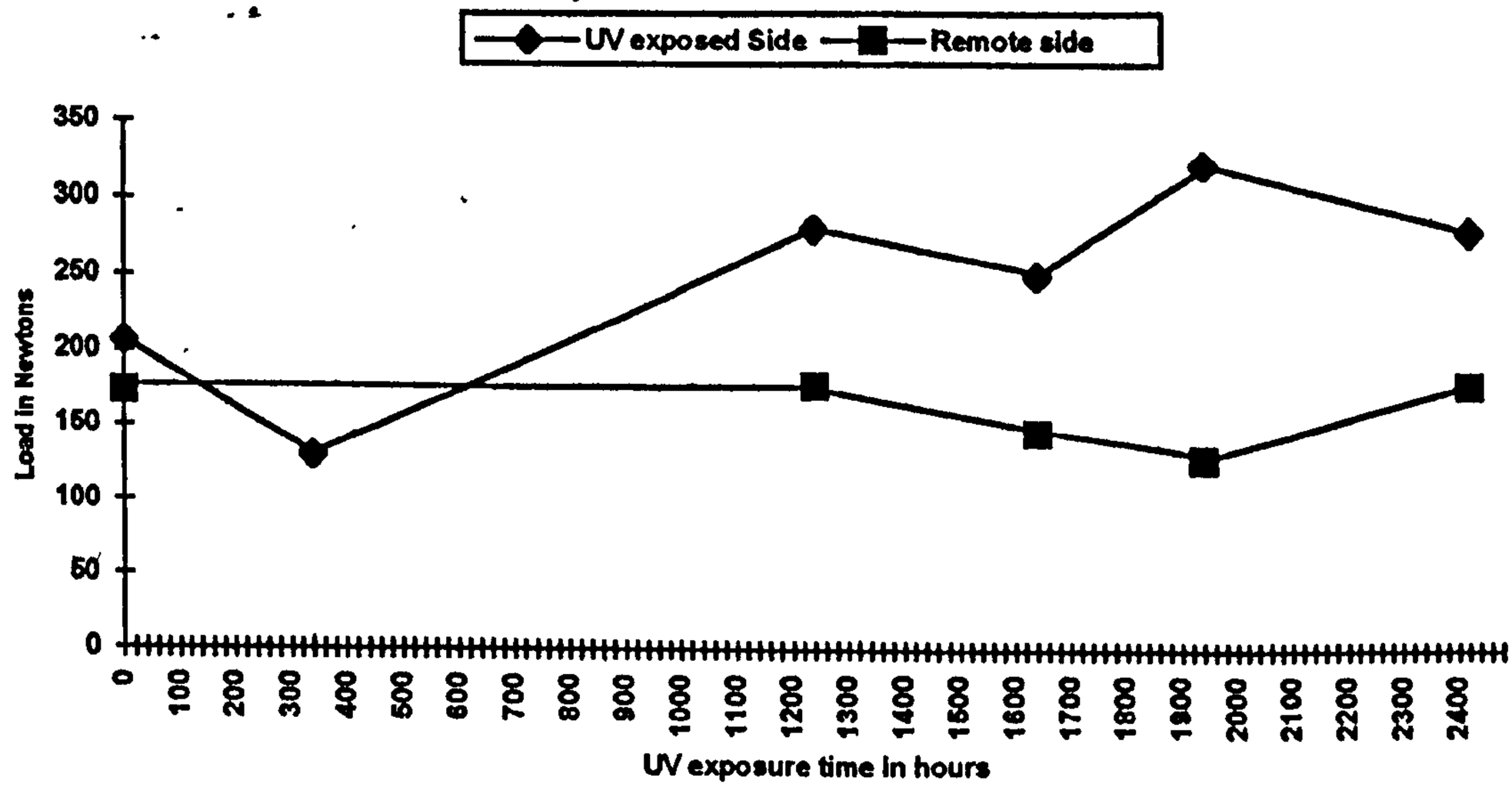

Fig. 8.14: Graph to show load in Newtons against UV exposure time in hours with 3 phr adhesion promoter present.

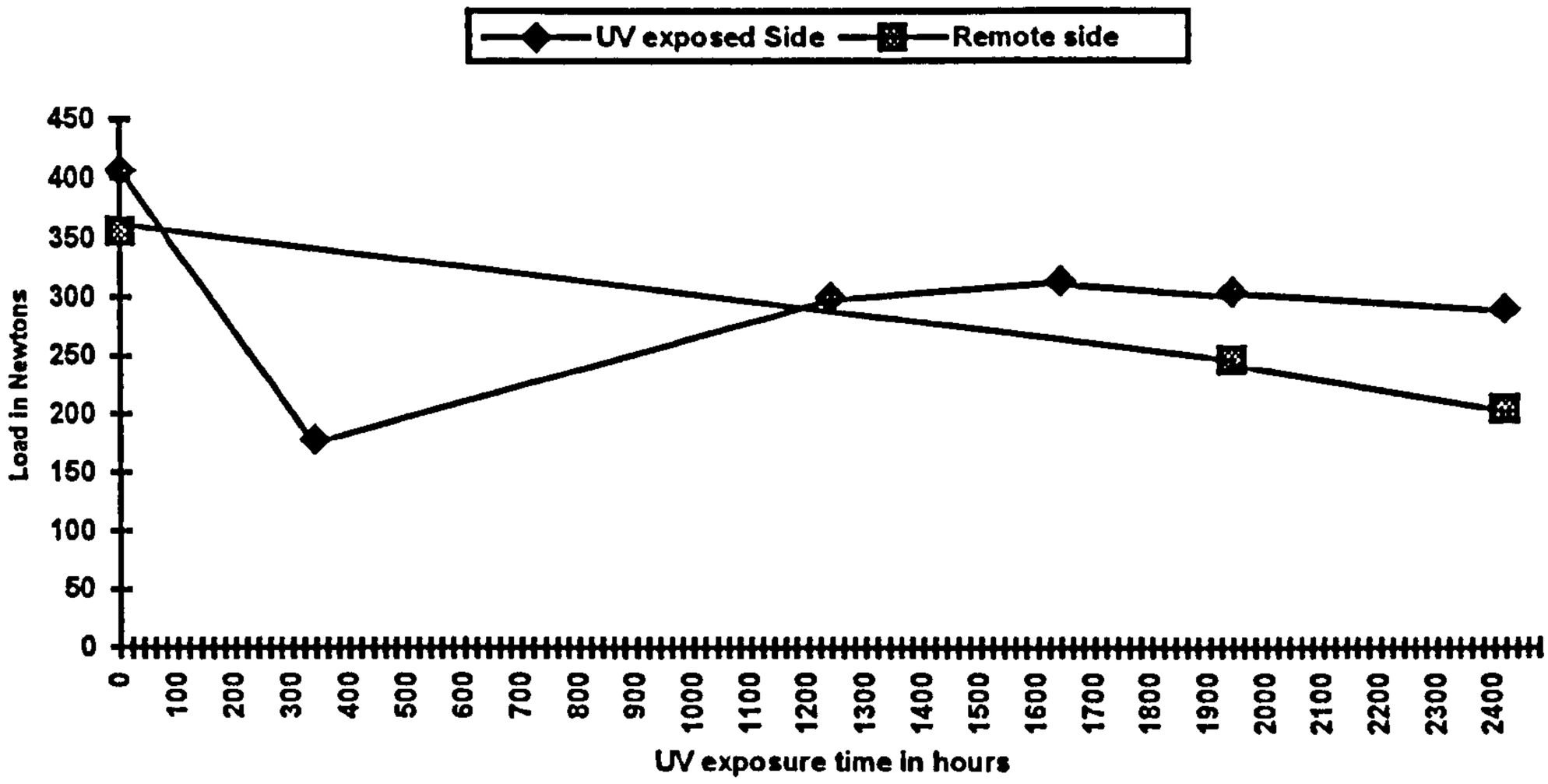

8.10 DISCUSSION AND CONCLUSIONS

Although extensive measures were undertaken to establish the nature of the discolouration at the polymer-glass interface in MnO_2-cured polysulfide-based sealants, the methods undertaken were relatively unsuccessful.

XPS is a technique which has become popular in recent years in analysing polymer surfaces, with numerous publications in the field[1-7] and so it was therefore logical to use this technique to analyse the changes occurring due to UV exposure at a polymer/glass interface. Although this technique was very informative in revealing the elements present at the surface, see table 8.1, we were unable to resolve chemical shifts owing to a build up of positive charge; moreover, the polymer samples also underwent radiation damage under the experiment, leading to further complication, and it was therefore impossible to obtain any accurate information on changes in functional groups occurring at the surface.

ATR-FTIR[10,11] and static SIMS[12] are also popular surface techniques for analysing polymer surfaces, but no useful information could be obtained for LP surfaces using these techniques. Surface Raman IR and EDAX analyses were also unsuccessful.

The elemental analysis (section 8.6) performed on the unexposed and exposed polymer blocks clearly showed that the material affording the discolouration at the interface was largely organic in nature. The leaching experiments of thin slices of bonds showed the presence of a carbonyl band at 1723 cm^{-1} in the UV-exposed polymer/glass surface. This result was confirmed by the IR spectrum obtained for a thin film sample of the material exhibiting the yellow discolouration (fig.8.11), although ^1H NMR analysis on the necessarily dilute leached solution was unable to

detect the peak at 8 ppm characteristic of a formate ester, and ATR-FTIR experiments failed to detect the development of the 1725 cm^{-1} band in UV-exposed surfaces, although a band at ca. 1600 cm^{-1} attributable to formate ions[13] was visible. From the shape and position of the carbonyl band appearing at the UV-exposed polymer/glass interface, it is highly probable that the photodegradation pathway occurring is the same as that for the pre-polymer samples discussed in section 5.9, and the cured polysulfide films, section 6.21, i.e. a free radical route resulting in the production of a formate ester. The detailed mechanism is illustrated in section 5.9.

The tensile experiment (section 8.9) shows that improved adhesion of the polymer to glass occurs following extensive UV irradiation, especially when an adhesion promoter such as A187 has been omitted from the formulation.

CHAPTER 8

REFERENCES

1. Ge, H., Qi. G., Kang, E.T., Neoh. K.G., *Polymer*, **35**, (1994) 504.
2. Zupp, T.A., Fulghum, J.E. Surman, D.J., *Surface and Interface Analysis*, **21**, (1994) 79.
3. Dutta, P.K., *Macromolecular Reports*, **A31**, (1994) 571.
4. Kaushik, V.K., Rao, P.V.C., Bhardwaj, I.S., *Polymer Testing*, **13**, (1994) 211.
5. Delamar, M., *Polimery*, **39**, (1994) 280.
6. Lacoste, J., Deslandes, Y., Black, P., Carlsson, D.J., *Polymer Degradation and Stability*, **49**, (1995) 21.
7. Watts, J.F., *Materials World*, (1993) 560.
8. Crooks, J.E., *The Spectrum in Chemistry*, Academic Press Inc., London. (1978) 185-201.
9. Woodruff, D.P., Delchar, T.A., *Modern Techniques of Surface Science*, Cambridge Solid State Science Series, Cambridge. (1986) 96-126.
10. Skourlis, T.P., McCullough, R.L., *J. Appl. Polym. Sci.*, **52**, (1994) 1241.
11. Pereira, M.R., Yarwood, J., *J. Polym. Sci. pt B*, **32**, (1994) 1881.
12. Benninghoven, A., Rading, D., *Macromol. Symp.* **83**, (1994) 27.
13. Lemaire, J., Gauvin, P., Sallet, D., *Makromol. Chem*, **188**, (1987) 1815.

CHAPTER 9

CONCLUSIONS AND FUTURE WORK

9.1 MASS SPECTROMETRIC CHARACTERISATION

We have developed a method of completely characterising the complex components that make up commercially used LPs, by means of electrospray ionisation mass spectrometry (ESI-MS), combined with collision induced dissociation (CID)[1,2]. This appears to be the most comprehensive study of LP characterisation to date, offering a much greater level of detail than previous studies[3-8].

ESI has proved to be a most useful addition to the armoury of mass spectroscopic techniques applicable to the characterisation of linear polysulfides. The individual spectra are well–resolved, enabling conclusions to be reached about the distribution of mers within a given formulation, about the presence of variant mers (usually associated with additional oxymethylene or oxyethylene units or a monosulfide linkage, or some combination of these), about the identity of end–groups and about the nature and extent of simple reactions of LPs, for example with acrylate esters. The CID spectra of ions derived from LPs reveal relatively simple fragmentation pathways, depending on the complexity of the LP structure.

ESI spectra offer a very direct insight into the presence of variant mers and of the end groups. Some of these features can be detected in LP oligomers by ^{1}H and ^{13}C NMR spectroscopy, but even then, the location of an anomalous group within the chain cannot be defined as precisely as it can be from CID spectra. Infra–red spectra

of LPs offer only general information about the functional groups present and cannot be used to observe the presence of additional groups such as CH_2O or C_2H_4O.

It is clear from the various ESI spectra portrayed, that while the technique provides very accurate mass information at RMM<2000, it gives a heavy bias towards the detection of low mass oligomers at the expense of those of higher mass, thus even when, as in LP–32C, the average RMM is *ca.* 4000, no peaks appear at $m/z > 2500$ and the ion abundances at $m/z > 1800$ do not reflect the abundances of oligomers present. This situation does not appear to arise from lower solubility of the high mass oligomers since changing the mobile phase offered no advantage; this could suggest that ESI discriminates against ions of higher *m/z* values and perhaps coupling a GPC column to the instrument would allow the higher oligomers to be detected, as advocated by Simonsick and Prokai[9,10]. An alternative explanation is that although ESI is a very soft ionisation technique, there is still some fragmentation before detection in LPs, most likely at the weak disulfide linkage.

Fast atom bombardment mass spectrometry (FAB-MS) studies of LPs gave rise to fragmentation spectra similar to those obtained by ESI/CID, thus characterisation by this technique is somewhat limited but results obtained were able to support assignment made using ESI-MS.

We have also been successful in obtaining detailed spectra of LPs using matrix assisted laser desorption ionisation time-of-flight mass spectrometry, (MALDI-TOF-MS); although these spectra are well resolved and exhibit a separation between peaks of 166 Da, the molecular weight of the repeat unit, they are not as informative as spectra obtained by ESI-MS. We also had a complication, i.e. the formation of silver clusters $[Ag(Ag_2S)_n]+$ at higher laser powers or high silver concentrations. The

correct molecular mass distribution for LPs is not obtained, with low mass oligomers being detected at the expense of high mass oligomers. Possible explanations for this are:

i) there is a bias for the detector to favour the detection of low mass oligomers, especially in very polydisperse samples, as with commercial LPs.

ii) the samples undergo fragmentation during ionisation, most likely at the weak disulfide linkage, and

iii) only low mass oligomers undergo ionisation into the gas phase.

Fractionation of an LP sample using a GPC column prior to MALDI-TOF-MS analysis may lead to high mass oligomers being detected using this technique, and hence the calculation of accurate molecular mass information for this class of polymers; this has been applied successfully by Montaudo et al.[11] for polydisperse samples of various well-known polymers, e.g. acrylates.

We have been unable to obtain spectra of the necessarily more complex degraded LP samples using MALDI-TOF-MS, whereas ESI-MS gave very useful data on the degradation process.

Field desorption mass spectrometry (FD-MS) has also been successful in characterising LP samples, but this technique is less generally accessible and much more time-consuming than either ESI-MS or MALDI-TOF-MS.

This thesis contains a detailed study of LPs using a wide variety of mass spectrometric ionisation techniques, of which there are no previous publications in the open literature.

9.2 DEGRADATION STUDIES OF LINEAR POLYSULFIDES.

In this thesis we have shown that linear polysulfides (LPs) are degraded thermally and photochemically by two competing degradation pathways:

i) a free radical autoxidation mechanism, and

ii) a hydrolysis mechanism.

UV photolysis or pyrolysis of LP pre-polymers in the presence of air or oxygen resulted in the development of carbonyl groups detectable by IR and NMR spectroscopy, while 2-D NMR studies and the highly characteristic field positions of the NMR resonances show the carbonyl group to be due to a formate ester.

Support for this assignment to a formate ester comes from studies of poly(propylene oxide)[12-14] and poly(ethylene oxide)[14], where attack at the C-H bond adjacent to the ether oxygen atom leads to a hydroperoxide and hence an alkoxyl radical, followed by scission to give a formate ester, as described in detail in section 5.9.

The formate ester arises as a result of a conventional free radical mechanism of autoxidation and is derived from two pathways, namely:

i) via the tertiary carbon centres (when present in LP) as proposed by Griffiths et al.[12], and

ii) via the secondary carbon atoms as indicated by Lemaire et al.[14]

The level of branching agent present in the pre-polymer appears to have little effect on the rate of degradation, supporting the theory that both secondary and tertiary carbon centres undergo attack.

All thin film samples of cured LP, irrespective of the LP structure and curing agent, including ZL-2264 (with an extra CH_2 linkage in the repeat unit), produce a carbonyl absorption at 1725 cm^{-1} when exposed to UV irradiation. This 1725 cm^{-1} band was also found for degraded LP pre-polymer samples (including ZL-2264) and assigned, using NMR techniques, as being due to the formation of a formate ester by a free radical route. The use of solid state ^1H NMR (above, section 6.21) was unable to confirm that the same degradation pathway is occurring in the cured film experiments, because the NMR spectra obtained were poorly resolved and the structural detail obtained was therefore limited. Irradiated films leached in $CDCl_3$ for long periods of time also failed to produce sufficient dissolved material to enable a search to be made for the 8 ppm peak assigned to the formate ester. Even so, the similarity in shape and position of the photoproduced carbonyl band make it highly probable that the carbonyl band developed in all polysulfide UV-irradiated films is due to the same degradation pathway as the carbonyl development seen in the pre-polymer samples, i.e. a free radical route leading to the formation of a formate ester, (see section 5.9).

The study of liquid exudates formed when TBHP- and HDDA- cured LP cast blocks are exposed to prolonged periods of heat or UV irradiation also show the development of carbonyl bands at 1724 cm^{-1} in their IR spectra, again indicating that degradation is occurring at least in part via a free radical mechanism.

ESI-MS studies of degraded pre-polymer samples and liquid exudates show that, in parallel with the degradation route involving oxygenation of a methylene group demonstrated by IR studies and NMR studies, there is a hydrolysis mechanism involving initial cleavage of the formal group to release formaldehyde, followed by

secondary reactions to give other products detected in the ESI-MS spectrum of the photolysate/pyrolysate. This mechanism is discussed in sections 5.8 and 5.9, and confirmed by the extremely slow degradation of ZL-2264, which has no formal group.

The hydrolysis mechanism is the principal route for the degradation of LP pre-polymers; the development of ^{13}C NMR peaks due to $S\underline{C}H_2CH_2OH$ and $SCH_2\underline{C}H_2OH$, at 41 ppm and 60 ppm respectively, finds support from model compound studies of bis-(2-hydroxyethyl)disulfide[15] which yielded ^{13}C resonances at 40 and 59.4 ppm. The stability of ZL-2264 as compared to all other LPs points to the crucial role of the formal groups as the locus of initial degradation.

As regards the relative role of the two degradation pathways, (see section 5.9), the relatively high intensity of peaks in the ESI-MS spectra of the degraded samples attributable to hydrolysed species, as opposed to oxidised species, indicates that, at least as regards pre-polymers, the hydrolysis pathway is dominant.

Interestingly, we have shown in chapters 6 and 7 that in the photodegradation of LP polymers cured with MnO_2- or $NaBO_3$- (but not t-BuOOH), the photo-oxidative route is much more significant. However, there is still evidence that the hydrolysis pathway is also occurring but to a lesser extent, since IR studies of UV irradiated films show the development of O-H bands in their spectra (see chapter 6).

In chapter 7 it is shown that TBHP- and HDDA- cured LP cast blocks decomposed under heat and UV to produce a liquid exudate which forms via the hydrolysis route; this is therefore the principal degradation route for LP samples cured using these curative agents, although the addition of carbon black is extremely efficient at inhibiting this process. ZL-2264 cured blocks did not form liquid exudates,

providing further evidence that the exudate is principally formed as a result of the hydrolysis mechanism.

Compared to a normally structured LP, ZL-2264 displays greatly improved photo- and thermal stability, a result offering confirmation of the hydrolysis mechanism illustrated in fig.5.18. This scheme depends critically on the presence of the formal linkage in the pre-polymer chain as the initial hydrolysis site to produce free formaldehyde, which then further attacks disulfide linkages. The variation in the repeat unit of ZL-2264 of replacing the CH_2O linkage with C_2H_4O eliminates any possibility of the formation of formaldehyde by this reaction, therefore making degradation by this particular hydrolysis route impossible. This is a key finding in the present search for means of extending the lifetimes of polymers based on LPs.

The results of chapters 5, 6 and 7 indicate the duality of the degradation mechanism of LPs. The hydrolysis mechanism, advocated by Rosenthal and Berenbaum[16], is the more significant for pre-polymers and HDDA- and TBHP-cured LP samples, while for LP samples cured using MnO_2- and $NaBO_3$-, the principal degradation route is that of free radical autoxidation. In this thesis a wide range of analytical techniques have been applied to the solution of the mechanism of polysulfide degradation, which is so mechanistically rich and diverse.

9.3 PHOTODEGRADATION OF MnO_2- CURED LINEAR POLYSULFIDES AT THEIR INTERFACE WITH GLASS.

Although extensive measures were undertaken to establish the nature of the discolouration at the polymer-glass interface in MnO_2-cured polysulfide-based sealants, the methods undertaken were relatively unsuccessful.

XPS was informative in revealing the elements present at the surface of a polysulfide sealant, but we were unable to resolve chemical shifts owing to a build up of positive charge; moreover, the polymer samples also underwent radiation damage during the experiment, leading to further complication. It was therefore impossible to obtain any accurate information on changes in functional groups occurring at the surface.

Using techniques such as ATR-FTIR, static SIMS, EDAX, surface Raman and IR gave no useful information on the nature of the yellow discolouration formed on photolysis. Elemental analysis performed on the unexposed and exposed polymer blocks clearly showed that the material affording the discolouration at the interface was largely organic in nature.

Leaching experiments of thin slices of bonds showed the presence of a carbonyl band at 1723 cm^{-1} in the UV-exposed polymer/glass surface. This result was confirmed by the IR spectrum obtained for a thin film sample of the material exhibiting the yellow discolouration (see fig.8.11), although ^{1}H NMR analysis on the necessarily dilute leached solution was unable to detect the peak at 8 ppm characteristic of a formate ester, and ATR-FTIR experiments failed to detect the development of the 1725 cm^{-1} band in UV-exposed surfaces, although a band at ca. 1600 cm^{-1} attributable to formate ions was visible. From the shape and position of the carbonyl band appearing at the UV-exposed polymer/glass interface, it is highly probable that the photodegradation pathway occurring is the same as that for the pre-polymer samples discussed in section 5.9, and the cured polysulfide films, section 6.21, i.e. a free radical route resulting in the production of a formate ester, which is

ultimately hydrolysed to formate ion. The detailed mechanism is illustrated in section 5.9.

The tensile experiment (section 8.9) shows that improved adhesion of the polymer to glass occurs following extensive UV irradiation, especially when an adhesion promoter such as A187 has been omitted from the formulation.

9.4 FUTURE WORK

Although we have been able to characterise fully the components that make up a commercial LP using mass spectrometric techniques such as ESI, MALDI and FD, we still have been unsuccessful in obtaining accurate molecular weight information for this class of polymer. To remedy this, separation of LP polymer samples using a GPC column could be undertaken and each fraction analysed by ESI-MS, MALDI-TOF-MS or FD-MS. This approach has been undertaken successfully in ESI-MS studies by Simonsick and Prokai[9,10], and by using MALDI-TOF-MS for accurate molecular weight analysis of polydisperse polymers by Montaudo et al.[11]

Another interesting approach to ESI-MS analysis of LP pre-polymers may be to use calcium- or copper- based salts in the solvent system, instead of ammonium chloride or potassium iodide, in an attempt to generate doubly charged ions, which might lead to more information about the higher molecular weight molecules present in these samples. Use of a silver salt would also be interesting in comparing ESI-MS results with MALDI-TOF-MS, to establish whether the silver cation becomes attached to the sulfur atom and whether Ag_2S clusters form under electrospray ionisation conditions. Further research into an ideal solvent/salt system for analysis of LP samples by ESI-MS and ideal matrix/salt system for analysis by MALDI-TOF-MS could also be undertaken.

In this thesis, we have clearly defined the two degradation pathways occurring within LP based samples. Further research could continue in this area to assign the A,B -30 amu series present in the ESI-MS of degraded pre-polymer samples and liquid exudates. Also, further studies to assign the new series seen in the heavily degraded liquid exudates could be undertaken to give an insight into secondary degradation reactions. Further studies could also be carried out to assess the degradation routes occurring when pre-polymer and cured samples are placed under an inert atmosphere. We could also look at the effects that infra-red irradiation, ozone, humidity, etc. may have on the service lifetimes of these polymers.

More research could continue into finding suitable inhibitors to prevent LP degradation. ZL-2264 clearly showed a greatly improved photo- and thermal stability compared to normally-structured LPs, and therefore studies into the degradation mechanisms of LPs with a slight variation in structure, i.e. a monosulfide linkage replacing the disulfide linkage, could be undertaken with a view to finding a more chemically stable LP.

Since LP-based commercial sealants contain various additives such as plasticisers, fillers, adhesion promoters, etc., further studies could be carried out to assess the effects these may have on the degradation and service lifetime of these sealants.

Further surface analysis could be undertaken to establish the exact nature of the yellow discolouration observed at the polymer/glass interface of MnO_2-cured LP polymers when exposed to UV irradiation.

CHAPTER 9

REFERENCES

1. Mahon, A., Kemp, T.J., Buzy, A., Jennings, K.R., *Polymer* **27,** (1996) 531.

2. Mahon, A., Kemp, T.J., Buzy, A., Jennings, K.R., *Polymer.* In the press.

3. Mazurek, W., Moritz, A.G., *Macromolecules*, **24**, (1991) 3261.

4. Averko-Antonovich, M.V.S., Zykova, L.A., Safina, V.V., *NP Kauch Rez* **4**, (1985) 23.

5. Berenbaum, M.B., Marck, H.F., Gaylord, N.G., Birkel, N.M., *Encyclopaedia of Polymer Science and Tech,* Wiley New York, **2**, (1969) 445.

6. Davidson, R.G., Mathys, C.I., *Anal. Chim. Acta* **160,** (1984) 197.

7. Morton Thiokol., *Internal Lab Reports.*, 1969, 1970, 1988.

8. Coates, R.J., Gilbert, B.C., Lee, T.C.P., *J. Chem.Soc, Perkin Trans 2,* (1992) 1387.

9. Simonsick, W.J., Prokai, L., '*Abstracts 42nd ASMS Conference on Mass Spectrometry*' Chicago (1994) 318.

10. Prokai, L., Simonsick, W.J., *Rapid Commun. Mass Spectrom.*, **7**, (1993) 853.

11. Montaudo, G., Garozzo, D., Montaudo, M.S., Puglisi, C., Samperi. F., *Macromolecules,* **28**, (1995) 7983.

12. Griffiths, P.J.F., Hughes, J.H., Park, G.S., *Eur. Polym. J,* **29**, (1993) 437.

13. Barton, Z., Kemp. T.J., Buzy, A., Jennings, K.R., *Polymer,* **36**, (1995) 4927.

14. Lemaire, J., Gauvin, P., Sallet, D., *Makromol. Chem,* **188**, (1987) 1815.

15. Scrivens, G., D.Phil. thesis, *An EPR Investigation into the Catalytic Oxidation of Thiols by Peroxides,* University of York, (1995).

16. Rosenthal, N.A., Berenbaum M.B., *Thermal Degradation of Ethyl Formal Polysulfide Polymers.* In-house report for Thiokol Chemical Corporation.